Heterocyclic Calix[4]arene Derivatives for Fluorescence Investigations

A thesis submitted to the National University of Ireland in fulfilment of the requirements for the degree of

Doctor of Philosophy

By

Niall John Maher B.Sc. (Hons.)

NUI MAYNOOTH

Ollscoil na hÉireann Má Nuad

Department of Chemistry,
Faculty of Science and Engineering,
National University of Ireland, Maynooth,
Maynooth,
Co. Kildare,
Éire.

September 2013

Research Supervisor: Dr. John McGinley

Head of Department: Dr. John C. Stephens

Declaration

This is to certify that the material presented within this thesis has not been submitted previously for a Degree to this or any other University. All material presented, except where acknowledged and cited, is the original work of the author.

Niall John Maher

_____

National University of Ireland, Maynooth September 2013

Acknowledgements

There are more than a few people who I would like to thank on finishing this thesis. First of all, I would like to thank my supervisor Dr. John McGinley who, even when commuting from Denmark, has never failed to provide me with guidance, encouragement and friendship over the past four years. I can only hope I have repaid the faith which he has shown in me since giving me this opportunity. I could not have asked for a better supervisor. I would also like to thank South Dublin County Council who provided me with the financial assistance needed for this project.

I extend my sincerest gratitude to all the staff in the department, in particular Dr. Frances Heaney for the many meetings and advice over the course of our collaboration. I also would like to thank the technicians in the department. Noel (who can fix anything and can chat about any sport) Ken (who never turned down a chemical order, and provided an insight into the Irish antiques scene) Ria, Ollie, Barbara and Maryanne Ryan I thank you all your help over the years. I would like to thank Dr. John Gallagher of Dublin City University for the X-ray crystallographic work performed and Dr. Elisa Fadda new to NUI Maynooth for the computational chemistry work.

To the postgrads who helped me settle in and welcomed me back into the lab your friendship has meant a lot to me. Particular thanks must go to John and Denis who provided me with great advice and helped me avoid the many pitfalls that come with calixarene chemistry. The rest of the McGinley group Laura, Haixin, Sam and of course Ursula without your friendship and random chats, the west side of the lab would have been very dull.

To the great number of people who had started before me, I wish to thank you all for providing such a fantastic atmosphere to enter into. From the lunchtime banter to the

many departmental parties, although most of you are no longer here your influence is still felt. I feel privileged to have started with such a great bunch of people and to the PhD's that started with me (Rob, Lorna, Gama, Wayne, Keeley, Emer, Orla, Dean and Pauaric) I thank you for your friendship. I apologise to anyone I forget to mention or who I mention more than once.

To everyone who toiled in the synthetic lab for all the advice, assistance and good old fashioned rants, I would like to say these were all greatly appreciated. Without you I don't think I could have endured the late nights and microwaved dinners as often as I did, I extend my warmest and most sincere thanks. Upstairs would just be a cold lab without the people who give it character. To Ross, Justine, Andrew, Collette, Adam (even though you left the McGinley group) and Xin I wish you all the very best in the future. To the downstairs postgrads (Paul, Ruth, Alice, Michelle Q, Chris, Barry, Michelle D, Andy) I too have shared your pain of working in the cave and I wish you the best of luck in the future. To the many postgrads whose time in the Maynooth has overlapped with mine, I thank you for all your help and advice (Colin, Murphy, Conor, Joey, Lynn, Dec, Rosin, Niamh, Louise, Ciárán M, Ciárán O'C, Owen, Richard, Rob C, Claire, Ken, Emer, Vickie, Anita, Alanna, Trish, Carol, Kaijie). I would like to thank Haowen who provided as interesting a work partner as you are likely to have over the course of our collaboration, I wish you all the best in the future and I greatly valued your friendship over those years. To the postdocs, past and present whose knowledge and advice were greatly appreciated, in particular Martin, Fiachra, Finno, Gillian and John K.

Special thanks must go to the Friday football crew, who have put up with my exuberant brand of defending over the past four years. Without the weekly run around on a Friday afternoon the weeks would have seemed a great deal longer.

I have been extremely lucky to have had incredible support outside of the lab and I would like to thank you all. I must reserve the most special thanks for my family, all of you, for your unwavering support and advice throughout this long slog. It is to my family that I wish to dedicate this thesis. I could not have done this without your support. To my extended family I thank you very much for everything.

Finally, I would like to thank Laura for her unfaltering love and support (even after hearing about calixarenes or rugby for the umpteenth time). It has been tough over the years but I must thank you for everything.

I told you all it would be grand.

Dedication

To my family, Dermot and Dolores my parents, Dermot and Anna my brother and sister.

Thank you for everything.

Abstract

This project entails the synthesis of a family of novel Schiff base capped calix[4]arenes. These ligands were prepared using three 1,3 *bis*-bromo-alkyl-disubstituted calix[4]arenes (ethyl, propyl and butyl), and *ortho*, *meta* and *para* substituted di-imine bridged diphenol units. All these reactions yielded the desired product with the exception of the *bis*-bromoethyl variants which did not result in capped calix[4]arene formation. The resulting ligands were subjected to attempted metal complexation reactions with metal perchlorate salts (Cu^{2+}, Co^{2+}, Hg^{2+}, Ni^{2+} and Zn^{2+}) and all these reactions resulted in hydrolysis of the imine moiety. Evidence of metal complexation was noted in some cases and it is thought that ethylenediamine metal (en(M)) chelate complexes have formed.

A class of novel 1,3 *bis*-triazole linked calix[4]arene benzaldehydes were prepared through difunctionalisation of the lower rim. A zinc(II) perchlorate complex of one of these was formed and the binding site was evaluated using ^{1}H and ^{13}C NMR spectroscopy. The fluorescent behaviour of two of these ligands was probed with a view to use as a fluorescent chemosensor. However, it was determined that this class of compounds was unsuitable for this role. The synthesis of a range of triazole linked Schiff base capped calix[4]arenes was attempted, but it was discovered the imine moiety was incompatible with the conditions used for triazole formation. A novel *bis*-propargyl di-imine diphenol precursor was prepared from the *meta* Schiff base linker.

Finally anthracene and pyrene isoxazole calix[4]arenes sensors were prepared in collaboration with the Heaney group of NUI Maynooth. The fluorescent emission spectra of these were recorded, and the effect a range of metal cations (Cd^{2+}, Co^{2+}, Cu^{2+}, Fe^{2+}, Hg^{2+}, Pb^{2+} and Zn^{2+}) had on the spectra was recorded. The calix[4]arene based sensors should good selectivity for Cu^{2+} cations. Exploitation of fluorescence

spectroscopic methods led to the determination of the stoichiometry (1:1) and binding constant for these chemosensors. The mode of binding was also examined by ^{1}H NMR spectra titration studies, and through molecular modelling studies which provides a coordination geometrical explanation of the selectivity for Cu^{2+}.

List of abbreviations

Ac	Acetyl
AcOH	Acetic acid
app	Apparent
AIC	Anthracene Isoxazole modified Calixarene
AIM	Anthracene Isoxazole modified Monomer
Anal. Calc.	Analytical calculation
Å	Ångstrom
Ar	Aryl
a.u.	Arbitrary Units
br	Broad
t-Bu	*tert*-butyl
Boc	*tert*-butyloxycarbonyl
$CDCl_3$	Deuterated chloroform
CD_3CN	Deuterated Acetonitrile
$CHCl_3$	Chloroform
cm	Centimetre
cm^{-1}	Wavenumbers
CsCl	Caesium Chloride
CuAAC	Copper(I)-catalysed 1,3 Huisgen Azide-Alkyne Cycloaddition
Cx	Calixarene
d	Doublet
dap	1,3-Diaminopropane
decomp	Decomposition
°C	Degrees Celsius
dd	Doublet of doublets
d.e.	Diastereomeric excess
Δ	Reflux temperature
δ	Chemical shift
DCM	Dichloromethane
DEPT	Distortionless Enhancement by Polarization Transfer
DFT	Density Functional Theory
DMF	*N*,*N*-dimethylformamide
d_6-DMSO	Deuterated dimethyl sulphoxide
dt	Doublet of triplets
en	Ethylenediamine
ESI	Electronspray ionisation
EtOH	Ethanol
FTIR	Fourier Transform Infrared
h	Hour
HCl	Hydrochloric acid

HOMO	Highest occupied molecular orbital
Hz	Hertz
I_f	Peak Fluorescence Intensity in presence of metal ion
I_o	Peak Fluorescence Intensity of free ligand
IR	Infrared
J	Coupling constant
K_a	Association Constant
KBr	Potassium bromide
KOH	Potassium hydroxide
K_s	Stability Constant
K_{SV}	Stern-Volmer Constant
λ	Wavelength (nm)
λ_f^{em}	Emission wavelength (nm)
λ_f^{ex}	Excitation wavelength (nm)
LC	Liquid chromatogram
LC/TOF-MS	Liquid chromatography time-of-flight mass spectrometer
L/min	Litres per minute
lit	Literature value
LUMO	Lowest unoccupied molecular orbital
M	Molar
m	Multiplet
Me	Methyl
MeCN	Acetonitrile
MeOH	Methanol
Me_4Si	Tetramethylsilane
MHz	Megahertz
min	Minute
mL	Millilitre
mmol	Millimole
m.p.	Melting point
μL	Microlitre
μM	Micromolar
N_2	Dinitrogen
NaCl	Sodium chloride
NaOH	Sodium hydroxide
NMR	Nuclear magnetic resonance
nm	Nanometre
NOAC	Huisgen Nitrile Oxide-Alkyne 1,3-dipolar Cycloaddition reaction
OEt	Ethoxide anion
O_2	Molecular oxygen
pH	Logarithmic scale of concentration of hydronium ions ($-\log[H_3O^+]$)
PhMe	Toluene

pK_a	Minus log of association constant K_a of a given solution ($-\log K_a$)
ppb	Parts per billion
ppm	Parts per million
PET	Photoinduced Electron Transfer
PIC	Pyrene Isoxazole modified Calixarene
PIM	Pyrene Isoxazole modified Monomer
py	Pyridine
q	Quartet
s	Singlet
qNR	*quasi*-Newton Raphson
sp.	Species
t	Triplet
τ	Fluorescent Lifetime
TLC	Thin Layer Chromatography
TFA	Trifluoroacetic acid
UV-Vis	Ultraviolet/visible
V	Volts
ν	Wavenumbers

Table of Contents

1. Introduction

1.1 Calixarene Chemistry

1.1.1 Overview

Calixarenes are versatile macromolecules, and it is due to this versatility and the ease of their preparation that calix[4]arenes have become increasingly popular in the field of supramolecular chemistry. The parent calix[4]arenes are easily functionalised, and these derivatives have a wide array of applications from capsules for drug delivery to metal ion chemosensors. Both the upper and lower rims have been subjected to countless transformations that bind metal ions at both sites. This section will provide an overview to the synthesis of the parent molecules and an insight into the methods used in functionalising the calix[4]arene. This thesis will focus solely on lower rim functionalisation, to bestow a taste of the vast array of roles for which these molecules have been utilized.

1.1.2 Calix[4]arene synthesis

The macrocyclic calixarene is formed *via* a base catalysed condensation between a *para*-substituted phenol and formaldehyde. The preparation of the different derivatives calix[4]arene, calix[5]arene, calix[6]arene and calix[8]arene is dependent on the base which is employed. Work undertaken by von Baeyer in 1872 involved the synthesis of macrocycles and represented his first foray into phenol and formaldehyde chemistry.[1-3] Unfortunately, the analytical tools which were at his disposal at the time led to the incomplete characterisation of the macrocycles prepared.[4] It was not until 1942, a full seventy years after von Baeyer, that Zinke and Ziegle would report the first crystalline product from this condensation reaction. Zinke sought to simplify the reaction and in pursuit of this used 4-*tert*-butyl phenol; the use of the *para* disubstituted phenol left

only the *ortho* positions open to reaction. The empirical formula of the crystals was determined to be $C_{11}H_{14}O$, this eventually lead to the assignment of the tetrameric structure.[5] This assignment was corroborated by Hayes and Hunter, who developed a stepwise synthesis which yielded a brown solid with a melting point >300 °C.[6,7]

The studies by Zinke served as the foundation for work which was undertaken by Cornforth in 1955.[8] Cornforth repeated the work of Zinke and he isolated two similar products, which interestingly had different melting points. Tetrameric structures were assigned to both of these products just as Zinke had done previously. Aided by Hodgkin, Cornforth proposed that the compounds were diastereoisomers.[9] These isomers are known to exist today as a result of the restriction in the rotation about the aromatic-methylene bond. The diasteroisomers have subsequently been comprehensively characterised: cone, partial cone, 1,2-alternate, 1,3-alternate conformations are shown (Figure 1.1).

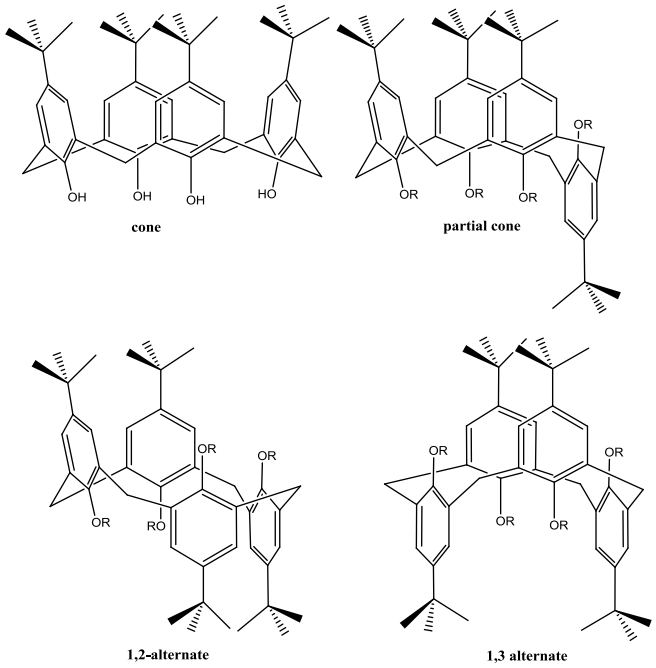

Figure 1.1: The four conformers of calix[4]arene.

It has been found that the cone conformation is the most stable conformer. This is due to the stabilising effect of the intramolecular hydrogen bonding which occurs between the hydroxyl groups.

It was C. David Gutsche who proposed that this family of macrocycles be named calixarenes. This was owing to the shape of these molecules which resembles a chalice and the Greek for chalice being *calix*. The work undertaken by Gutsche's group was exploring the use of calixarenes as cavities to mimic enzyme active sites.[4] Andretti *et al*. solved the X-ray crystal structure of *p-tert*-butylcalix[4]arene in 1979, which provided a definitive assignment of structure.[10] It was found that the calix[4]arene crystal grown, formed an inclusion complex with a molecule of toluene situated in the macrocyclic cavity. Hayes and Hunter proposed a ten step synthetic pathway for the synthesis of *p*-methylcalix[4]arene, Scheme 1.1.[6] This method involves (i) the protection of one of the reaction sites with bromine. Next (ii) is the base promoted hydroxymethylation which provides the methyl linker. After this, steps (i) and (ii) are repeated as necessary to give the appropriate number of repeat units for the linear oligomer. The bromine is removed by palladium hydrogenolysis, and this leads to self-condensation of the linear oligomer in the presence of acid at high dilution. Although there are advantages for this method, it is quite a laborious task when compared to later developments.

Munch developed a method between 1976 and 1977 which yielded a convenient route to the calix[8]arene precursor.[4] Munch used a slurry of *p-tert*-butyl-phenol and paraformaldehyde in xylenes.[11] This was heated to reflux with a catalytic amount of 50 % potassium hydroxide, with a Dean-Stark apparatus attached to remove water from the reaction system.

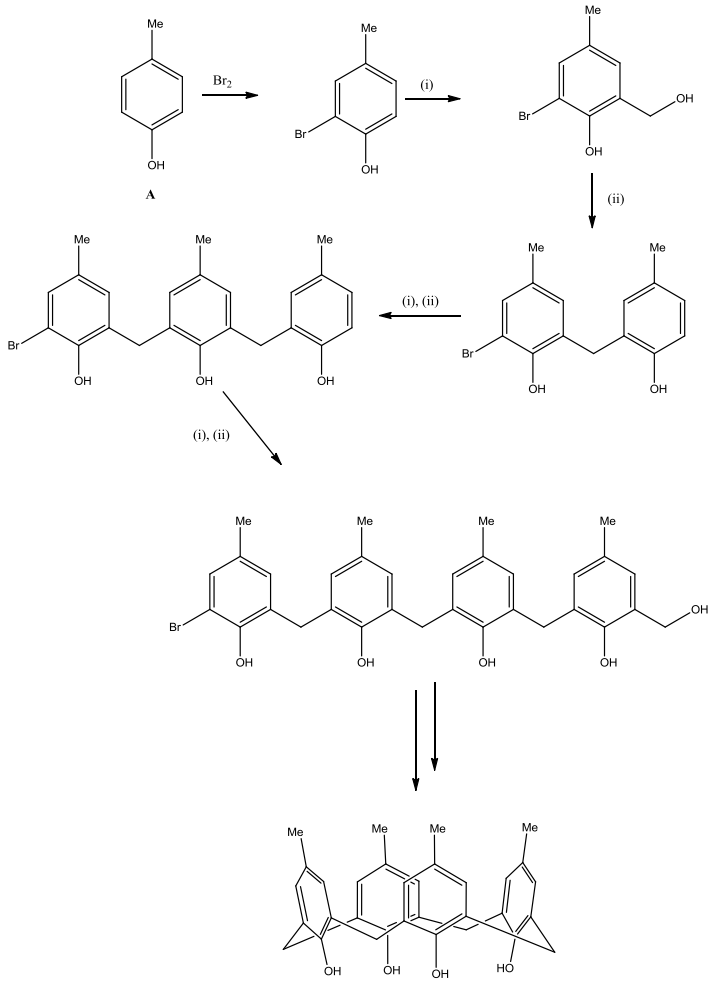

Scheme 1.1: Hayes and Hunter stepwise synthesis of cyclic macromolecule.[4] (i) HCHO, NaOH (ii) **A**, HCl.

Gutsche's group adopted the method which Munch had developed, with much of this work concerned with optimising the conditions by varying the catalyst, the ratio of reactants and solvents used.[12] The product was examined by mass spectroscopy; with a *m/e* value obtained which was in agreement with a cyclic octamer. However, the appearance of a strong mass signal at *m/e* 648 suggested that it could be due to a pair of cyclic tetramers. A trimethylsilyl derivative was also examined by mass spectroscopy and this showed a strong mass signal at *m/e* 1872 which pointed towards an octameric rather than a tetrameric structure. In 1985 X-ray crystallographic data which was published by Gutsche provided definite proof of the existence of calix[8]arene which is now known as octamer.[13]

Whilst this method is high yielding, it unfortunately only yields the calix[8]arene derivative, and as such requires conversion to the tetrameric form. A method which requires heating the octamer to reflux in diphenyl ether with a catalytic amount of sodium hydroxide was published by Gutsche.[14] The product was isolated successfully by precipitation upon addition of ethyl acetate to the warm diphenyl ether solution. The exact mechanism for this conversion is unknown. It is thought to involve the calix[8]arene "pinching" in the middle causing cleavage of the molecule and yielding two equivalents of calix[4]arene. This process has been dubbed 'molecular mitosis' by Gutsche. In a paper published in 1999, Gutsche and his group investigated the mechanism of formation of the tetramer. They concluded that although this 'molecular mitosis' is seen to occur, it is just one of several different formation pathways which occur simultaneously.[14]

Due to the highly symmetric nature of the tetramer and octamer, one would expect it to be difficult to distinguish between them, however this is not the case. As a result of this symmetry both calixarenes have very simple ^{1}H NMR spectra, but it is possible to differentiate between the octamer and tetramer by the shift of the phenolic proton in the ^{1}H NMR spectra. This can be explained by the different sizes of the macrocyclic cavity, the octamer lower rim has a larger circumference so the phenolic groups have weaker hydrogen bonding interactions. Tetramer has a lower rim which is smaller, so the phenolic groups are closer and thus, have stronger hydrogen bonding interactions. The result of this is seen in the ^{1}H NMR spectra of both products with octamer OH resonating at 9.63 ppm as a singlet, and the tetramer OH resonates at 10.34 ppm.

1.1.3 Lower rim functionalisation of calix[4]arene

Only one of the four main conformers of calix[4]arene, the cone conformation, will be covered in this thesis. In this conformation, the phenolic hydroxyl groups are aligned

on the same side of the cavity. The tetramer is drawn with the narrow rim, which possesses the hydroxyl groups, below the wider rim which possess the *tert*-butyl groups. As a result of this convention, the wider rim is denoted the upper rim and the narrower rim is the lower rim (Figure 1.2).

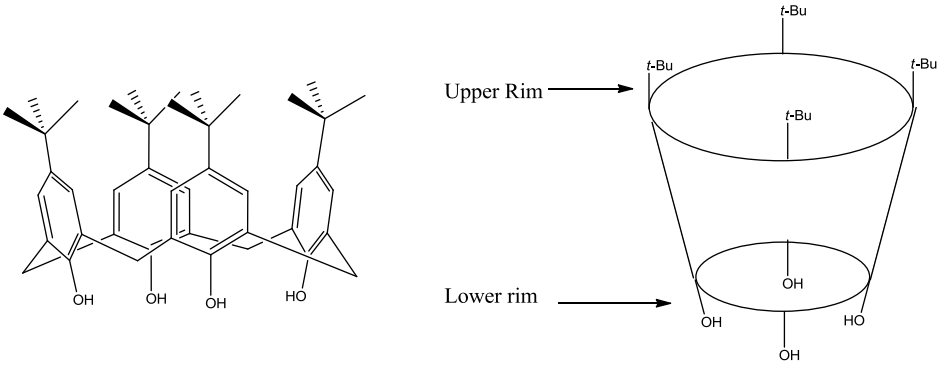

Figure 1.2: Upper and Lower rim positions of Calix[4]arene.

Both the upper[15] and lower rim[16,17] have been successfully modified and the extent of these modifications are the subject of several reviews. With the calix[4]arene derivatives prepared in this thesis solely focused on attachment *via* the lower rim, the scope of this introduction will extend only to modification of the lower rim of the calix[4]arene. In this thesis, calix[4]arene is modified with Schiff base, triazole and isoxazole moieties and as such this introduction will deal with examples of this type of modification.

The lower rim of the calix[4]arene is easily functionalised. This is achieved using widely employed acid-base and nucleophilic reactions. A base, such as potassium carbonate, is usually used in the modification, which gives rise to the calix[4]arene alkali salt. The desired alky-halide is introduced, where it participates in an *in situ* reaction to yield the phenoxy-ether product. Chloro, bromo or iodo variants of the alkyl halides are generally used in these reactions.[18,19]

Regioselectivity can be an issue for difunctionalised calix[4]arenes, as a result of the products being either 1,2-proximal or 1,3-distal substituted (Figure 1.3). The 1,3-distal product is obtained as the major product, which is due to hydrogen bonding interactions which stabilise the alkoxide intermediate.

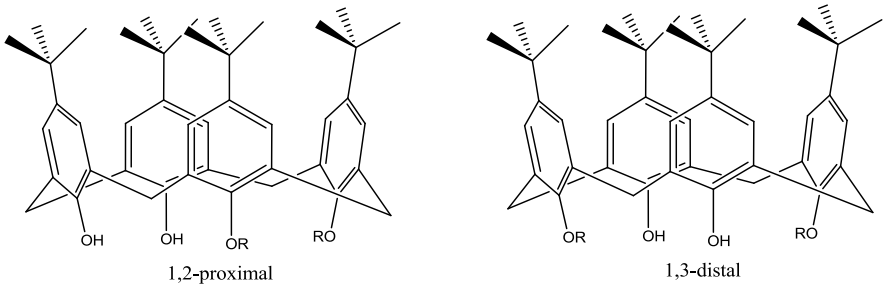

Figure 1.3: Substitution patterns of disubstituted calix[4]arene.

The first phenol is deprotonated by the first equivalent of base, and as this proceeds the two proximal phenoxide moieties act as hydrogen bond donors. This stabilises the intermediate and is shown in Figure 1.4. A monosubstituted derivative is produced first by a nucleophilic substitution with one equivalent of the alkyl halide. This can be isolated at this stage, however, monosubstituted calix[4]arenes usually require chromatography for purification. Due to the proximal hydroxyl moieties ability to act as stabilising hydrogen bond donors (Figure 1.4), the monosubstituted calix[4]arene is selectively deprotonated at the distal position. If deprotonation was to occur at the proximal hydroxyl group, the alkoxide would be stabilised by one hydrogen bond. This is a result of the distance between two distal orientated phenolic oxygens, which would be at a distance too great for hydrogen bonding to occur, this has been calculated to be in the range 3.1-3.6 Å.[20]

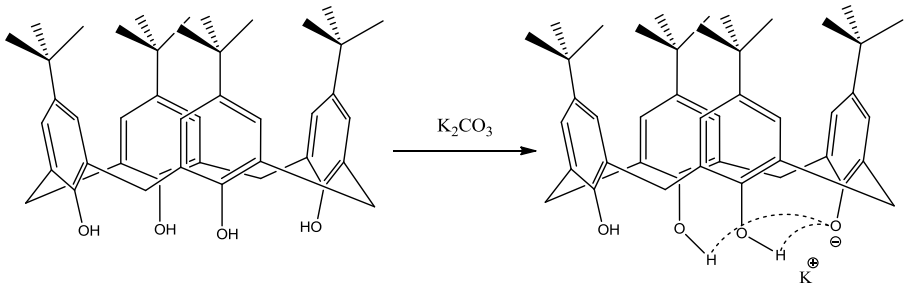

Figure 1.4: Hydrogen bonding interactions following deprotonation of lower rim hydroxyl.

The influence that these hydrogen bond interactions have on the lower rim can be seen when functionalisation of the remaining two phenoxy groups is undertaken. Whilst *mono* or *bis* substitution requires only a mild base, such as potassium carbonate, a significantly stronger base is required to deprotonate the residual phenol groups. This is a consequence of an absence of any hydroxyl protons which could participate in stabilising the alkoxide ion formed. As a result, the deprotonated phenol is more basic in nature, which leaves it more reactive. Stronger bases such as sodium hydride and barium oxide have been exploited for this purpose.[21,22]

1.2 Schiff bases

1.2.1 Overview

There is a vast array of publications in the literature which detail the use of Schiff bases as ligands for binding metal ions. The formation of Schiff base ligands can be performed under a variety of reaction conditions making this reaction quite flexible. The main concern in the formation of Schiff bases is the necessity to remove water which is created from the condensation reaction between an aldehyde or ketone and the amine. These ligands are suitable for metal ion complex formation because of the lone pair of electrons which are on the nitrogen atom of the imine moiety. These Schiff base ligands are markedly proficient at binding transition metal ions. The complexes formed have a wide array of applications from biological mimics to catalysts.[23,24]

1.2.2 Schiff base synthesis

Schiff bases, named after Hugo Schiff, are molecules which contain an imine with an alkyl or aryl group attached to the imine nitrogen.[25] The reaction for the formation of a Schiff-base is a reversible acid-catalysed condensation reaction, which takes place between a primary amine and either an aldehyde or a ketone. This does not prove to be successful for reactions with ammonia. The typical reaction conditions for imine formation require a protic solvent, such as methanol or ethanol, which is sufficiently dry to prevent subsequent hydrolysis of the newly formed imine bond. These condensation reactions proceed smoothly in general, although some reactants can require more energy so harsher conditions such as heating to reflux in a high boiling solvent are used and may include the use of a Dean-Stark apparatus or molecular sieves to remove the water. This usually depends on the electronic effects.[26,27]

The mechanism of formation of the imine bond is well agreed upon (Mechanism 1.1), with the general consensus being that the carbonyl oxygen must be protonated, or that a Lewis acid must be used. This will enhance the electrophilicity of the carbonyl carbon which will assist the later nucleophilic attack.

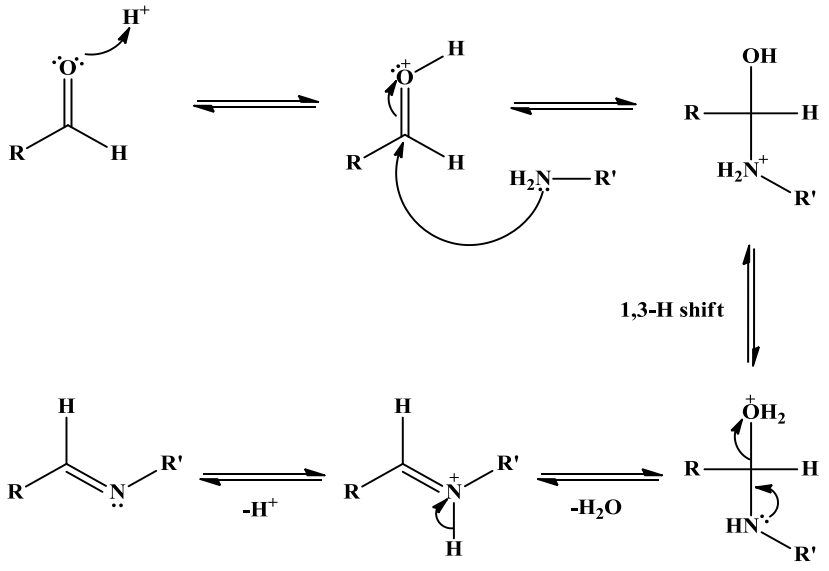

Mechanism 1.1: Mechanism of imine formation.

The protonation of the carbonyl oxygen precedes the nucleophilic attack of the amine on the carbonyl carbon. This is followed by a 1,3-H shift, which leads to the elimination of water. Subsequent disassociation of this species yields the imine product. As a result of the steric interactions between the bulkier R groups, as R is either an aryl or alkyl substituent, the imine double bond generally adopts a *trans* geometrical orientation. This helps to limit the aforementioned steric interactions.

Whilst the formation and purification of most Schiff base ligands is relatively straight forward, some more complex derivatives such as tripodal ligands (Figure 1.5) prove to be more elusive. As Schiff bases can undergo hydrolysis under chromatographic conditions, methods such as employing zinc(II) perchlorate as a template to circumvent these problems have been devised. Hundal *et al*. proposed a mechanism where coordination of the Zn^{2+} ion leads to an increased electrophilic nature of the aldehyde.[28]

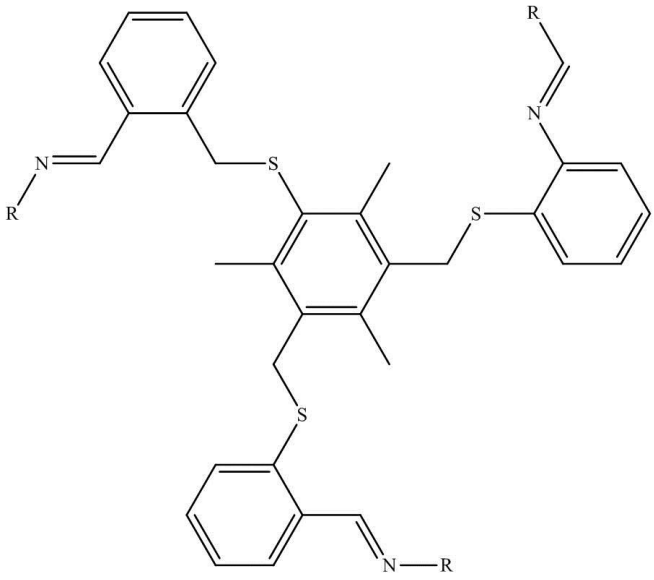

Figure 1.5: Tripodal Schiff base ligand synthesised using a zinc template method

R = aromatic moiety.[28]

It is suggested that the zinc(II) ion localises the electron density of the aromatic amine on the nitrogen atom. This consequently makes it a stronger nucleophile which allows the Schiff base reaction to occur. Due to the Zn^{2+} ion being quite labile, liberation of the newly formed tripodal ligand can occur (Figure 1.5). This reaction is high yielding and gives a product of high purity.

1.2.3 Schiff base derivatives

The use of Schiff base compounds which are derived from salicylaldehyde or another one of its derivatives is well documented. *Mono*, di and multinuclear complexes have been successfully prepared using these salicylaldehyde derivatives. The synthesis of these and the considerable extent of ligands which have been prepared is evident from extensive reviews.[29,30]

Salicylaldehyde has had extensive use as a framework upon which some well-known reagents are based. The substitution pattern of the ring is the reason for this extensive use, and this is clear when compared to the *meta* and *para* derivatives which have been used to a much lesser degree. After an imine has been formed with salicylaldehyde, this imine is *ortho* to the hydroxyl functional group. As a result of this orientation, a six member chelate ring could be formed with the bound metal ion if complexation takes place at the N_2O_2 binding site. A broad selection of *d*- and *f*-block metals have been bound at this site,[31,32] which demonstrates the versatility of this approach.

A recent review by Matsunaga and Shibasaki exhibits the broad scope of catalysts which have been developed based on Schiff bases.[33] Of particular interest is work by Jacobsen and co-workers who reported on the synthesis of Mn(III)Cl(salen),[34] $Cr(III)N_3$(salen),[35] Co(III)OAc(salen)[36] and Al(III)X(salen) complexes (X = Cl, Me, CN, imidate).[37] As a result of the similarity that these Schiff base complexes bear to

the Schiff base capped calix[4]arenes which are prepared in this thesis, the coordination geometry displayed by these complexes should provide a template for the complexes attempted in this project.

The manganese(III) complex (Figure 1.6a) was found to stereoselectively convert unfunctionalised alkenes to epoxides, with enantiomeric excesses (e.e) of up to 97 % reported.[34] The cobalt(III) complex (Figure 1.6b) has been employed in the conversion of racemic of various epoxide derivatives (aliphatic, halogenated, ether/carbonyl baring, aryl, yinyl, and alkynyl) into a single enantiomer with e.e in excess of 99 % reported.[36]

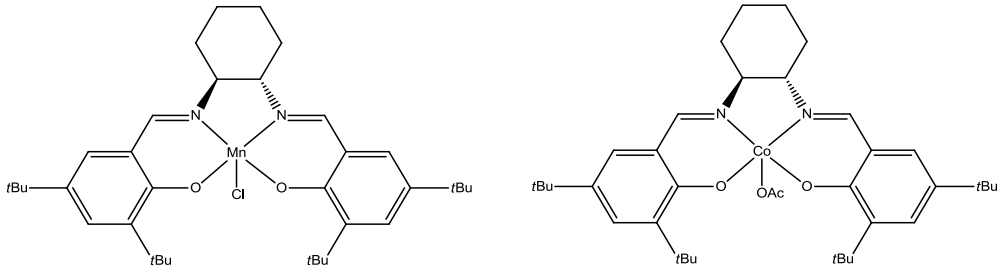

(a) (b)

Figure 1.6: (a) Jacobsen's Mn-salen complex[34] (b) Co-salen complex.[36]

The central diamine is at the core of this extensive variety of binding properties seen for these compounds. The bridging linkage between the two nitrogens can be aromatic or aliphatic in nature. The one requirement which can act as a limitation is that the functional groups must be compatible with amines.

1,2-diaminoethane or ethylene diamine (en) is the most widely used diamine in the literature. When ethylene diamine is employed in imine formation it incorporates a two carbon chain between the two imine moieties. Complexation of a metal through the imine nitrogens results in the formation of a five member ring through the N-M-N bonds. This can be seen in the Jacobsen complexes (Figure 1.6a & b). It is possible to prepare asymmetric centres on the chain *via* functionalisation of the carbon chain. A

wide range of derivatives have been prepared with the introduction of naphthyl, phenyl and isooctyl moieties. These ligands have also been utilised in the synthesis of derivatives which have applications as catalysis[33] and fluorescent sensors.[38,39]

1.2.4 Calix[4]arene Schiff bases

The functionalisation of calix[4]arenes with Schiff bases has been extensively studied with a multitude of examples present in the literature. This section will provide a brief overview of the range of Schiff base modified calix[4]arenes. Calixarenes which have been modified at the upper[40,41] and lower rims with Schiff base moieties have been previously prepared. The Schiff base moiety is often introduced *via* reaction of a benzaldehyde moiety or with an amine modified calix[4]arene.

Of particular interest for this thesis are calix[4]arene Schiff base derivatives which have been prepared that use salicylaldehyde moiety as a linker. Work which was undertaken by Vicens *et al*. utilized a cross linking reaction of a 1,3-distal-dialdehyde calix[4]arene with appropriate diamines, such as ethylene diamine, to yield a bridged lower rim calix[4]arene derivative (Figure 1.7). It was expected that this molecule would bind metals in a similar fashion to salen ligands, which bind through a N_2O_2 coordination sphere. Whilst preliminary metal extraction studies by this group resulted in moderate affinity for Cu^{2+} ions,[42] further work on this ligand which resulted in the preparation of the derivatives, shown in Figure 1.7, slightly improved the metal ion extraction potential.[43]

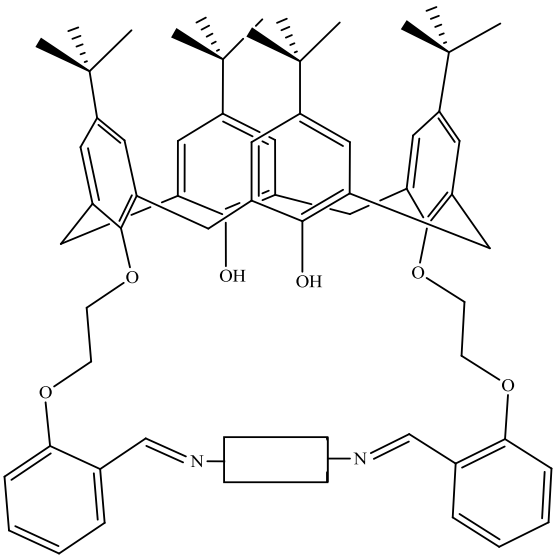

= $(CH_2)n$ (n = 2-4), *o*- and *m*-C_6H_4

Figure 1.7: Schiff base bridged calix[4]arenes prepared by Viscens *et al*.[42]

Schiff base modified calix[4]arenes have also been used as fluorescent sensors. Mahon *et al*. reported on the synthesis of a zinc(II) responsive fluorescent sensor which contains a Schiff base link (Figure 1.8a).[44] This ligand is prepared by reaction of the calixarene dialdehyde with salicylaldhyde hydrazine in the presence of acetic acid, which acts as a catalyst, to form the imine link.

McGinley *et al*. subjected this ligand **(a)** to fluorescence emission spectroscopy. The study proposes that the Zn^{2+} ion binds between the imine nitrogen and the hydroxyl group (Figure 1.8b). It was found that the free calix[4]arene ligand **(a)** exhibited weak fluorescent emission. Enhancement of the fluorescent emission profile was observed upon complexation of Zn^{2+} **(b)**.[45] It is also noted that this sensor is responsive to zinc and cadmium ions only.

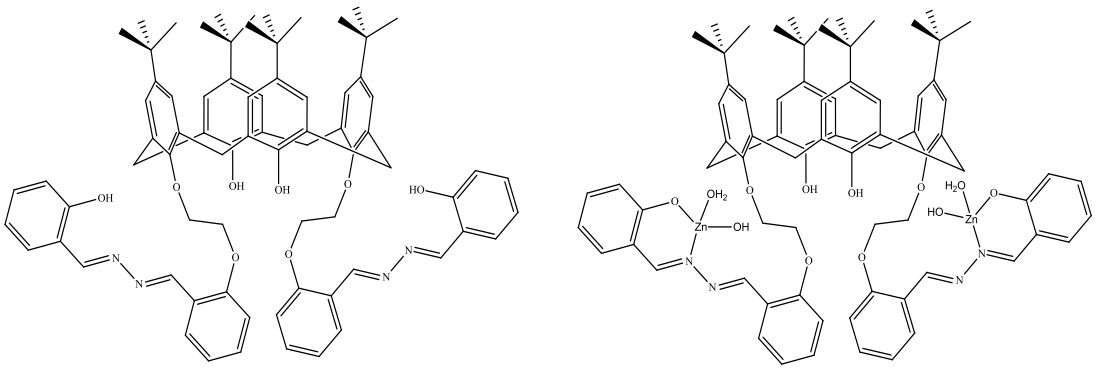

(a) (b)

Figure 1.8: Zn(II) responsive sensor prepared by McGinley *et al*.[45]

Functionalization of the lower rim of the calixarene has been expanded to prepare calix[4]arene 'tubes'. This is where two calix[4]arenes are joined by their lower rims, a tail-to-tail arrangement, *via* a Schiff base linkage, or with another similar functional group such as a hydrazide. Murray and co-workers reported on the preparation of one of these 'calixtubes' (Figure 1.9), whereby an imine was used to link an aldehyde and amine functionalised calixarene together.[46]

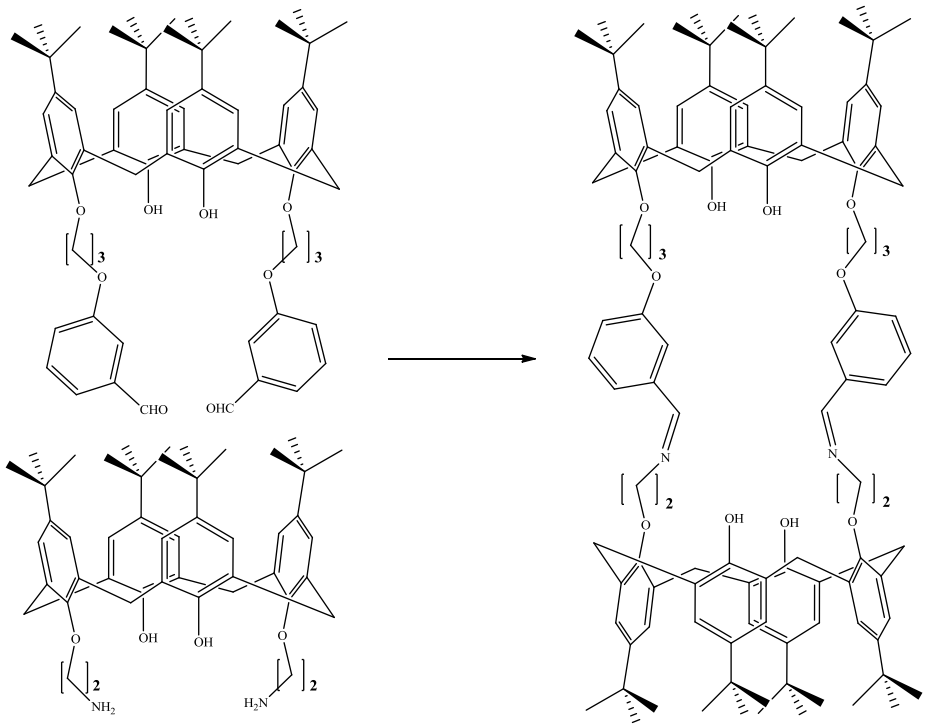

Figure 1.9: Synthesis of calix[4]tube.[46]

1.2.5 Schiff base metal complexation

Schiff bases are often exploited to create metal ion binding ligands, and as such are regarded as good ligands. The lone pair on the nitrogen atom is orientated in such a manner as to allow it to donate into the metal ion. In conjunction with the adjacent oxygen atom in salicylaldehyde Schiff base derivatives, this donation results in the ability to coordinate a broad range of transition metals. As a direct result of the excellent metal binding characteristics which these ligands exhibit, numerous examples of complexes have been prepared. A great number of these complexes have found use as transition metal catalysts, which is discussed in several reviews, Shibasaki and co-workers[33] and Gupta *et al*. being notable examples.[47] The *meta*-benzaldehyde and *para*-benzaldehyde Schiff base derivatives in comparison have not been subjected to exhaustive study, but there are some examples in the literature. A *meta*-derivative has been used by Herbert *et al.* to form binuclear palladium complexes,[48,49] while Pal and co-workers have used *para*-analogues in combination with cobalt(II) chloride to enhance the enantioselectivity of lipase-mediated alkylation of racemic secondary alcohols.[49]

1.3 Triazole Chemistry

1.3.1 Overview

Ever since the seminal paper by Finn, Klob and Sharpless on click chemistry in 2001,[50] triazoles formed by Copper(I)-catalysed Azide-Alkyne Cycloaddition (CuAAC) type chemistry have been studied with increased interest. The usefulness of this type of reaction is dictated by two characteristics shared by both azides and alkynes. These functional groups can equally be introduced into an organic molecule with relative ease and, just as importantly, they are quite stable under a variety of conditions.

Because of this diversity, triazole containing compounds have been used in a variety of roles ranging from fluorescent metal ion sensors[51] to biological enzyme inhibitors.[52] Due to the lone pair of electrons on the nitrogen atoms on the triazole ring and their heterocyclic π-conjugated nature, these compounds have been widely used for coordination to metal centres.[53]

1.3.2 CuAAC Triazole Synthesis

The Huisgen 1,3-dipolar cycloaddition of alkynes and azides to yield 1,2,3-triazoles is the premier example of the click reactions which Sharpless described. The subsequent discovery of the dramatic effect which copper(I) catalysis had on the rate of reaction (an increase of a factor of 10^7) thrust this reaction into the limelight.[54] A recent review by Fokin highlights the broad scope of this reaction.[55] The synthesis of triazoles *via* the CuAAC pathway can be carried out in a variety of solvents, both protic and aprotic. Importantly, it is also unaffected by most inorganic and organic functional groups, which negates the use of protecting groups.

With the notable exception of ruthenium (which is exploited in the preparation of 1,3 disubstituted triazoles), copper is the only metal to stand out as a reliable and regioselective catalyst for the azide-alkyne cycloaddition. This unique catalytic function which Cu(I) exhibits may be explained by a combination of factors. Cu(I) is able to react with terminal alkynes through both σ and π interactions and, particularly in aqueous conditions, rapid exchange of the alkyne and other ligands in the coordination sphere of Cu(I) is possible.

The reaction can proceed with the use of almost any solvated source of Cu(I).[56] A review of this reaction by Meldal *et al*. provides a comprehensive list of all sources used at that point.[57] This group proposes that one of the key factors which has an

influence on this pathway is the ability to keep the level of Cu(I) sufficiently high at all times throughout the reaction period. As a consequence of this, the *in situ* reduction of Cu(II) with a large excess of a reducing agent has become one of the preferred sources of Cu(I). A result of having the reducing agent in excess is that the reaction is less susceptible to oxygen, so these reactions can be carried out in open air conditions which further improve the versatility of the reaction. CuI, CuBr, and Cu^0 are among the most commonly utilized sources of copper, but the most widely used is $CuSO_4$ in the presence of a reducing agent. Sodium ascorbate acts as the reducing agent in a large proportion of the literature,[58] and it is this partnership which is used in this thesis.

A stepwise mechanism for this reaction has been proposed by Himo *et al.*[59] (Mechanism 1.2a). This stepwise mechanism is proposed on the basis of DFT calculations, which indicate that the concerted mechanism that occurs for the thermal dipolar cycloaddition of azides and alkynes is strongly disfavoured.

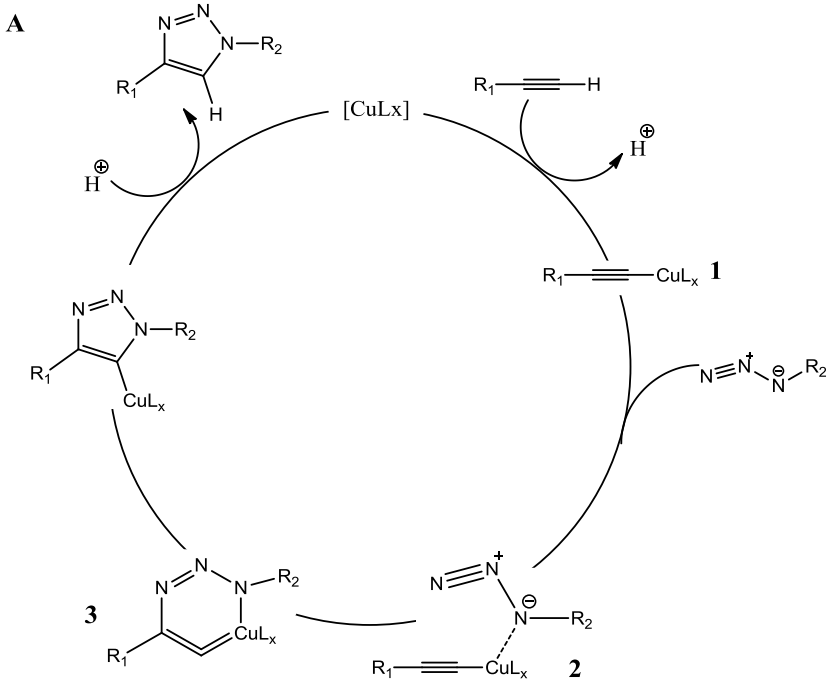

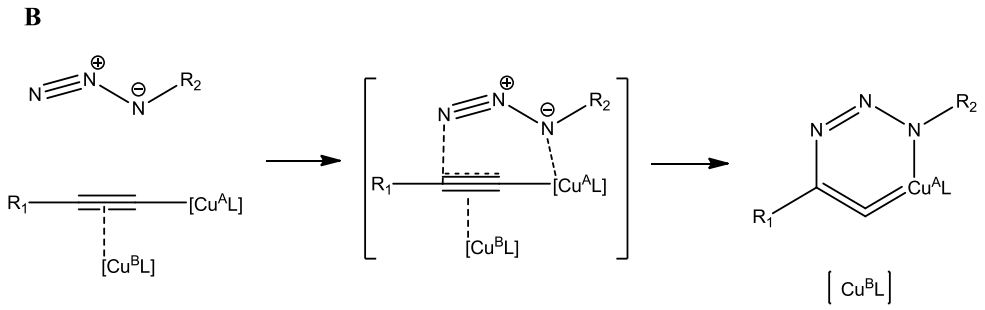

Mechanism 1.2: (A) Proposed catalytic cycle for the CuAAC reaction based on DFT calculations. **(B)** Introduction of second copper results in a lower energy barrier.[55]

The mechanism is comprehensively reviewed by van Maarseveen *et al.*[56] It has been proposed that this stepwise catalytic cycle begins with the formation of a Cu(I) acetylide via a π complex **1**. Although experimental evidence suggests that the copper acetylide complexes determine the rate and success of the catalysis, remarkably little is known about their exact nature.[56] It was found through kinetic studies that the rate of the catalytic process is second order in copper, however when the concentration of copper increases, this results in the formation of less reactive metal aggregates.[60] The azide is then activated by coordination to copper to form complex **2**. The possible role of a second copper atom can be seen in **(B)** and the introduction of this second copper favourably influences the energetic profile of the reaction through a reduction in the activation barrier by approximately 3-6 kcal mol^{-1}.[55,61] A strained copper metallacycle **3** is formed by through the first C-N bond formation event.

1.3.3 Triazole Derivatives

The literature has countless examples of disubstituted triazoles formed by "Click Chemisty". It is clear that there are two major derivatives which are repeatedly mentioned, the 1,4-disubstituted and 1,5-disubstituted-1*H*-1,2,3-triazoles. The 1,4-disubstitured variant is commonly prepared by CuAAC,[62] whilst the 1,5-disubstituted

derivative is more often prepared using a ruthenium catalyst (RuAAC),[63] (Scheme 1.2).

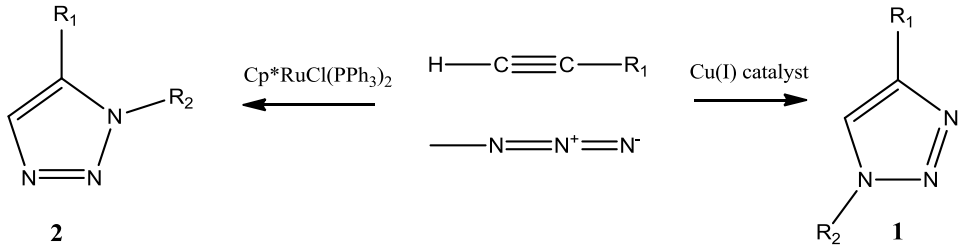

Scheme 1.2: Catalyst for 1,4-disubstituted triazole (**1**) and 1,5-disubstituted triazole (**2**).

After extensive investigation undertaken by Fokin *et al*, [Cp*RuCl] compounds have been found to be the most efficient and regioselective catalysts. This group found through computational studies that the regioselectivity is determined by the oxidative step. This is an irreversible oxidative coupling of azide and alkyne which gives a ruthenacycle, this is followed by the rate-determining reductive elimination.[64]

Creary and co-workers of the University of Notre Dame reported on a simple method of distinguishing between these two triazole derivatives using ^{13}C NMR spectroscopy.[65] Using a 'low tech' gated decoupling sequence, this group determined that the C_5 signal of a 1,4-disubstituted triazole will resonate at ≈120 ppm, the C_4 of the 1,5-disubstituted triazole will resonate at ≈133 ppm.

1.3.4 Calix[4]arene Triazoles

In recent years there has been an explosion in studies which functionalise calix[4]arenes with triazole units, and this brief introduction will provide a taste of the scope of these reactions. Modification of both the upper[66] and lower rims can be found in the literature, and the vast majority of these reactions utilize Copper(I)-catalysed Azide-Alkyne Cycloaddition (CuAAC). The triazole is generally formed through a reaction between a calix[4]arene alkyne and an azide.

In 2008 Kim and co-workers developed a pyrenyl appended triazole linked calix[4]arene, which was used as a fluorescent sensor for Cd^{2+} and Zn^{2+} (Figure 1.10).[67] This macrocycle was synthesised through the application of CuAAC chemistry between a 1,3-distal dipropargyl calix[4]arene and an azide pyrene derivative. Fluorescent spectroscopic studies reveal that this sensor binds selectively for Cd^{2+} and Zn^{2+} ions. It was found that upon complexation of these metal ions that the monomer emission increases while the excimer emission decreases. ^{1}H NMR studies which were conducted upon Cd^{2+} or Zn^{2+} complexes of the sensor indicate that binding occurs between the top of the triazole and the phenolic oxygens of the calixarene.

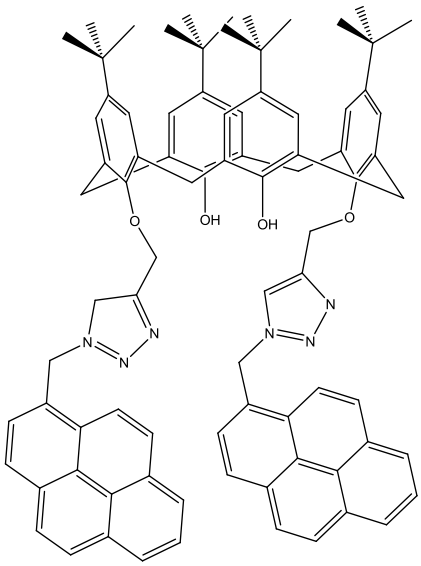

Figure 1.10: Calix[4]arene based fluorescent sensor developed by Kim *et al*.[67]

Chung *et al*. prepared a proximal derivative of this pyrenyl appended calix[4]arene (Figure 1.11).[68] This sensor with a proximal substitution pattern had an emission spectrum which was less intense than the 1,3-distal variant. Chung and co-workers discovered that each of these sensors displayed very different responses to the addition of Ag^{+}. While for the 1,3-distal sensor heightened fluorescence was observed in both the monomer and excimer, the proximal sensor displayed a quenching of the excimer and concurrent enhancement of monomer emission. Metal titration ^{1}H NMR

spectroscopic studies led to a proposed mode of binding between Ag^{+} and the macrocycle, which is similar to that seen between Cu^{2+} and the sensor developed by Park.[67] The 1,3-distal variant doesn't bind in this fashion which gives rise to the contrasting effects upon complexation.

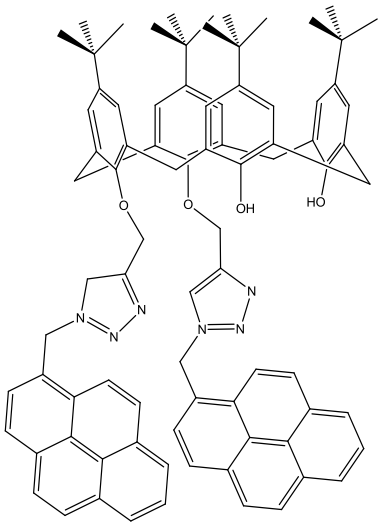

Figure 1.11: Proximal sensor prepared by Chung and co-workers.[68]

Triazoles have also been exploited to link several calixarenes into multivalent structures. A recent review by Sameni *et al.*[69] outlines the synthesis of two tris-calix[4]arenes which were prepared by Santoyo-Gonzales *et al.*[70,71] (Figure 1.12). These compounds were produced in 57% yields; however, no metal extraction studies were carried out on these compounds.

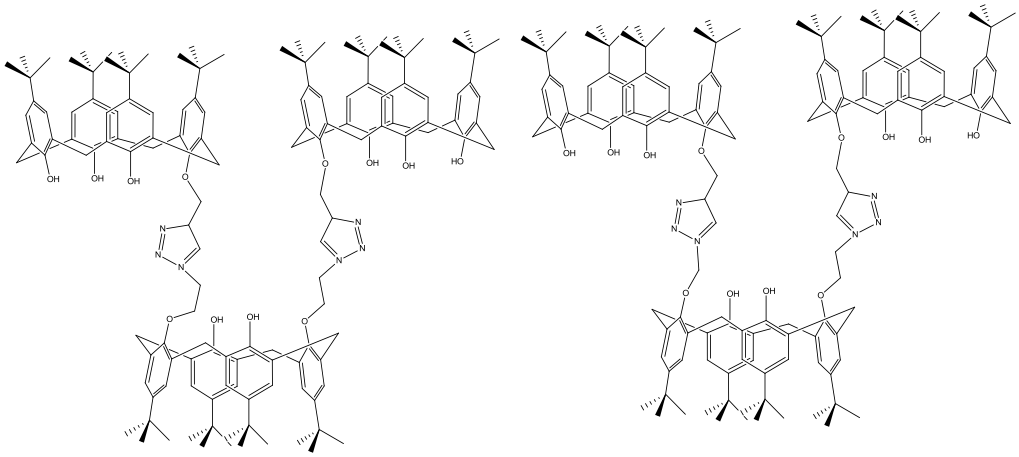

Figure 1.12: Tris-calix[4]arenes prepared by Santoyo-Gonzales and co-workers.[69]

1.4 Isoxazole Chemistry

1.4.1 Overview

While much of 'click chemistry' found in the literature is concerned with triazole formation *via* CuAAC, the interest in the formation of isoxazoles through 'click chemistry' has experienced exponential growth in the past decade. Isoxazoles are a class of heterocycles which bear both oxygen and nitrogen atoms.[72] These heterocycles have been used in a variety of roles ranging from scaffolds for achiral ligands[73] to ionophores in chemosensors for both cations and anions.[74] As is the case for triazole rings, due to the lone pairs of electrons on both the oxygen and nitrogen atoms and the conjugated π-bond nature of the heterocycle, isoxazoles have been widely utilized in metal coordination complexes.[75] In keeping with what was observed for triazoles, metal catalysed cycloaddition reactions allow for control of the regiochemisty of the desired isoxazole. Use of a Cu(I) catalyst yields a 3,5-disubstituted isoxazole and utilizing a Ru(II) catalyst results in a 3,4-disubstituted isoxazole. Once again this is very similar to what was seen for the formation of the 1,2,3-triazoles.[76] Interestingly however, isoxazoles can be synthesised in the absence of a metal catalyst through nitrile oxide-alkyne 1,3-dipolar cycloaddition (NOAC).[77] The material covered in this thesis will concentrate only on this method of isoxazole formation.

1.4.2 NOAC Isoxazole Synthesis

A recent review by Heaney from NUI Maynooth illustrates the broad scope of applications for this type of chemical reaction.[76] There are many reasons why NOAC is utilized in the preparation of isoxazoles. The formation of a dipole from oxime substrates are easily prepared from a broad range of procedures, either by direct or indirect oxidative methods. This dipole can also be formed from nitro precursors in the

presence of aryl isocyanates.[78] The NOAC reaction has been observed experimentally to be kinetically favoured when compared to similar azide cycloadditions.[79] Importantly, these reactions are regioselective, reactions between monosubstituted alkynes and nitrile oxides results in the formation of 3,5-disubstituted isoxazoles.[80]

The major obstacle of dipole instability, which can result in nitrile oxide dimerization[81] or nucleophile trapping,[82] can be circumvented by the *in situ* generation of the dipole. Chloramine-T has been widely used in the generation of nitrile oxides from aldoxime precursors; it has also been utilized in the transformation of hydrazones to nitrile imines.[83] A key advantage which results from using chloramine-T is its ability to be used with both acid and base-sensitive substrates. Padmavathi and co-workers proposed a mechanism for the transformation of aldoxime to the nitrile oxide in 2003 (Mechanism 1.3).[83] Although this is a reasonable mechanism for dipole formation, there are a number of factors which should be considered. Padmavathi observed that the nitrile oxide which is initially generated can undergo side reactions in the presence of excess chloramine-T, thus providing undesired side products.[83] Rai *et al*. observed that some compounds, such as vinyl sulfones, are not inert to the oxidising power of chloramine-T, however, a solution has been proposed to combat this problem. This requires the oxime to be exposed to the chloroamine-T prior to the addition of the dipolarophile.[84]

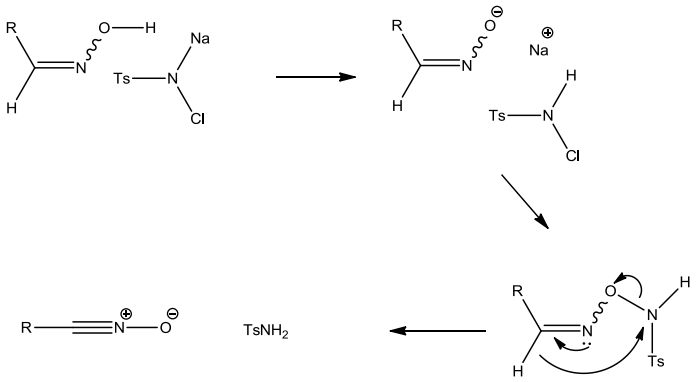

Mechanism 1.3: Mechanism of nitrile oxide formation from oxime by chloramine-T.[83]

This nitrile oxide dipole then reacts with a dipolarophile, propargyl modified substrates are commonly employed in this role. The use of terminal alkynes allows for selective formation of 3,5-disubstituted isoxazoles, which can be distinguished from the 3,4 variant by their ^{1}H NMR spectra.[85] The reaction mechanism follows a typical 1,3-dipolar cycloaddition (Mechanism 1.4), to yield the desired isoxazole. These reactions typically are performed as a one pot synthesis.

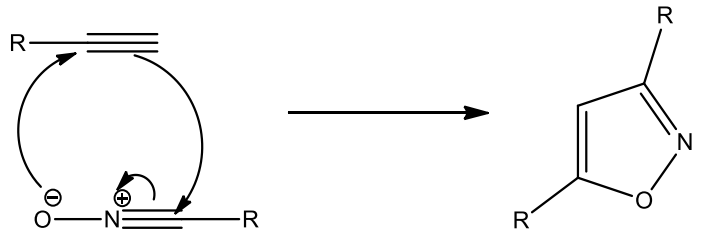

Mechanism 1.4: General mechanism for 1,3-dipolar cycloaddition.

1.4.3 Isoxazole Derivatives

As is the case with triazoles, isoxazoles are generally prepared as one of two major regioisomers, the 3,5-disubstituted and 3,4-disubstituted isoxazoles (Figure 1.13). Both the 3,5-disubstituted[77] and 3,4-disubstituted[86] variants have been prepared selectively.

(a) (b)

Figure 1.13: 3,5-disubstituted **(a)** and 3,4 disubstituted isoxazoles **(b)**.

Furthermore, Kaiser and co-workers reported that the selectivity for the two variants is highly temperature dependent. When they performed the reaction at room temperature they yielded the 3,4-disubstituted isomer in a 47 % yield. Elevation of the reaction

temperature to 60 °C yields the 3,5-disubstituted product in a 45 % yield and 20 % of the previously product isomer. This group also discovered that they could convert the 3,4 isomer to the 3,5 product by heating it to 80 °C for 92 h.[86]

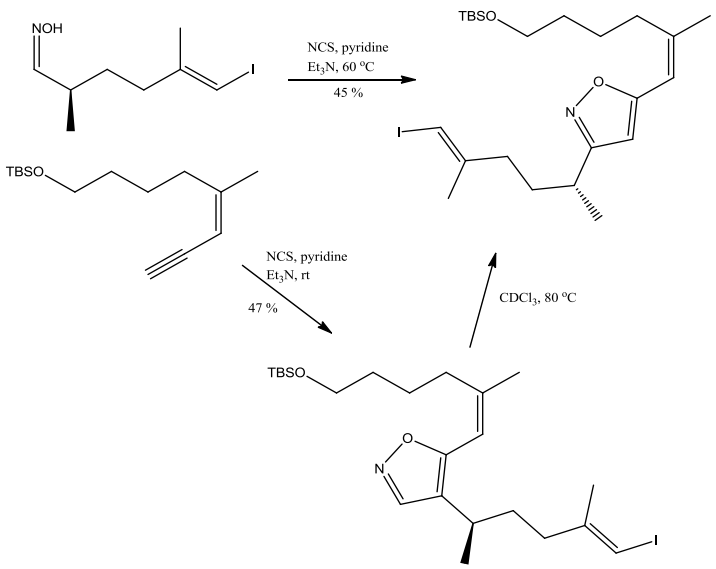

Scheme 1.3: Kinetic and thermodynamic products reported by Kaiser.[86]

1.4.4 Calix[4]arene Isoxazoles

While triazoles have been widely exploited in calixarene chemistry, the application of isoxazoles has been comparatively limited. The isoxazole moiety can act as an efficient metal ion binding site, and as a result of this efforts have been made to prepare fluorescent chemosensors which contain isoxazoles. Isoxazole modification of calixarenes has been achieved at both the upper[87] and lower rims.

Senthilvelan and co-workers reported the synthesis of a naphthalene isoxazole modified calix[4]arene in 2009 (Figure 1.14a),[88] with conjugation between the isoxazole and the naphthalene moieties. This group reports that the macrocyclic molecule displayed a weak monomer and strong excimer emission when examined by fluorescent emission spectroscopy. Ten metal perchlorate salts were added to an acetonitrile solution of the molecule. However, only Cu^{2+} caused any dramatic

quenching of the excimer emission. Following analysis of these fluorescence experiments, the binding was determined to be a 1:1 complex with a K_a of 2080 M^{-1}. Further work by this group modified this ligand to include a β-amino-α,β-unsaturated ketone instead of an isoxazole (Figure 1.14b). In contrast to the isoxazole modified derivative, complexation of Cu^{2+} leads to an enhancement of the fluorescent emission profile.

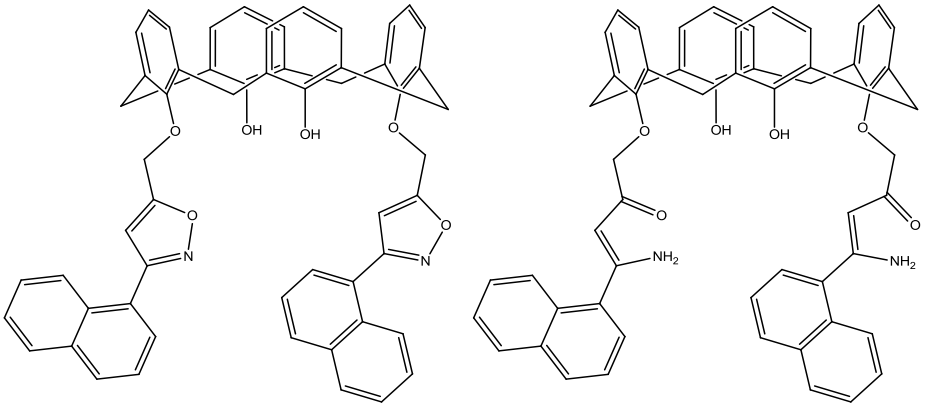

(a) (b)

Figure 1.14: Fluorescent sensors based on calix[4]arene prepared by Senthilvelan *et al*.[88]

Isoxazole chemistry has also been utilised by Tsai *et al*. to prepare an isoxazolylanthryl linked dicalixarene (Figure 1.15a).[89] Tsai prepared this compound *via* two synthetic routes. In principle, the product could be prepared by a quadruple cycloaddition reaction between a *bis*-propargyl calix[4]arene and the anthracene *bis*-carbonitrile oxide. However, purification of this reaction proved to be difficult even by column chromatography. Thus Tsai and co-workers devised a two-step reaction which initially prepares a *mono* bridged precursor followed by a second cycloaddition reaction to prepare the desired *bis*-bridged product.

Due to the presence of the anthracene fluorophore in the structure this molecule was screened for fluorescent emission. A range of aromatic and alkyl diamine guests were introduced to the host macrocycle all of which resulted in little to no change in the

emission profile. Dramatic quenching was observed upon titration of methyl viologen (Figure 1.15b). More recently, this group has explored the ability of these dicalixarenes to undergo self-assembly into supramolecular organogels.[90]

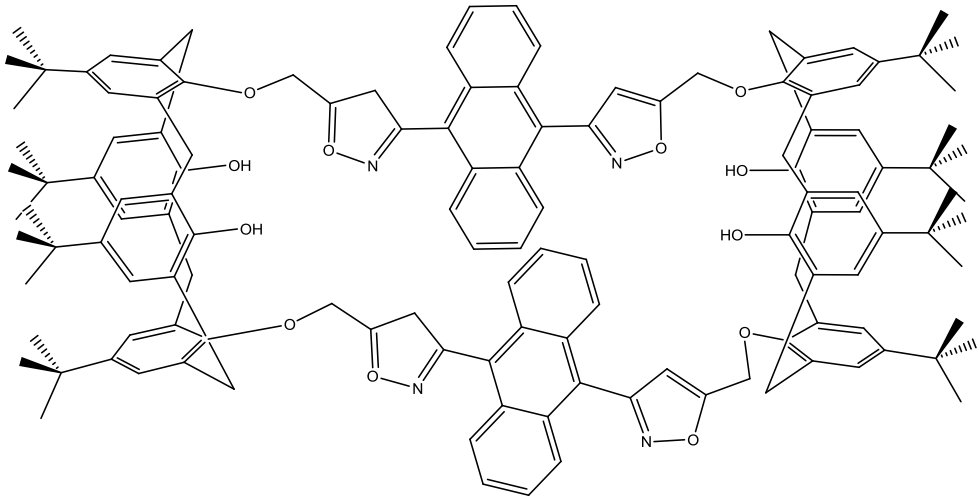

Figure 1.15a: Dicalixarene prepared by Tsai and co-workers.[89]

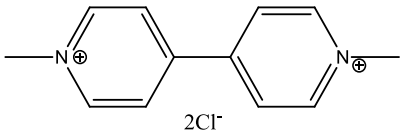

Figure 1.15b: Methyl viologen.

1.5 Fluorescence

1.5.1 Overview

As this thesis deals with the preparation of fluorescent metal ion sensors which contain either pyrene or anthracene fluorescent reporter units, the materials covered in this introduction will deal primarily with the fluorescence properties of pyrene and anthracene containing molecules. Fluorescence spectroscopy is an area of chemistry which encompasses a broad spectrum of concepts, and as such this thesis will focus on methods which have been applied in this project.

Stokes observed that when a fluorescent molecule absorbs UV light, the light emitted is of lower energy (wavelength). This difference in energy is known as the Stokes shift. As a result, fluorescence, which is a natural phenomenon, can be defined as the emission of a photon from an electronic excited state of a molecule with a lower energy than the wavelength at which the photon was absorbed.[91] The Stokes shift can be explained by the Franck-Condon principle. This states that 'an electronic transition is most likely to occur without changes in the positions of the nuclei in the molecular entity and its environment'.[92] The resultant state is known as the *Franck-Condon* state, and the transition is known as a *vertical transiton*. A direct result of the higher energy potential of the excited state is that the vertical transition for the lowest vibrational energy level of ground state ν''_0, intersects the excited state at the ν'_n energy level (Figure 1.16). Through non-radiative decay to the lowest vibrational energy level of the excited state ν'_0, the excited electron loses energy. The transition of the electron from ν'_0 to ν''_n, a point where its vertical transition intersects the ground state potential energy curve, results in emission of the photon. Non-radiative decay returns the electron to the lowest vibronic energy level ν''_0 (Figure 1.16). The energy difference

between the absorption (ν''_0 to ν'_n) and the emission (ν'_0 to ν''_n) is the reason why a Stokes shift occurs.

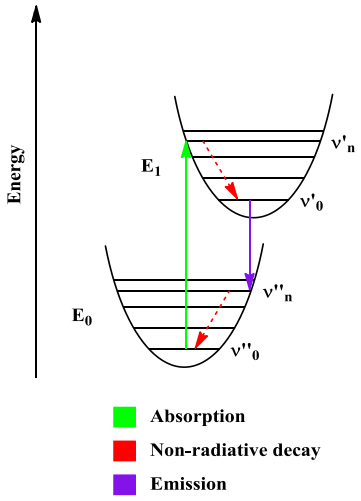

Figure 1.16: Vibrational level transitions of an electron for both absorption and emission processes.

Fluorescence typically has very short lifetimes in the order of less than 10 nanoseconds. This is the time between excitation of the electron by absorption and emission on its return to the ground state. The short lifetime is a major difference which distinguishes fluorescence from the other luminescent phenomenon, phosphorescence. Phosphorescence has a much longer lifetime in comparison to fluorescence and can have extended lifetimes which can be in excess of one millisecond.[92]

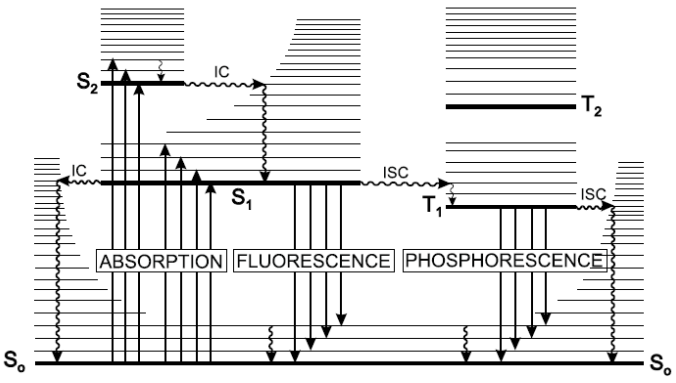

Figure 1.17: Jablonski diagram which shows all the possible transitions between electronic states. S = singlet state, T = triplet state, IC-internal conversion and ISC-intersystem crossing.[92]

For the process of fluorescence a molecule absorbs a photon. This is required as thermal factors cannot provide enough energy to effect an electronic transition. The energy from this photon is absorbed by a single electron, this electron undergoes an electronic transition from the S_0 singlet ground state to the S_1 singlet excited state. This excited electron *a*, with a spin of +1/2 (S*a* = +1/2), is spin paired with a corresponding electron in the ground state orbital *a** (S*a** = -1/2). This is a singlet-singlet transition and is spin allowed following the M = 2S + 1 formula, ($\Delta S = 0$). To return to this more stable ground state, the electron must lose energy, and it can do this by a number of processes, such as luminescence (emission of light) or through non-radiative transitions (transference of energy to the surrounding solvent, vibrations, rotations). If the electron loses the excess energy through the emission of a photon, fluorescence occurs.[93]

Phosphorescence, contrastingly, involves a spin forbidden triplet transition ($\Delta S \neq 0$). As with the previously discussed fluorescence process, absorption occurs in the same fashion. In this process, the electron undergoes a change of spin (S*a* = +1/2 to -1/2) to the triplet excited state T_1, which is slightly lower in energy than the singlet excited state S_1. The lower energy of this excited state is a result of Hund's rule. Conversion from the S_1 to the T_1 state through intersystem crossing becomes possible due to spin orbit coupling. A consequence of this is that the wavefunction of the singlet state always contains a small but not insignificant fraction of a triplet wavefunction.

1.5.2 Monomer & Excimer Emission

All fluorescent compounds have a monomer emission, but aromatic fluorophores can also exhibit an excimer emission profile. Excimers are dimers which are in an excited state, the name is a contraction of *exc*ited and d*imer*. An excimer is formed by the

collision between identical excited and unexcited molecules. The excitation energy is delocalised over the two moieties, which is denoted by the $(MM)^*$ in the equation below. The formation of these excimers is a diffusion controlled process, and thusly the photophysical effects are detected at relatively high concentration of the species.[92]

$$^1M^* + {}^1M \leftrightharpoons {}^1(MM)^*$$

Many aromatic hydrocarbons such as pyrene, naphthalene or anthracene are known to form excimers. The peak emission wavelength λ_f^{em} for the excimer is at a higher wavelength than that of the monomer, this can be seen clearly from the graphical representation of generic emission bands (Figure 1.18a), and also from the experimental recorded spectrum of pyrene (Figure 1.18b).

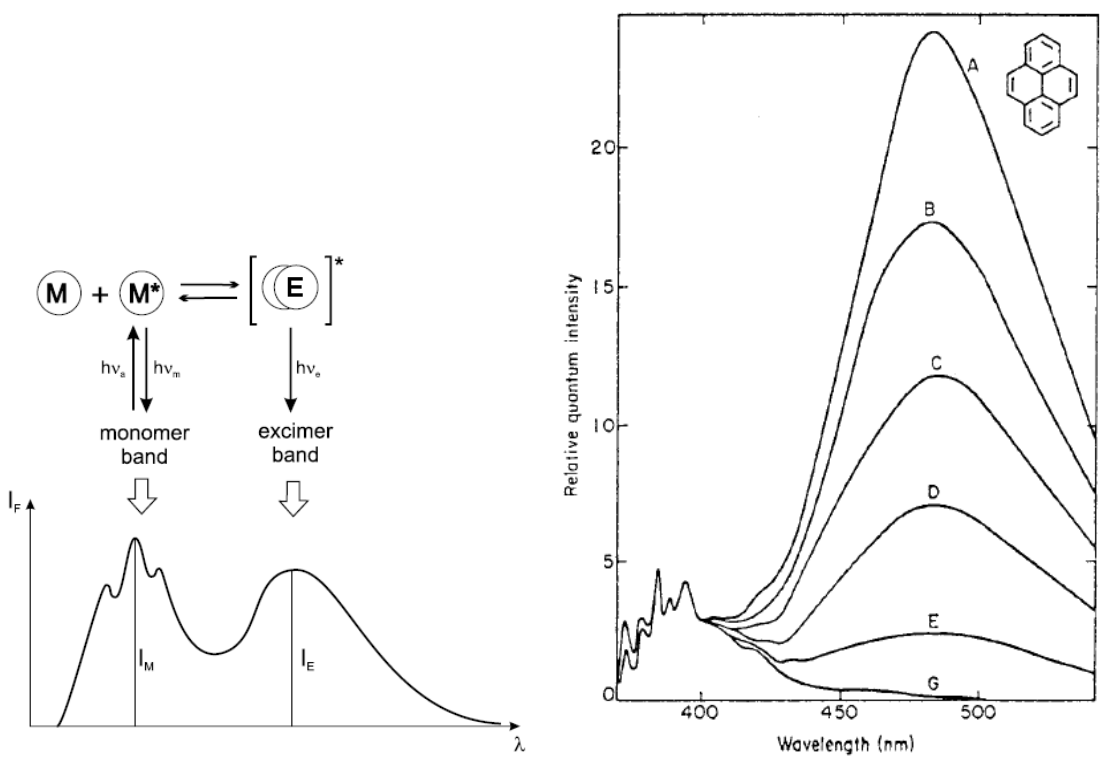

(a) (b)

Figure 1.18: (a) Generic monomer and excimer emission bands **(b)** Fluorescence Emission spectrum of pyrene recorded by Birks and Christophorou in cyclohexane.[92]

In 1963, Birks and Christophorou reported on the effect that concentration has on the monomer and excimer excitations. They found that the relative fluorescent intensity of the monomer stays constant, however, the intensity of the excimer band increases with increasing concentration (Figure 1.18b).[94]

These features of the excimer can be explained through the use of energy surfaces (Figure 1.19), the lower smooth curve represents the repulsive energy between two ground state molecules. The upper curve is representative of two molecules, one of which is in the excited state. A minimum which corresponds to formation of excimer emission is observed when two aromatic rings are facing each other at a distance of ≈3-4 Å. For pyrene this distance has been found to be 3.37 Å, and the stabilisation energy of ΔH for the excimer has been determined experimentally to be 170 kJ mol^{-1}.

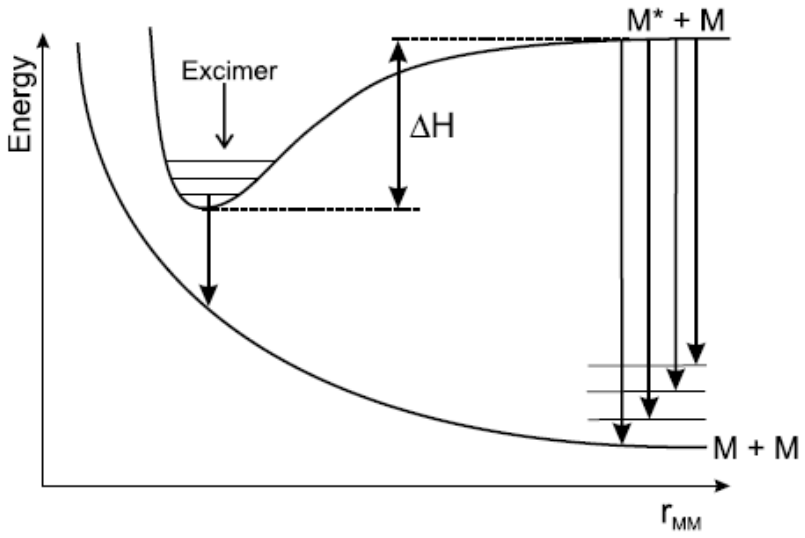

Figure 1.19: Energy surface diagram for formation of the excimer.[92]

Excimer formation is seen for most calixarene based fluorescent compounds, this is due to the vast majority of these being based on 1,3 distal disubstituted calixarenes. A review of calixarene-derived fluorescent probes by Kim and Quang describes the synthesis and fluorescent properties of a broad range of these modified calixarenes.[95]

Jin *et al*. developed one of the first calix[4]arene derivatives to show excimer formation (Figure 1.20b). They found that this sensor showed good selectivity for the Na^+ ion in MeOH/THF (Figure 1.20a).[96] The fluorescent spectrum of this derivative shows a dual emission with the excimer and monomer bands at 480 nm and 390 nm respectively. Upon addition of increasing amounts of Na^+ this group observed that as the excimer emission band was quenched the monomer band was enhanced.

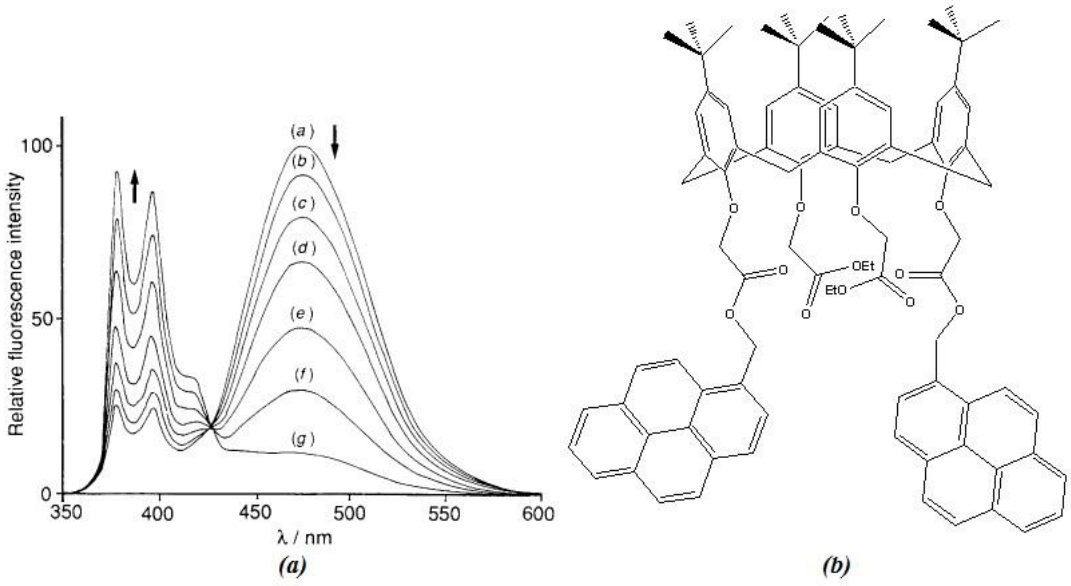

Figure 1.20: (a) Fluorescent emission spectrum of the Calix[4]arene developed by Jin and co-workers in the presence of increasing concentrations of Na^+, **(b)** Structure of the calixarene derivative.[96]

1.5.3 Quenching and Stern-Volmer relationship

Quenching is simply any process which decreases the fluorescence intensity, and so can result from a variety of processes. The majority of these processes, such as concentration changes, light scattering or photobleaching, are not of interest experimentally. The quenching processes which are experimentally interesting are *dynamic quenching*, *static quenching* and *resonance energy transfer*. The materials covered in this thesis will primarily deal with *dynamic* and *static* quenching.

Dynamic Quenching requires contact between the quencher (Q) and the fluorophore, which arises from random collisional events (Figure 1.21). The *dynamic quenching* agent (quencher) provides a non-radiative route for loss of the excited state energy.

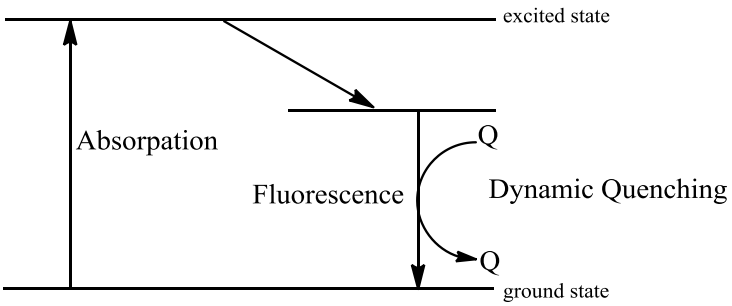

Figure 1.21: Mechanism of dynamic quenching, Q denotes quencher (usually metal ion).

This mode of quenching exhibits a concentration dependence which is described by the Stern Volmer equation.

$$\frac{\phi_o}{\phi} = \frac{I_o}{I} = 1 + k_q \tau_o [Q] = 1 + K_D [Q]$$

Where I_o and I are the intensity of the unquenched and quenched fluorescent emission spectra respectively, and τ_o is the life time of the fluorescent state in the absence of a quencher, when τ_o is known the value for k_p can be calculated.[92]

Static quenching can occur through two processes, (a) sphere of effective quenching or through the (b) formation of a non-fluorescent complex (Figure 1.22).

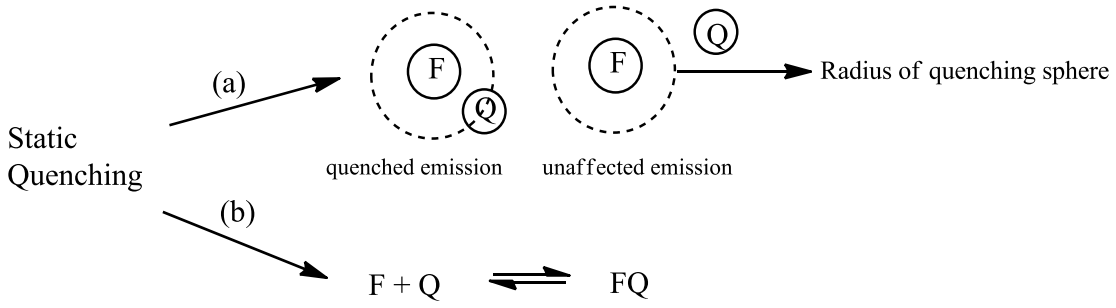

Figure 1.22: Forms of static quenching **(a)** Sphere of effective quenching and **(b)** ground state non-fluorescent complex formation.

Perrin proposed a model of quenching where neither the fluorophore (F) or the quencher (Q) can change positions relative to each other in the excited state of F^*. If Q is located with the effective quenching sphere that surrounds the fluorophore which is of volume V_q the quenching is assumed to be complete (Figure 1.22).[92] If it lies outside this sphere it will have no effect on the emission profile. It can be explained by the following equation, where V_q is the volume of the quenching sphere, N_a is Avogadro's number and [Q] is quencher concentration.

$$\frac{I_O}{I} = \exp(V_q N_a [Q])$$

This mode of quenching applies to rigid matrices or viscous media. This type of *static quenching* is unlikely to be applicable, because all fluorescent experiments in this project were performed in the liquid phase.

The formation of a ground state 1:1 non-fluorescent complex can be expressed by the equilibrium seen in Figure 1.22. In contrast to *dynamic quenching*, the excited state lifetime of the uncomplexed fluorophore F is unaffected. The fluorescence intensity is found to decrease upon addition of Q. The stability of this complex is given by the following equation.

$$K_S = \frac{[FQ]}{[F][Q]}$$

The total concentration of F is given by $[F]_o = [F] + [FQ]$. From this the fraction of uncomplexed fluorophores can be determined.

$$\frac{[M]}{[M]_o} = \frac{1}{1 + K_S[Q]}$$

Due to fluorescence intensities being inversely proportional to concentration this is rewritten as

$$\frac{I_o}{I} = 1 + K_S[Q]$$

A plot of I_o/I for this type of quenching will follow a linear Stern-Volmer like line. If the type of quenching is unknown the equation is rewritten as

$$\frac{I_o}{I} = 1 + K_{SV}[Q]$$

Where K_{SV} is the Stern Volmer constant which is equal to the slope of the line, this leads to a simple determination of the association constant (K_a=K_{SV}). However, it is not so simple when more than one quenching process occurs concurrently.

Combined *static* and *dynamic quenching* occurs in many instances with quenching occurring through both random collisions and through complex formation. This results in a deviation from linearity to an upward concave curve (Figure 1.23). For this plot, the fraction of fluorescence which remains (I/I_o) is found from the portion not complexed (f) and the fraction which is unquenched by collision encounters.[93]

$$\frac{I}{I_o} = f\frac{\gamma}{\gamma + k_q[Q]}$$

f^{-1} is equal to $1 + K_S[Q]$ so inversion of this equation gives an equation which is second order with respect to $[Q]$, this explains the upward curve of this plot.

$$\frac{I_O}{I} = (1 + K_{SV}[Q])(1 + K_S[Q])$$

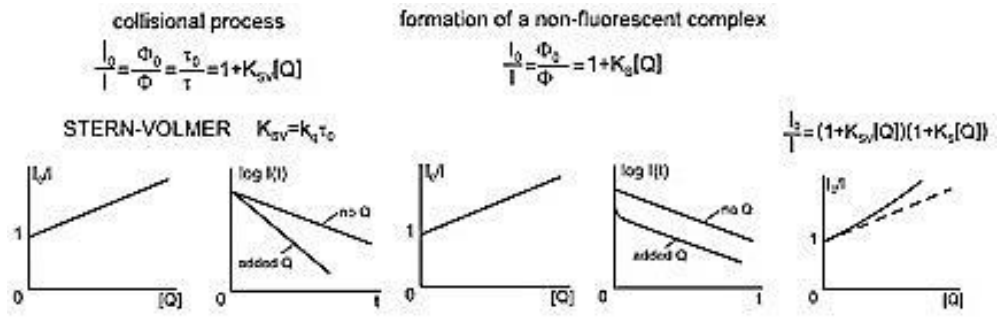

(a) **(b)** **(c)**

Figure 1.23: Summary of quenching process and their 'Stern-Volmer' plots **(a)** Dynamic quenching **(b)** Static quenching complex formation **(c)** combined quenching.[92]

1.5.4 Binding constant determination

If the 'Stern-Volmer' type plot is linear, K_{SV}, which is the slope of the line, is the binding constant for the system. This is an efficient and simple method of determining this value from the fluorescence spectral data obtained, and it has been exploited by numerous groups.[97-99] However, this method is not useful if more than one type of quenching occurs.

In 1988, Valeur *et al.* developed three methods for the determination of the stability constant K_s which is equal to K_a from fluorescent spectral data.[100] These methods enable the determination of the binding constant K_a when the Stern-Volmer plot deviates from linearity, and have been employed by a number of groups.[101, 102]

$I_F{}^o$ is the peak fluorescence for the free ligand spectrum and $I_F{}^{max}$ is the maximum fluorescent emission observed in the presence of the quencher. The concentration of the metal and ligand are given by [M] and [L].

Method One:

$$\frac{I_F - I_F{}^o}{I_F{}^{max} - I_F} = K_S[M]$$

In this method the ratio of $(I_F–I_F^o)$ / $(I_F^{max}–I_F)$ is plotted against the metal concentration [M], and the stability constant K_s is obtained from the slope of the line. A major drawback of this method is the requirement to determine I_F^{max}. This is difficult to determine with a high degree of accuracy at high concentrations of metal ions.

Method Two:

$$\frac{\left[1-\left(\frac{I_F{}^O}{I_F}\right)\right]}{[M]} = K_S\left(\frac{b}{a}\right)\left(\frac{I_F{}^O}{I_F}\right) - K_S$$

This method is used when the determination of I_F^{max} proves to be problematic.[103] K_s is determined from the intercept of a plot of $[1-(I_F^o/I_F)]$/[M] against I_F^o/I_F. Due to the emphasis that this method places on the error for the points close to I_F^o, it is unsuitable for weak variations in the fluorescence intensity.

Method Three:

$$\frac{I_F{}^O}{I_F - I_F{}^O} = \left[\frac{a}{b-a}\right]\left[\left(\frac{1}{K_S[M]}\right) + 1\right]$$

For this method, $I_F^O/(I_F\text{-}I_F^O)$ is plotted against 1/[M] and the stability constant K_s is determined from the ratio of intercept to slope. This third method was employed in the work of this project to determine the binding constants for the fluorescent sensors prepared.

1.5.5 Job's Method (Method of Continuous Variation)

The stoichiometry of a complex can be determined by using Job's method of continuous variation. For a complex H*h*G*g* which is formed according to the following equilibrium:

$$hH + gG \leftrightharpoons HhGg$$

The principle behind this method is that the fluorescence intensity is measured for a series of solutions which contains the host and guest, within which the total concentrations of host and guest is kept constant. The mole fraction [X] of the host is given by the following equation.

$$[H] + [G] = [H + G] = Constant$$

where [H] = host concentration and [G] = guest concentration

$$[X] = [H]/([H + G])$$

The difference in the fluorescence intensity of the host F_o and the host in the presence of guest F is found for each solution and for curve fitting this ΔF is multiplied by the mole fraction *[X]*

$$\Delta F * [X] \quad \Delta F = F_0 - F$$

This *ΔF*[X]* is plotted versus *[X]* to give the Job plot. The stoichiometry of the complex can be determined by observing at what mole fraction the maximum change in fluorescence occurs.

1.5.6 Classes of Fluoroionophores

Three major classes of fluorescent molecular sensors have been identified. A schematic summary of these is shown in Figure 1.24.

Class 1: This class of fluorophore undergoes quenching after collision with an analyte such as O_2.

Class 2: A class of fluorophore which can reversibly bind an analyte, depending on the nature of the analyte these are classed as a fluorescent pH indicator or a fluorescent chelating agent, for a proton or an ion respectively.

Class 3: This class contains two moieties with different functions. The fluorophore which acts as the reported unit is linked to a receptor for the analyte, either *via* a spacer of directly. Supramolecular chemistry uses this class of sensors extensively. Sensors of this class are designed with selectivity and affinity in mind, which enables usage as selective ion sensors and as such are known as ionophores. When a fluorophore is incorporated into a system with an ionophore it is known as a fluoroionophore.

Class 2 and **class 3** sensors can function either by Chelation Enhancement of Fluorescence (**CEF**) or by Chelation Enhancement of Quenching (**CEQ**).[92] The sensors which are prepared in this thesis are **Class 3 CEQ** type sensors.

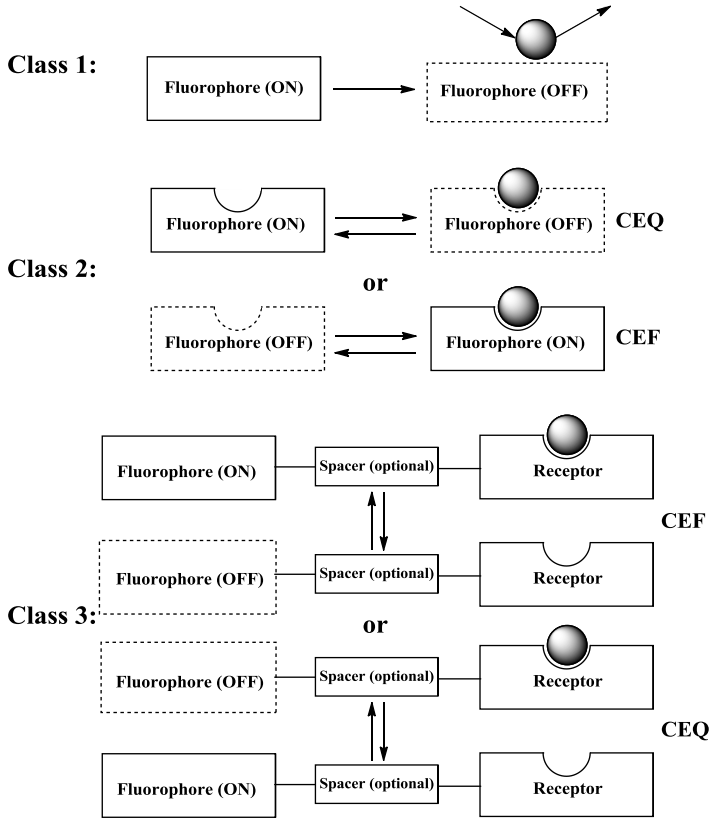

Figure 1.24: Schematic of three major classes of fluorescent sensors.[92]

1.5.7 Aims of thesis

The overarching goal of this project was the expansion of the coordination calix[4]arene ligands, with a view to potential roles as fluorescent chemosensors. This approach encapsulated three branches; Schiff-bases, triazoles and isoxazoles. The first part of this project explored the synthesis of six novel Schiff-base capped calixarenes through a compartmentalisation method, and the subsequent attempted metal complexation reactions. The binding characteristics of these ligands with cobalt(II), copper(II), mercury(II), nickel(II) and zinc(II) were compared to that of the model *Salen* type ligand metal complexes. These ligands were screened for examination of their fluorescent emission spectra.

Continuing on this theme, an investigation into the synthesis of a range of triazole linked aldehyde calix[4]arenes, and triazole linked Schiff bases capped calix[4]arenes were run in tandem. Once again the compartmentalisation method was employed. It was intended that this would introduce unusual or multiple metal binding sites into the structure. Preliminary fluorescent emission spectroscopic studies were performed on the ligands from this investigation to establish their suitability as fluorescent chemosensors.

The final approach in this project utilized isoxazole linked pyrene and anthracene calixarenes to prepare fluoroionophores. These ligands were screened for their fluorescent behaviour, and the affect, if any, a range of metal perchlorate salts, cadmium(II), cobalt(II), copper(II), iron(II), lead(II), nickel(II) and zinc(II) had on the emission spectrum. The stoichiometry and kinetics of the binding with copper(II) was scrutinised. Finally, a parallel ^{1}H NMR spectroscopic and computational investigation of the mode of binding was undertaken.

2. Experimental

2.1 Instrumentation

Reactants and reagents were supplied by Alfa Aesar, Apollo or Sigma Aldrich and were used as received without further purification. HPLC grade solvents were used and, where needed, dried according to standard procedures.

^{1}H and ^{13}C NMR spectra were recorded on a Bruker Avance 300MHz spectrometer at a probe temperature of 25°C using saturated $CDCl_3$ solutions with Me_4Si unless otherwise stated. ^{1}H NMR and ^{13}C NMR spectra were run at 300 MHz and 75 MHz, respectively.

For metal titration NMR analysis, ^{1}H NMR spectra were recorded on a Bruker Avance II 500MHz spectrometer with a 25°C probe temperature using a CD_3CN:$CDCl_3$ (3:1) mixture at Institute of Technology Tallaght Dublin.

Infrared spectra (cm^{-1}) were recorded as KBr discs or liquid films between NaCl plates using a Perkin Elmer system 2000 FT-IR spectrophotometer.

UV-vis spectra were recorded as solutions with HPLC grade solvents, using a Unicam UV-Visible 540 spectrometer in the stated regions. The results were analysed using Vision software V3.40.

Melting point analyses were carried out using a Stewart Scientific SMP 11 melting point apparatus and are uncorrected.

Mass spectrometry was carried out on a LC/TOF-MS model 6210 Time-Of-Flight LC/MS with an electrospray source positive and negative (ESI+/−), capillary 3500 V, nebuliser spray 30 psig, drying gas 5 L/min and source temperature 325 °C. The fragmentor was used at 175 V. The LC was run on a 1200 series model and injection volumes were typically 10 μL. The column used was an Agilent Eclipse XBD-C18. A

diameter of 5-micron was employed. The mobile phase constituted A (acetonitrile with 0.1 % formic acid) and B (0.1 % aqueous formic acid) with a gradient of 5 % A to 100 % at a flow rate of 0.5 mL/min over 15 minutes.

Microanalysis was carried out at the National University of Ireland Maynooth, using a Thermo Finnigan Elementary Analyzer Flash EA 1112. The results of which were analysed using the Eager 300 software.

Fluorescence studies were performed using a Jasco FP-6300 spectrofluorometer at NUI Maynooth, and the results were analysed using the Spectra Manager 1.0 software supplied. All fluorescence studies were carried out in emission mode, with an excitation bandwidth of 2.5 nm and emission bandwidth of 2.5 nm unless otherwise stated. All fluorescence experiments were carried out as acetonitrile solutions unless otherwise stated.

2.2 Synthesis of Calix[4]arene Schiff base derivatives and their metal complexes

2.2.1 5,11,17,23,29,35,41,47-octa-*tert*-butyl-49,50,51,52,53,54,55,56-octa-hydroxycalix[8]arene: (1)[104]

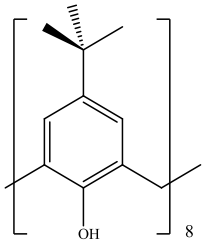

tert-Butylphenol (112 g, 720 mmol), paraformaldehyde (36 g, 1200 mmol) along with 10M KOH (1.8 mL) in xylene (600 mL) were placed in a 2 L round bottomed flask, fitted with a Dean-Stark apparatus. This mixture was refluxed for 4 h with efficient stirring. After cooling a precipitate formed which was collected by filtration, washed with toluene, diethyl ether, acetone and water (4 X 200 mL). The precipitate was then dried in an oven for seven days to give **1** as a white solid.

Yield: 69.7 g, 60 %. m.p.: > 300 °C (lit: 411-412 °C).[104] δ_H ($CDCl_3$): 1.28 (72H, s, *t*-Bu), 3.48 (8H, br d, Ar-C*H*$_2$-Ar, *J* = 13.0 Hz), 4.39 (8H, br d, Ar-C*H*$_2$-Ar, *J* = 13.0 Hz), 7.17 (16H, s, Ar*H*), 9.63 (8H, s, O*H*). δ_C ($CDCl_3$): 31.4, 32.3, 34.0, 125.5, 128.7, 144.7, 146.6. ν_{max} (KBr): 3409, 3235, 2956, 1487, 1451, 1393, 1362, 1291, 1249, 1204, 1117, 875, 816, 784, 728 cm^{-1}.

2.2.2 5,11,17,23-Tetra-*tert*-butyl-25,26,27,28-tetrahydroxy-calix[4]arene: (2)[104]

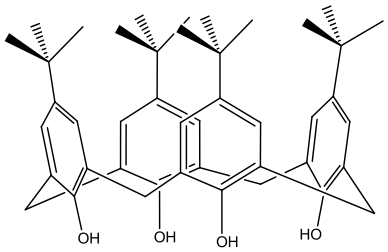

A slurry of **1** (32 g, 24.65 mmol) and 10M NaOH (1.0 mL) and diphenyl ether (400 mL) was placed in a 2 L round bottomed flask equipped with a Dean-Stark water trap. The mixture was heated to reflux for 1.5 h with mechanical stirring. After reflux a black liquid had formed. This liquid was left to cool to 80 °C – 100 °C at which point it was treated with ethyl acetate (400 mL). This gave a white solid; which was washed with consecutive portions of toluene, ether, acetone, and water (100 mL of each) and placed in the oven to dry for five days, to yield a white solid (**2**).

Yield 16.9 g, 40 %. m.p: > 300 °C (lit: 344-346 °C).[104] δ_H ($CDCl_3$): 1.21 (36H, s, *t*-Bu), 3.50 (4H, br d, Ar-C*H*$_2$-Ar, *J* = 12.4 Hz), 4.26 (4H, br d, Ar-C*H*$_2$-Ar, *J* = 12.4 Hz), 7.04 (8H, s, Ar*H*), 10.34 (8H, s, O*H*). δ_C ($CDCl_3$): 31.4, 32.6, 34.0, 125.9, 127.7, 144.4, 146.7. ν_{max} (KBr): 3167, 2960, 2905, 2868, 1482, 1392, 1362, 1201, 871, 818, 782, 710, 675, 592 cm^{-1}.

2.2.3 5,11,17,23-Tetra-*tert*-butyl-25,27–dihydroxy-26,28-bis(2-bromoethoxy)calix[4]arene: (3)[105]

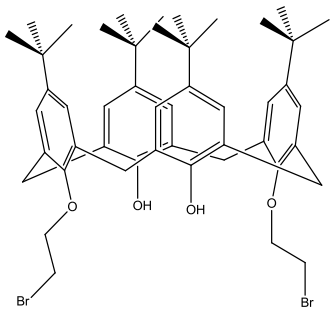

Compound **2** (2.5 g, 3.85 mmol) and potassium carbonate (1.06 g, 7.7 mmol) were dissolved in acetonitrile (200 mL) in a round bottomed flask. This mixture was stirred for 1 h, at which point 1,2-dibromoethane (14.47 g, 77 mmol) was added dropwise. The mixture was then heated to reflux for 48 hours with vigorous stirring. The reaction was then cooled to room temp and left to stir for 12 hours. The inorganic salts formed were filtered off and the filtrate was then concentrated under vacuum to yield a yellow

solid. This solid was dissolved in a $CHCl_3$/EtOH mix (1:1). A powdery white solid (**3**) was precipitated after a day.

Yield: 2.65 g, 80 %. m.p.: > 260 °C (Lit. 278-280 °C).[106] Anal. Calc. for $C_{48}H_{62}Br_2O_4$: C, 66.82; H, 7.24 %; Found C, 66.50; H, 7.24 %. δ_H ($CDCl_3$): 0.95 (18H, s, *t*-Bu), 1.29 (18H, s, *t*-Bu), 3.31 (4H, d, Ar-C*H*$_2$-Ar, *J* = 13.2 Hz), 3.82 (4H, t, Br-C*H*$_2$, *J* = 6.6 Hz), 4.28-4.33 (8H, m, O-C*H*$_2$, Ar-C*H*$_2$-Ar), 6.79 (4H, s, Ar-*H*), 6.99 (2H, s, Ar-O*H*), 7.06 (4H, s, Ar-*H*). δ_C (CDCl3): 29.4, 30.9, 31.6, 33.0, 75.5, 125.1, 125.6, 132.7, 142, 147, 149, 151. ν_{max} (KBr): 3450, 2960, 2905, 2866, 1626, 1598, 1484, 1459, 1414, 1392, 1373, 1362, 1301, 1270, 1238, 1195, 1176, 1124, 1100, 1068, 1007, 947, 873, 821, 635 cm^{-1}.

2.2.4 5,11,17,23-Tetra-*tert*-butyl-25,27–dihydroxy-26,28-bis(2-bromopropoxy)calix[4]arene: (4)[106]

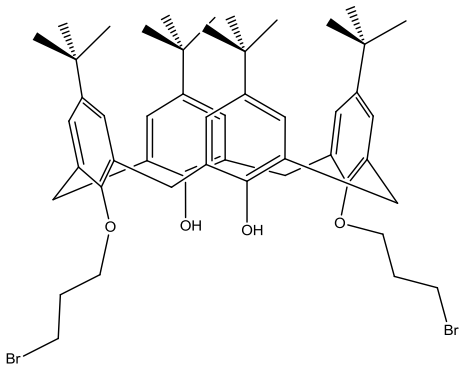

Compound **2** (5 g, 7.7 mmol) and potassium carbonate (2.12 g, 15.4 mmol) were dissolved in MeCN (200 mL) in a 500mL round bottomed flask, and stirred for 1 h, at which point 1,3 dibromopropane (31.09 g, 154 mmol) was added dropwise. The mixture was then heated to reflux for 67 h with vigorous stirring. This was then cooled for a 1 h period. The inorganic salts formed were filtered off, and the filtrate was then concentrated under vacuum to yield a yellow oil. This solid was dissolved in a $CHCl_3$/EtOH mix (1:1). A powdery white solid (**4**) was precipitated after two days.

Yield: 4.5 g, 65 %. m.p.: > 260 °C (Lit 288-290 °C).[106] Anal. Calc. for $C_{50}H_{66}Br_2O_4$: C, 67.41; H, 7.47; N, 0 %; Found C, 71.08; H, 7.78; N, 0.04 %. δ_H ($CDCl_3$): 1.22 (18H, s, *t*-Bu), 1.27 (18H, s, *t*-Bu), 2.51 (4H, app q, CH_2-C*H*$_2$-CH_2, *J* = 12 Hz), 3.32 (4H, d, Ar-C*H*$_2$-Ar, *J* = 12.9 Hz), 3.95 (4H, t, Br-C*H*$_2$, *J* = 6.9 Hz), 4.09 (4H, t, O-C*H*$_2$, *J* = 5.4 Hz), 4.24 (4H, d, Ar-C*H*$_2$-Ar, *J* = 12.9 Hz), 6.87 (4H, s, Ar-*H*), 7.05 (4H, s, Ar-*H*), 7.63 (2H, s, Ar-O*H*). δ_C (CDCl3): 30.3, 31.1, 31.7 31.9, 33.5, 34.0, 73.3, 125.2, 125.7, 127.5, 132.7, 141.7, 145.6, 147.2, 149.2. ν_{max} (KBr): 3408, 3044, 2954, 2902, 2866, 1598, 1485, 1435, 1414, 1392, 1380, 1362, 1334, 1302, 1284, 1255, 1239, 1201, 1172, 1123, 1098, 1023, 977, 927, 873, 780, 759, 634, 568 cm^{-1}.

2.2.5 5,11,17,23-Tetra-*tert*-butyl-25,27–dihydroxy-26,28-bis(2-bromobutoxy)calix[4]arene: (5)[107]

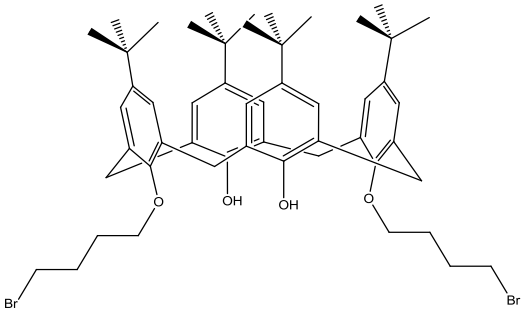

A mixture of potassium carbonate (1.91 g, 13.8 mmol) and compound **2** (3 g, 4.62 mmol) were dissolved in 250 mL of MeCN in a 500 mL round bottom flask, after 1 h of stirring at room temperature 1,4 dibromobutane (19.95 g, 9.24 mmol) was added dropwise. The resulting mixture was refluxed for 72 h and then cooled to room temperature. The insoluble salts were filtered off and the filtrate reduced to dryness, a yellow solid formed. This solid was taken up in hot $CHCl_3$ and a white ppt. formed upon addition of EtOH. **5** was collected by filtration and washed with cold EtOH.

Yield: 1.25 g, 30 %. m.p.: 250 -258 °C (Lit. 204-206 °C).[106] Anal. Calc. for $C_{52}H_{70}Br_2O_4$: C, 67.97; H, 7.68; N, 0%; Found C, 65.4; H, 7.52; N, 0%. δ_H ($CDCl_3$):

1.02 (18H, s, *t*-Bu), 1.35 (18H, s, *t*-Bu), 2.19 (4H, app q, O-CH_2-CH_2, J = 6 Hz), 2.34 (4H, app q, CH_2-CH_2-Br, J = 6.6 Hz), 3.35(4H, d, Ar-CH_2-Ar, J = 13.2 Hz), 3.67 (4H, t, CH_2-Br, J = 6.6 Hz), 4.04 (4H, t, O-CH_2, J = 6 Hz), 4.27 (4H, d, Ar-CH_2-Ar, J = 12.9Hz), 6.86(4H, s, Ar-*H*), 7.11(4H, s, Ar-*H*), 7.47(2H, s, Ar-O*H*). δ_C (CDCl3): 28.4, 29.6, 31.1, 31.7, 32.5, 33.8, 34.1, 75.2, 124.8, 125.6, 127.8, 132.5, 141.5, 146.9, 149.7, 151.5. ν_{max} (KBr): 3400, 2961, 2905, 2866, 1598, 1485, 1443, 1391, 1384, 1362, 1332, 1300, 1241, 1200, 1123, 1037, 998, 978, 945, 928, 872, 634 cm^{-1}.

2.2.6 4,4'-((Ethane-1,2-diylbis(azanylylidene))bis(methanylylidene))diphenol: (6)[108]

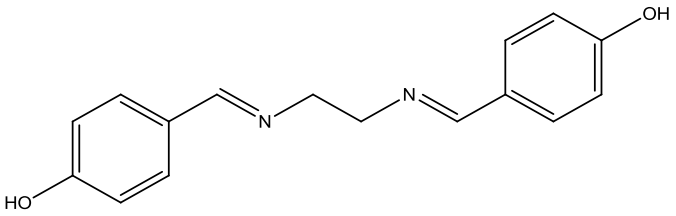

In a 100 mL round bottom flask 4-Hydroxybenzaldehyde (1 g, 8.18 mmol) was dissolved in ethanol (50 mL), to this solution ethylenediamine (0.246 g, 4.09 mmol) was added over 1 h dropwise. The resulting solution was heated to 120°C and kept at this temperature for 1 h with stirring. This was then cooled to room temperature and placed in an ice bath, **6** precipitated out of solution as yellow crystals.

Yield: 0.682 g, 62%. m.p.: 220- 222 °C, (Lit 220 °C).[109] Anal. Calc. for $C_{16}H_{16}N_2O_2$: C, 71.62; H, 6.01; N, 10.44 %; Found C, 66.75; H, 6.19; N, 9.32 %. δ_H (DMSO): 3.76 (4H, s, N-CH_2), 6.77 (4H, d, Ar-*H*, J = 8.5 Hz), 7.51 (4H, d, Ar-*H*, J = 8.6 Hz), 8.17 (2H, s, *H*C=N). δ_C (DMSO): 61.3, 115.4, 127.6, 129.7, 159.8, 161.5. ν_{max} (KBr): 3471, 2892, 2682, 1639, 1606, 1584, 1516, 1456, 1437, 1377, 1341, 1287, 1259, 1181, 1163, 1034, 981, 826 cm^{-1}.

2.2.7 *p*-Schiff Base linked propoxy calix[4]arene: (7)

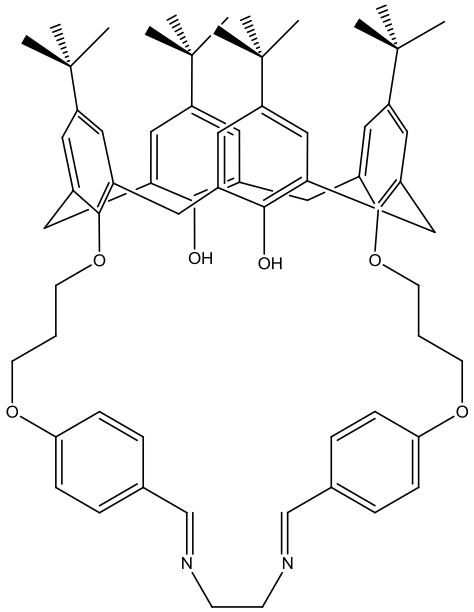

A mixture of **6** (81.13 mg, 0.30 mmol) and potassium carbonate (97 mg, 0.75 mmol) in MeCN (100 mL) was stirred at room temperature for 1h. To this stirring mixture **4** (270 mg, 0.30 mmol) in MeCN (100 mL) was added, and heated to reflux for 24 h, followed by cooling to room temperature. Inorganic salts were filtered, and the filtrate reduced to dryness. This residue was taken up in a hot EtOH/$CHCl_3$ mix. A white crystalline solid (**7**) precipitated out of solution.

Yield: 225 mg, 74%. m.p.: >260 °C. Anal. Calc. for $C_{66}H_{50}N_2O_6$: C, 79.48; H, 8.08; N, 2.81%; Found C, 72.02; H, 7.42; N, 2.52 %. δ_H ($CDCl_3$): 1.01 (18H, s, *t*-Bu), 1.27 (18H, s, *t*-Bu), 2.31 (4H, m, CH_2-C*H*$_2$-CH_2), 3.33 (4H, d, Ar-C*H*$_2$-Ar, *J* = 12.57 Hz), 3.77 (4H, s, C=N-C*H*$_2$), 4.06-4.11 (4H, m,C*H*$_2$), 4.19-4.28 (8H, m, Ar-C*H*$_2$-Ar, O-C*H*$_2$), 6.82 (4H, d, Ar-*H*, *J* = 9 Hz), 6.87 (4H, s, Ar-*H*), 7.05 (4H, s, Ar-*H*), 7.53 (4H, d, Ar-*H*, *J* = 8.7 Hz), 7.82 (2H, s, Ar-O*H*), 8.04 (2H, s, *H*C=N). δ_C ($CDCl_3$): 29.8, 31.0, 31.7, 34.0, 64.7, 114.4, 125.1, 125.6, 129.7, 132.0, 132.8, 141.6, 147.1, 149.4, 150.9, 160.7, 161.7. ν_{max} (KBr): 3411, 2959, 2905, 2870, 1644, 1606, 1578, 1511, 1485, 1362, 1305, 1242, 1165, 1124, 1053, 871, 831 cm^{-1}.

2.2.8 Metal Complexes of Ligand 7

2.2.8.1 Attempted synthesis of Complex Zn(7)(ClO_4)$_2$

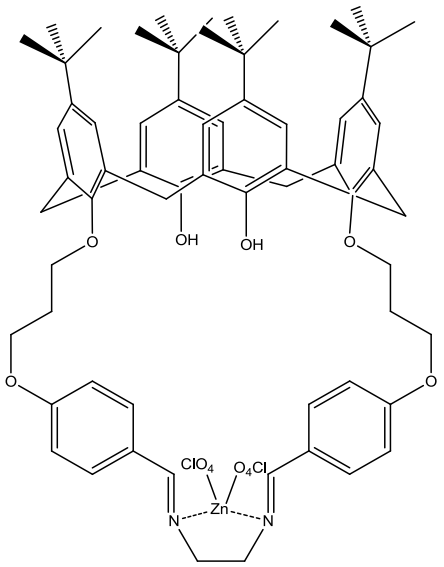

Compound **7** (10 mg, 0.01 mmol) was dissolved in $CHCl_3$ (2 mL), to this zinc(II) perchlorate (9.3 mg, 0.025 mmol) in MeOH (5 mL) was added. The resulting mixture was stirred at room temperature for 4 h. A white ppt. formed, this was filtered and the filtrate reduced to dryness to yield a pale yellow solid, which was the aldehyde product.

Crude Yield: 5 mg, 40 %. m.p.: 154-160 °C. δ_H ($CDCl_3$): 0.99 (18H, s, *t*-Bu), 1.27 (18H, s, *t*-Bu), 2.32 (4H, m, CH_2-C*H*$_2$-CH_2), 3.30 (4H, d, Ar-C*H*$_2$-Ar, *J* = 13.0 Hz), 4.09 (4H, t, Cx-O-C*H*$_2$, *J* = 5.6 Hz), 4.19 (4H, d, Ar-C*H*$_2$-Ar, *J* = 12.9 Hz), 4.44 (4H, t, Ar-O-C*H*$_2$, *J* = 6.6 Hz), 6.85 (4H, s, Ar-*H*), 7.03-7.06 (6H, m, Ar-*H*, Ar-*H*), 7.64 (1H, s, Ar-O*H*), 7.79 (2H, d, Ar-*H*, *J* = 8.6 Hz), 9.84 (1H, s, *H*C=O). δ_C ($CDCl_3$): 21.6, 28.5, 28.6, 29.9, 30.6, 30.7, 32.8, 56.3, 113.8, 124.1, 124.6, 126.5, 131.0, 131.6, 148.2, 189.8. ν_{max} (KBr) : 3410, 2960, 2951, 2932, 2904, 2870, 1646, 1598, 1581, 1485, 1447, 1362, 1315, 1270, 1195, 1174, 1068, 1055, 871, 791, 690 cm^{-1}.

2.2.8.2 Attempted Synthesis of Complex Zn(7)Cl_2

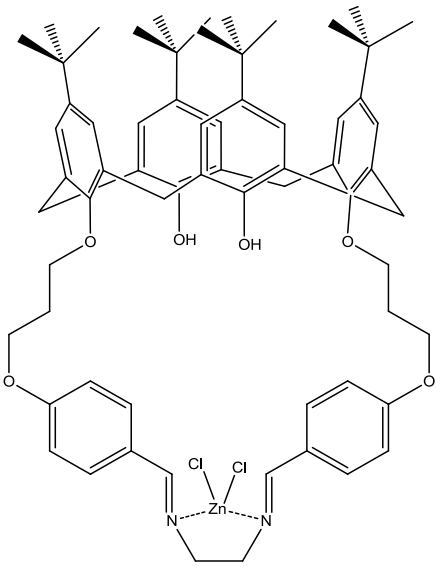

Compound **7** (22 mg, 0.022 mmol) was dissolved in toluene (2 mL) to this stirring mixture zinc(II) chloride (7 mg, 0.051 mmol) in MeOH (5 mL) was added dropwise. The cloudy reaction mixture turned clear after addition of all the MeOH, this was stirred for 4 h and at this point the reaction turned white. The solution was concentrated at reduced pressure to yield a yellow solid which was dried in an oven overnight. This solid was determined to be the aldehyde product.

Crude Yield 10 mg, 40 %. m.p.: 124-136 °C. δ_H ($CDCl_3$): 1.00 (18H, s, *t*-Bu), 1.27 (18H,s *t*-Bu), 2.12-2.34 (4H, m, CH_2-C*H*$_2$-CH_2), 3.31 (4H, d, Ar-C*H*2-Ar, J = 12.6 Hz), 3.70-4.46 (16H, m, Ar-C*H*$_2$-Ar, O-C*H*$_2$, O-C*H*$_2$, C=N-C*H*$_2$), 6.85-7.04 (14H, m, Ar-*H*), 8.46 (2H, s, Ar-O*H*), 10.09 (2H, s, *H*C=O). δ_C ($CDCl_3$): 31.0, 31.7, 33.8, 34.0, 65.1, 72.4, 114.8, 115.0, 115.1, 125.1, 125.6, 127.6, 129.9, 132.0, 132.6, 132.7, 141.6, 141.7, 147.3, 149.2, 150.5, 163.9, 190.8. ν_{max} (KBr): 3494, 3445, 3271, 2958, 2905, 2868, 1692, 1601, 1578, 1509, 1485, 1362, 1310, 1259, 1211, 1160, 1047, 831, 619 cm^{-1}.

2.2.8.3 Attempted Synthesis of Complex Ni(7)$(ClO_4)_2$

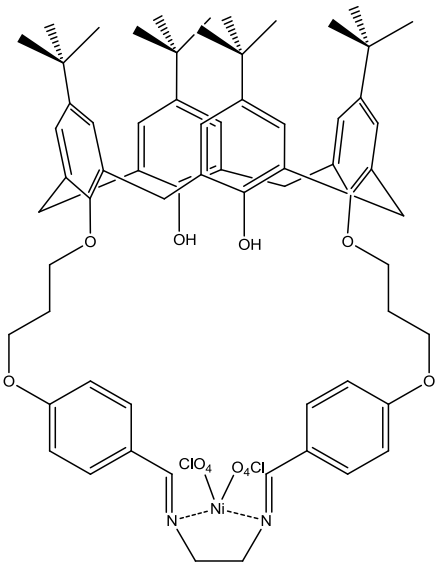

Compound **7** (10 mg, 0.01 mmol) was dissolved in $CHCl_3$ (2 mL), nickel(II) perchlorate (9.2 mg, 0.025 mmol) in MeOH (5 mL) was titrated into the stirring mixture. The reaction mixture was stirred at room temperature for 8 h. A yellow/green solution formed, the solvents were removed under vacuum and the product extracted from excess perchlorate by addition of $CHCl_3$ to yield a light green solid. The solid was determined to be the aldehyde product.

Crude Yield: 8 mg, 64 %. m.p.: 180-192 °C. ν_{max} (KBr): 3405, 3235, 2960, 1689, 1650, 1623, 1600, 1576, 1510, 1486, 1262, 1089, 832, 627 cm^{-1}.

2.2.8.4 Attempted Synthesis of Complex Co(7)(ClO_4)$_2$

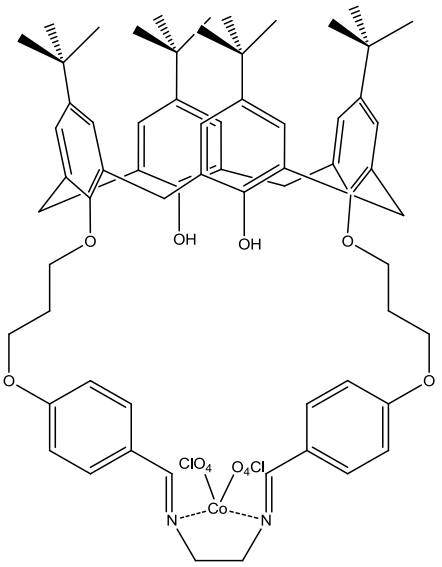

7 (10 mg, 0.01 mmol) was dissolved in $CHCl_3$ (3 mL) and to this cobalt perchlorate (9.2 mg, 0.025 mmol) in MeOH (6 mL) was added, the resulting mixture was stirred at room temperature for 8 h. A red/yellow solution formed, the solvents were removed under reduced pressure and the product was extracted from excess perchlorate through addition of $CHCl_3$. A red solid was formed from concentration of solvent at reduced pressure, this was the aldehyde product from hydrolysis of the imine.

Crude Yield: 6 mg, 48 %. m.p.: >260 °C. ν_{max} (KBr): 3529, 3417, 3233, 2960, 2905, 2874, 1687, 1651, 1600, 1576, 1510, 1486, 1362, 1262, 1161, 1089, 832, 627 cm^{-1}.

2.2.8.5 Attempted Synthesis of Complex Hg(7)$(ClO_4)_2$

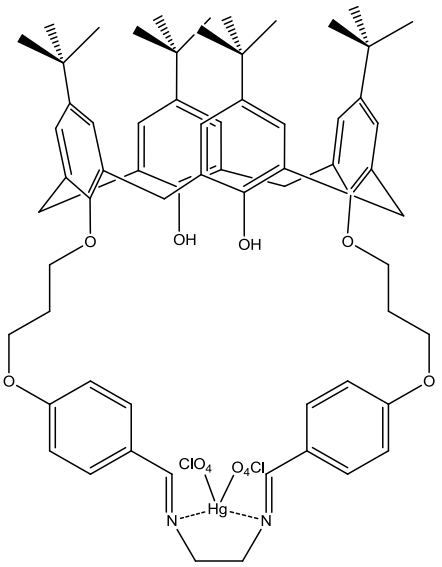

A mixture of compound **7** (10 mg, 0.01 mmol) in $CHCl_3$ (3 mL) and mercury(II) perchlorate (10 mg, 0.025 mmol) in MeOH (7 mL) was stirred at room temperature for 16 h. The solvents were removed on a rotary evaporator, to give a yellow/orange solid. The product was removed from the excess perchlorate by addition of $CHCl_3$, concentration under reduced pressure yields a purple solid. This solid was found to be the aldehyde product.

Crude Yield: 9 mg, 64 %. m.p.: >260 °C. δ_H ($CDCl_3$): 0.99 (18H, s, *t*-Bu), 1.27 (18H, s, *t*-Bu), 2.32 (4H, q, CH_2-C*H*$_2$-CH_2, *J* = 6.2 Hz), 3.31 (4H, d, Ar-C*H*$_2$-Ar, *J* = 12.9 Hz), 4.19 (12H, m, Ar-CH_2-Ar, O-C*H*$_2$, C=N-C*H*$_2$), 4.44 (4H, t, O-C*H*$_2$, *J* = 6.5 Hz), 6.76 (4H, d, Ar-*H*, *J* = 13.8 Hz), 6.85 (4H, s, Ar-*H*), 7.04 (4H, s, Ar-*H*), 7.60 (2H, s, Ar-O*H*), 7.79 (4H, d, Ar-*H*, *J* = 8.6 Hz), 9.84 (2H, s, *H*C=O). ν_{max} (KBr): 3412, 3230, 2960, 2904, 2879, 1671, 1599, 1509, 1485, 1362, 1303, 1259, 1204, 1103, 981, 872, 627 cm^{-1}.

2.2.8.6 Attempted Synthesis of Complex Cu(7)(ClO_4)$_2$

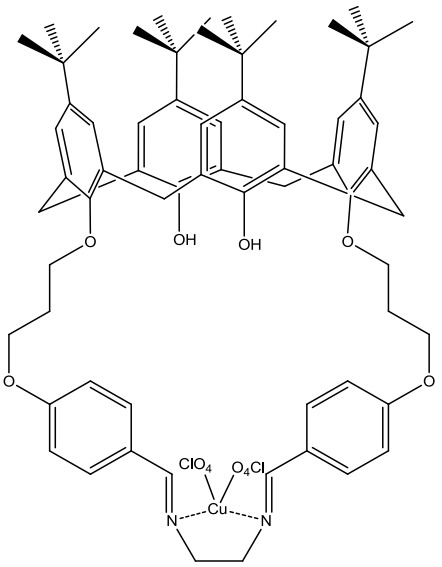

Compound **7** (10 mg, 0.01 mmol) in $CHCl_3$ (5 mL) and copper perchlorate (4.5 mg, 0.12 mmol) in MeOH (5 mL) were heated to reflux for 3 h. The mixture was then cooled and the solvent was removed at reduced pressure, this yielded a blue-green solid, which was recrystallized from EtOH to yield a pale green solid, which was found to be the aldehyde product.

Crude Yield: 10 mg, 79 %. m.p.: 124-136 °C. ν_{max} (KBr): 3395, 2960, 2904, 2868, 1693, 1599, 1577, 1509, 1485, 1362, 1308, 1258, 1210, 1160, 1124, 1102, 1051, 831, 615 cm^{-1}.

2.2.9 *p*-Schiff Base linked butoxy calix[4]arene: (8)

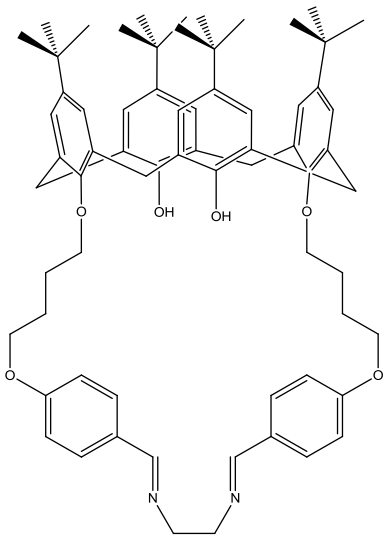

In a 100 mL round bottom flask **6** (0.1 g, 0.37 mmol) and potassium carbonate (0.13 g, 0.99 mmol) were dissolved in MeCN (60 mL) and stirred at room temperature for 1 h. To this compound **4** (0.32 g, 0.35 mmol) was added and the resulting mixture was headed to reflux for 72 hours, and then cooled to room temperature. The potassium salts which had formed were filtered off and the filtrate was dried under vacuum. The residue was taken up in hot $CHCl_3$ and EtOH, to yield **8** as a pale yellow solid.

Yield: 132 mg, 35 %. m.p.: >260 °C. Anal. Calc. for $C_{68}H_{84}N_2O_6$: C, 79.65; H, 8.26; N, 2.73%; Found C, 77.31; H, 8.17; N, 2.33%. δ_H ($CDCl_3$): 0.99 (18H, s, *t*-but), 1.29 (18H, s, *t*-but), 2.07 (8H, m, CH_2-C*H*$_2$-CH_2), 3.31 (4H, d, Ar-C*H*$_2$-Ar, *J* = 13.2), 3.99-4.11 (12H, m, Br-C*H*$_2$,O-C*H*$_2$,N-C*H*$_2$), 4.29 (4H, d, Ar-C*H*$_2$-Ar, *J* = 12.9 Hz), 6.84 (4H, s, Ar-*H*), 6.97 (4H, d, Ar-*H*, *J* = 6.9 Hz), 7.06 (4H, s, Ar-*H*), 7.17 (4H, m, Ar-*H*), 7.75 (2H, s, Ar-O*H*), 8.05 (2H, s, *H*C=N). δ_C ($CDCl_3$): 30.9, 31.1, 31.7, 31.9, 33.8, 66.3, 124.0, 124.5, 125.1, 126.2, 126.6, 128.4, 128.9, 131.6, 133.7, 140.4, 145.8, 148.7, 149.6, 158.2. ν_{max} (KBr): 3388, 3046, 2958, 2868, 1710, 1670, 1644, 1600, 1485, 1446, 1391, 1362, 1296, 1241, 1202, 1123, 1096, 1042, 1018, 981, 871, 781, 698 cm^{-1}.

2.2.10 Metal Complexes of Ligand 8

2.2.10.1 Attempted Synthesis of Complex $Zn(8)(ClO_4)_2$

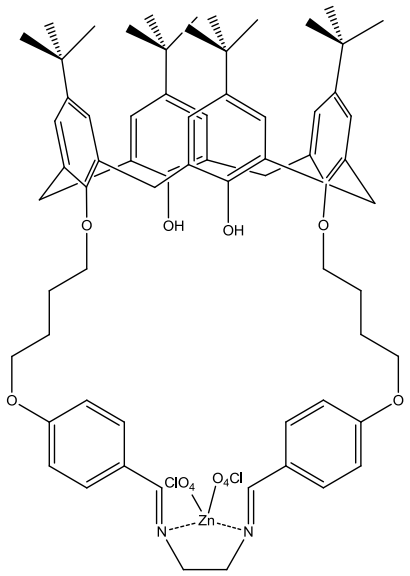

A mixture of compound **8** (25 mg, 0.024 mmol) and zinc(II) perchlorate (22 mg, 0.059 mmol) in a MeOH:$CHCl_3$ mixture (1:1, 20ml) was placed in a 50 ml round bottomed flask. The mixture was stirred at room temperature for 4 h. The solvents were removed under vacuum to obtain a yellow solid; complex was separated from excess metal salt using $CHCl_3$. Concentration under reduced pressure yielded an orange solid, which was determined to be the aldehyde product.

Crude Yield: 12 mg, 39 %. m.p.: 150-164 °C. δ_H ($CDCl_3$): 0.97 (18H, s, *t*-Bu), 1.29 (18H, s, *t*-Bu), 2.20 (8H, m, CH_2-C*H*$_2$-C*H*$_2$-CH_2), 3.31 (4H, d, Ar-C*H*$_2$-Ar, J = 12.9 Hz), 4.03 (4H, t, C*H*$_2$-O-Ar, J = 5.4 Hz), 4.12 (4H, t, O-C*H*$_2$, J = 5.7 Hz), 4.26 (4H, d, Ar-C*H*$_2$-Ar, J = 12.9 Hz), 6.82 (4H, s, Ar-*H*), 6.94 (4H, d, Ar-*H*, J = 8.7 Hz), 7.06 (4H, s, Ar-*H*), 7.56 (2H, s, Ar-O*H*), 7.75 (4H, d, Ar-*H*), 9.84 (2H, s, *H*C=O). ν_{max} (KBr): 3428, 3235, 2960, 2905, 2868, 1693, 1601, 1577, 1509, 1485, 1431, 1392, 1362, 1311, 1258, 1209, 1159, 1121, 1108, 1011, 872, 627 cm^{-1}.

2.2.10.2 Attempted Synthesis of Complex Hg(8)(ClO_4)$_2$

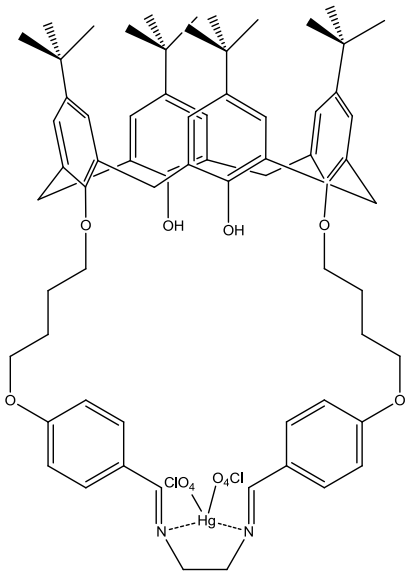

Compound **8** (15 mg, 0.014 mmol) was dissolved in $CHCl_3$ (3 mL), mercury perchlorate (11.68 mg, 0.029 mmol) in MeOH (6 mL) was added to this stirring solution, the mixture was stirred at room temperature for 8 h. The solution was concentrated under reduced pressure, the complex was separated from excess perchlorate by addition of $CHCl_3$, and concentration under vacuum yielded the a dark purple solid which was found to be the aldehyde product from imine hydrolysis.

Crude Yield: 10 mg, 50 %. m.p.: > 260 °C. δ_H ($CDCl_3$): 0.97 (18H, s, *t*-Bu), 1.21 (18H, s, *t*-Bu), 2.32 (8H, m, CH_2-CH_2-CH_2-CH_2), 3.31 (4H, d, Ar-CH_2-Ar, J = 12.9 Hz), 3.46 (4H, m, O-CH_2), 4.03 (4H, m, Ar-CH_2-Ar), 4.13 (4H, m, C=N-CH_2), 4.24 (4H, m, O-CH_2),6.75 (4H, s, Ar-*H*), 7.05 (12H, m, Ar-*H*), 7.60 (2H, s, Ar-O*H*), 10.34 (2H, s, *H*C=O). ν_{max} (KBr): 3423, 2958, 2868, 1601, 1510, 1484, 1362, 1251, 1204, 1109, 1091, 872, 626 cm^{-1}.

2.2.10.3 Attempted Synthesis of Complex Cu(7)(ClO_4)$_2$

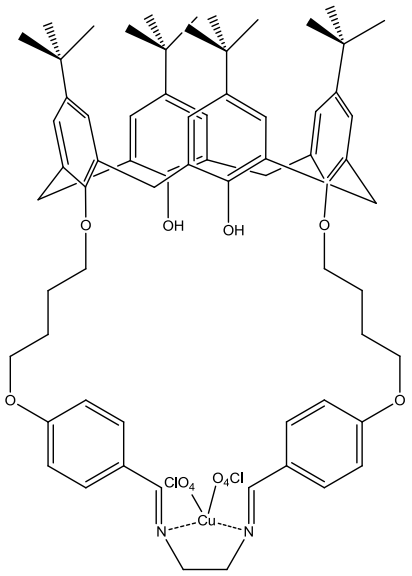

Compound **8** (17.2 mg, 0.016 mmol) was dissolved in $CHCl_3$ (3 mL), to this copper perchlorate (12.43 mg, 0.033 mmol) dissolved in EtOH (6 mL) was added. The resulting mixture was stirred at room temperature for 8 h. The solution was concentrated under vacuum to yield a brown solid which was the aldehyde product.

Crude Yield: 10 mg, 49 %. m.p.: >300 °C. ν_{max} (KBr): 3436, 2959, 2910, 2903, 2868, 1625, 1602, 1485, 1455, 1260, 1202, 1143, 1120, 1110, 1088, 872, 782, 626 cm^{-1}.

2.2.11 Attempted Synthesis of *p*-Schiff base capped ethoxy-calixarene

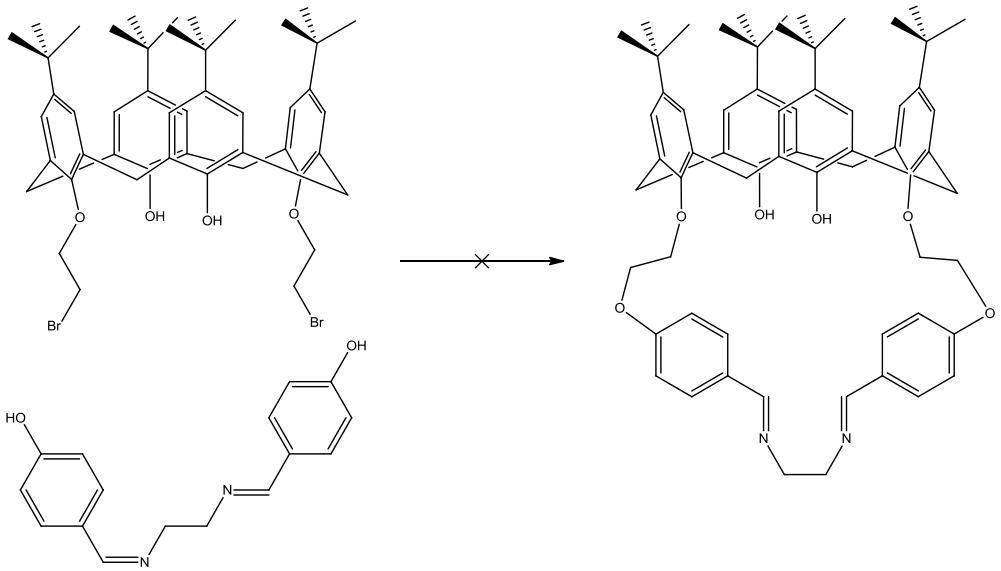

A mixture of compound **6** (0.01 g, 0.037 mmol) and potassium carbonate (0.013 g, 0.093 mmol) dissolved in MeCN (50 mL) and stirred for 1 h at ambient temperature. At this point compound **3** (0.032g, 0.037 mmol) was added and heated to reflux for 48 h. The mixture was cooled to room temperature and the inorganic salts formed filtered off. The filtrate was dried on a rotary evaporator and the residue was redissolved in $CHCl_3$:EtOH solvent mix.

2.2.12 3,3'-((ethane-1,2-bis(azanylylidene))bis(methanylylidene))diphenol: (9)

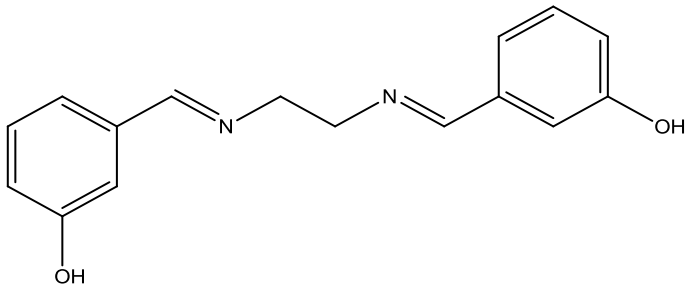

In a 100 mL round bottom flask 3-Hydroxybenzaldehyde (1 g, 8.18 mmol) was dissolved in ethanol (50 mL), to this solution ethylenediamine (0.246 g, 4.09 mmol) was added over 1 h dropwise. The resulting solution was heated to 120 °C and kept at

this temperature for one hour with stirring. This was then cooled to room temperature and placed in ice. An off white crystalline solid (**9**) was obtained.

Yield: 0.615 g, 56%. m.p.: 198-200 °C (Lit 198-200 °C).[110] Anal. Calc. for $C_{16}H_{16}N_2O_2$: C, 71.62; H, 6.01; N, 10.44 %; Found C, 65.75; H, 5.76; N, 9.53 %. δ_H (DMSO): 3.83 (4H, s, N-C*H*$_2$), 6.81 (2H, dd, Ar-*H*, J = 7.1 Hz), 7.10 (4H, m, Ar-*H*), 7.19 (2H, t, Ar-*H*, *J* = 7.7 Hz), 8.23 (2H, s, *H*C=N). δ_C (DMSO): 60.8, 113.3, 117.8, 119.3, 129.6, 137.0, 157.1, 161.9. ν_{max} (KBr): 3418, 3051, 2928, 2884, 2850, 2823, 2721, 2599, 2484, 1647, 1596, 1457, 1392, 1275, 1245, 1174, 1154, 1020, 867, 779, 685 cm^{-1}.

2.2.13 *m*-Schiff Base linked propoxy-calix[4]arene: (10)

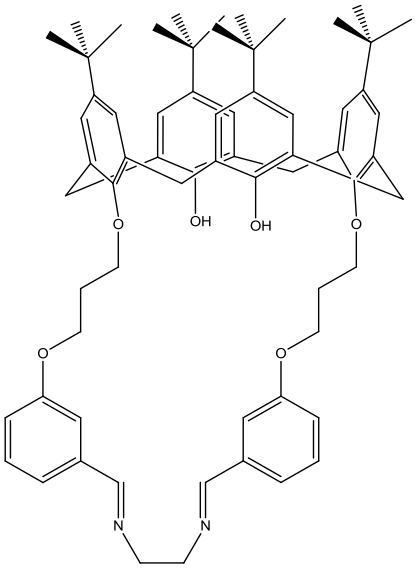

A mixture of compound **9** (50 mg, 0.18 mmol) and potassium carbonate (65 mg, 0.51 mmol) in MeCN (100 mL) was stirred at room temperature for 1 h. After 1 h compound **4** (166 mg, 0.18 mmol) was added, the mixture was then heated to reflux for 72 h with vigorous stirring. This was then cooled and left to stir for 24 h at room temperature. The solvent was removed under vacuum to obtain a yellow/off white

solid; this was triturated with MeOH, and the solid taken up in a $CHCl_3$:EtOH mixture (1:1). **10** precipitated as a white solid.

Yield: 147 mg, 82%. m.p.: 218-224 °C. Anal. Calc. for $C_{68}H_{84}N_2O_6$: C, 79.48; H, 8.08; N, 2.81 %; Found C, 77.42; H, 8.27; N, 2.70 %. δ_H ($CDCl_3$): 1.05 (18H, s, *t*-Bu), 1.26 (18H, s, *t*-Bu), 2.30 (4H, t, CH_2-CH_2-CH_2, *J* = 6.9 Hz), 3.31 (4H, d, Ar-CH_2-Ar, *J* = 12.9 Hz), 3.93 (4H, s, C=N-CH_2), 4.06 (4H, t, O-CH_2, *J* = 6.3 Hz), 4.24 (4H, d, Ar-CH_2-Ar, *J* = 12.9 Hz), 4.37 (4H, t, CH_2-O-Ar, *J* = 6.6 Hz), 6.91 (4H, s, Ar-*H*), 6.99 (12H, m, Ar-*H*), 7.96 (2H, s, Ar-O*H*), 8.06 (2H, s, *H*C=N). δ_C ($CDCl_3$): 29.9, 31.1, 31.7, 31.9, 33.8, 34.0, 59.8, 64.7, 72.5, 113.4, 117.6, 120.0, 125.1, 125.6, 127.7, 129.7, 132.9, 137.7, 141.6, 147.1, 149.4, 150.6, 159.0, 163.7.ν_{max} (KBr): 3404, 2960, 2870, 1646, 1598, 1581, 1485, 1447, 1362, 1266, 1195, 1174, 1157, 1123, 1096, 1068, 1055, 946, 871, 791, 690 cm^{-1}.

2.2.14 Metal Complexes of ligand 10

2.2.14.1 Attempted Synthesis of Complex Zn(10)$(ClO_4)_2$

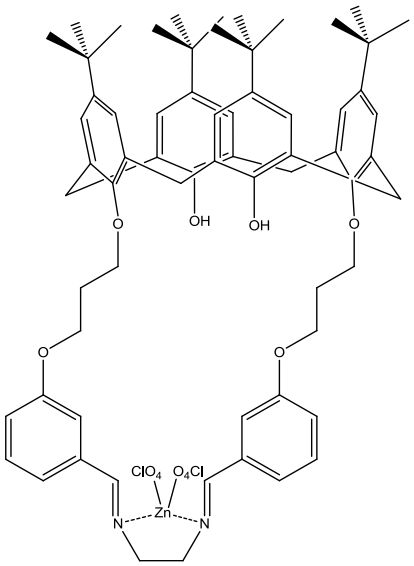

A mixture of **13** (62 mg, 0.06 mmol) and zinc (II) perchlorate (27 mg, 0.07 mmol) in a MeOH:$CHCl_3$ mixture (1:1, 20ml) was placed in a 50 ml round bottomed flask. The

mixture was then heated to reflux in an inert N_2 atmosphere for 4 hours with vigorous stirring. This was then cooled for a period of 1 h. The solvents were removed under vacuum to obtain a yellow/off white solid, this was the aldehyde product from imine hydrolysis.

Crude Yield: 34 mg, 45 %. m.p.: 122-136 °C. δ_H ($CDCl_3$): 0.99 (18H, s, *t*-Bu), 1.31 (18H, s, *t*-Bu), 2.17-2.24 (4H, m, CH_2-C*H*$_2$-CH_2, *J* = 13.2 Hz), 3.31 (4H, d, Ar-C*H*$_2$-Ar, *J* = 12.9 Hz), 4.04 - 4.07 (4H, t, Br-C*H*$_2$, *J* = 5.7 Hz), 4.1 – 4.14 (4H, t, O-C*H*$_2$, *J* = 5.4 Hz), 4.27 (4H, d, Ar-C*H*$_2$-Ar, *J* = 12.9 Hz), 5.3 (4H, s, N-C*H*$_2$), 6.84 (4H, s, Ar-*H*), 7.06 (4H, s, Ar-*H*), 7.124-7.156 (4H, d, Ar-*H*, *J* = 9.6 Hz), 7.368-7.393 (4H, d, Ar-*H*, *J* = 7.5 Hz), 7.71 (2H, s, Ar-O*H*), 9.97 (2H, s, Ar-C*H*=O). δ_C ($CDCl_3$): 25.97, 31.04, 31.71, 31.83, 33.97, 67.92, 113.17, 121.76, 123.11, 125.12, 125.55, 127.73, 130.02, 132.62, 137.76, 141.53, 146.93, 149.82, 150.71, 159.56, 192.13. ν_{max} (KBr): 3417, 2961, 2969, 1698, 1598, 1486, 1262, 1094, 627 cm^{-1}.

2.2.14.2 Attempted Synthesis of Complex Cu(10)$(ClO_4)_2$

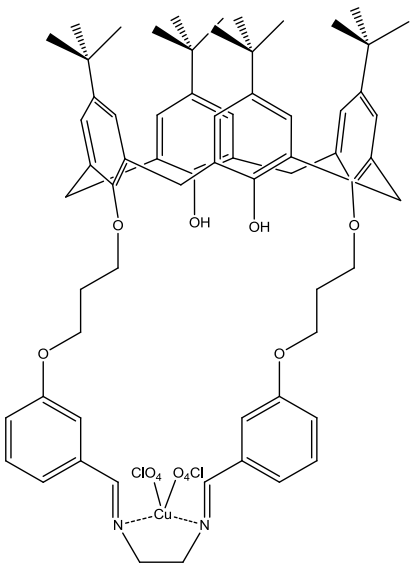

Ligand **10** (50 mg, 0.0488 mmol) and $Cu(ClO_4)_2$ (21.7 mg, 0.0586 mmol) were dissolved in $CHCl_3$:MeOH an (1:2) mix. The mixture was stirred for 8 h at room

temperature. The solvents were removed under vacuum to obtain a pale green solid, which was determined to be the aldehyde product resulting from hydrolysis.

Crude Yield: 24 mg, 39 %. m.p.: 86-98 °C. ν_{max} (KBr): 3411, 2960, 2872, 2829, 1698, 1599, 1486, 1392, 1362, 1261, 1102, 1055, 871, 627 cm^{-1}.

2.2.15 *m*-Schiff Base linked butoxy calix[4]arene: (11)

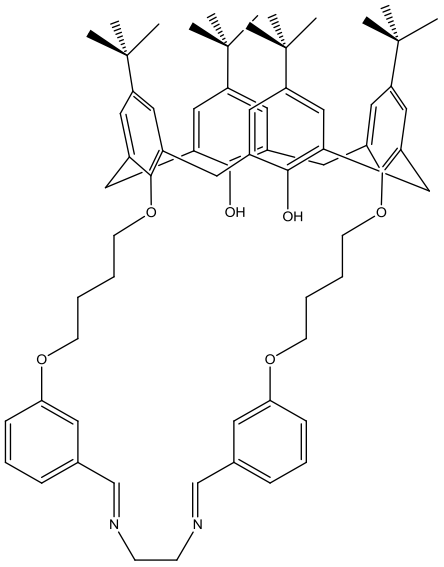

A mixture of **12** (87 mg, 0.32 mmol) and potassium carbonate (111 mg, 1.1 mmol) in MeCN (50 mL) was stirred at room temperature for 1 h. After this **5** (295 g, 0.32 mmol) was added, the mixture was then heated to reflux in an inert N_2 atmosphere for 48 h with vigorous stirring. This was then cooled and left to stir for 8 h at room temp. The solvent was removed under vacuum to obtain a yellow/off white solid. This was redissolved in $CHCl_3$:EtOH (1:1). Compound **11** precipitated as an off white crystalline solid after a day.

Yield: 200 mg, 60%. m.p.: 154°C-184°C. Anal. Calc. for $C_{68}H_{84}N_2O_6$: C, 79.65; H, 8.26; N, 2.73 %; Found C, 75.52; H, 7.68; N, 2.85 %. δ_H ($CDCl_3$): 0.99 (18H, s, *t*-Bu), 1.29 (18H, s, *t*-Bu), 3.31 (4H, d, Ar-C*H*$_2$-Ar, *J* = 12.6 Hz), 3.71 (8H, m, O-C*H*$_2$), 3.93-4.04 (12H, m, O-CH2-C*H*$_2$, C=N-C*H*$_2$), 4.28 (4H, d, Ar-C*H*$_2$-Ar, *J* = 12.9 Hz), 6.84

(4H, s, Ar-*H*), 6.97-6.99 (6H, m, Ar-*H*), 7.06 (4H, m, Ar-*H*), 7.21 (2H, s, Ar-*H*), 7.74 (2H, s, Ar-O*H*), 8.05 (2H, s, *H*C=N). δ_C ($CDCl_3$): 26.5, 27.1, 31.0, 31.7, 34.0, 33.8, 60.1, 67.8, 111.4, 118.9, 120.4, 125.1, 125.5, 127.7, 129.6, 132.8, 137.3 ,141.4, 146.9, 149.7, 150.7, 159.3, 165.1. ν_{max} (KBr): 3398, 3045, 2954, 2905, 2866, 1646, 1598, 1582, 1485, 1446, 1362, 1264, 1200, 1123, 1042, 1016, 978, 871, 781, 688 cm^{-1}.

2.2.16 Metal Complexes of ligand 11

2.2.16.1 Attempted Synthesis of Complex $Zn(11)(ClO_4)_2$

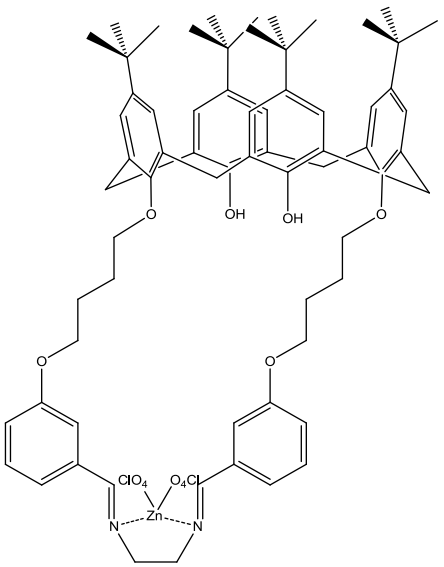

A mixture of ligand **11** (25 mg, 0.025 mmol) and zinc(II) perchlorate (22.39 mg, 0.06 mmol) in a $CHCl_3$/MeOH (1:2) was stirred at room temperature for 8h. The organic solvents were removed under vacuum to leave a white solid. The complex was separated from excess perchlorate using $CHCl_3$. After removal of solvent an off white/yellow solid was obtained, this solid was found to be the aldehyde product due to imine hydrolysis.

Crude Yield: 20 mg, 62 %. m.p.: 128-138 °C. δ_H ($CDCl_3$): 1.01 (18H, s, *t*-but), 1.26 (18H, s, *t*-but), 2.36 (4H, q, CH_2-C*H*$_2$-CH_2, *J* = 6 Hz), 3.26-3.33 (8H, m, Ar-C*H*$_2$-Ar, C=N-C*H*$_2$), 4.13 (4H, t, O-C*H*$_2$, *J* = 5.7 Hz), 4.21 (4H, d, Ar-CH2-Ar, *J* = 12.6 Hz),

4.47 (4H, t, Ar-O-C*H*$_2$, *J* = 6.3 Hz), 6.87 (4H s, Ar-*H*), 7.02 (4H, s, Ar-*H*), 7.14 (2 H, m, Ar-*H*), 7.40-7.46 (6H, m, Ar-*H*), 7.78 (2H, s, Ar-O*H*), 9.89 (2H, s, *H*C=O). ν_{max} (KBr): 3409, 3328, 2959, 2928, 2868, 1699, 1567, 1485, 1446, 1384, 1260, 1198, 1041, 872, 682 cm^{-1}.

2.2.16.2 Attempted Synthesis of Complex Co(11)(ClO$_4$)$_2$

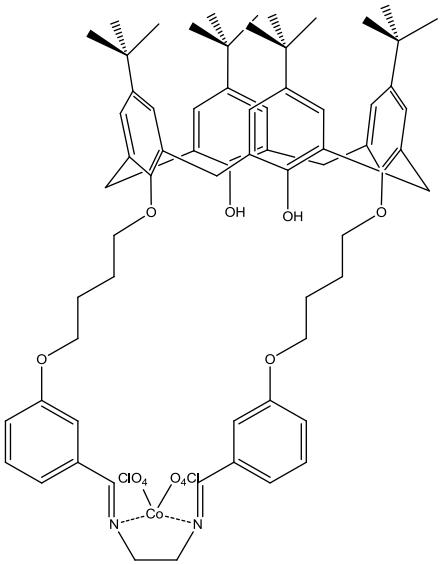

Ligand **11** (10 mg, 0.009 mmol) and cobalt(II) perchlorate (4.3 mg, 0.012 mmol) were dissolved in $CHCl_3$/MeOH (1:2), which was stirred at room temperature for 4 h. The mixture was separated from the excess metal salt, using $CHCl_3$. Removal of solvent yielded a red brown solid which was the aldehyde product.

Crude Yield: 8 mg, 69 %. m.p.: >300 °C. ν_{max} (KBr): 3417, 2960, 1698, 1598, 1486, 1262, 1094, 791, 627 cm^{-1}.

2.2.16.3 Attempted Synthesis of Complex Cu(11)$(ClO_4)_2$

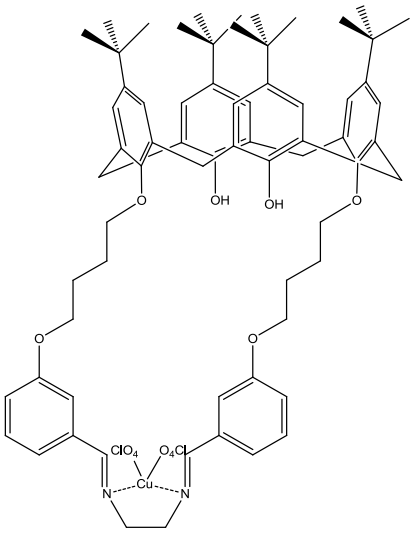

Compound **11** (10 mg, 0.01 mmol) in $CHCl_3$ (5 mL) and copper perchlorate (4.5 mg, 0.12 mmol) in MeOH (5 mL) were heated to reflux for 3 h. The mixture was then cooled and the solvent was removed at reduced pressure, this yielded a blue-green solid, which was the aldehyde product from hydrolysis of the imine.

Crude Yield: 10 mg, 77 %. m.p.: 122-168 °C. ν_{max} (KBr): 3395, 2960, 2904, 2868, 1693, 1599, 1577, 1509, 1485, 1362, 1308, 1258, 1210, 1160, 1124, 1102, 1051, 831, 615 cm^{-1}.

2.2.16.4 Attempted Synthesis of Complex Ni(11)$(ClO_4)_2$

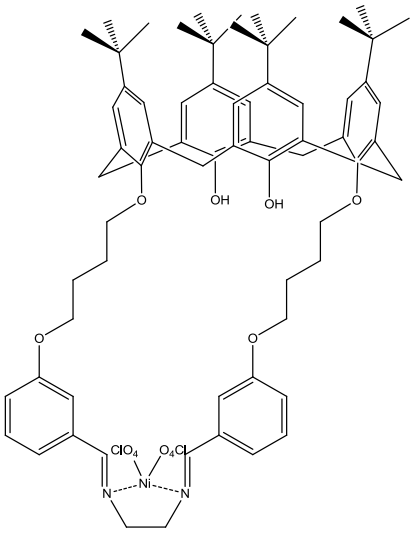

Compound **11** (25 mg, 0.024 mmol) was dissolved in $CHCl_3$ (2 mL), nickel perchlorate (10.5 mg, 0.029 mmol) in MeOH (6 mL) was added, the reaction mixture was heated to reflux for 4 h. The mixture was cooled, and was concentrated under reduced pressure. The solvents were removed under vacuum to yield a yellow solid, which was determined to be the aldehyde product from the imine hydrolysis reaction.

Crude Yield: 18 mg, 58 %. m.p.: 130-138 °C. ν_{max} (KBr) : 3436, 2960, 2909, 2870, 1697, 1633, 1599, 1485, 1384, 1261, 1200, 1121, 799, 626 cm^{-1}.

2.2.16.5 Attempted Synthesis of Complex $Hg(11)(ClO_4)_2$

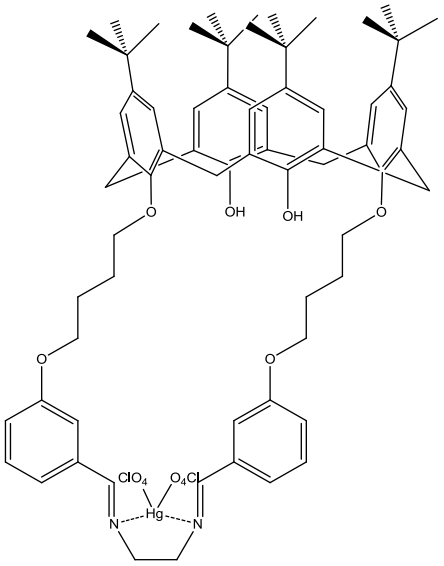

Compound **11** (15 mg, 0.02 mmol) was dissolved in $CHCl_3$ (3 mL), mercury perchlorate (11.68 mg, 0.03 mmol) in MeOH (6 mL) was added, and the reaction mixture was stirred at room temperature for 8 h. The solution was concentrated under vacuum to yield a brown solid, which was found to be the aldehyde product.

Crude Yield: 7 mg, 33 %. m.p.: > 260 °C. δ_H ($CDCl_3$): 0.96 (18H, s, *t*-Bu), 1.28 (18H, s, *t*-Bu), 2.32 (4H, t, CH_2-C*H*$_2$-C*H*$_2$-CH_2, J = 7.0 Hz), 3.31 (4H, d, Ar-C*H*$_2$-Ar, J = 12.9 Hz), 4.10 (8H, m, O-C*H*$_2$, O-C*H*$_2$), 4.24 (4H, m, Ar-C*H*$_2$), 6.83 (4H, s, Ar-*H*), 7.05 (8H, m, Ar-*H*), 7.33 (4H, m, Ar-*H*), 7.65 (2H, s, Ar-O*H*), 9.89 (2H, s, *H*C=O).

ν_{max} (KBr): 3409, 3227, 2959, 2870, 1695, 1598, 1506, 1485, 1391, 1362, 1261, 1202, 1107, 1092, 872, 783, 627 cm^{-1}.

2.2.17 *m*-Schiff Base linked ethoxy-calix[4]arene: (12)

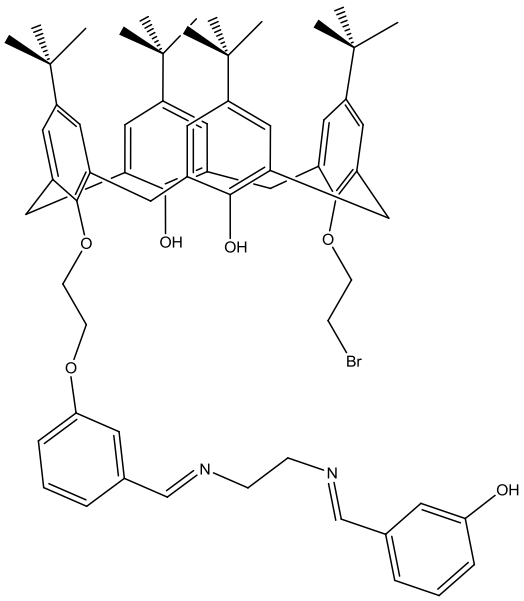

Potassium carbonate (0.13 g, 0.99 mmol) and compound **9** (0.10 g, 0.37 mmol) were dissolved in MeCN (250 mL) and heated to reflux for 1 h. At this point **3** (0.32 g, 0.35 mmol) was added and the mixture was heated to reflux for 16 h. The reaction mixture was then cooled to room temperature and the inorganic salts formed were removed by filtration. Solvent was removed under vacuum and the residue was redissolved in $CHCl_3$. **12** was obtained as an off white solid through addition of cold EtOH.

Yield: 64 mg, 62 %. m.p.: 222-226 °C. Anal. Calc. for $C_{64}H_{77}BrN_2O_6$: C, 73.19; H, 7.39; N, 2.67 %; Found C, 74.48; H, 7.26; N, 2.98 %. δ_H ($CDCl_3$): 1.04 (18H, s, *t*-Bu), 1.26 (18H, s, *t*-Bu), 3.30 (4H, d, Ar-C*H*$_2$-Ar, *J* = 12.9 Hz), 3.93 (4H, s, C=N-C*H*$_2$), 4.06 (4H, t, O-C*H*$_2$-CH$_2$, *J* = 5.7 Hz), 4.23(4H, d, Ar-C*H*$_2$, *J* = 12.9 Hz), 4.37 (4H, t, O-CH$_2$-C*H*$_2$-O-Ar, *J* = 6.9 Hz), 6.89 (4H, s, Ar-*H*), 6.98-7.03 (6H, m, Ar-*H*, Ar-*H*, Ar-*H*), 7.08 (2H, s, Ar-*H*), 7.23-7.30 (4H, m, Ar-*H*, Ar-*H*), 7.95 (2H, s, Ar-O*H*), 7.98 (2H, s, N=C*H*). δ_C ($CDCl_3$): 29.8, 30.9, 31.0, 31.6, 31.9, 33.8, 34.0, 59.8, 64.7, 72.5, 113.4,

117.5, 119.9, 125.2, 125.7, 127.7, 129.7, 132.9, 137.7, 141.6, 147.2, 149.4, 150.6, 159.0, 163.7. ν_{max} (KBr): 3408, 2960, 2904, 2870, 1646, 1598, 1581, 1485, 1447, 1392, 1362, 1314, 1270, 1240, 1195, 1174, 1156, 1097, 1068, 1055, 871, 791, 690 cm^{-1}.

2.2.18 2,2'-(ethane-1,2-diylbis(azanylylidene))bis(methanylylidene))diphenol: (13)[111]

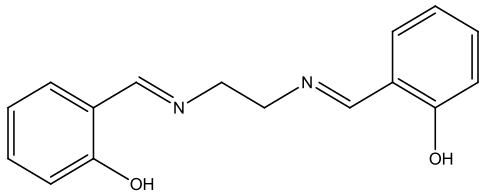

Salicylaldehyde (1.00 g, 8.18 mmol) was dissolved in methanol (50 mL), ethylenediamine (0.25 g, 4.09 mmol) was added dropwise, and heated to 120 °C for 2 h. The mixture was then cooled to room temperature and the round bottom placed in ice. A bright yellow crystalline solid (**13**) was formed. This was collected by filtration and washed with cool MeOH.

Yield: 0.88 g, 81 %. m.p.: 112-118 °C (Lit 105 °C).[112] Anal. Calc. for $C_{16}H_{16}N_2O_2$: C, 71.62; H, 6.01; N, 10.44 %; Found C, 65.75; H, 5.76; N, 9.53 %. δ_H (DMSO): 3.91 (2H, s, N-CH_2), 6.85-6.9 (4H, m, Ar-*H*), 7.29 (2H, t, Ar-*H*, *J* = 7.2 Hz), 7.40 (2H, dd, Ar-*H*, *J* = 7.6 Hz), 8.58 (2H, s, *H*C=N), 13.39 (2H, s, Ar-O*H*). δ_C (DMSO): 58.7, 116.4, 118.5, 131.6, 132.3, 160.5, 166.89. ν_{max} (KBr): 3456, 2900, 1636, 1577, 1497, 1460, 1455, 1418, 1371, 1283, 1199, 1149, 1042, 1021, 857, 742 cm^{-1}.

2.2.19 *o*-Schiff Base linked propoxy-calix[4]arene: (14)

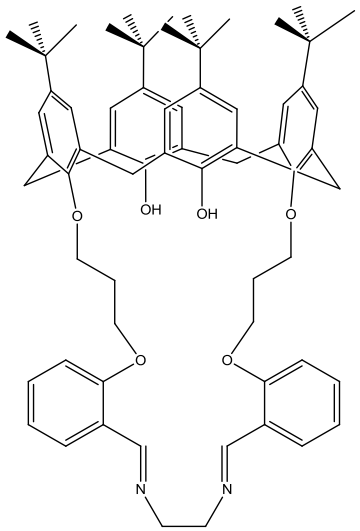

A mixture of compound **13** (100 mg, 0.36 mmol) and potassium carbonate (121 mg, 1.02 mmol) in MeCN (100 mL) was stirred at room temperature for 1 h. After this hour compound **4** (321 mg, 0.36 mmol) was added, the mixture was then heated to reflux for 72 h with vigorous stirring. This was then cooled and left to stir for 24 h at room temperature. The solvent was removed under vacuum to obtain a yellow/off white solid; this was triturated with MeOH, and the solid redissolved in $CHCl_3$:EtOH (1:1). Compound **14** precipitated as a yellow crystalline solid after two days.

Yield: 255 mg, 71%. m.p.: 188-196 °C. Anal. Calc. for $C_{68}H_{84}N_2O_6$: C, 79.65; H, 8.26; N, 2.73 %; Found C, 75.52; H, 7.68; N, 2.85 %. δ_H ($CDCl_3$): 1.01 (18H, s, *t*-Bu), 1.33 (18H, s, *t*-Bu), 2.503 (4H, t, CH_2-C*H*$_2$-CH_2, *J* = 6 Hz), 3.32 (4H, d, Ar-C*H*$_2$-Ar, *J* = 12.9 Hz), 3.951 (4H, s, C=N-C*H*$_2$), 3.99 (4H, t, O-C*H*$_2$, *J* = 6.3 Hz), 4.09 (4H, t, C*H*$_2$-O-Ar, *J* = 5.4 Hz), 4.24 (4H, d, Ar-C*H*$_2$-Ar, *J* = 12.9), 6.83-6.88 (12H, m, Ar-*H*), 6.927 (4H, d, Ar-*H*, *J* = 8.1 Hz), 7.04 (4H, s, Ar-*H*), 7.22-7.32 (14H, m, Ar-*H*), 7.72 (2H, s, Ar-O*H*), 8.36 (2H, s, *H*C=N). δ_C ($CDCl_3$): 29.3, 30.0, 30.6, 30.8, 32.4, 32.8, 33.0, 58.7, 115.9, 117.6, 124.7, 126.5, 130.4, 131.3, 131.8, 148.12, 149.5, 159.9, 165.5. ν_{max} (KBr): 3400, 3046, 2963, 2904, 2867, 1633, 1600, 1485, 1362, 1282, 1196, 1152, 932, 754 cm^{-1}.

2.2.20 Metal Complexes of ligand 14

2.2.20.1 Attempted Synthesis of Complex $Zn(14)(ClO_4)_2$

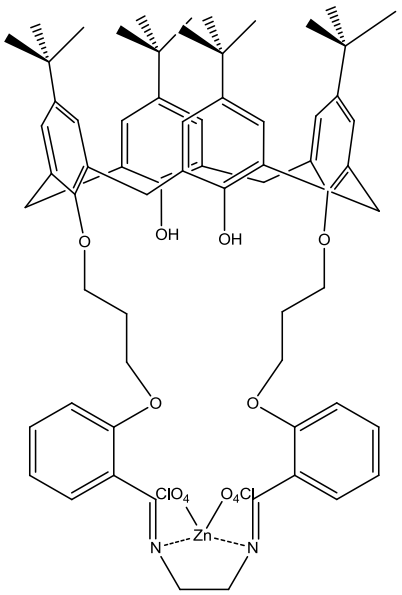

Compound **21** (10 mg, 0.010 mmol) was dissolved in $CHCl_3$ (2 mL), to this zinc perchlorate (9.33 mg, 0.025 mmol) in MeOH (5 mL) was added. This mixture was stirred for 4 h at room temperature, and the solvents removed at reduced pressure. This gave a yellow/off white solid, which was found to be the aldehyde product.

Crude Yield: 5 mg, 40 %. m.p.: 122-140 °C. δH ($CDCl_3$): ν_{max} (KBr): 3423, 2959, 2926, 2867, 1731, 1632, 1623, 1606, 1485, 1469, 1423, 1384, 1363, 1287, 1261, 1201, 1121, 1107, 1098, 1023, 873, 626 cm^{-1}.

2.2.20.2 Attempted Synthesis of Complex Hg(14)(ClO_4)$_2$

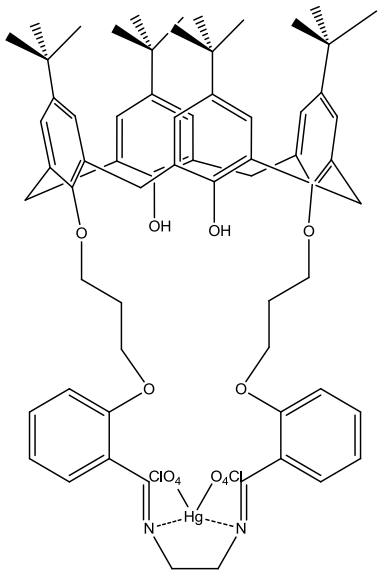

Mercury perchlorate (10 mg, 0.025 mmol) in MeOH (5 mL) was added to a stirring solution of compound **14** (10 mg, 0.010 mmol) in $CHCl_3$ (2 mL), the reaction mixture was stirred at room temperature for 12 h. A red-brown solid was obtained upon concentration of the solution, which was found to be the aldehyde product from imine hydrolysis.

Crude Yield: 6 mg, 17 %. m.p.: > 260 °C. σ_H (CDCl3): 0.99 (18H, s, *t*-Bu), 2.35 (4H, m, CH2-C*H*2-CH2), 3.64 (12H, m, O-CH_2, O-CH_2, C=N-CH_2), 4.23 (4H, m, Ar-CH_2-Ar), 6.91 (4H, s, Ar-*H*), 7.05 (12H, m, Ar-*H*), 7.60 (2H, s, Ar-O*H*), 10.34 (2H, s, *H*C=O). ν_{max} (KBr): 3406, 3237, 2961, 2905, 2868, 1658, 1600, 1484, 1460, 1393, 1362, 1297, 1240, 1201, 1121, 1108, 1104, 872, 756, 626 cm^{-1}.

2.2.20.3 Attempted Synthesis of Complex Co(14)$(ClO_4)_2$

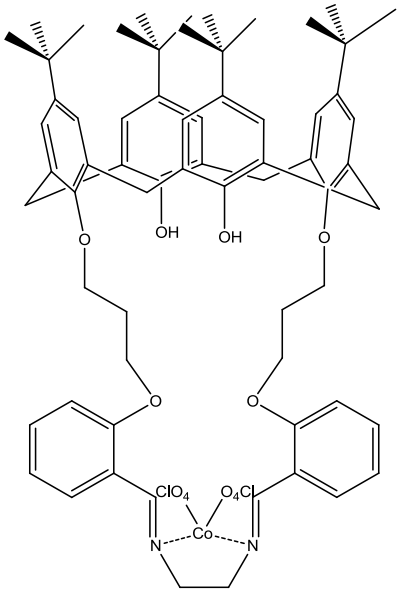

Compound **14** (10 mg, 0.010 mmol) in $CHCl_3$ (3 mL) and cobalt perchlorate (9.2 mg, 0.025 mmol) in MeOH (6 mL) were stirred at room temperature for 8 h. The solution was concentrated under reduced pressure to yield a brown solid, which was determined to be the aldehyde product from imine hydrolysis.

Crude Yield: 6 mg, 48 %. m.p.: 120-122 °C. ν_{max} (KBr): 3613, 3529, 3414, 2960, 2904, 2867, 1686, 1639, 1600, 1484, 1458, 1392, 1362, 1298, 1195, 1097, 872, 756, 626 cm^{-1}.

2.2.20.4 Attempted Synthesis of Complex Cu(14)$(ClO_4)_2$

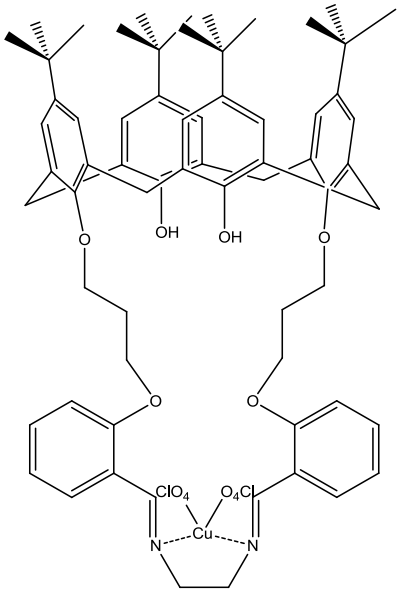

Compound **14** (10.0 mg, 0.010 mmol) was dissolved in $CHCl_3$ (3 mL). To this copper perchlorate (9.3 mg, 0.025 mmol) in MeOH (6 mL) was added, the reaction mixture was stirred at room temperature for 8 h. The solvents were removed under reduced pressure to yield a green solid, which was found to be the aldehyde product.

Crude Yield: 8 mg, 64 %. m.p.: 188-190 °C. ν_{max} (KBr): 3453, 2961, 2905, 2867, 1639, 1600, 1484, 1459, 1362, 1298, 1288, 1241, 1195, 1112, 1088, 872, 757, 626 cm^{-1}.

2.2.20.5 Attempted Synthesis of Complex Ni(14)$(ClO_4)_2$

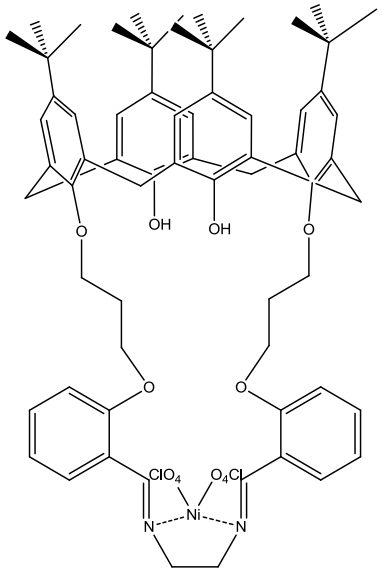

Nickel perchlorate (9.2 mg, 0.025 mmol) in MeOH (6 mL) was added to a stirring solution of compound **14** (10.0 mg, 0.01 mmol) in $CHCl_3$ (3 mL), the resulting mixture was stirred at room temperature for 8 h. The solution was concentrated under vacuum to yield yellow/green solid which was found to be the aldehyde product.

Crude Yield: 7 mg, 22 %. m.p.: 162- 168 °C. ν_{max} (KBr): 3405, 2961, 2905, 2872, 1687, 1625, 1600, 1484, 1459, 1362, 1298, 1288, 1240, 1194, 1139, 1110, 1089, 872, 757, 626 cm^{-1}.

2.2.21 *o*-Schiff Base linked butoxy-calix[4]arene: (15)

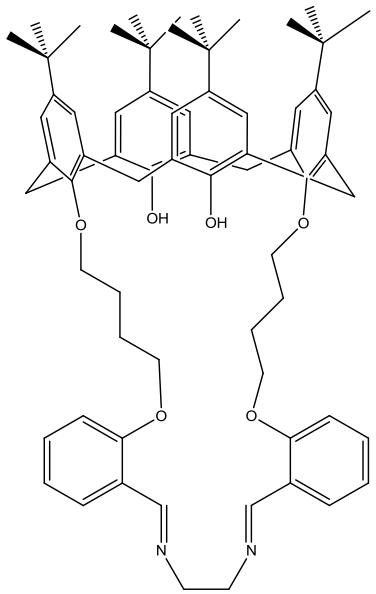

A mixture of compound **13** (26.8 mg, 10 mmol) and potassium carbonate (34.5 mg, 25 mmol) was dissolved in MeCN (250 mL) and heated to reflux for 1 h. Compound **5** (166 mg, 0.186 mmol) was added, and the reaction mixture was heated to reflux for 48 h, and then cooled to room temperature. The inorganic salts formed were filtered and the filtrate concentrated on a rotary evaporator, **15** was obtained as a pale yellow solid by slow diffusion of MeOH in DCM.

Yield: 51 mg, 27 %. m.p.: 168-178 °C. Anal. Calc. for $C_{68}H_{84}N_2O_6$: C, 79.65; H, 8.26; N, 2.73; Found: C, 77.96; H, 8.41; N, 2.20 %. δ_H ($CDCl_3$): 0.99 (18H, s, *t*-Bu), 1.34

(18H, s, *t*-Bu), 2.82 (8H, q, CH_2-C*H*$_2$-C*H*$_2$-CH_2, *J* = 6.6 Hz), 3.29 (4H, d, Ar-C*H*$_2$-Ar, *J* = 12.9 Hz), 4.03 (12H, m, O-C*H*$_2$, O-C*H*$_2$, C=N-C*H*$_2$), 4.21 (4H, d, Ar-C*H*$_2$-Ar, *J* = 12.9 Hz), 6.82 (4H, s, Ar-*H*), 6.89 (4H, m, Ar-*H*), 7.10 (4H, s, Ar-*H*), 7.36 (2H, s, Ar-O*H*), 7.93 (2H, dd, Ar-*H*, *J* = 7.6 Hz), 8.71 (2H, s, *H*C=N). δ_C ($CDCl_3$): 29.7, 30.0, 30.6, 32.7, 32.9, 60.9, 66.7, 74.7, 110.8, 119.5, 124.1, 124.5, 126.6, 131.7, 140.4, 145.9, 148.7, 149.7, 157.0, 158.5, 160.2. ν_{max} (KBr): 3398, 2958, 2930, 2867, 1668, 1633, 1599, 1485, 1456, 1391, 1362, 1298, 1240, 1200, 1122, 871, 819, 801, 752 cm^{-1}.

2.2.22 Metal complexes of ligand 15

2.2.22.1 Attempted Synthesis of Complex Zn(15)$(ClO_4)_2$

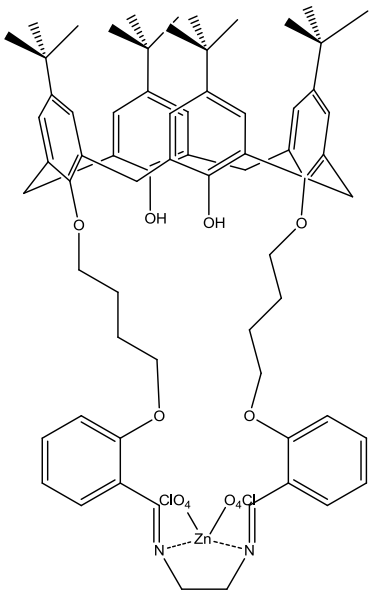

A mixture of ligand **15** (25 mg, 0.025 mmol) and zinc(II) perchlorate (22.39 mg, 0.06mmol) in a $CHCl_3$/MeOH (1:2) was stirred at room temperature for 8 h. The organic solvents were removed under vacuum to leave a white solid. The complex was separated from excess perchlorate using $CHCl_3$. After removal of solvent an off white/yellow solid was obtained, which was found to be the aldehyde product.

Crude Yield: 19 mg, 59 %. m.p.: 168-226 °C. ν_{max} (KBr): 3489, 2961, 2906, 2868, 1689, 1599, 1485, 1458, 1391, 1362, 1300, 1260, 1241, 1196, 1106, 1093, 871, 802, 755, 627 cm^{-1}.

2.2.22.2 Attempted Synthesis of Complex $Cu(15)(ClO_4)_2$

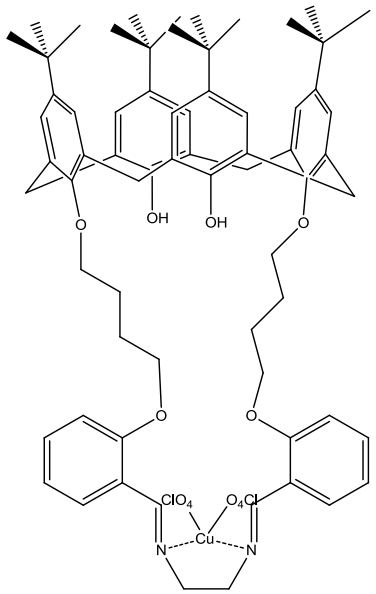

Compound **15** (11.2 mg, 0.011 mmol) was dissolved in $CHCl_3$ (3 mL). To this stirring solution copper perchlorate (8.1 mg, 0.022 mmol) in MeOH (6 mL) was added, the reaction mixture was stirred at room temperature for 8 h. The solution was concentrated under reduced pressure and dried in an oven (75 °C) overnight. This gave a brown solid which was determined to be the aldehyde product.

Crude Yield: 8 mg, 56 %. m.p.: >300 °C. ν_{max} (KBr): 3432, 2956, 2875, 2863, 1600, 1485, 1362, 1299, 1121, 1108, 871, 720, 625 cm^{-1}.

2.2.23 Attempted synthesis of *o*-Schiff Base linked ethoxy-calix[4]arene: (16)

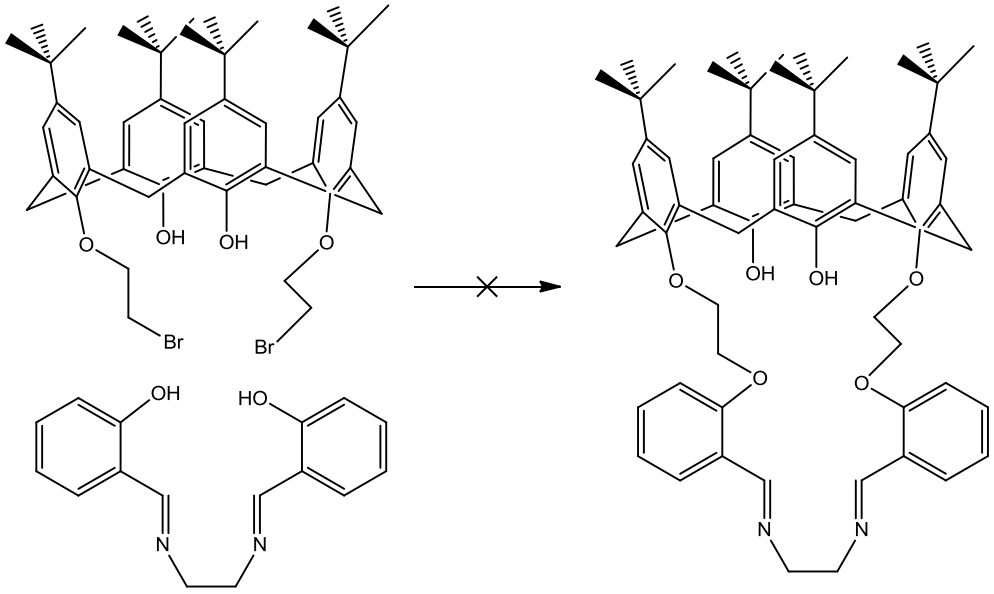

A mixture of compound **14** (0.125 g, 0.46 mmol) and potassium carbonate (0.161 g, 1.16 mmol) dissolved in MeCN (50 mL) and stirred for 1 h at ambient temperature. At this point compound **3** (0.40 g, 0.46 mmol) was added and heated to reflux for 48 hours, the mixture was cooled to room temperature and the inorganic salts formed filtered. The filtrate was concentrated under reduced vacuum and the residue was redissolved in $CHCl_3$:EtOH solvent mix to yield a brown ppt.

2.3 Fluorescence Spectroscopy of Ligands from section 2.2

2.3.1 Overview and Parameters

$CHCl_3$ solutions of the Schiff base linked calix[4]arenes were successfully prepared. All samples were run at room temperature as 100 μM solutions of their proposed structures. UV-Vis spectra were recorded to determine the absorption maxima. The parent calix[4]arene has an absorption max at 280 nm.[4]

2.3.2 Fluorescence Data

Table 2.1: Absorption maxima were used as an excitation parameter to generate emission spectra, with maximum (λ_f^{em}). It was intended to use this parameter to generate an excitation spectrum but No Fluorescence was Observed (NFO) for any of the ligands.

Sample No.	**Absorption Peaks nm**			λ_f^{em}
7	228.0	272.0		NFO
8	269.2	243.6		NFO
10	242.5	291.5		NFO
11	250	291	310	NFO
14	230.0	284.0		NFO

2.3.3 Fluorescence Spectroscopy of selected metal complexes

Although the parent ligands exhibited no observable fluorescence, some of the metal complexes which showed interesting colour changes (2.2.8.5 and 2.2.10.2) were screened for fluorescent behaviour. The UV-Vis spectrum of each compound was used to determine the excitation wavelength (λ_f^{ex}). The emission would be recorded upon excitation at this wavelength. The peak emission wavelength (λ_f^{em}) was recorded, but as in the case of the parent ligands no fluorescent behaviour was observed (NFO).

Table 2.2: Absorption peaks and fluorescence emission max (nm) for screened metal complexes.

Sample	**Absorption Peaks nm**	λ_f^{em}
Hg(**7**)$(ClO_4)_2$	280	NFO
Hg(**8**)$(ClO_4)_2$	280	NFO

2.4 Synthesis of Calix[4]arene triazole derivatives and their metal complexes

2.4.1 5,11,17,23-tetra-*tert*-butyl-25,27–dihydroxy-26,28-bis(propargyl)calix[4]arene: (17)[113]

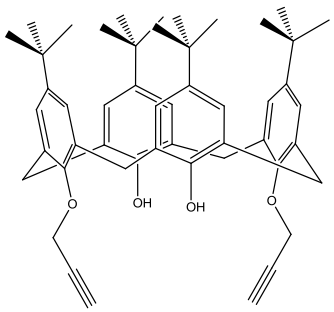

A mixture of **2** (3.86 g, 5.90 mmol) and potassium carbonate (1.97 g, 14.3 mmol) in acetone (100 mL) were heated to reflux with stirring for 2 h. Aat this point propargyl bromide (2.40 g, 20.3 mmol) was added dropwise. The resulting mixture was heated to reflux for 24 h. After cooling the reaction mixture was filtered, and filtrated reduced to dryness, the residue was triturated with MeOH to give a white solid. This solid was recrystallized from $CHCl_3$ by addition of MeOH, and purified further on silica gel using ethyl acetate/petroleum ether mix (1:2), giving **17**.

Yield: (2.65 g, 62 %), m.p.: 222-226 °C (Lit. 220-222 °C)[114], Anal Calc. C, 82.83; H, 8.34; N, 0.0; Found: C, 80.21; H, 8.34; N, 0.0 %. δ_H ($CDCl_3$): 0.90 (18H, s, *t*-Bu), 1.30 (18H, s, *t*-Bu), 2.53 (2H, t, C≡C*H*, *J* = 2.4 Hz), 3.31 (4H, d, Ar-CH_2-Ar, *J* = 13.35), 4.35 (4H, d, Ar-CH_2-Ar, *J* = 13.29 Hz), 4.74 (4H, d, O-CH_2, *J* = 2.43 Hz), 6.49 (2H, s, Ar-O*H*), 6.72 (4H, s, Ar-*H*), 7.07 (4H, s, Ar-*H*). δ_C ($CDCl_3$): 30.9, 31.7, 32.0, 33.9, 63.31, 76.3, 125.0, 125.5, 128.0, 132.5, 141.6, 147.2, 149.4, 150.3. ν_{max} (KBr): 3435, 3312, 3289, 2957, 2905, 2866, 2119, 1485, 1392, 1362, 1302, 1024, 1189, 1174, 1122, 1004, 924, 872, 666, 641 cm^{-1}.

2.4.2 5,11,17,23-tetra-*tert*-butyl-25,27–dihydroxy-26,28-bis(2-azidoethoxy)calix[4]arene: (18)[70]

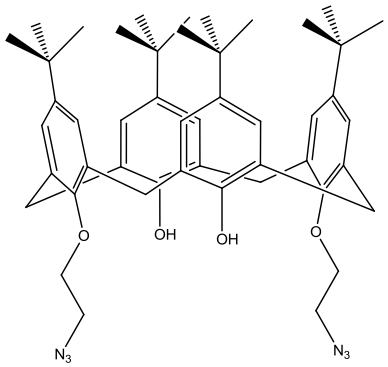

3 (100 mg, 0.11 mmol), sodium azide (28 mg, 0.46 mmol) and caesium chloride (10 mg) were dissolved in DMF (10 mL) in a round bottomed flask. This mixture was heated to 90°C for 4.5 hours; the mixture was then cooled to room temperature. A white ppt was obtained when this mixture was added to cold water. **18** was collected by filtration and washed with water (3 X 50 mL).

Yield: 74.8 mg, 82 %. δ_H ($CDCl_3$): 0.99 (18H, s, *t*-Bu), 1.30 (18H, s, *t*-Bu), 3.30 (4H, d, Ar-C*H*$_2$-Ar, *J* = 13.2 Hz), 3.83 (4H, t, C*H*$_2$-N_3, *J* = 5.1 Hz), 4.05 (4H, t, O-C*H*$_2$, *J* = 4.2 Hz), 4.29 (4H, d, Ar-C*H*2-Ar, *J* = 13.5 Hz), 6.77 (4H, s, Ar-*H*), 6.98 (2H, s, Ar-O*H*), 7.07 (4H, s, Ar-*H*). δ_C ($CDCl_3$): 30.9, 31.4, 31.7, 32.2, 51.2, 74.4, 125.0, 125.6. ν_{max} (KBr): 3428, 2961, 2904, 2867, 2107, 1677, 1484, 1362, 1300, 1239, 1200, 1123, 1107, 872 cm^{-1}.

2.4.3 5,11,17,23-tetra-*tert*-butyl-25,27–dihydroxy-26,28-bis(2-azidopropoxy)calix[4]arene: (19)[115]

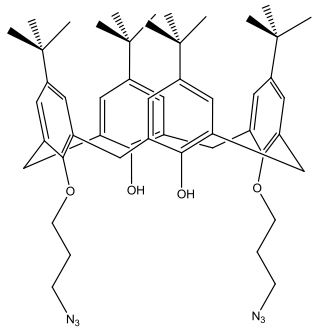

Compound **4** (1.0 g, 1.20 mmol), sodium azide (0.313 g, 4.81 mmol) and caesium chloride (5 mg) were dissolved in DMF (30 mL) in a round bottomed flask. This mixture was heated to 90 °C for 4.5 hours; the mixture was then cooled to room temperature. A white ppt was obtained when this mixture was added to cold water. **19** was collected by filtration and washed with water (3 X 50 mL).

Yield: 0.67 g, 74%. δ_H ($CDCl_3$): 1.00 (18H, s, *t*-Bu), 1.27 (18H, s, *t*-Bu), 2.23 (4H, q, CH_2-C*H*$_2$-CH_2, *J* = 6.0 Hz), 3.32 (4H, d, Ar-C*H*$_2$-Ar, *J* = 12.9 Hz), 3.86 (4H, t, Br-C*H*$_2$, *J* = 6.6 Hz), 4.04 (4H, t, O-C*H*$_2$, *J* = 5.7 Hz), 4.20 (4H, d, Ar-C*H*$_2$-Ar, *J* = 12.9 Hz), 6.85 (4H, s, Ar-*H*), 7.04 (2H, s, Ar-O*H*), 7.60 (4H, s, Ar-*H*). δ_C ($CDCl_3$): 29.67, 31.08, 31.73, 34.05, 48.25, 72.64, 125.23, 125.70, 127.58, 131.89, 141.55, 145.63, 147.26, 149.31. ν_{max} (KBr): 3419, 2960, 2904, 2867, 2097, 1480, 1435, 1414, 1362, 1302, 1285, 1239, 1201, 1123, 1097, 1023, 927, 873 cm^{-1}.

2.4.4 5,11,17,23-tetra-*tert*-butyl-25,27–dihydroxy-26,28-bis(2-azidobutoxy)calix[4]arene: (20)[115]

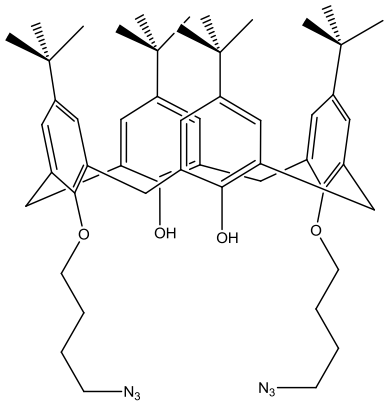

5 (1.0 g, 1.20 mmol), sodium azide (0.313 g, 4.81 mmol) and caesium chloride (5 mg) were dissolved in DMF (30 mL) in a round bottomed flask. This mixture was heated to 90 °C for 4.5 hours; the mixture was then cooled to room temperature. A white ppt. was obtained under vacuum after this mixture was added to cold water. **20** was collected by filtration and washed with water (3 X 50 mL).

Yield: 56.67 mg, 56 %. δ_H ($CDCl_3$): 0.96 (18H, s, *t*-Bu), 1.28 (18H, s, *t*-Bu), 2.06 (8H, m, CH_2-C*H*$_2$-C*H*$_2$-CH_2), 3.29 (4H, d, Ar-C*H*$_2$-Ar, *J* = 12.9 Hz), 3.47 (4H, t, C*H*$_2$-N_3, *J* = 6.3 Hz), 3.97 (4H, t, O-C*H*$_2$, *J* = 5.4 Hz), 4.21 (4H, d, Ar-C*H*$_2$-Ar, *J* = 12.9 Hz), 6.80 (4H, s, Ar-*H*), 7.05 (2H, s, Ar-*H*), 7.43 (4H, s, Ar-O*H*). δ_C ($CDCl_3$): 25.8, 27.3, 31.0, 33.8, 33.9, 51.3, 75.6, 125.1, 125.5, 127.6, 132.5, 141.5, 146.9, 149.7, 150.6. ν_{max} (KBr): 3405, 2961, 2905, 2868, 2096, 1485, 1362, 1300, 1266, 1255, 1201, 1123, 872 cm^{-1}.

2.4.5 5,11,17,23-tetra-*tert*-butyl-25,27–dihydroxy-26,28-bis(ethoxy-triazo-methoxy) dicalix[4]arene: (21)

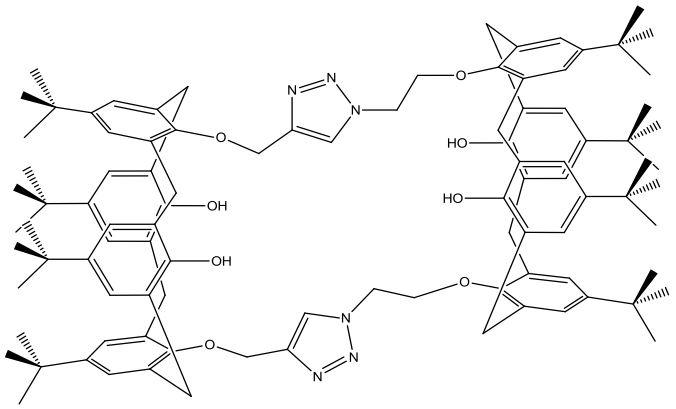

Compound **18** (83 mg, 0.10 mmol) and compound **17** (76.5 mg, 0.10 mmol) were dissolved in DMF (10 mL). To this stirring mixture copper sulphate (3 mg, 0.01 mmol) and sodium ascorbate (21 mg, 0.10 mmol) were added. The mixture was heated to 90 °C for 86 h. After cooling to room temperature the reaction mixture was poured into water (50 mL), and the product was extracted with EtOAc (200 mL), this was then dried over $MgSO_4$. The crude product was purified by column chromatography (silica gel) with DCM as eluent. **21** obtained as an off white solid.

Yield: 20 mg, 13 %. m.p.: >260 °C (Lit > 250 °C).[71] *m/z* Calc $[M+H]^+$ for $C_{98}H_{122}N_6O_8$ Calculated; 1512.943, Found; 1512.944. δ_H ($CDCl_3$): 0.97 (36H, s, *t*-but), 1.20 (36H, s, *t*-Bu), 3.29 (8H, m, Ar-CH_2-Ar), 4.10 (8H, m, Ar-CH_2-Ar), 4.50 (4H, t, CH_2-O, J = 4.8 Hz), 5.14 (4H, t, CH_2-Triazole, J = 7.5 Hz), 5.25 (4H, s, Triazole-CH_2-O), 6.83 (8H, s, Ar-*H*), 6.91 (2H, s, Ar-O*H*), 7.02 (16H, m, Ar-*H*), 7.60 (2H, s Ar-O*H*), 8.55 (2H, s, Triazole-*H*). δ_C ($CDCl_3$): 29.7, 31.0, 31.5, 31.7, 33.8, 33.9, 46.2, 70.4, 111.9, 125.2, 125.6, 125.9, 127.6, 150.2. ν_{max} (KBr): 3440, 2996, 2961, 1635, 1484, 1384, 1362, 1201, 1123, 872, 727 cm^{-1}.

2.4.6 5,11,17,23-tetra-*tert*-butyl-25,27–dihydroxy-26,28-bis(propoxy-triazo-methoxy) dicalix[4]arene: (22)

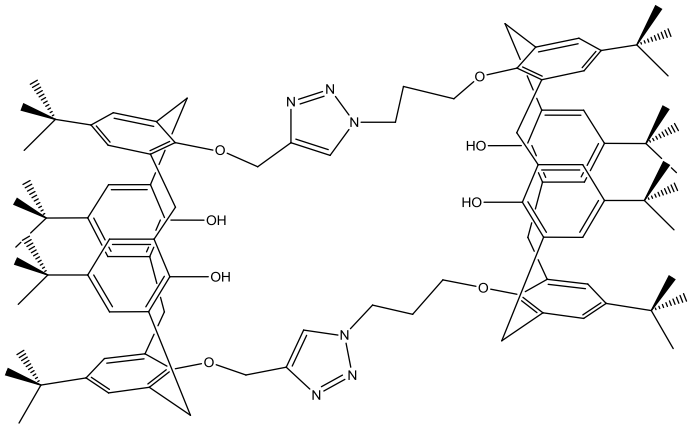

Compound **17** (82 mg, 0.11 mmol) and compound **19** (100 mg, 0.11 mmol) were dissolved in DMF (15 mL) to this stirring mixture sodium ascorbate (23 mg, 0.11 mmol) and copper sulphate pentahydrate (2.8 mg, 0.011 mmol) were added. The resulting mixture was heated to 90 °C for 17 h, and then cooled to room temperature. The reaction mixture was poured into water (50 mL), and then extracted with ethyl acetate (200 mL), the solvent was removed by vacuum. The red solid formed was taken up in DCM:EtOAC to give white crystals **22**.

Yield: 32 mg, 19 %. m.p.: 172-178 °C. *m/z* Calc $[M+H]^+$ for $C_{100}H_{126}N_6O_8$ Calculated; 1540.9743, Found; 1540.9766. δ_H ($CDCl_3$): 0.95 (18H, s, *t*-Bu), 1.04 (18H, s, *t*-Bu), 1.27 (18H, s, *t*-Bu), 1.29 (18H, s, *t*-Bu), 2.67 (4H, m, CH_2-C*H*$_2$-CH_2), 3.31-3.38 (8H, m, Ar-C*H*$_2$-Ar), 4.30 (8H, m, Ar-C*H*$_2$-Ar), 4.50 (4H, t, O-C*H*$_2$, *J* = 5.7 Hz), 5.13 (4H, t, Triazole-C*H*$_2$, *J* = 6.0 Hz), 5.25 (4H, s, Triazole-C*H*$_2$-OAr), 6.81 (4H, s, Ar-*H*), 6.91 (4H, s, Ar-*H*), 7.04 (8H, d, Ar-*H*, *J* = 5.7 Hz), 7.22 (2H, s, Ar-O*H*), 7.94 (2H, s, Triazole-*H*), 8.13 (2H, s, Ar-O*H*). δ_C ($CDCl_3$): 30.9, 31.0, 31.6, 31.7, 33.8, 34.0, 125.0, 125.2, 125.5, 125.7, 125.8, 132.5, 132.8, 150.5. ν_{max} (KBr): 3416, 2961, 2926, 2866, 1736, 1600, 1485, 1464, 1392, 1362, 1300, 1240, 1202, 1123, 1096, 1044, 946, 871, 720 cm^{-1}.

2.4.7 5,11,17,23-tetra-*tert*-butyl-25,27–dihydroxy-26,28-bis(butoxy-triazo-ethoxy) dicalix[4]arene: (23)

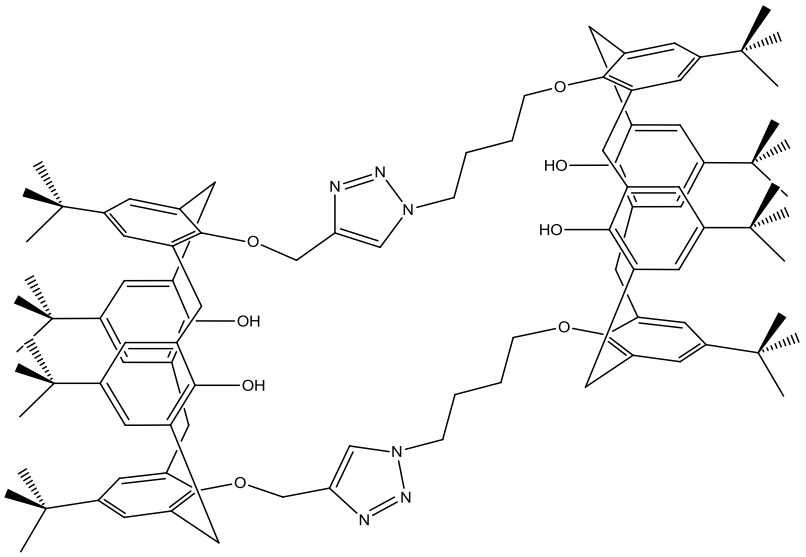

Compound **17** (30 mg, 0.035 mmol) and compound **20** (26 mg, 0.035 mmol) were stirred in DMF (5 mL) and sodium ascorbate (6.35 mg, 0.030 mmol) and copper sulphate (1 mg, 0.08 mmol) were added. The reaction mixture was heated to 90 °C for 18 h, and then cooled to room temperature. This was then poured into water 50 mL and the product extracted with EtOAc (200 mL), the solution was concentrated under reduced pressure and the red residue obtained was purified, by elution with DCM on silica gel, and crystallisation with DCM:Petroleum Ether (1:1) mixture to give light brown crystals **23**.

Yield: 29 mg, 52 %. m.p.: 232- 236 °C. *m/z* Calc $[M-H]^+$ for $C_{102}H_{126}N_6O_8$ Calculated; 1567.996, Found; 1563.961. δ_H ($CDCl_3$): 0.89 (32H, s, *t*-Bu), 1.11 (32H, s, *t*-Bu), 2.63 (4H, m, CH_2-C*H*$_2$-C*H*$_2$-CH_2), 3.30 (8H, m, Ar-C*H*$_2$-Ar, Ar-C*H*$_2$-Ar), 4.18 (4H, t, O-C*H*$_2$, *J* = 6.4 Hz), 4.27 (8H, m, Ar-C*H*$_2$-Ar, Ar-C*H*$_2$-Ar), 4.98 (4H, t, triazole-C*H*$_2$, *J* = 6 Hz), 5.13 (4H, s, triazole-C*H*$_2$-O), 6.81 (4H, s, Ar-*H*), 6.90 (4H, s, Ar-*H*), 7.04/7.06 (8H, 2 x s, Ar-*H*), 7.21 (2H, s, Ar-O*H*), 7.90 (2H, s, Ar-O*H*), 8.13 (2H, s, Triazole-*H*). δ_C ($CDCl_3$): 28.6, 29.9, 30.3, 30.4, 30.6, 32.8, 113.1, 122.4, 124.2, 124.7, 156.5,

130.8, 131.5, 131.8, 137.7, 146.3, 148.6, 149.5, 192.2. ν_{max} (KBr): 3425, 2963, 1633, 1484, 1464, 1384, 1367, 1362, 1261, 1203, 1123, 1097, 1023, 803 cm^{-1}.

2.4.8 4-(prop-2-yn-1-yloxy)benzaldehyde: (24)[116]

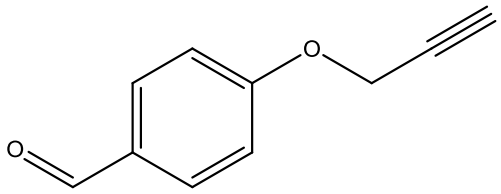

4-Hydroxybenzaldehyde (2.00 g, 16.4 mmol) and potassium carbonate (4.53 g, 32.8 mmol) were dissolved in acetone (250 mL), and this mixture was stirred at room temperature for 2 h. Propargyl bromide (2.34 g, 19.68 mmol) was added to this stirring mixture, which was then heated to reflux for 5 h, after which the reaction mixture was cooled to room temperature. The solvent was removed under vacuum, yielding **24**.

Yield: 2.44 g, 93 %. m.p.: 66-70 °C (Lit 85 °C).[117] *m/z* Calc $[M+H]^+$ for $C_{10}H_8O_2$ Calculated; 161.0597, Found; 161.0593. Anal. Calc. for $C_{10}H_8O_2$: C, 74.99; H, 5.03; N, 0.0 %; Found C, 73.53; H, 4.69; N, 3.61 %. δ_H ($CDCl_3$): 2.57 (1H, t, C≡C*H*, *J* = 2.4Hz), 4.77 (2H, s, O-CH_2), 7.07 (2H, d, Ar-*H*, *J* = 4.5 Hz), 7.84 (2H, d, Ar-*H*, *J* = 4.8 Hz), 9.90 (1H, s, *H*C=O). δ_C ($CDCl_3$): 55.8, 76.4, 78.3, 115.1, 130.8, 131.6, 162.3, 190.8. ν_{max} (NaCl): 3213, 2833, 1681, 1603, 1578, 1507, 1248, 1216, 1169, 1022, 832 cm^{-1}.

2.4.9 5,11,17,23-tetra-*tert*-butyl-25,27–dihydroxy-26,28-bis-propoxy-(triazo-*p*-benzaldehyde) calix[4]arene: (25)

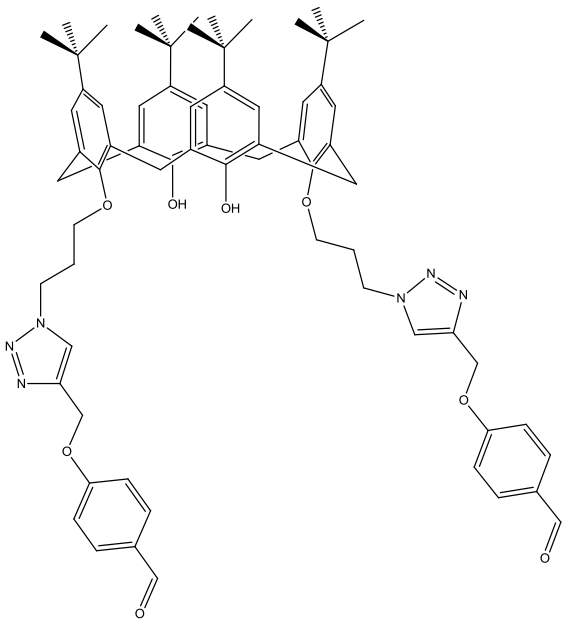

A mixture of compound **24** (42 mg, 0.25 mmol) and compound **19** (100 mg, 0.12 mol) was dissolved in DCM (25 mL) and water (25 mL). To this mixture copper sulphate (3.1 mg, 0.01 mmol) and sodium ascorbate (25 mg, 0.12 mmol) were added. This reaction mixture was heated to reflux for 24 h, and then cooled to room temperature. The product **25** was precipitated as an off-white solid from DCM: Petroleum Ether.

Yield: 84 mg, 62 %. m.p.: 214-228 °C. *m/z* Calc [M+H] for $C_{70}H_{82}N_6O_8$ Calculated; 1135.6267, Found; 1135.6181. δ_H ($CDCl_3$): 0.96 (18H, s, *t*-Bu), 1.29 (18H, s, *t*-Bu), 2.61 (4H, m, CH_2-C*H*$_2$-CH_2), 3.29 (4H, d, Ar-C*H*$_2$-Ar, *J* = 12.9 Hz), 3.99 (4H, t, O-C*H*$_2$, *J* = 5.4 Hz), 4.13 (4H, d, Ar-C*H*$_2$-Ar, *J* = 12.9 Hz), 4.88 (4H, m, C*H*$_2$-Triazole), 5.24 (4H, s, Trizaole-C*H*$_2$-O), 6.81 (4H, s, Ar-*H*), 7.03 (4H, d, Ar-*H*, *J* = 11.1 Hz), 7.11 (4H, s, Ar-*H*), 7.42 (2H, s, Ar-O*H*), 7.77 (4H, d, Ar-*H*, *J* = 8.4 Hz), 7.95 (2H, s, Triazole-*H*), 9.90 (2H, s, *H*C=O). δ_C ($CDCl_3$): 30.8, 30.9, 31.7, 33.9, 34.0, 47.3, 62.0, 72.1, 115.0, 125.3, 125.7, 127.6, 130.3, 132.0, 132.3, 142.3, 147.6, 149.1, 150.2, 163.1, 190.8. ν_{max} (KBr): 3423, 2960, 2920, 2903, 2867, 1687, 1657, 1647, 1601, 1579, 1509, 1485, 1384, 1347, 1249, 1217, 1161, 871, 673 cm^{-1}.

2.4.10 3-(prop-2-yn-1-yloxy)benzaldehyde: (26)

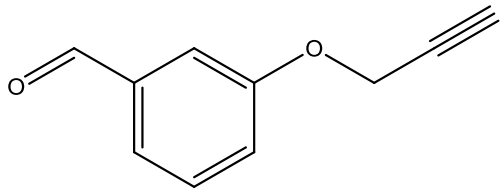

3-Hydroxybenzaldehyde (2.00 g, 16.4 mmol) was dissolved in MeCN (250 mL) with potassium carbonate (4.53 g, 32.8 mmol) and stirred for 1 h. To this mixture propargyl bromide (2.34 g, 19.68 mmol) was added, and the reaction mixture was heated to reflux for 5 h. The mixture was then cooled and filtered, and the solvent was removed at low pressure. The yellow oil yielded was purified by column chromatography with dichloromethane as eluent to give **26** as yellow oil. Cooling with in ice gives yellow crystalline solid.

Yield: 1.63 g, 62 %. m.p.: 30-34 °C. *m/z* Calc $[M+H]^+$ for $C_{10}H_8O_2$ Calculated; 161.0597, Found; 161.0592. δ_H ($CDCl_3$): 2.55 (1H, t, C≡C*H*, *J* = 2.4 Hz), 4.76 (2H, s, O-CH_2), 7.25 (1H, m, Ar-*H*), 7.45-7.54 (3H, m, Ar-*H*), 9.98 (1H, s, *H*C=O). δ_C ($CDCl_3$): 59.9, 76.1, 77.8, 113.4, 122.1, 124.2, 130.2, 137.7, 158.0, 191.9. ν_{max} (NaCl): 3300, 3055, 2826, 1701, 1594, 1484, 1387, 1321, 1265, 1243, 1167, 1148, 1037, 790, 738 cm^{-1}.

2.4.11 5,11,17,23-tetra-*tert*-butyl-25,27–dihydroxy-26,28-bis-propoxy-(triazo-*o*-benzaldehyde) calix[4]arene: (27)

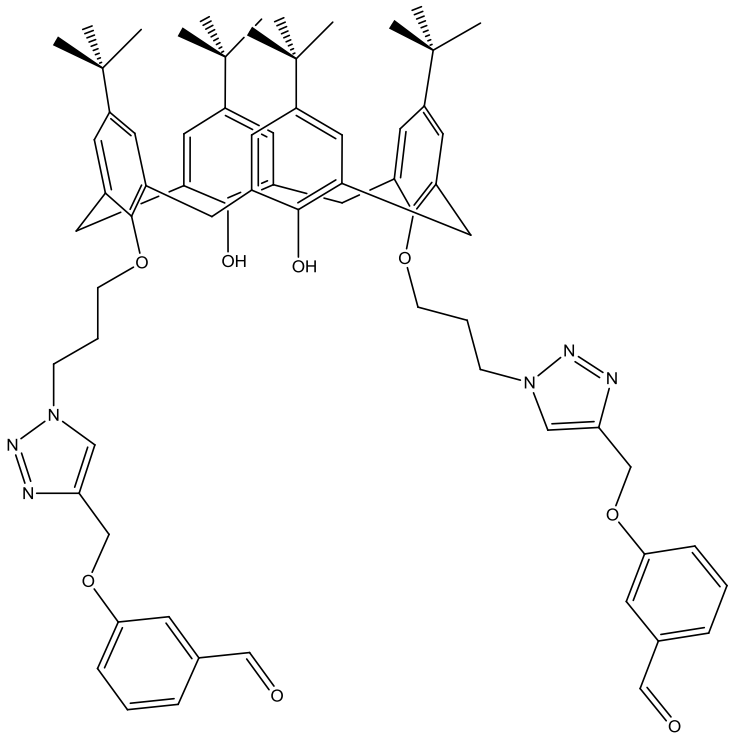

A mixture of compound **26** (42 mg, 0.25 mmol) and compound **19** (100 mg, 0.12 mol) was dissolved in DCM (25 mL) and water (25 mL). To this mixture copper sulphate (3.1 mg, 0.01 mmol) and sodium ascorbate (25 mg, 0.12 mmol) were added. This reaction mixture was heated to reflux for 24 h, and then cooled to room temperature. The product **27** was precipitated as an off-white solid from DCM: Petroleum Ether.

Yield: 66 mg, 48 %. m.p.: 218-232 °C. *m/z* Calc [M+H] for $C_{70}H_{82}N_6O_8$ Calculated; 1135.6267, Found; 1135.6252. δ_H ($CDCl_3$): 0.97 (18H, s, *t*-Bu), 1.28 (18H, s, *t*-Bu), 2.62 (4H, m, CH_2-C*H*$_2$-CH_2), 3.29 (4H, d, Ar-CH2-Ar, *J* = 13.2 Hz), 3.98 (4H, t, O-C*H*$_2$, *J* = 5.4 Hz), 4.88 (4H, m, C*H*$_2$-Triazole), 5.22 (4H, s, O-C*H*$_2$-Triazole), 6.82 (4H, s, Ar-*H*), 7.08 (4H, s, Ar-*H*), 7.16 (2H, d, Ar-*H*, *J* = 7.8 Hz), 7.46 (8H, m, Ar-*H*, Ar-O*H*), 7.98 (2H, s, Triazole-*H*), 9.98 (2H, s, *H*C=O). δ_C($CDCl_3$): 30.8, 30.9, 31.49, 31.6, 33.8, 34.0, 47.2, 55.9, 62.1, 72.2, 113.6, 121.8, 122.1, 123.5, 125.3, 125.7, 127.6, 132.3, 137.7, 142.1, 147.5, 149.2, 150.2, 158.8, 192.0. ν_{max} (KBr): 3425, 2960, 2924,

2904, 2868, 2906, 1698, 1596, 1587, 1485, 1461, 1449, 1391, 1385, 1362, 1287, 1260, 1243, 1201, 1168, 1034, 872 cm^{-1}.

2.4.12 2-(prop-2-yn-1-yloxy)benzaldehyde: (28)

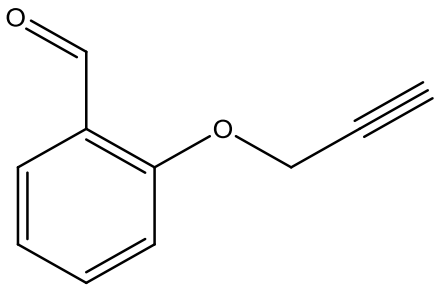

Salicylaldehyde (2.00 g, 16.4 mmol) was dissolved in MeCN (250 mL) with potassium carbonate (4.53 g, 32.8 mmol) and stirred for 2 h; propargyl bromide (2.34 g, 19.68 mmol) was added. This reaction mixture was heated to reflux for 5 h, it was then cooled, filtered and the solvent removed under vacuum. This yielded **28** as a brown crystalline solid.

Yield: 2.37 g, 90 %. m.p.: 60-62 °C (Lit 60-62 °C).[58] *m/z* Calc $[M+H]^+$ for $C_{10}H_8O_2$ Calculated; 161.0597, Found; 161.0593. Anal. Calc. for $C_{10}H_8O_2$: C, 74.99; H, 5.03; N, 0.0 %; Found C, 73.21; H, 4.79; N, 3.22%. δ_H ($CDCl_3$): 2.56 (1H, t, C≡C*H*, *J* = 2.4 Hz), 4.83 (2H, s, O-CH_2), 7.07-7.14 (2H, m, Ar-*H*), 7.55-7.59 (1H, m, Ar-*H*), 7.85-7.88 (1H, m, Ar-*H*), 10.49 (1H, s, *H*C=O) δ_C ($CDCl_3$): 56.3, 76.5, 77.7, 113.2, 121.6, 125.4, 128.5, 135.4, 159.7, 189.5. ν_{max} (NaCl): 3301, 3054, 2872, 1690, 1600, 1483, 1460, 1400, 1304, 1288, 1265, 1220, 1191, 1163, 1021, 737, 703 cm^{-1}.

2.4.13 5,11,17,23-tetra-*tert*-butyl-25,27–dihydroxy-26,28-bis-propoxy-(triazo-salicyalydehye) calix[4]arene: (29)

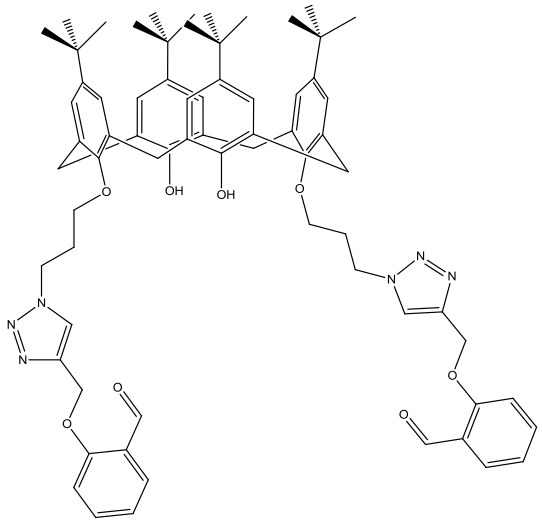

Compound **19** (250 mg, 0.03 mmol) and compound **28** (98.25 mg, 0.06 mmol) were dissolved in a DCM and water mixture (25 mL: 25 mL), copper sulphate (153.16 mg, 0.06 mmol) and sodium ascorbate (121.52 mg, 0.06 mmol) were added and the mixture heated to reflux for 120 h. The reaction mixture was cooled and the product extracted with DCM (100 mL), the combined organic extracts were washed with brine (200 mL) and dried over $MgSO_4$. The solution was dried under reduced pressure and the product was precipitated from DCM:Petroleum Ether, giving **29** as an off white solid.

Yield: 30 mg, 88 %; m.p.: 230-234 °C, *m/z* Calc [M+H] for $C_{70}H_{82}N_6O_8$ Calculated; 1135.6267, Found; 1135.6191. δ_H ($CDCl_3$): 0.96 (18H, s, *t*-Bu), 1.27 (18H, s, *t*-Bu), 2.61 (4H, q, CH_2-C*H*$_2$-CH_2, *J* = 6 Hz), 3.28 (4H, d, Ar-C*H*$_2$-Ar, *J* = 12.9 Hz), 3.99 (4H, t, O-C*H*$_2$, *J* = 5.7 Hz), 4.13 (4H, d, Ar-C*H*$_2$-Ar, *J* = 12.9 Hz), 4.87 (4H, t, C*H*$_2$-Triazole, *J* = 6.6 Hz), 5.29 (2H, s, Triazole-C*H*$_2$-O), 6.81 (4H, s, Ar-*H*), 7.03 (2H, m, Ar-*H*), 7.05 (4H, s, Ar-*H*), 7.13 (2H, d, Ar-*H*, *J* = 8.7 Hz), 7.43 (2H, s, Ar-O*H*), 7.46 (2H, m, Ar-*H*), 7.79 (2H, d, Ar-*H*, *J* = 5.7 Hz), 7.95 (2H, s, Triazole-*H*), 10.40 (2H, s, *H*C=O). δ_C ($CDCl_3$): 30.9, 31.7, 34.0, 47.3, 62.5, 113.0, 121.2, 125.0, 125.3, 125.7,

127.5, 128.6, 132.3, 135.9, 142.1, 149.1, 150.2, 160.5, 189.6. ν_{max} (KBr): 3397, 2958, 2903, 2867, 1687, 1598, 1584, 1484, 1458, 1392, 1362, 1301, 1286, 1241, 1209, 1162, 1124, 1045, 1027, 945, 872, 832, 758 cm^{-1}.

2.4.14 5,11,17,23-tetra-*tert*-butyl-25,27–dihydroxy-26,28-bis-butoxy-(triazo-salicyalydehye) calix[4]arene: (30)

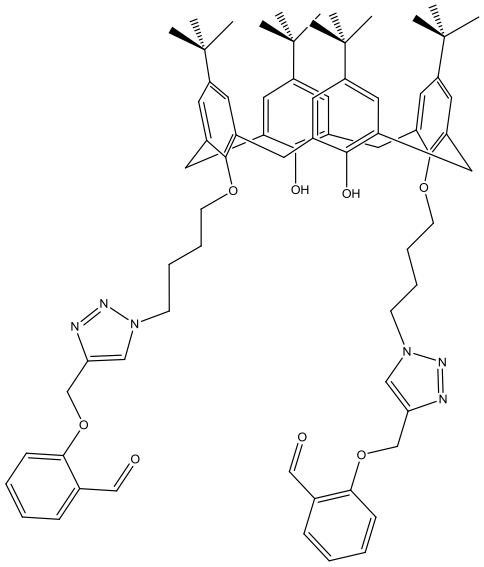

In a mixture of DCM (25 mL) and water (25 mL) compound **28** (100 mg, 0.01 mmol) and compound **20** (38 mg, 0.023 mmol) were dissolved. To this copper sulphate pentahydrate (59.22 mg, 0.023 mmol) and sodium ascorbate (47 mg, 0.023 mmol) were added. The mixture was heated to reflux for 115 h, the reaction mixture was cooled and the product was extracted with DCM (100 mL). The organic layers were combined and washed with brine (200 mL), dried over $MgSO_4$ and concentrated under reduced pressure, the residue was redissolved in diethyl ether, and the solvent was removed under vacuum, **30** was collected as a white solid.

Yield: 34 mg, 83 %. m.p.: 218-224 °C. *m/z* Calc [M+H] for $C_{72}H_{86}N_6O_8$ Calculated; 1163.658, Found; 1163.660. δ_H ($CDCl_3$): 0.89 (18H, s, *t*-Bu), 1.24 (18H, s, *t*-Bu), 1.72 (4H, q, CH_2-C*H*$_2$-CH_2, *J* = 6.9 Hz), 2.19 (4H, q, CH_2-CH_2-C*H*$_2$-CH_2, *J* = 6.9 Hz), 3.28 (4H, d, Ar-C*H*$_2$-Ar, *J* = 13.2 Hz), 3.86 (4H, t, O-C*H*$_2$, *J* = 5.7 Hz), 4.10 (4H, d, Ar-

CH_2-Ar, J = 12.9 Hz), 4.56 (4H, t, CH_2-Triazole, J = 7.5 Hz), 5.32 (4H, s, Ar-O-CH_2-Triazole), 6.72 (4H, s, Ar-*H*), 7.02 (4H, m Ar-*H*, Ar-O*H*), 7.07 (4H, s, Ar-*H*), 7.17 (2H, d, Ar-*H*, J = 8.4 Hz), 7.48 (2H, t, Ar-*H*, J = 7.5 Hz), 7.78 (2H, d, Ar-*H*, J = 7.8 Hz), 8.01 (2H, s, Triazole-*H*), 10.45 (2H, s, *H*C=O). δ_C ($CDCl_3$): 18.4, 26.5, 27.7, 30.9, 31.2, 31.4, 31.7, 33.9, 50.2, 58.4, 62.5, 113.1, 121.2, 123.9, 125.05, 125.6, 127.7, 128.6, 132.0, 136.0, 142.0, 143.2, 147.2, 149.4, 150.2, 160.6, 189.6. ν_{max} (KBr) : 3416, 2957, 2904, 2867, 1687, 1598, 1484, 1458, 1392, 1362, 1285, 1239, 1210, 1195, 1162, 1049, 872, 758 cm^{-1}.

2.4.14.1 Reaction of 30 with $Zn(ClO_4)_2.6H_2O$ in MeOH/$CHCl_3$: Complex $Zn(30)(ClO_4)_2$

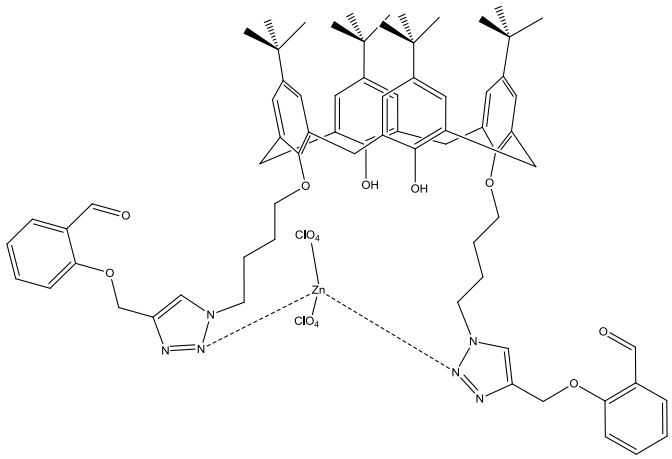

A mixture of **30** (10 mg, 0.008 mmol) in $CHCl_3$ (5 mL) and zinc(II) perchlorate (12 mg, 0.032 mmol) in MeOH (10 mL) were stirred at room temperature for 8 h. The solvent was removed on a rotary evaporator, to leave a yellow solid.

Yield: 8 mg, 70 %: m.p.: 154-164 °C, δ_H ($CDCl_3$): 0.84 (18H, s, *t*-Bu), 1.30 (18H, s, *t*-Bu), 2.18 (8H, m, CH_2-CH_2-CH_2-CH_2), 3.26 (4H, d, Ar-CH_2-Ar, J = 12.9 Hz), 3.88 (4H, m, O-CH_2), 4.08 (4H, d, Ar-CH_2-Ar, J = 12.9 Hz), 4.69 (4H, m, CH_2-Triazole), 5.45 (4H, s, Ar-O-CH_2-Triazole), 6.68 (4H, s, Ar-*H*), 6.99 (6H, m, Ar-*H*), 7.48 (2H, m, Ar-*H*), 7.76 (2H, m, Ar-*H*), 8.19 (2H, s, Triazole-*H*), 10.28 (2H, s, *H*C=O). ν_{max} (KBr)

: 3469, 2958, 2907, 2868, 1688, 1599, 1484, 1458, 1240, 1208, 1145, 1110, 1090, 757, 626 cm^{-1}.

2.4.15 Bis(3-(prop-2-yn-1-yloxy)benzylidene)ethane-1,2-diamine (30)

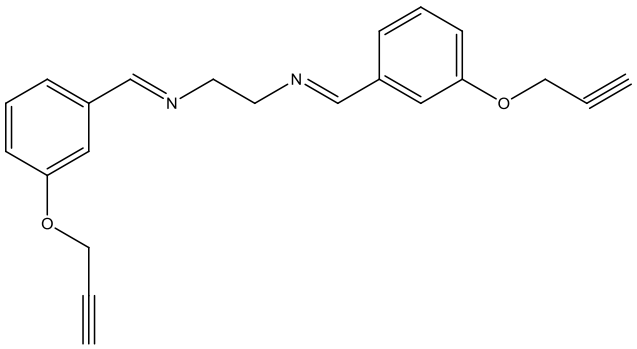

A mixture of compound **9** (0.1 g, 0.37 mmol) and potassium carbonate (0.7 g, 5.11 mmol) were dissolved in acetone and heated to reflux for one hour, at this point propargyl bromide (0.39 g, 3.27 mmol) was added dropwise, and the reaction mixture was heated to reflux for 48 h. After cooling to room temperature the potassium salts formed were filtered and the filtrate concentrated under vacuum, the residue was dissolved in $CHCl_3$ and **30 w**as obtained by addition of EtOH.

Yield: 44 mg, 35%. m.p.: 88-94 °C. Anal. Calc. for $C_{22}H_{20}N_2O_2$: C, 76.72; H, 5.85; N, 8.13 %; Found C, 70.27; H, 5.46 N, 7.24 %. δ_H ($CDCl_3$): 2.49 (2H, t, C≡C*H*, *J* = 2.4 Hz), 3.96 (4H, s, C=N-CH_2-CH_2-N), 4.70 (4H, d, HC≡CH_2, *J* = 2.4 Hz), 7.00-7.04 (2H, m, Ar-*H*), 7.28-7.34 (6H, m, Ar-*H*,Ar-*H*,Ar-*H*), 8.24 (2H, s, *H*C=N). δ_C ($CDCl_3$): 55.8, 61.4, 75.6, 112.9, 117.9, 122.00, 129.64, 137.60, 157.78, 162.40. ν_{max} (KBr) : 3237, 2837, 1639, 1598, 1447, 1378, 1277, 1263, 1175, 1156, 1042, 781, 686 cm^{-1}.

2.4.16 Reaction of 19 with 30 in DCM and MeOH

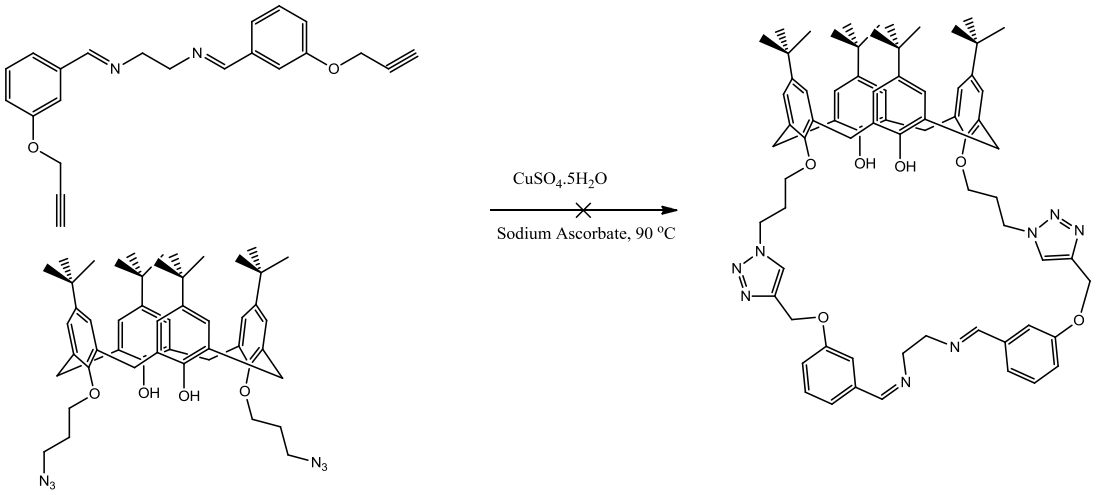

A mixture of **30** (10 mg, 0.0029 mmol) and **19** (23.7 mg, 0.0029 mmol) were dissolved in a DCM (10 mL) to this stirring mixture copper sulphate pentahydrate (2 mg, 0.008 mmol) and sodium ascorbate (5 mg, 0.025 mmol) in MeOH (2 mL) was added. The resulting mixture was heated to 90°C for 7 h. The solvent was removed under vacuum and the residue was taken up in $CHCl_3$ to which EtOH was added. A white ppt formed which was insoluble in all NMR solvents. The solution was reduced under vaccum, the ^1H NMR spectrum includes an aldehyde peak, which is consistent with imine hydrolysis.

2.4.17 Reaction of 19 with 30 in DCM and MeOH with a drying agent

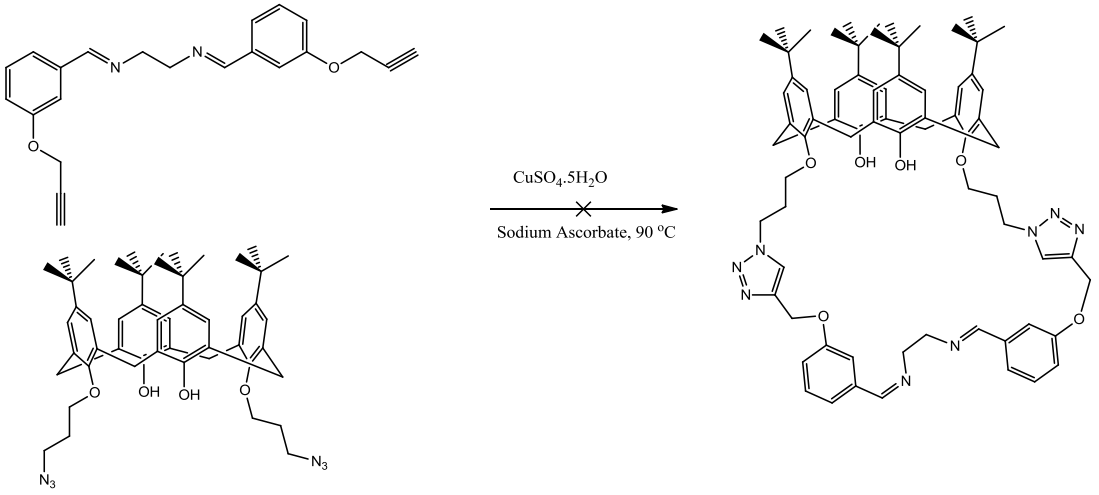

A mixture of **30** (10 mg, 0.0029 mmol), **19** (23.7 mg, 0.0029 mmol) and magnesium sulphate (3.5 mg, 0.029 mmol) were dissolved in DCM (10 mL) to this stirring mixture copper sulphate pentahydrate (2 mg, 0.008 mmol) and sodium ascorbate (5 mg, 0.025 mmol) in MeOH (2 mL) was added. The resulting mixture was heated to 90 °C for 7 h. The solvent was removed under vacuum and the residue was taken up in $CHCl_3$ to which EtOH was added. The ^{1}H NMR includes an aldehyde peak, which is consistent with imine hydrolysis.

2.4.18 Reaction of 6 with propargyl bromide in acetone: (31)

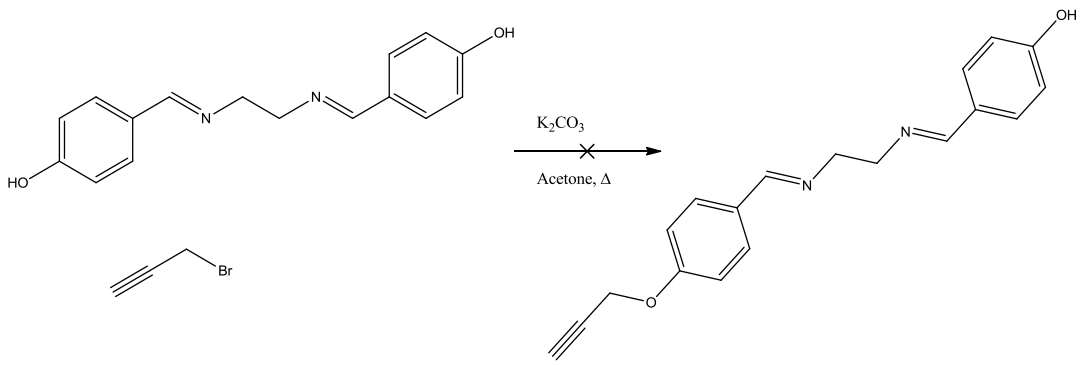

Potassium carbonate (143 mg, 1.12 mmol) and **6** (200 mg, 0.74 mmol) were dissolved in acetone (100 mL) and heated to reflux for 1 hour, propargyl bromide (133 mg, 1.12 mmol) was added and heated to reflux for 24 h. The mixture was cooled to room temperature and Buchner filtered, the filtrate was reduced to dryness under vacuum. The residue was dissolved in DCM addition of Pet Ether gave a brown ppt., this was removed and the solvents were removed under vacuum, a yellow solid precipitate from DCM: Pet Ether, this was found to be the **16**, which indicates that the imine underwent hydrolysis.

δ_H ($CDCl_3$): 2.56 (1H, t, C≡C*H*, *J* = 2.5 Hz), 3.92 (4H, s, C=N-CH_2), 4.78 (2H, d, O-CH_2, *J* = 2.4 Hz), 6.96 (4H, d, Ar-*H*, *J* = 8.8), 7.63 (4H, d, Ar-*H*, *J* = 8.9 Hz), 8.21

(2H, s, *H*C=N), 9.91 (1H, s, *H*C=O). δ_C ($CDCl_3$): 55.9, 76.3, 76.6, 115.2, 130.6, 131.9, 162.3, 190.8. ν_{max} (KBr): 3448, 3214, 2964, 1683, 1604, 1578, 1508, 1453, 1260, 1095, 1022, 805 cm^{-1}.

2.4.19 Reaction of 13 with propargyl bromide in acetonitrile: (32)

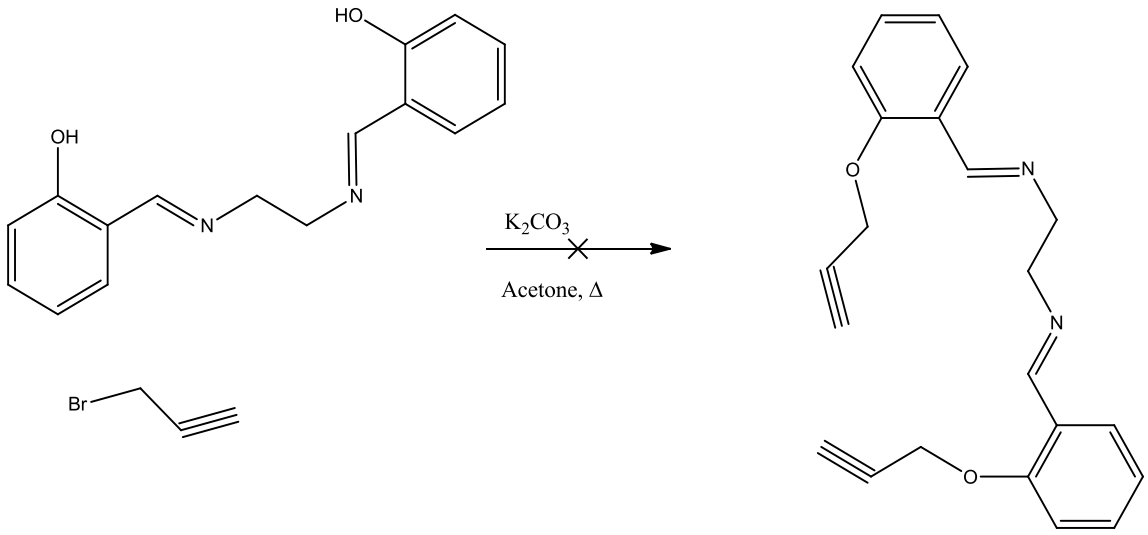

Compound **13** (0.1 g, 0.37 mmol) and potassium carbonate (0.13 g, 0.93 mmol) were dissolved in acetonitrile (100 mL) and heated to reflux for 1 h. At this point propargyl bromide (0.13 g, 1.49 mmol) was added dropwise, and the mixture was heated to reflux for 48 h, and then cooled to room temperature. The inorganic salts formed were filtered, and the filtrate concentrated under reduced pressure. This yielded a brown solid, ^{1}H NMR analysis of the crude product revealed that significant imine hydrolysis had occurred. It was attempted to purify the product by column chromatography, but it was only possible to isolate the aldehyde hydrolysis product.

2.4.20 Reaction of 13 with propargyl bromide in acetonitrile: (33)

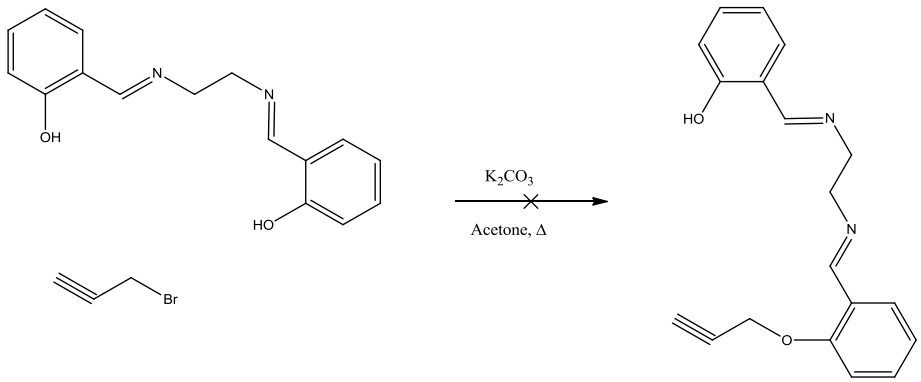

Compound **13** (0.1 g, 0.37 mmol) and potassium carbonate (0.05 g, 0.46 mmol) were dissolved in acetonitrile (100 mL) and heated to reflux for 1 h. At this point propargyl bromide (0.11 g, 0.93 mmol) was added dropwise, and the mixture was heated to reflux for 24 h, and then cooled to room temperature. The inorganic salts formed were filtered, and the filtrate concentrated under reduced pressure. It was clear from the ^{1}H NMR spectrum that significant aldehyde formation had occurred.

2.5 Fluorescence Spectroscopy of Ligands from section 2.4

2.5.1 Overview and Parameters

Two of the triazole ligands were of sufficient purity to be screened for fluorescent behaviour, **29** and **30**, 100 μM solutions of both ligands in $CHCl_3$ were successfully prepared. All samples were run at room temperature; UV-Vis spectra were recorded to determine the absorption maxima. The parent calix[4]arene has an absorption max at 280 nm.[4]

2.5.2 Fluorescent Data

The UV-Vis spectral plot of the ligands, **29** and **30**, showed three absorption peaks (Table 2.3). Each of these peaks were then used as the excitation wavelength, (λ_f^{ex}),

and the emission spectrum was recorded with peak emission (λ_f^{em}). Excitation of **29** at 252 and 316 nm resulted in no fluorescence emission spectra, while a λ_f^{ex} = 292 resulted in a weak emission spectrum with λ_f^{em} = 344 nm. A similar result was noted for ligand **30**.

Table 2.3: UV-Vis absorption peaks, which are used as the excitation wavelength, λ_f^{ex}, to obtain fluorescent emission spectrum with peak emission, λ_f^{em}.

Sample no.	Absorption Peaks (nm)			λ_f^{em}
29	252	292	316	344
30	250	290	316	346

2.6 Synthesis of Isoxazole modified Calix[4]arenes for Fluorescence studies

2.6.1 Anthracene modified Isoxazole Calix[4]arene: (AIC)

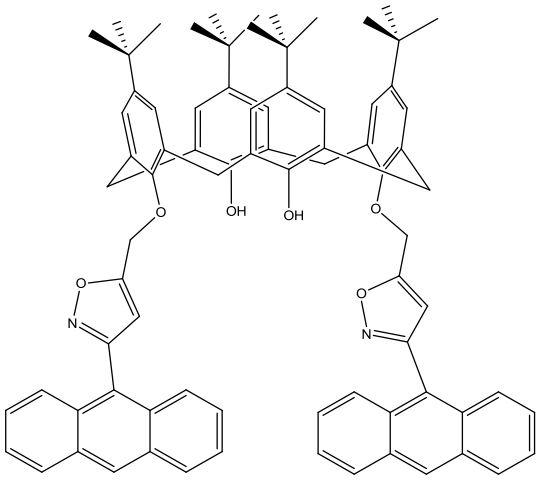

AIC was prepared by Haowen Diao using the following method.

Anthracene-9-carbaldehyde oxime (0.19 g, 0.75 mmol) and chloramine-T (0.20 g, 0.90 mmol) were placed in a 100 mL round bottomed flask and dissolved in EtOH (60 mL). Compound **17** (0.30 g, 0.43 mmol) was added. The mixture was heated at reflux (80 °C) for 3 hours and another portion of oxime (0.90 g) and chloramine-T (0.20 g) were

added. The mixture was heated at reflux (80 °C) overnight. On completion of the reaction, water (30 mL) was added and the mixture was extracted with chloroform (10 mL x 3). The organic layers were combined, washed with 5% NaOH (10 mL x 2) and dried over anhydrous $MgSO_4$. The solvent was removed under vacuum. The crude product was purified by flash column chromatography (SiO_2, petroleum ether: ethyl acetate, 3: 1). The crude product was crystallised from a Per Ether:EtOAc mixture (3: 1) yielding the desired product as a white solid.

Yield: 0.25 g, 51 %. m.p.: 174-190 °C. *m/z*: $[M+Na]^+$ calculated for $C_{80}H_{78}N_2NaO_6$, 1185.5752, found 1185.5670. δ_H ($CDCl_3$) : 0.94 (18H, s, *t*-Bu), 1.31 (18H, s, *t*-Bu), 3.37 (4H, d, Ar-C*H*$_2$-Ar, *J* = 13.2 Hz), 4.29 (4H, d, Ar-C*H*$_2$-Ar, *J* = 13.2 Hz), 5.27 (4H, s, Ar-O-C*H*$_2$), 6.48 (2H, s, isoxazole C*H*), 6.70 (2H, s, Ar-O*H*), 7.09 (4H, s, Ar-*H*), 7.33-7.43 (8H, m, Ar-*H*), 7.79 (4H, d, Ar-*H*, *J* = 7.8 Hz), 7.93 (4H, d, Ar-*H*, *J* = 7.8 Hz), 8.43 (2H, s, Ar-*H*). δ_C ($CDCl_3$) δ:31.0, 31.7, 33.9, 34.0 67.7, 108.1, 125.2, 125.3, 125.6, 125.8, 126.5, 127.8, 128.4, 129.0, 130.6, 131.1, 132.5, 141.9, 147.7, 149.6, 150.4, 161.0, 167.9. ν_{max} (KBr): 3447.81, 2960.41, 1625.69, 1483.97, 1362.69, 1207.46, 888.35, 735.12 cm^{-1}.

2.6.2 1-(tert-butyl)-4-(prop-2-yn-1-yloxy)benzene: (34)

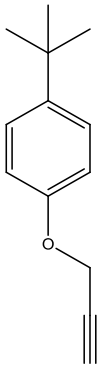

p-Tert-butyl phenol (1 g, 6.65 mmol) and potassium carbonate (1.75 g, 12.65 mmol) were dissolved in acetone (100 mL) and stirred for 2 h, at this point propargyl bromide (1.18 g, 9.98 mmol) was added dropwise. The mixture was heated to reflux for 8 h

under N_2. The reaction mixture was cooled to room temperature and the inorganic salts filtered. The mixture was washed with water (50 mL) and the product extracted by DCM (150 mL), and dried over $MgSO_4$. The solvent was removed under vacuum to yield yellow oil **34**.

Yield: 1.13 g, 90%. *m/z* Calc [M+H] for $C_{13}H_{16}O$ Calculated; 189.1270, Found; 189.1274. δ_H ($CDCl_3$): 1.37 (9H, s, *t*-Bu), 2.55 (1H, t, C≡C*H*, *J* = 2.4 Hz), 4.71 (2H, d, O-CH_2, *J* = 2.43), 6.96 (2H, d, Ar-*H*, *J* = 8.9 Hz), 7.36 (2H, d, Ar-*H*, *J* = 8.9 Hz). δ_C ($CDCl_3$): 31.5, 38.8, 55.8, 75.3, 78.8, 114.3, 126.3, 144.4, 155.5. ν_{max} (NaCl): 3435, 3290, 3276, 3046, 2958, 2906, 2867, 1595, 1482, 1445, 1388, 1366, 1306, 1205, 1187, 1120, 1095, 1002, 867, 640 cm^{-1}.

2.6.3 Reaction of 34 with paraformaldehyde in MeOH:

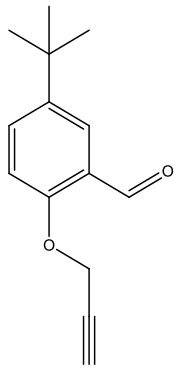

Compound **34** (500 mg, 2.65 mmol) was dissolved in MeOH (50 mL) to this 30% formaldehyde in H_2O (200 mg, 6.63 mmol) and sodium hydroxide (287 mg, 7.17 mmol) was added. The reaction mixture was heated to 67 °C for 3 h, and then cooled to room temperature, filtered and the solvents were removed from the filtrate at reduced pressure, to give brown oil. The ^1H NMR showed no signal for the aldehyde proton.

2.6.4 Anthracene modified isoxazole t*ert*-butyl-phenol: (AIM)

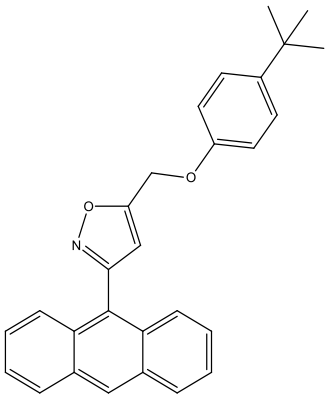

AIM was prepared by Haowen Diao using the following method.

34 (0.25 g, 1.35 mmol) and EtOH (40 mL) were added into a 100 mL round bottomed flask. Anthracene-9-carbaldehyde oxime (0.15 g, 0.68 mmol) and chloramine-T (0.15 g, 0.66 mmol) were added. The mixture was heated at reflux for 2 hours. After 2 h **34** (0.128 g, 0.68 mmol) and chloramine-T (0.154 g, 0.68 mmol) were added. The mixture was heated at reflux for another 2 hours. After this interval further portions of **34** (0.128 g, 0.68 mmol) and chloramine-T (0.154 g, 0.68 mmol) were added. After a total of 6 h the reaction was cooled and water (100 mL) was added. The mixture was extracted with chloroform (3 x 30 mL). The organic layers were combined and washed with 5 % NaOH (3 x 15 mL) and dried over anhydrous $MgSO_4$. The solvent was removed by evaporation under reduced pressure. The crude product was purified by flash column chromatography (SiO_2, DCM: petroleum ether, 1:2, R_f = 0.4). The desired product (**AIM**) was obtained as a yellow liquid

Yield: 0.27 g, 98 %. *m/z* [2M+Na] +calculated for $C_{56}H_{50}N_2NaO_4$, 837.3663, found 837.3681. δ_H ($CDCl_3$): 1.32 (9H, s, *t*-Bu), 5.38 (2H, s, O-C*H*$_2$), 6.61 (1H, s, isoxazole C*H*), 7.01-6.97 (2H, m, Ar-*H*), 7.36 (2H, m, Ar-*H*), 7.52-7.42 (4H, m, Ar-*H*), 7.85 (2H, m, Ar-*H*), 8.06 (2H, dd, Ar-*H*, *J*= 1.8, 7.2 Hz), 8.58 (1H, s, Ar-*H*). δ_C ($CDCl_3$): 31.5, 34.2, 61.8, 106.9, 114.5, 122.9, 125.4, 125.6, 126.5, 126.6, 128.55, 129.1, 130.6,

131.2, 144.8, 155.7, 161.0, 167.7. ν_{max} (KBr): 2962.5, 1605.5, 1512.3, 1363.5, 1363.5, 1232.0, 998.2, 893.6, 732.3 cm^{-1}.

2.7 Fluorescent properties of ssoxazole modified calix[4]arenes from section 2.6

2.7.1 Overview and Parameters

Fluorescence spectra measurements were performed using a Jascow FP6300 fluorescence spectrometer. The samples were prepared in a 3000 μL quartz fluorescence cell with a 10 mm path length. The excitation wavelength (λ_f^{ex}) was determined using UV-Vis spectroscopy to be 274 nm, 343 nm and 364 nm for **PIM**, **PIC**, **AIC** and **AIM**, respectively, with all results recorded in triplicate. Stock solutions of the host and guest (metal salts) were prepared in HPLC grade acetonitrile to concentrations of 12 μM host and 1200 μM guest. A total volume of 3000 μL was maintained in the cell at all times, with the host volume of 1500 μL for each reading, resulting in a constant concentration of 6 μM. The concentration of the metal salts was varied from 0.6 μM to 600 μM by dilution using additional acetonitrile in the remaining 1500 μL portion. Upon addition, mixing was performed by inversion; this mixing was completed after sixty seconds ensuring adequate equilibration of host and guest. Before each sample was run, a cell filled with acetonitrile was placed in the spectrometer and the emission spectra was recorded, the equipment was then auto zeroed for the solvent. The data obtained was processed using Microsoft Excel to obtain a spectral plot of relative fluorescence intensity (a.u.) versus emission wavelength (nm).

2.7.2 Fluorescence Data

Absorption maxima were used as an excitation parameter (λ_f^{ex}) to generate emission spectra, with maximum (λ_f^{em}), Table 2.4. All the excitation wavelengths were tested but some resulted in higher quality emission spectra. Once the optimum excitation wavelength was found, the emission spectra in the presence of a variety of metal perchlorate salts and copper salts were recorded.

Table 2.4: Absorption maxima used as excitation wavelength (λ_f^{ex}), and the corresponding peak emission wavelength recorded (λ_f^{em}).

Sample Name	**UV-Vis absorption peaks (nm)**			**λ_f^{em} (nm)**
AIC	356	364	384	439
PIC	235	278	343	498
AIM	252	304	364	421
PIM	274		346	386

3. Results and Discussion

3.1 Introduction

This thesis represents the results of an investigation into the discovery of novel metal binders based on *tert*-butyl-calix[4]arene, which is exploited as a macromolecular scaffold. This was further expanded to include analytical proprieties, which display when metal complexation had occurred. Preparation of novel compounds through standard Schiff base conditions proved to be a success. UV-Vis and fluorescence spectroscopic methods were performed on the ligands and select metal complex reactions. Once this avenue was exhausted, the development of unusual metal binding sites was investigated; it was decided to include both Schiff base and triazole sites within the same lower rim cavity. Due to the sensitivity of the di-imine link to the reaction conditions needed for the *click* reaction, the desired calix-triazole-Schiff base compounds proved elusive. However, lower rim link triazole double calixarenes (*click-calixtubes*) and triazole linked calix[4]arene aldehydes were successfully prepared.

3.2 Schiff base capped calix[4]arenes

3.2.1 Overview

It was initially decided to substitute the lower rim of *tert*-butyl calix[4]arene with a simple metal binding site, within which the size and shape of the binding site could be altered. To this end it was decided that simple di-imine bridged diphenol link units would be exploited, with the position of the aldehyde relative to the hydroxyl group being changed to enable the construction of calix[4]arenes with metal binding sites with different shapes, Figure 3.1. Schiff base capped calix[4]arenes have been previously reported,[42,43] but these have been achieved *via* a cross linking fashion. This thesis focused on creating a compartmentalised approach to synthesising these

compounds. This was attempted in order to maximise the yield and optimise the purification steps needed. To this end a range of bromoalkoxy-calix[4]arenes and di-hydroxybenzyldiimines were synthesised so that they could be combined in a simple one step reaction to give the desired compounds.

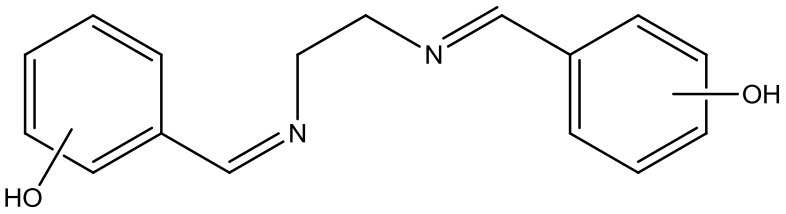

Figure 3.1: General structure for di-imine bridged diphenol units used

3.2.2 Synthesis and characterisation of calix[4]arene precursors

The calix[4]arene, **2**, (tetramer) which was to serve as the scaffold upon which all subsequent compounds would be constructed, was prepared using the method developed by Gutsche *et al.*[104] which first prepares the calix[8]arene precursor, **1**, (octamer), through the base catalysed condensation of paraformaldehyde and *p-tert*-butylphenol shown in Scheme 3.1. The expected highly symmetric nature of the octamer was confirmed by examination of the ^{1}H NMR spectrum, with a single uncoupled peak representing the *tert*-butyl groups resonating at 1.28 ppm. Due to the position of the *t*-butyl groups, the aromatic protons are chemically equivalent and as such are observed as a singlet at 7.17 ppm. The methylene bridges resonate as a pair of doublets at 3.48 and 4.39 ppm, which is indicative of their diastereotopic character, resulting in one proton pointing into the macrocyclic cavity. Consequently, the geminal protons exist in two different chemical environments. Extensive hydrogen bonding occurs between the phenolic protons because of their relative close proximity within the cavity, giving rise to a lower than expected lower field resonance at 9.63 ppm.

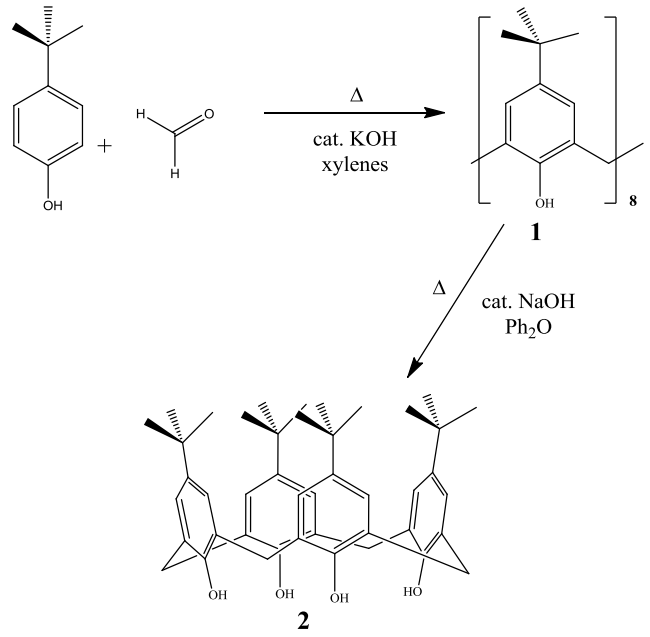

Scheme 3.1: Synthesis of calix[8]arene,**1**, and calix[4]arene, **2**, with conditions used.

By heating the octamer to reflux in diphenyl ether in the presence of a base catalyst the octamer, **1**, was converted to tetramer, **2**, which is shown in Scheme 3.1. This yields **2** as a glinting white solid. The resonance signals for the *tert*-butyl groups, aromatics and phenolic groups occurring as singlets at 1.21, 7.04 and 10.34 ppm, respectively, is indicative of preservation of symmetry, as in the case of the octamer. The lower field position observed for the phenolic proton is as a result of the tighter proximity of the hydroxyl groups due to the smaller macrocycle size. As in the case of the octamer, the methylene protons are diastereotopic in nature and resonate as a set of doublets at 3.50 and 4.26 ppm.

The phenolic rim of the tetramer is easily functionalised using potassium carbonate as a base with the addition of a desired electrophile. This route was utilised to fashion 1,3-*bis*-bromoalkoxy substituted calix[4]arenes, **3**, **4**, and **5** as shown in Scheme 3.2. In the synthesis of the bromoethoxy derivative, the tetramer was heated to reflux with potassium carbonate for one hour. The 1,2-dibromoethane was added in tenfold excess and refluxed for two days. The 1,3-distal substituted calixarene, **3**, was obtained after

precipitation from a mixture of hot chloroform and methanol and was confirmed by analysis of its ^{1}H NMR spectrum.

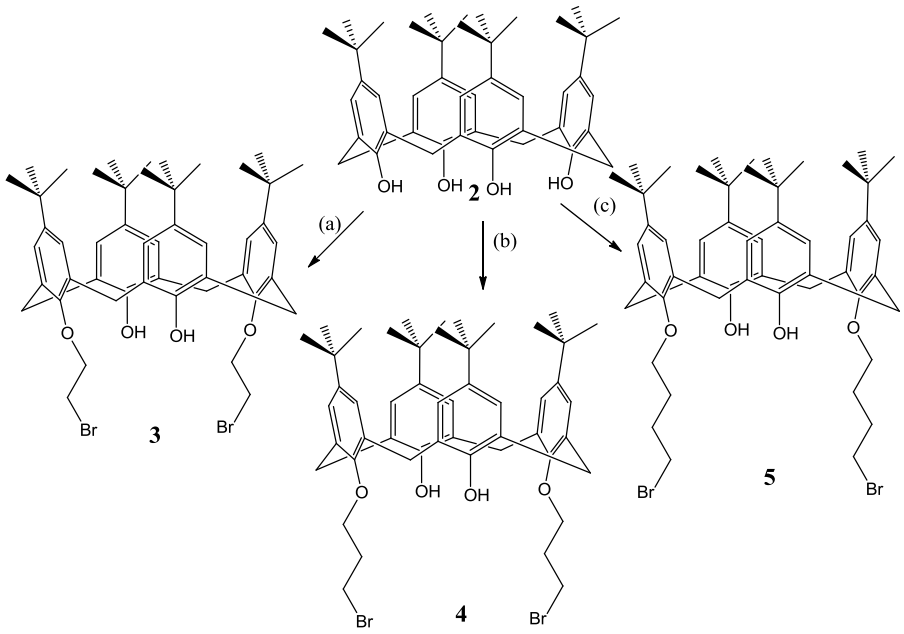

Scheme 3.2: Synthesis of **3**, **4**, **5 (a)** 1,2-dibromoethane, K_2CO_3, Δ; **(b)** 1,3-dibromopropane, K_2CO_3, Δ; **(c)** 1,4-dibromobutane, K_2CO_3, Δ.

The effect of the symmetry that exists in the molecule can be seen in its ^{1}H NMR spectrum which is clear from the two *tert*-butyl group signals resonating as singlets at 0.95 and 1.29 ppm. This pattern is also observed for the aromatic protons, which are observed as two singlets at 6.79 and 7.06 ppm. The phenolic proton signal is shifted upfield significantly to 6.99 ppm; this is due to two of the phenolic groups being substituted to form phenolic ethers. The presence of the ethers results in a reduction in the degree of hydrogen bonding with which the remaining phenolic protons can participate. From the data analysed in this thesis, this characteristic is observed for all 1,3-distal substituted calixarenes synthesised. The bromoethoxy pendant arm protons are represented by a triplet at 3.82 ppm and as part of a multiplet at 4.28 ppm, both of which are shifted downfield due to the close proximity to electronegative atoms, O and Br. The bridging methylene protons occur as a doublet at 3.31 ppm with a coupling constant of J = 13.2 Hz and in the multiplet at 4.28 ppm. The value for the coupling

constant was within the expected range for geminal protons.[118] As with unmodified calixarenes, these protons retain their diastereotopic nature in all functionalised calixarenes which are described in this thesis with the chemical shifts, and coupling constants being similar.

The procedure for preparing 1,3 *bis*-bromopropoxy-calix[4]arene, **4**, was the same as for the bromoethoxy variant, with symmetry once again being retained in the macrocycle. This is clear from the two *tert*-butyl signals which are seen as singlets at 1.10 and 1.27 ppm, and from a pair of singlets representing the aromatic protons at 6.86 and 7.04 ppm. Because of the reasons outlined above the phenolic proton appears at 7.63 ppm. The proton signals for the bromopropoxy pendant arm are present as a quintet at 2.47 ppm, and two triplets at 3.98 and 4.09 ppm, while the methylene bridges are represented by two doublets at 3.32 and 4.23 ppm. Synthesis of the bromobutoxy substituted derivative was similar to both the bromoethoxy and bromopropoxy derivatives, with a slight modification of the reaction time being lengthened to three days to maximise yield. The work up also required washing with copious amounts of water (>1000 mL) to remove excess 1,4-dibromobutane. As with the previously described calixarene derivatives **3** and **4**, symmetry is retained. This is clear from the ^{1}H NMR spectrum, with the *tert*-butyl groups present as a pair of singlets at 1.02 and 1.35 ppm. Two singlets at 6.85 and 7.11 ppm represent the aromatic protons. A singlet at 7.47 ppm is representative of the phenolic proton, and the methylene protons resonate at 3.35 and 4.27 ppm as doublets. The bromobutyl fragment of the molecule is represented by two quintets at 2.16 and 2.34 ppm and two triplets at 3.67 and 4.03 ppm. The characteristic ^{1}H NMR spectra described above can be seen in all substituted calixarenes synthesised.

Changing the alkoxy chain length from two to three and finally to four carbons had an observable effect on the percentage yields obtained, shown in Table 3.1. This trend holds true in general for all substituted calix[4]arenes studied in this thesis.

Table 3.1: Varying reaction times and yields obtained for bromoalkoxy substituted calix[4]arenes.

Chain Length	Reaction Time (hours)	% yield
2	48	80
3	48	65
4	72	30

3.2.3 Synthesis and characterisation of Schiff Base linkers

The diphenol di-imines that were used to form capped calix[4]arene derivatives were prepared using standard Schiff base conditions.[108] These linkers were selected because the *ortho*-benzaldhyde based *Salen* and the *meta*-benzaldhyde derivatives have been extensively studied for their metal binding capabilities.[48,111] The *para*-benzaldeyde derivative is relatively unstudied in comparison.

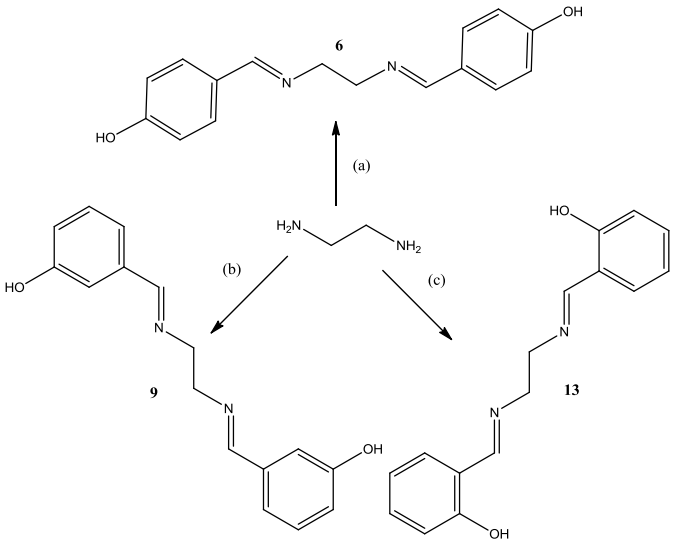

Scheme 3.3: Synthesis of dialdehyde Schiff bases **(a)** 4-Hydroxybenzaldehyde, EtOH, 120 °C, 2 h **(b)** 3-Hydroxybenzaldehyde, EtOH, 120 °C, 2h **(c)** 2-Hydroxybenzaldehyde, EtOH, 120 °C, 2h.

The synthesis of the *para*, *meta*, and *ortho*-Schiff base linkers, **6**, **9**, and **13**, is outlined in Scheme 3.3. The effect the symmetrical nature of **6** has on the ^{1}H NMR spectrum is clear upon analysis. This is evident from the two doublets at 6.77 and 7.51 ppm, which are representative of the aromatic protons that integrate for four protons each. This splitting pattern is characteristic for a *para*-disubsituted aromatic compound. The signal for the ethyl bridge protons resonate at 3.75 ppm as a singlet which integrates for four protons. This is further evidence of the symmetry in this molecule, and is seen in all Schiff bases prepared in this thesis. The characteristic signal for the imine proton is seen as a singlet which resonates at 8.17 ppm, which is integrated for two protons. The evidence for formation of the imine is confirmed further by examination of the ^{13}C NMR spectrum which shows a peak at 161.5 ppm which is in the region the imine would be expected to resonate. The IR spectrum of the compound shows an absorption band at 1639 cm^{-1}, which is within the region of the spectrum where the imine would be expected to appear. The phenolic proton does not appear in the ^{1}H NMR spectrum, but its presence is indicated in the IR spectrum by a broad absorption band at 3471 cm^{-1}, and the ^{13}C NMR with a signal that resonates at 159.8 ppm, which is common for a carbon bound to a phenolic OH.

From analysis of the ^{1}H NMR spectrum of *meta*-Schiff base linker **9**, the effect of the symmetry is once again clearly seen. The aromatic region contains a doublet of doublets which resonates at 6.81 ppm, representing two protons, with a coupling constant of J = 7.1 Hz, a multiplet which is centred at 7.10 ppm which integrates for four protons, and a triplet which resonates at 7.19 ppm, and, integrates for two protons with a coupling constant of J = 7.7 Hz. As with **6**, the ethylene bridging protons are represented by a signal which resonates at 3.81 ppm as a singlet. The imine proton resonates in the expected region with a signal with chemical shift of 8.23 ppm; the presence of the imine is again supported by the ^{13}C NMR with a signal occurring at

161.9 ppm, and an absorption band in the IR spectrum occurring at 1647 cm^{-1}. As was the case in **6**, the phenolic proton signal is not present in the ^{1}H NMR, but again can be accounted for from the ^{13}C NMR which has a signal resonating at 157.5 ppm, and from the IR spectrum with an absorption band which peaks at 3418 cm^{-1}.

Ortho-Schiff base linker, **13**, also known as *Salen*, exhibits the same symmetry which has been discussed for **6** and **9** above. Analysis by ^{1}H NMR spectroscopy shows that the aromatic signals resonate as a multiplet at 6.86 ppm, a triplet at 7.28 ppm, and a doublet of doublets at 7.40 ppm, which integrate for eight protons collectively. The signal for the bridging ethyl fragment resonates at 3.92 ppm as a singlet, and the imine signal resonates at 8.58 ppm as a singlet. Once again, confirmation is obtained from analysis of the ^{13}C NMR spectrum within which a signal resonates at 166.9 ppm and also by the IR spectrum, which clearly shows an absorption band observed at 1636 cm^{-1}. In contrast to the earlier discussed **6** and **9**, the phenolic proton signal is observed in the ^{1}H NMR spectrum is due to the hydrogen bonding interaction between the OH and the imine (Scheme 3.4).

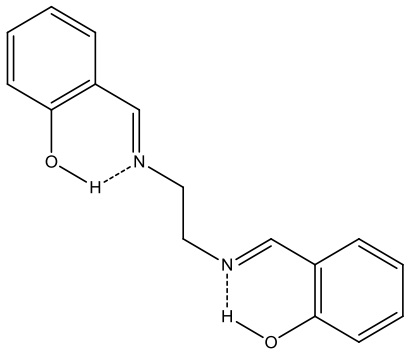

Scheme 3.4: *Ortho* Schiff base linker **13**, showing the hydrogen bonding interactions.

The phenolic proton resonates at 13.38 ppm as a singlet, which is in agreement to the data obtained from the ^{13}C NMR, which has a signal resonating at 160.5 ppm, and the IR spectrum, which once again shows a characteristic absorption band at 3456cm^{-1}.

The symmetry found in the dialdehyde Schiff bases discussed above is found to be conserved when they are used to functionalise the lower rim of the calixarene.

3.2.4 Synthesis and characterisation of Schiff base capped calix[4]arenes

The 1,3-distal-bromoalkoxy-calix[4]arenes **3**, **4**, and **5** were used as the basic scaffold unit which would be capped by the di-imine linked diphenol Schiff bases **6**, **9,** and **13**. Scheme 3.5 shows the reaction conditions for the formation of the *para*-Schiff base benzyl linked propoxy-calix[4]arene **7** and *para*-Schiff base benzyl linked butoxy-calix[4]arene **8**. The synthesis is straightforward, with deprotonation of the Schiff base phenols preceding addition of the alkyl bromide, with the products **7** and **8** obtained in high purity as a solid precipitated from a $CHCl_3$:EtOH solution in moderate yields of 74 % and 35 %, respectively. The lower yield that was obtained for the butyl derivative follows the trend which was originally noted in Section 3.2.2.

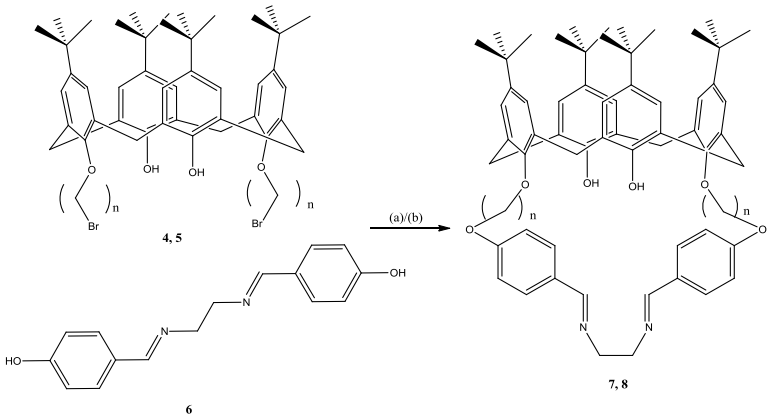

Scheme 3.5: Synthesis of *para*-Schiff base linked alkoxy calix[4]arenes, where n = 3,4. **(a)** *(i)* K_2CO_3, Δ, MeCN,*(ii)* **4**, Δ, MeCN. **(b)** *(i)* K_2CO_3, Δ, MeCN, *(ii)* **5**, Δ, MeCN.

It is clear from analysis of the ^{1}H NMR spectrum of **7**, that the symmetry which was exhibited by the starting materials is retained for the capped calix[4]arene. This is illustrated by two signals which represent the *tert*-butyl groups which resonate as singlets at 1.03 and 1.27 ppm. When this is compared to the bromopropoxy-calixarene

ligand **4**, no significant shifting of the signals is observed. The methylene bridges are again observed as two doublets with signals that resonate at 3.33 and 4.23 ppm. This clearly shows the diastereotopic nature of the genimal protons. The aromatic proton signals resonate as two singlets at 6.86 and 7.04 ppm which is characteristic for a *bis*-substitution pattern. Once again this shows minimal shifting of the spectrum in comparison to **4**. The propoxy fragment signals resonate at 2.31, 4.04 and 4.15 ppm as a multiplet and two triplets respectively. In comparison to the previously discussed calixarene scaffold **4**, the alkoxy chain shows the most significant shifting. The central CH_2 in the propoxy chain is shifted upfield by 0.20 ppm while the ether CH_2 signals are not shifted significantly. The phenolic proton resonates at 7.90 ppm as a singlet and is shifted by 0.27 ppm downfield when compared to the free ligand. The signals for the Schiff base portion of the molecule again shows the characteristic symmetry observed in the starting compound. The bridging CH_2 resonates as a singlet at 3.77 ppm integrating for four protons and shows no significant shift up or downfield. The aromatic region once again shows the characteristic *para* splitting pattern with a pair of doublets resonating at 6.81 and 7.53 ppm, which represent no significant shifting. The imine proton is represented as a singlet that resonates at 8.02 ppm, which is a 0.15 ppm upfield shift in comparison to **6**. A summary of these shifts is shown in Table 3.2. The presence of the imine is also corroborated by the ^{13}C NMR spectrum by a signal with a resonance of 161.7 ppm.

Table 3.2: Comparison of chemical shifts for capped calix[4]arene **7** and starting compounds **4** and **6**.

δH in S.M (ppm)	δH in 7 (ppm)	ΔδH (ppm)	Assignment
1.01, 1.27	1.03, 1.27	+ 0.02, 0.00	*t*-Bu
3.32, 4.24	3.32, 4.24	0.00, 0.00	Ar-CH_2-Ar
2.51, 3.98, 4.09	2.31, 4.04, 4.15	- 0.02, + 0.06, + 0.06	CH_2-CH_2-CH_2
6.86, 7.04	6.89, 7.05	+ 0.03, + 0.01	CxAr-H
7.63	7.90	+ 0.28	Ar-OH
3.76	3.77	+ 0.01	N-CH_2-CH_2-N
6.76, 7.51	6.81, 7.53	+ 0.05, + 0.02	Ar-H
8.17	8.03	- 0.14	HC=N

Upon analysis of the ^{1}H NMR spectrum of **8**, the retention of symmetry is again quite clear. The *tert*-butyl groups resonate as a pair of doublets at 0.99 and 1.29 ppm and the aromatic protons resonate as singlets at 6.84 and 7.06 ppm. The methylene bridges retain their diastereotopic nature and appear as two doublets that resonate at 3.31 and 4.28 ppm. The phenolic proton signal is represented by a singlet at 7.76 ppm. As was observed for compound **7**, the alkoxy chain is seen to undergo the most noticeable shifting when compared to the calix[4]arene cone. The butoxy chain is represented by two signals that resonate as two multiplets at 2.19 and 3.99 ppm. The bridging CH_2 of the Schiff base moiety is represented by this multiplet. Due to shifting of the signals, the characteristic splitting pattern is not observed for the aromatic protons. Instead, the signals resonate as two multiplets at 6.99 ppm and 7.23 ppm. As is the case with **7**, the imine proton has been shifted upfield to 8.05 ppm and, as with the capped calix[4]arene discussed earlier, the imine moiety was confirmed by ^{13}C NMR spectroscopy which exhibits a signal at 164.4 ppm. The approximate shifts are shown in Table 3.3.

Table 3.3: Comparison of chemical shifts for capped calix[4]arene **8** and starting compounds **5** and **6**.

δH in S.M (ppm)	**δH in 8 (ppm)**	**ΔδH (ppm)**	**Assignment**
1.02, 1.35	1.03, 1.29	+ 0.01, - 0.06	*t*-Bu
3.35, 4.27	3.32, 4.24	-0.03, - 0.03	Ar-CH_2-Ar
2.16, 2.34, 3.67, 4.04	2.19, 3.99	Indeterminate	CH_2-CH_2-CH_2-CH_2
6.85, 7.11	6.84, 7.07	- 0.01, - 0.04	CxAr-H
7.47	7.76	+ 0.29	Ar-OH
3.76	3.99	+ 0.23	N-CH_2-CH_2-N
6.76, 7.51	6.99, 7.23	+ 0.05, + 0.02	Ar-H
8.17	8.05	- 0.12	HC=N

IR spectroscopy was employed to aid in validation of the proposed structures. Imines are known to have a sharp absorbance band for the R_2C=N-R stretch between 1640-1690 cm^{-1}. Therefore, the presence of this, along with the phenolic stretch for the tetramer (≈ 3400 cm^{-1}), would back up the data from the ^1H and ^{13}C NMR spectra. This spectral method is of importance due to the desire to complex metals to the ligands. Examination of the IR spectrum of **7** shows the characteristic peaks for both the imine at 1644 cm^{-1} and the phenol group at 3411 cm^{-1}. When the spectrum for **8**, is studied these peaks are again seen at 1644 cm^{-1}, representing the imine, and 3395 cm^{-1} for the phenolic OH.

The syntheses of *meta* capped ligands **10** and **11** are shown in Scheme 3.6. The synthetic route is essentially the same as the *para* based compounds. As was the case with **7** and **8**, the reflux time is increased from twenty four hours to forty eight hours upon increasing the chain length from the 1,3-dibromopropane to the 1,4-dibromobutane.

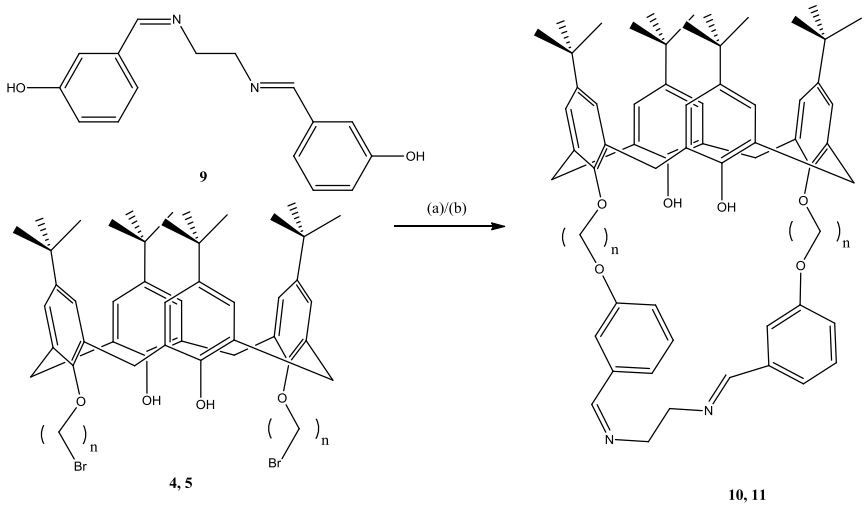

Scheme 3.6: Synthesis of *para*-Schiff base linked alkoxy calix[4]arenes, where n = 3,4. **(a)** *(i)* K_2CO_3, Δ, MeCN, *(ii)* **4**, Δ, MeCN. **(b)** *(i)* K_2CO_3, Δ, MeCN, *(ii)* **5**, Δ, MeCN.

For the reasons which have previously been discussed, the high degree of symmetry was once again observed for both compounds **10** and **11**. Analysis of the ^{1}H NMR spectrum reveals similar trends to what was seen previously with the *para* ligands; the *tert*-butyl groups resonate as two singlets at 1.05 and 1.26 ppm, and the calixarene aromatic protons are represented by two singlets at 6.91 and 7.03 ppm. Diastereotopic behaviour is again observed at the methylene bridges, which is evident from the pair of doublets at 3.31 and 4.24 ppm. The phenolic proton occurs at 7.96 ppm due to the same reasons discussed as the precursors. The propoxy pendant arm which links the tetramer to the Schiff base experiences some notable shifting in comparison to the precursor's spectrum. This segment of the compound is represented by a quintet and two triplet signals that resonate at 2.28, 4.06 and 4.37 ppm, respectively. A summary of these shifts can be seen in Table 3.4. The signals for the capping unit conform to the precursor spectrum quite well, with the ethylene bridge represented by a singlet that resonates at 3.93 ppm. The aromatic protons are represented by multiplets at 7.01 and 7.07 ppm and another multiplet at 7.29 ppm which is partially obscured by the $CDCl_3$ peak. The two imine protons are represented by a singlet at 8.06 ppm. When compared to the Schiff base linker starting material, this represents a 0.17 ppm upfield shift.

Table 3.4: Comparison of chemical shifts for capped calix[4]arene **10** and starting compounds **4** and **9**.

δH in S.M (ppm)	δH in 10 (ppm)	ΔδH (ppm)	Assignment
1.01, 1.27	1.05, 1.26	+ 0.04, - 0.01	*t*-Bu
3.32, 4.24	3.31, 4.24	- 0.01, 0.00	Ar-CH_2-Ar
2.51, 3.98, 4.09	2.28, 4.06, 4.37	- 0.23, + 0.08, + 0.28	CH_2-CH_2-CH_2
6.86, 7.04	6.84, 7.07	- 0.02, + 0.03	CxAr-H
7.63	7.96	+ 0.33	Ar-OH
3.83	3.93	+ 0.10	N-CH_2-CH_2-N
6.85, 7.09, 7.18	7.01, 7.07 ,7.29	+ 0.16, + 0.02, + 0.11	Ar-H
8.23	8.06	- 0.17	HC=N

Examination of the ^{13}C NMR spectrum aids in confirmation of the proposed structure indicated by a signal peak that resonates at 163.7 ppm which represents the imine carbon. Analysis of the IR spectrum shows stretching bands at 3404 and 1646 cm^{-1}. These bands are in the expected range for both the phenolic and imine groups, respectively.

As was the case for the propoxy capped calixarene **10**, the structure of the butoxy derivative **11** was confirmed by ^{1}H NMR spectroscopy. This is further backed up by the ^{13}C NMR and IR spectra of the ligand. Symmetry is confirmed by the presence of two *tert*-butyl groups at 0.99 and 1.29 ppm which resonate as singlets and the two aromatic proton signals for the calix-core, which are represented by two singlets at 6.84 and 7.07 ppm. This pattern in the ^{1}H NMR spectrum is indicative of a 1,3-distal substituted calix[4]arene. The methylene bridges are represented by two doublets at 3.31 and 4.29 ppm. The butoxy chain signals are shifted as is seen in **8**. They are represented by two multiplets at 2.18 ppm and 4.00 ppm which integrate for eight and twelve protons, respectively. The multiplet, which resonates at 4.00 ppm, also includes

the bridging ethyl protons; this is indicated by its integration for twelve protons. The phenolic proton calixarene scaffold is represented as a singlet at 7.74 ppm. The signals for the Schiff base portion of the structure are represented by a singlet at 8.05 ppm for the imine proton and a singlet at 3.99 ppm, which is in the midst of the butoxy multiplet representing the bridging ethyl protons. The aromatic protons for the Schiff base can be seen as multiplets centred at 6.84, 7.05 and 7.17 ppm. These signals are slightly obscured by the aromatic signals from the calixarene core. Table 3.5 shows a summary of the relative shifts in the ^{1}H NMR spectrum of the *meta*-Schiff base capped butoxy calixarene **11**.

Table 3.5: Comparison of chemical shifts for capped calix[4]arene **11** and starting compounds **5** and **9**.

δH in S.M (ppm)	**δH in 11 (ppm)**	**ΔδH (ppm)**	**Assignment**
1.02, 1.35	0.99, 1.29	- 0.03, - 0.09	*t*-Bu
3.35, 4.27	3.31, 4.29	- 0.04,+ 0.02	Ar-CH_2-Ar
2.16, 2.34, 3.67, 4.04	2.18, 4.00	Indeterminate	CH_2-CH_2-CH_2-CH_2
6.85, 7.11	6.84, 7.07	- 0.01, - 0.04	CxAr-H
7.47	7.74	+ 0.27	Ar-OH
3.83	3.99	+ 0.16	N-CH_2-CH_2-N
6.85, 7.09, 7.18	6.84, 7.05, 7.17	- 0.01, - 0.04, - 0.01	Ar-H
8.23	8.05	- 0.18	HC=N

This structural assignment was confirmed by the ^{13}C NMR spectrum, which has a resonance at 164.4 ppm indicative of an imine. Again, IR spectroscopy was used as a tertiary analytical method and shows bands at 3459 and 1646 cm^{-1}.

The *ortho*-Schiff base capped calix[4]arenes were synthesised in the same manner as both the *para* and *meta* variants but it was found that this addition to the system resulted in negatively affected yields and, particularly in the case of the butoxy chain,

made purification more difficult to achieve. The reaction conditions and synthetic route are shown in Scheme 3.7.

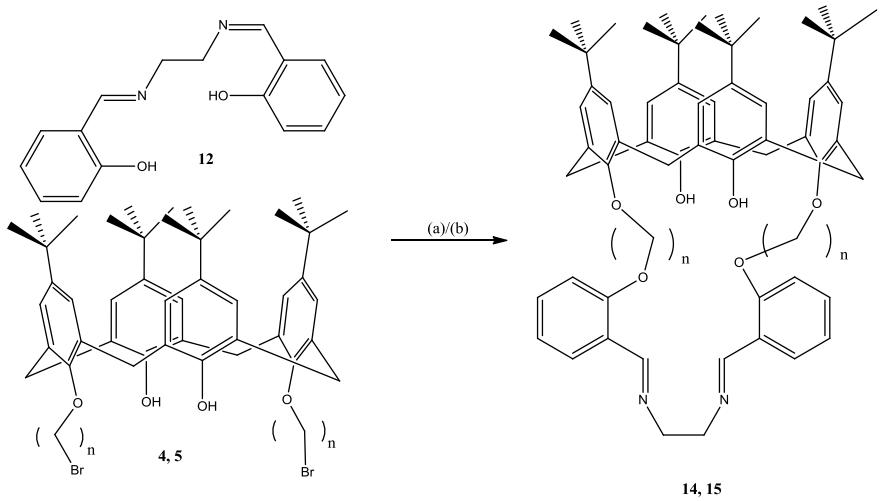

Scheme 3.7: Synthesis of *para*-Schiff base linked alkoxy calix[4]arenes, where n = 3,4. **(a)** *(i)* K_2CO_3, Δ, MeCN,*(ii)* **4**, Δ, MeCN. **(b)***(i)* K_2CO_3, Δ, MeCN, *(ii)* **5**, Δ, MeCN.

The propoxy derivative **14** was successfully isolated as a yellow solid. Analysis of the product through ^{1}H NMR spectroscopy provides a clear indication of the symmetry in the macrocyclic molecule. This is clear from the two *tert*-butyl groups resonating at 1.01 and 1.33 ppm as a pair of singlets, and the calixarene aromatic protons, which are represented as a pair of singlets that resonate at 6.88 and 7.04 ppm. The methylene bridging protons appear as a pair of doublets at 3.32 and 4.24 ppm and, as discussed earlier, retain their diastereotopic nature. The propoxy chain is represented by a quintet and two triplets which resonate at 2.48, 3.99 and 4.09 ppm, respectively. The phenolic proton resonates at 7.76 ppm as a singlet. The ethyl bridging protons resonate as a singlet at 3.95 ppm, whilst the imine protons are represented as a singlet resonating at 8.37 ppm. In a trend which was established with the other capped calix[4]arenes, the aromatic protons in the Schiff base are represented by multiplets that are somewhat concealed by the tetramer aromatic protons which resonate at 6.86 and 7.24 ppm. A doublet is also seen to resonate at 6.92 ppm. A summary of the shifting compared to

the starting materials is shown in Table 3.6. The ^{13}C NMR spectrum of **14** shows a resonance at 165.5 ppm which backs up the presence of the imine. This is given further backing by the IR spectrum, which upon analysis shows absorption bands at 3410 and 1634 cm^{-1}, which are indicative of the presence of phenolic OH and imine.

Table 3.6: Comparison of chemical shifts for capped calix[4]arene **14** and starting compounds **4** and **12**.

δH in S.M (ppm)	δH in 14 (ppm)	ΔδH (ppm)	Assignment
1.01, 1.27	1.01, 1.33	+ 0.00, + 0.06	*t*-Bu
3.32, 4.24	3.32, 4.24	0.00, 0.00	Ar-CH_2-Ar
2.51, 3.98, 4.09	2.48, 3.99, 4.09	- 0.03, + 0.01, + 0.00	CH_2-CH_2-CH_2
6.86, 7.04	6.88, 7.04	+ 0.02, + 0.00	CxAr-H
7.63	7.76	+ 0.13	Ar-OH
3.91	3.95	+ 0.05	N-CH_2-CH_2-N
6.86, 7.29, 7.74	6.86, 6.92, 7.24	Indeterminate	Ar-H
8.58	8.37	- 0.21	HC=N

Upon analysis of the ^{1}H NMR spectrum of **15**, the symmetry is again clear and is indicated by the presence of two singlets which resonate at 0.99 and 1.34 ppm, and the two singlets for the aromatic protons which resonate at 6.82 and 7.10 ppm. The butoxy fragment is represented by a multiplet at 2.16 ppm, which represents eight protons, and a multiplet which resonates at 3.90 ppm, which integrates for twelve protons. As for the previous butyl chain calixarenes, the protons for the ethyl bridge on the Schiff base also resonate in the middle of this multiplet. The aromatic protons are observed as two singlets which resonate at 6.84 and 7.05 ppm, and the phenol group is represented by a singlet at 7.36 ppm. The ethyl bridge is represented in a multiplet at 3.99 ppm, the imine group resonates as a singlet at 8.71 ppm. The aromatic protons are represented by a multiplet at 6.89 ppm, a multiplet centred at 7.01 ppm and a doublet of doublets at 7.93 ppm. The ^{13}C NMR and IR spectra again confirm the presence of both the imine

proton and phenolic hydroxyl group, with a signal resonating at 160.2 ppm, and absorption bands at 3398 and 1633 cm^{-1} for the imine and phenol, respectively.

Due to the difficulty in purifying the product, the ^{1}H NMR spectrum is not quite as clearly defined as in the case of either *para* or *meta* variants. As such, comparison with the starting materials to determine relative shifts is ineffectual in this case.

This reduced yield may possibly be due to steric hindrance which arises as a consequence of the position of the imine group within the cavity. As a result of strain, the Schiff base bridge would also be required to adopt a distorted conformation. This effect seems to be more obvious for the *ortho* when it is compared with the *para* and *meta* derivatives, which can be seen in the proposed structures in Figure 3.2. However without crystallographic data, the structure cannot be determined unambiguously.

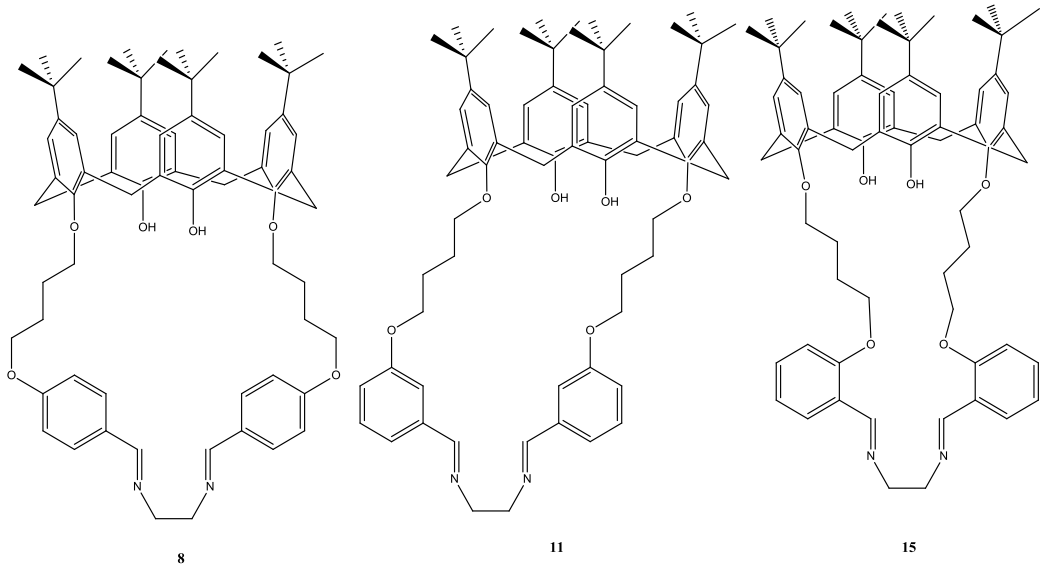

Figure 3.2: Proposed structures of **8**, **11** and **15**.

This proposed strain could explain why there is such a dramatic reduction in yield. This trend has been previously reported by Vicens *et al*.[43] This group created a range of Schiff base calix[4]arenes which were then screened for their metal ion extraction ability. However, these capped calixarenes were synthesised by way of a cross linking

reaction. While this is not a definitive trend, it is seen when the length of the bridge is increased that an initial increase in yield is observed.[43] The extra flexibility afforded to the scaffold from the lengthened alkyl chain results in the need for an extended reaction time to maximise yield, but as expected leads to lesser yields than the propoxy derivatives. This combination of factors negatively affects the synthesis of **15**.

3.2.5 Reactions of 1,3-distal bromoethoxy calixarene with Schiff base linkers 6, 9 and 13.

The successful synthesis of an *ortho*-capped ethoxy-calixarene has been previously reported,[43] but in this synthesis a cross linking reaction was exploited. Therefore, it was expected that the compartmental route employed in this thesis would yield similar results. The synthesis plan followed is shown in Scheme 3.8, which was the standard route adhered to throughout the synthesis of capped calixarenes. After the twenty four hour reflux period, ^{1}H NMR spectroscopy was carried out on the crude product, however this did not yield the expected product.

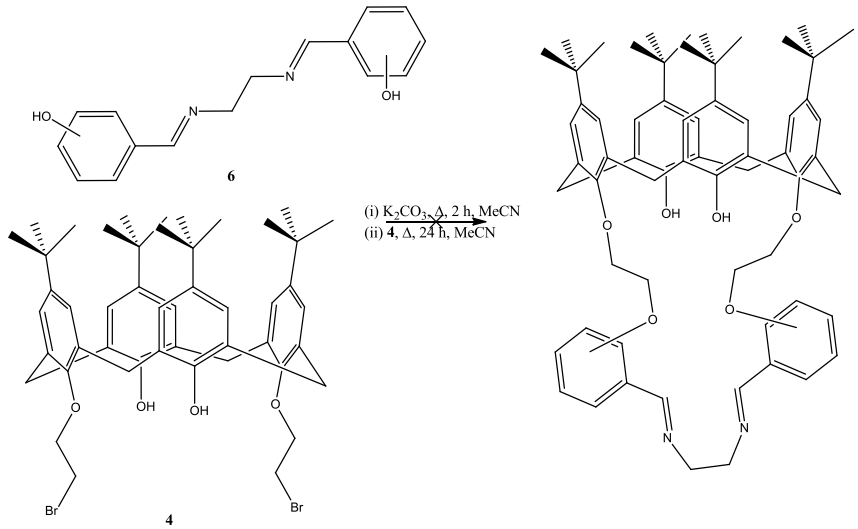

Scheme 3.8: Attempted synthesis of the Schiff linked ethoxycalix[4]arenes with conditions used and proposed structure shown.

The same method was attempted with the *ortho* and *meta* Schiff base linkers, which is shown in Scheme 3.8, as with all 1,3-distal-substituted calixarenes studied in the course of this project. As was the case with the previous reaction analysis of the ^{1}H NMR spectrum reveals that the desired products were not obtained.

In previous studies reported on the reaction of *bis*(tetrazole)phenylenes with 1,2 dibromoethane,[119] a vinyl group is formed by the presence of unreacted triethylamine abstracting HBr from the initially formed alkylbromo compounds. An alternate route is that the bromo ion that is formed in the first displacement can act as a base in 1,2-dibromoethane in the absence of solvent, which results in an ion that is not solvated. However, the spectroscopic data obtained did not provide evidence for the formation of a vinyl compound. Therefore, it is reasonable to conclude that the synthetic method employed in this thesis is not suitable for the 1,3-*bis*bromoethyl tetramer.

3.2.6 Spectroscopic Studies

The ligands which were obtained with sufficient purity (**7**, **8**, **10**, **11** and **12**) were screened to acquire their UV-Vis absorbance spectrum (Figure 3.3). Due to the insolubility of the ligands in other commonly used solvents, e.g. MeCN, the spectra were all obtained using a HPLC grade $CHCl_3$ solution of the compound at a concentration of 100 μM of the proposed structures. A summary of the absorbance peaks observed is shown in Table 3.7. These peaks were used to determine the excitation wavelength for fluorescent emission spectroscopy λ_f^{ex}. None of the ligands were found to exhibit any observable fluorescent behaviour (NFO).

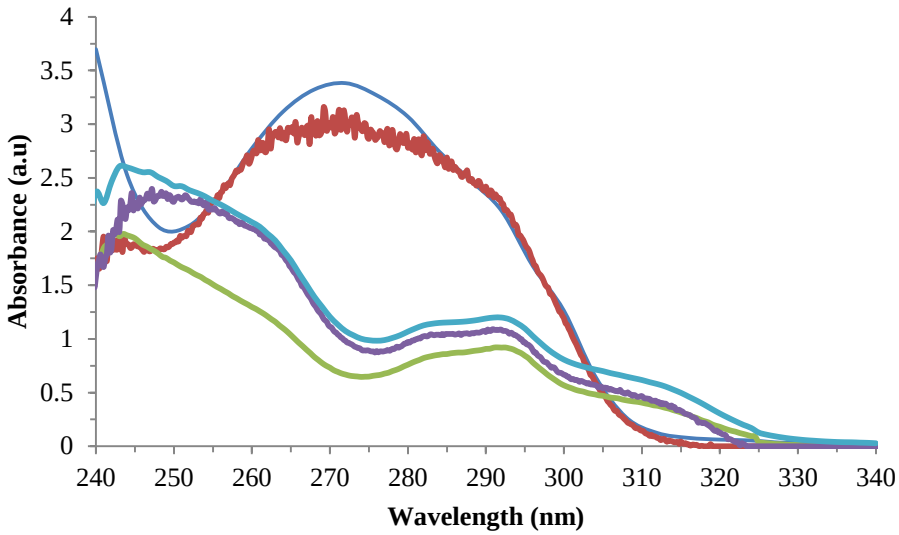

Figure 3.3: UV-Vis Spectra of **7** (blue), **8** (red), **10** (green), **11** (light blue), **12** (purple) ($CHCl_3$) 100 μM.

Table 3.7: Summary of absorbance peaks observed for Schiff base ligands.

Sample No.	Absorption Peaks nm		λ_f^{em}
7	228.0	272.0	NFO
8	269.2	243.6	NFO
10	242.5	291.5	NFO
11	243.0	292.0	NFO
14	230.0	284.0	NFO

3.3 Metal Complexation Reactions of Schiff base calix[4]arenes

3.3.1 Overview

The metal binding abilities of Schiff bases is a major factor in their selection for the construction of Schiff base capped calixarenes. The imine moiety makes them effective metal binders as it has a nitrogen atom which possesses a lone pair of electrons; it is these electrons which then donate into the metal to form a coordination bond. The extent to which the imine moiety has been employed in the preparation of

molecules that have ligating qualities has been reviewed by Vigatio *et al.*[30] Metal complexation reactions were performed between ligands **7**, **8**, **10**, **11**, **14** and **15**, and the metal perchlorate salts of copper, cobalt, mercury, nickel and zinc. For ligand **7**, a complex formation was attempted with the anhydrous zinc chloride salt. Due to the general insolubility for the calixarene ligands in typical co-ordination solvents, such as ethanol or methanol, it was required to perform these reactions in a mixed solvent system. The solvent system, which was almost exclusively used, was a mixture of methanol and chloroform, with the exception being the reaction of ligand **7** with zinc chloride carried out in a toluene and methanol mixture. Where possible, the result of the reaction was monitored with ^{1}H and ^{13}C NMR spectroscopy, but this was only available for the proposed mercury and zinc complexes due to the paramagnetism of the other metals studied. Infrared spectroscopy was also used to characterise the products from these reactions. As was discussed in section 3.2.3 and 3.2.4, the imine absorption band occurs between 1630 and 1670 cm^{-1}, so changes to this would indicate complexation at this site. Also, this could be used to establish if ligand hydrolysis had occurred.

3.3.2 Schiff base hydrolysis and cleavage

A major problem with using Schiff bases in attempting to complex metal ions is that Schiff base ligands readily undergo hydrolysis. Cleavage of the imine bond can occur even under mild conditions. In the metal complexation reactions which were attempted in Section 2.2, every precaution was taken to ensure that anhydrous solvents and conditions were used. However, the addition of water to the system was unavoidable due to the metal salts, which were obtained commercially in their hydrated form. In the course of this project, it was found that this did indeed supply enough water to lead to ligand hydrolysis and this could also be accelerated by metal cations which have Lewis

acid properties. The mechanism for imine formation (acid catalyst and dehydration) and its reversible reaction (aqueous acid) are shown in mechanism 3.1.

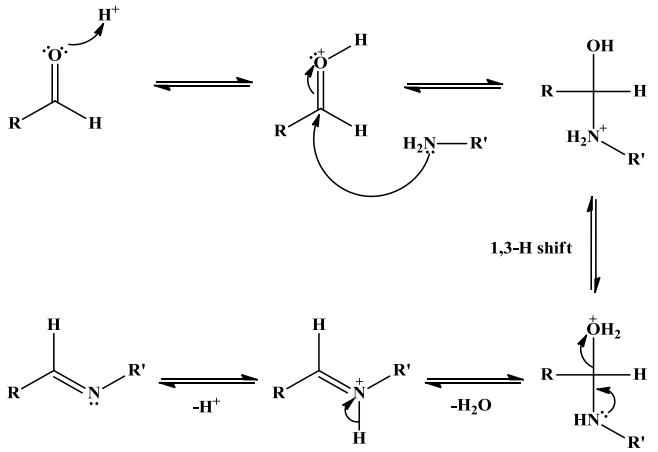

Mechanism 3.1: Mechanism of imine formation.

In nearly all cases, evidence of metal complexation was observed with coordinate perchlorate groups being evident from the IR spectra. In cases where ^{1}H NMR spectroscopy was possible, imine hydrolysis was evident from a shift seen at approximately 9.70-10.0 ppm depending on the position of the aldehyde. In certain cases this was confirmed by ^{13}C NMR spectroscopy with a signal occurring in the region of 190 ppm, contrasting with the expected 160-165 ppm for the imine carbon. Elemental analysis was also used to determine the structure of any complexes formed by these reactions.

3.3.3 Ethlyene Diamine (en) metal complexes

As a result of imine hydrolysis it is possible that the diamine is now available for complexation reactions. This has been previously noted in work carried out by our group. Attempted metal complexation reactions with *m*-Schiff base ligands (Figure 3.4) results in cleavage of the imine moiety and subsequent formation of bidentate en(M) complexes.[120]

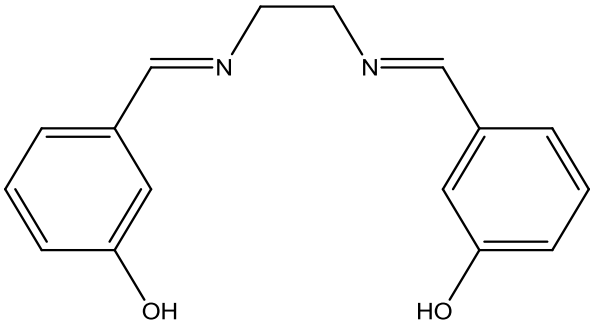

Figure 3.4: *m*-Schiff base ligand prepared by Mahon and co-workers.[120]

Chattopadhyay *et al*. reported on the influence the counter anions of a metal salt on hydrolysis of the imine bond in metal complex reactions. It was found that when the counter ion was chloride, hydrolysis of the imine occurred and an en complex of the metal was formed (en(M)) (Figure 3.5).[121]

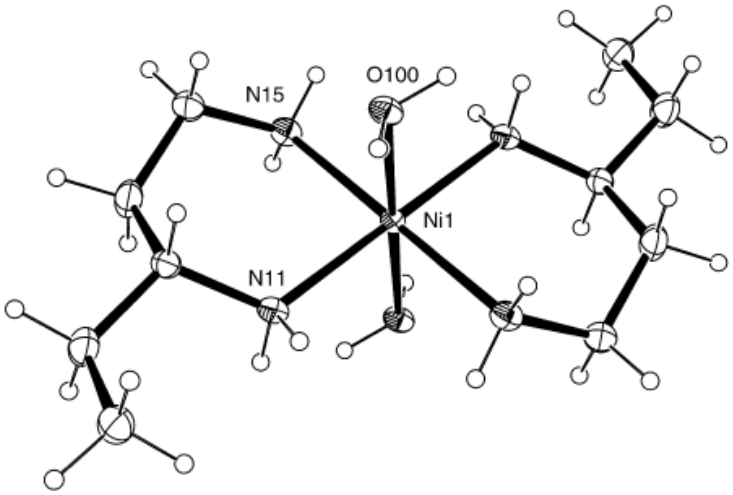

Figure 3.5: en(Ni) complex isolated by Chattopadhyay and co-workers.[121]

Both of these studies successfully isolated the en(M) complex which was formed. However, in the current study, even after numerous attempts at recrystallization, isolation of the probable resultant complex proved fruitless. The micro analytical data which was acquired for the attempted complexes does suggest there are both nitrogen and metal salts present in the product obtained. The IR spectroscopic data which indicates the presence of the perchlorate counter anion also points towards this. It is

proposed that after hydrolysis of the imine to yield the calix[4]arene dialdehyde, the free diamine could form a metal complex.

3.3.4 Metal Complexation reactions of ligand 7

3.3.4.1 Reaction of 7 with zinc(II) perchlorate

A solution of **7** in chloroform was stirred in a 100 mL round bottom flask and to this a methanolic solution of zinc(II) perchlorate was added, whereupon a white precipitate formed. This was collected and analysed and found to be the starting ligand **7** (Figure 3.6).

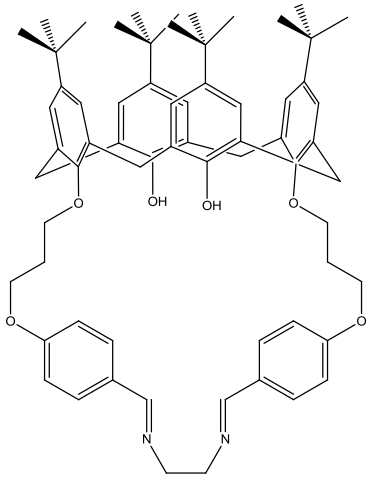

Figure 3.6: Ligand **7**.

As a result, the filtrate was concentrated and the residue was analysed by ^{1}H NMR spectroscopy. The spectrum of **7** and the spectrum of the zinc perchlorate complex are shown in Figure 3.7. The proton signals, which are labelled as per Figure 3.8, show the largest degree of shifting in the complex form. The signal that represents the phenolic protons H_f undergoes an upfield shift of 0.26 ppm from 7.90 ppm in **7**, to 7.64 ppm in the product obtained. There is also a shift for the non-calixcore aromatic signals: H_d undergoes a shift from 6.81 to 7.03 ppm, and H_e from 7.53 to 7.79 ppm, downfield shifts of 0.22 and 0.26 ppm, respectively. The most notable apparent shift is seen in

H_g, which resonates at 8.02 ppm in the starting ligand spectrum, and at 9.84 ppm in the spectrum of complex Zn(**7**)$(ClO_4)_2$ which would have represented a downfield shift of 1.82 ppm. A shift in position was expected for the imine proton H_g, which was the proposed site for metal complexation. Studies on similar Schiff bases have reported shifts of between 0.05-0.5 ppm on complexation,[48,122] and, as such, this strikingly obvious shift was not unexpected. However, the magnitude of this shift may indicate that ligand hydrolysis had occurred, particularly when viewed with the apparent disappearance of the bridging ethyl signal at 3.77 ppm.

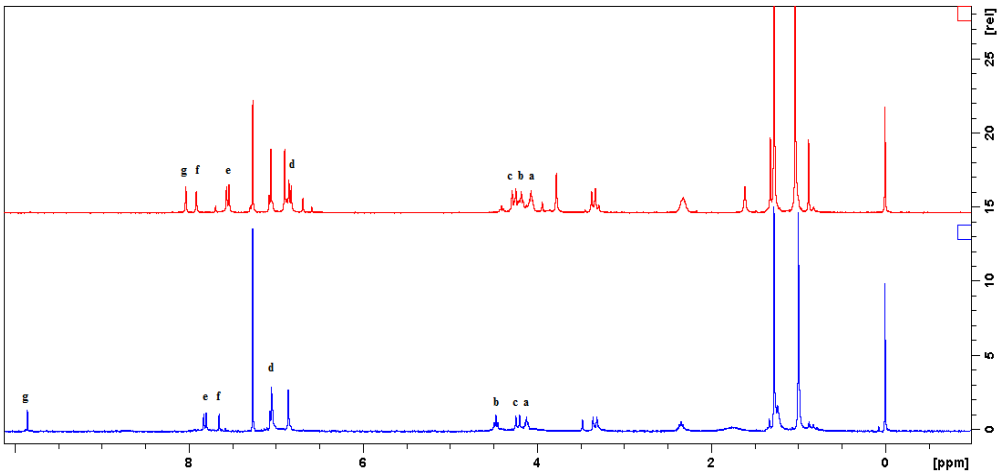

Figure 3.7: Comparison of ^{1}H NMR spectrum of Complex Zn(7)$(ClO_4)_2$ (blue) and **7** (red).

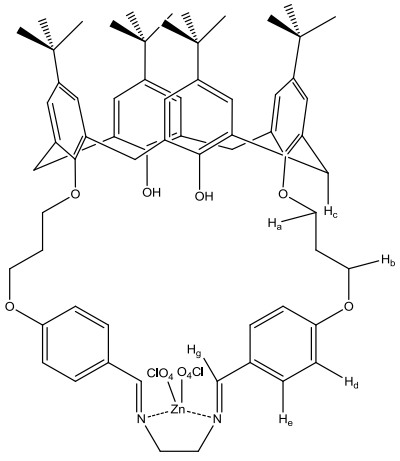

Figure 3.8: Originally proposed structure for Complex Zn(**7**)$(ClO_4)_2$ with protons which undergo shifts labelled.

As the ^{1}H NMR spectrum strongly suggested aldehyde formation, the ^{13}C NMR spectrum was next to be studied. The spectral trace of **7** clearly includes a signal at 161.7 ppm, which is indicative of an imine carbon in the structure. This has been previously discussed in section 3.2.3 and 3.2.4. Some shifting in the signal position would be reasonable to expect, but analysis of the spectrum for the complex reveals a stark difference; a new signal is now seen at 189.1 ppm. This signal resonates in the region of the spectrum where one would expect an aldehyde carbon to appear, so with this and the ^{1}H NMR spectrum it was becoming clear that ligand hydrolysis had taken place. These signals can be seen in Figure 3.9a and 3.9b below.

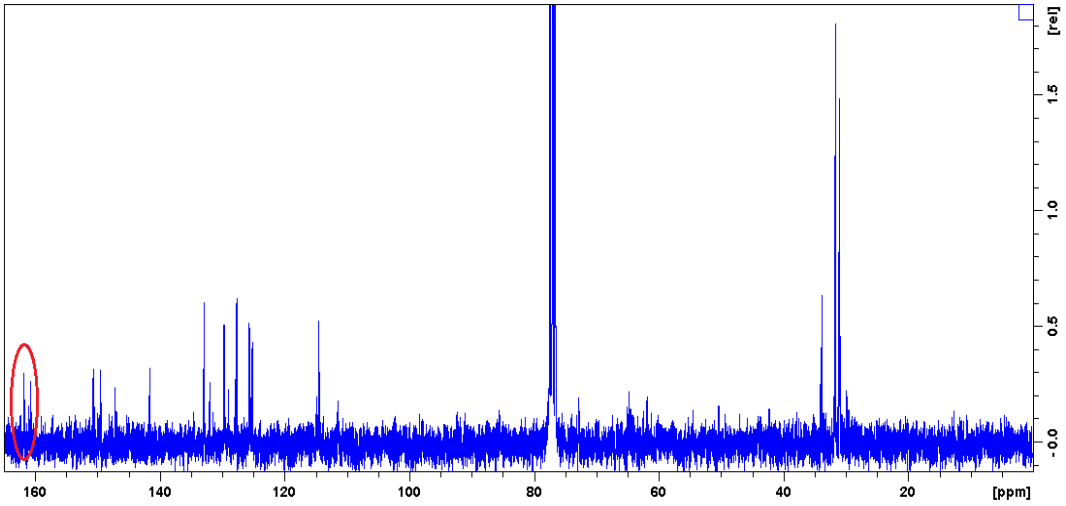

Figure 3.9a: ^{13}C NMR spectrum of **7**.

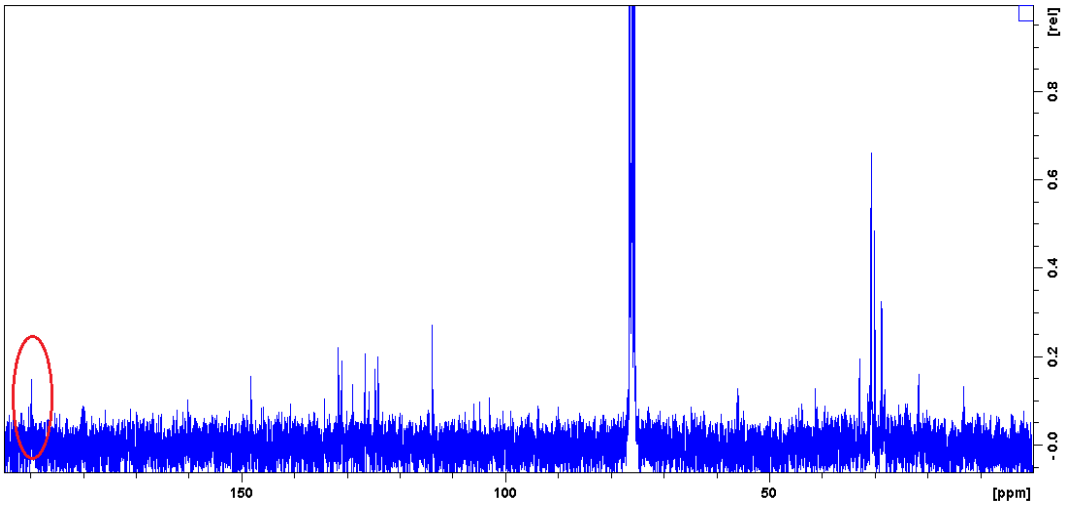

Figure 3.9b: ^{13}C NMR spectrum of complex Zn(**7**)$(ClO_4)_2$.

Analysis of the IR spectra of **7** (Figure 3.10a), and of Zn(**7**)$(ClO_4)_2$ (Figure 3.10b), reveals clearly that the absorption band which appears at 1644 cm^{-1} in the spectrum of **7** is now seen at 1735 cm^{-1}. This new higher wavenumber is most likely attributable to the formation of an aldehyde in the structure. This effect can also be seen in the appearance of two absorption bands at 2742 cm^{-1} and at 2856 cm^{-1}. These bands are typical of the C-H aldehyde stretch. The presence of the perchlorate anion is suggested by the observation of absorption bands at 1097 cm^{-1} and 1195 cm^{-1}, suggesting that some metal complexation has occurred.

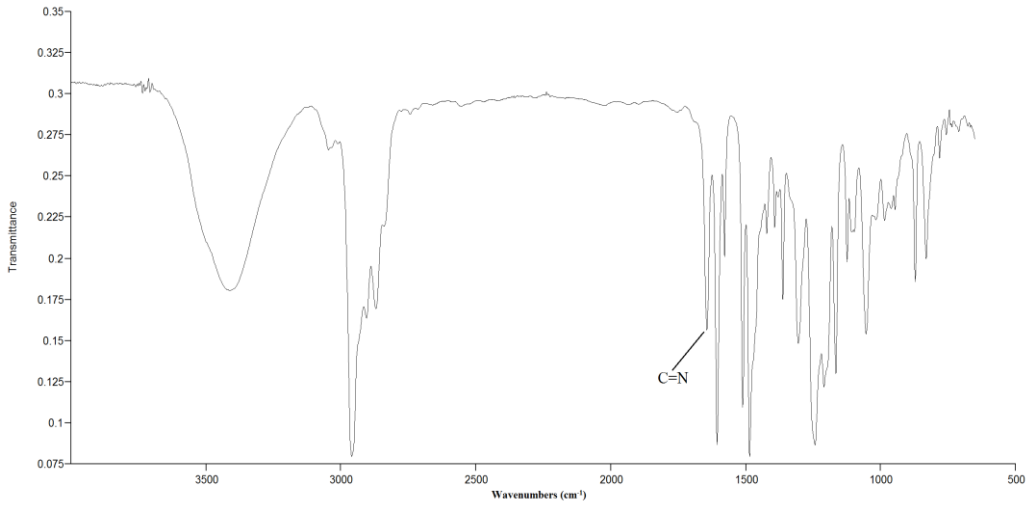

Figure 3.10a: IR Spectrum of **7.**

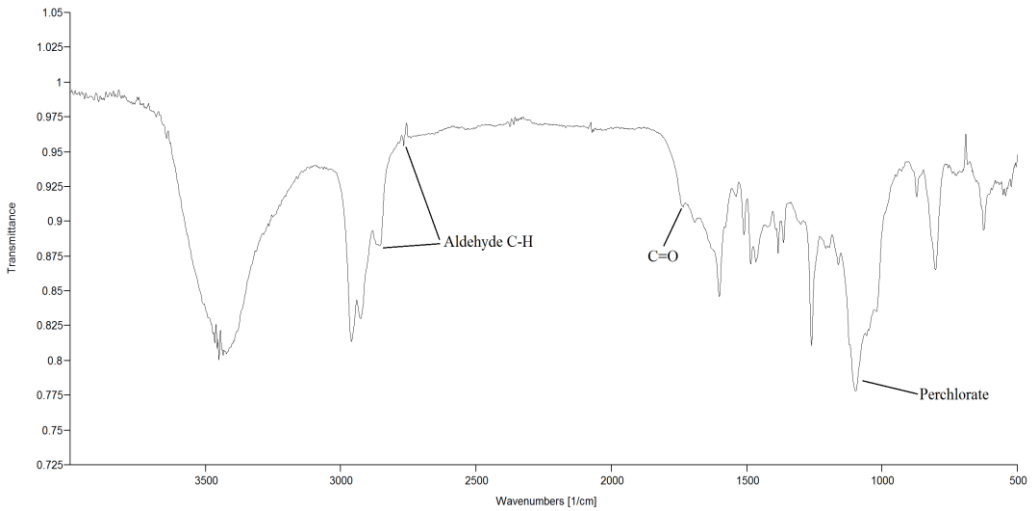

Figure 3.10b: IR spectrum of Zn(**7**)$(ClO_4)_2$.

Elemental analysis was also performed on this compound. The calculated results for the proposed structure in Figure 3.8 would account for carbon comprising 62.83 % of the structure, with hydrogen and nitrogen responsible for 6.39 % and 2.22 %, respectively. The returned experimental results differ from this with carbon accounting for 62.60 %, with hydrogen and nitrogen as 7.65 % and 1.44 %, respectively. The result for nitrogen of 1.44% indicates that there may still be an imine or amine present in the structure.

3.3.4.2 Reaction of 7 with mercury(II) perchlorate

The same procedure was used for the attempted complexation of **7** with mercury(II) perchlorate as for complex Zn(**7**)$(ClO_4)_2$. No starting material precipitated out of solution during the course of this reaction. The product was obtained as a purple solid. This colour change was unexpected as previously reported mercury complexes tend to retain the colour of the parent ligand. As mercury is diamagnetic, ^{1}H NMR spectroscopic analysis was possible and as a result the spectrum was studied in the same manner as the zinc(II) perchlorate complex. Shown and labelled in Figure 3.11, is the ^{1}H NMR spectrum of the ligand **7** and the product from the complex reaction as well as significant shifts within the spectra. The effect of symmetry is noted in the spectrum by the appearance of two singlets at 0.99 and 1.27 ppm which represent the *tert*-butyl groups, and by a set of singlets at 6.85 and 7.04 ppm which is representative of the calixarene aromatic protons. The signal for H_c, which is attributed to the imine proton in the calixarene compound **7**, seems to undergo a shift from 8.02 ppm to 9.84 ppm. This would be a 1.82 ppm downfield shift and, when compared to shifts observed in other Schiff base metal complexes, this seems excessive. It would seem that this ligand underwent hydrolysis during the complexation reaction. The phenolic proton H_b

shifts upfield from 7.90 to 7.66 ppm, a shift of 0.24 ppm. This is consistent with the shifts seen in the zinc perchlorate complex reaction in section 3.3.3.1.

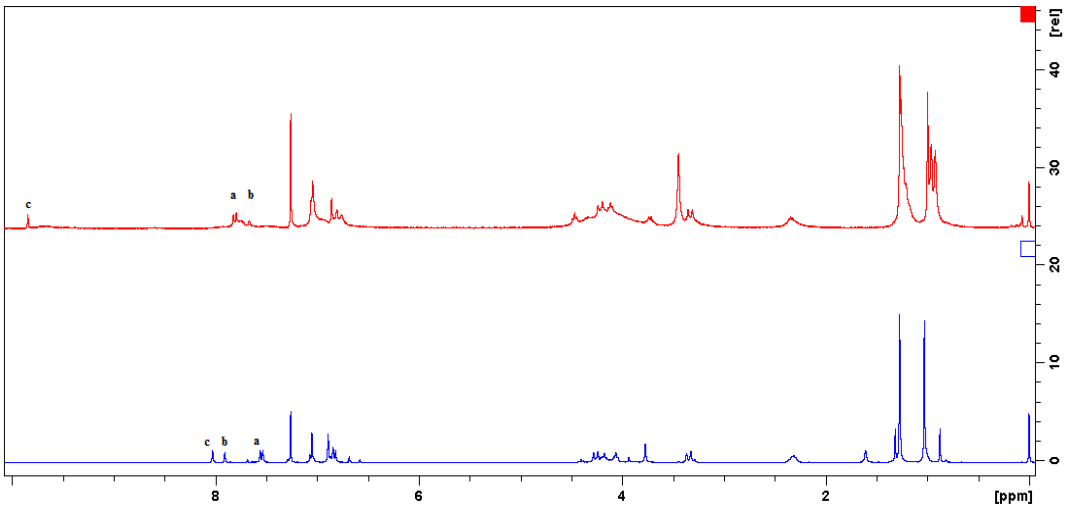

Figure 3.11: ^{1}H NMR spectrum of **7** (blue) and Complex Hg(**7**)$(ClO_4)_2$.

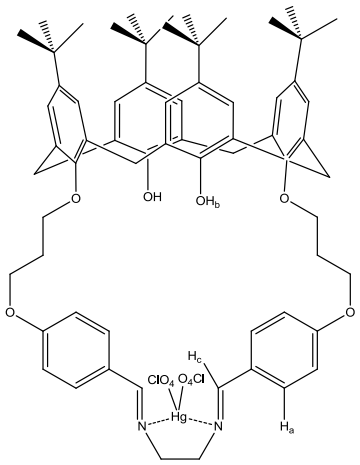

Figure 3.12: Originally proposed structure for Hg(**7**)$(ClO_4)_2$.

The IR spectrum of the product obtained (Figure 3.13), was compared to the spectrum for the starting material **7**, shown in Figure 3.10a. It can be seen that a slightly broad band occurs at 1671 cm^{-1}, differing from **7**, which has a sharper band at 1644 cm^{-1}. A typical imine stretch occurs between 1640-1690 cm^{-1}, while an aldehyde usually has stretching bands at 1685-1710 cm^{-1} for the C=O, and 2850 and 2750 cm^{-1} for C-H stretch. The stretching bands observed at 2745 cm^{-1} and 2873 cm^{-1}, along with the

previously mentioned band at 1671 cm^{-1}, points to an aldehyde incorporated into the compound. The conjugated nature of the benzaldehyde which would result for imine hydrolysis would account for this low wavenumber for a C=O aldehyde stretch. This effect has been previous reported in the case of 4-Hydroxybenzaldehdye.[123] It is clear from the spectrum that the perchlorate is also present, which is shown by the band at 1103 cm^{-1}.

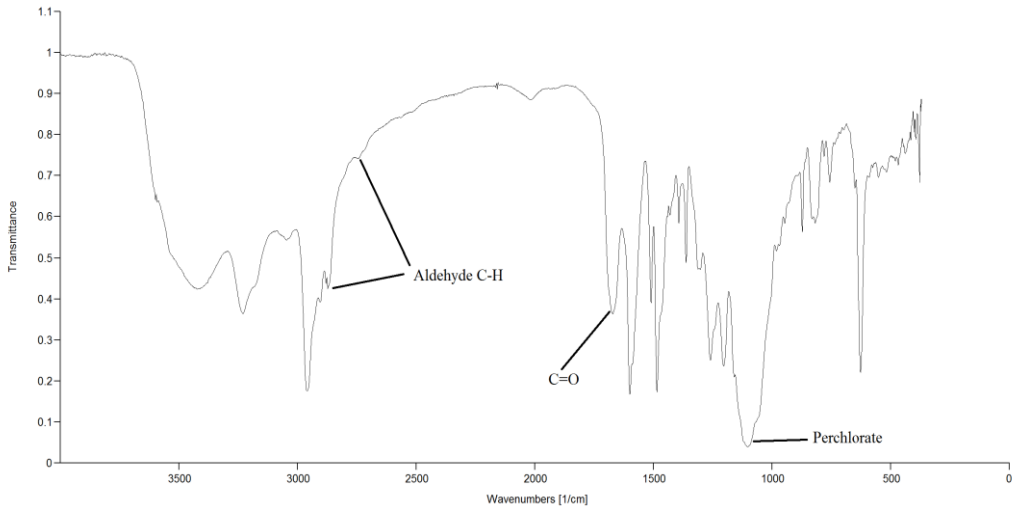

Figure 3.13: IR spectrum of Complex Hg(**7**)$(ClO_4)_2$.

Elemental analysis was also performed on the product from this reaction, with the expected result for the structure proposed in Figure 3.8 being carbon 56.75%, Hydrogen 5.77% and Nitrogen 2.01%. The results returned were quite different with the carbon comprising 71.70 %, hydrogen 4.54 %, and nitrogen 1.42 % of the structure.

3.3.4.1 Reaction of 7 with zinc(II)chloride

A solution of **7** in toluene was stirred in a 50 mL round bottomed flask, to this a methanolic solution of zinc(II)chloride was added dropwise. No precipitate was formed, so the solution was reduced to dryness under reduced pressure and the yellow

substance formed was analysed by ^{1}H NMR spectroscopy. Complexation of the zinc(II)chloride salt was explored, due to its availability in an anhydrous basis. Despite the hydroscopic nature of the metal salt, meaning that it would be impossible to guarantee total exclusion of water from the reaction, it was expected that there would be less available than in the case of the perchlorates. This would give more of an insight into whether the hydrolysis is a result of the water complexed to the perchlorate salts, or due to the interaction with the metals themselves. As was the case with the Zn(**7**)$(ClO_4)_2$, a signal occurs at 9.84 ppm as a singlet, which had been previously thought to represent the aldehyde proton formed as a result of the hydrolysis reaction. However, there was also evidence of the imine within the spectrum, as can be seen in Figure 3.14.

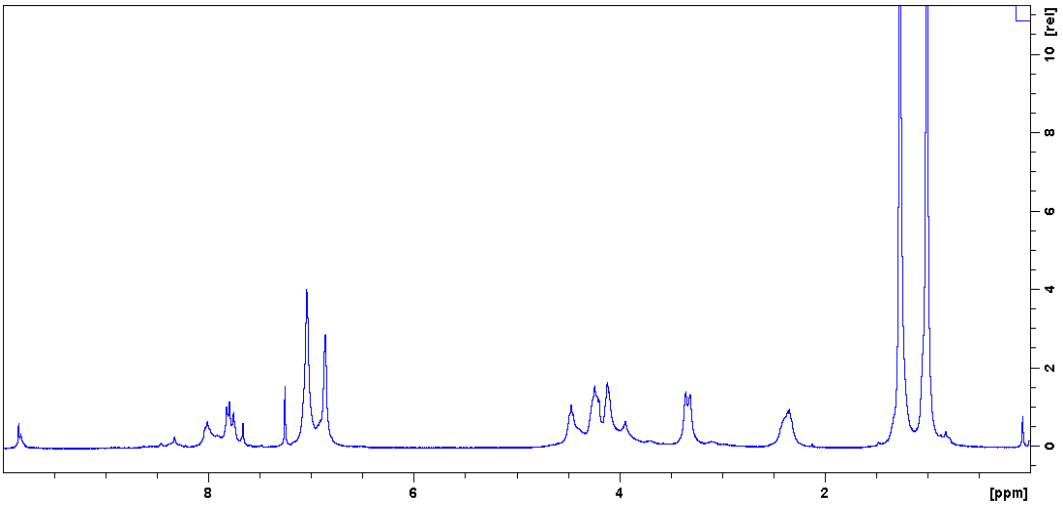

Figure 3.14: ^{1}H NMR of Zn(**7**)Cl_2.

The ^{13}C NMR spectrum also seems to confirm the presence of both aldehyde and imine within the structure with a peak at 190.8 ppm and another at 163.9 ppm, as can be seen in Figure 3.15.

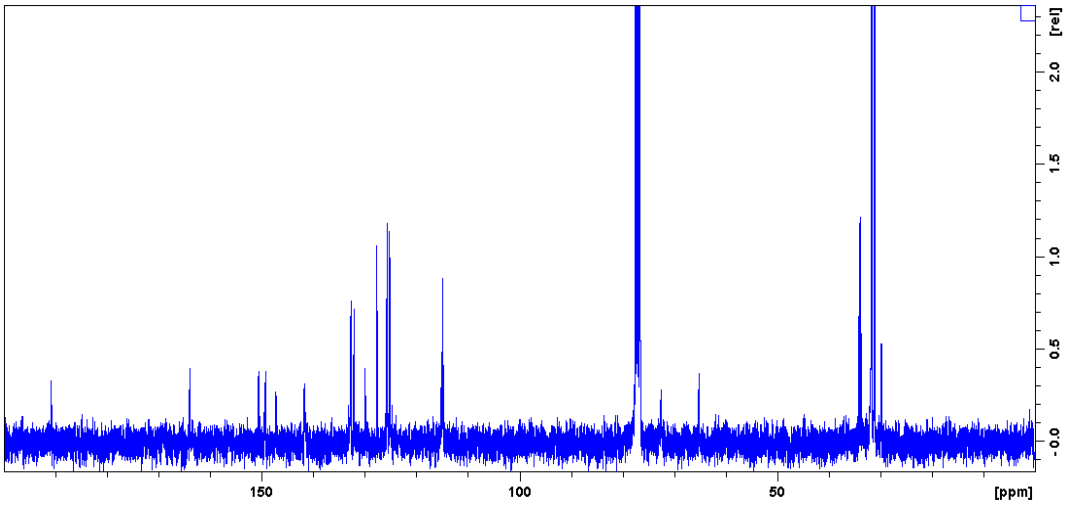

Figure 3.15: ^{13}C NMR of Zn(**7**)Cl_2.

The IR spectrum was also examined (Figure 3.16) and the presence of an aldehyde is clear from the C=O stretching band which occurs at 1692 cm^{-1}, but there is also evidence of the imine being present from a weak band at 1635 cm^{-1}. The bands which appear at 2740 and 2868 cm^{-1} once again seem to be in line with the imine hydrolysis hypothesis.

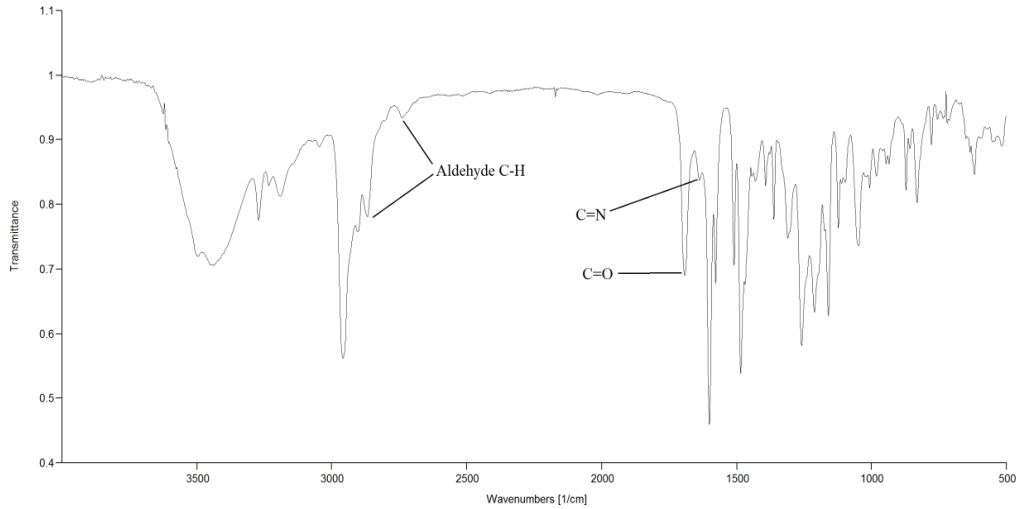

Figure 3.16: Infrared spectra Zn(**7**)Cl_2.

Elemental analysis was performed on the isolated product. It was found that the experimental results deviated from those which had been calculated. However, this deviation was to a lesser extent than previously observed. The calculated results were

carbon 69.93 %, hydrogen 7.11 % and nitrogen 2.47 %, but the experimentally found results came back as carbon 66.60 %, hydrogen 6.33 % and nitrogen 1.30 %. Therefore, it is clear that this proposed structure varies from the actual structure formed.

3.3.4.2 Reaction of 7 with paramagnetic perchlorate metal salts

A similar procedure was followed for the preparation of the paramagnetic complexes Cu(**7**)$(ClO_4)_2$, Co(**7**)$(ClO_4)_2$ and Ni(**7**)$(ClO_4)_2$ as was discussed for Zn(**7**)$(ClO_4)_2$ and Hg(**7**)$(ClO_4)_2$. As these metals are paramagnetic, ^{1}H NMR and ^{13}C NMR spectroscopic analysis could not be used to characterise the product. Therefore, IR spectroscopy was the main technique used and these spectra could be compared with the spectra obtained for the diamagnetic compounds. The product from the copper complexation reaction was a blue-green solid. The IR spectrum in Figure 3.17 shows a sharp absorbance peak at 1694 cm^{-1}, which is just outside the range expected for the imine stretch, most likely due to an α,β benzaldehyde. The argument for imine hydrolysis is further strengthened by the shoulder stretches at 2739 and 2869 cm^{-1} which are also normally seen in aldehydic systems. It is clear from this spectrum that no perchlorate is present.

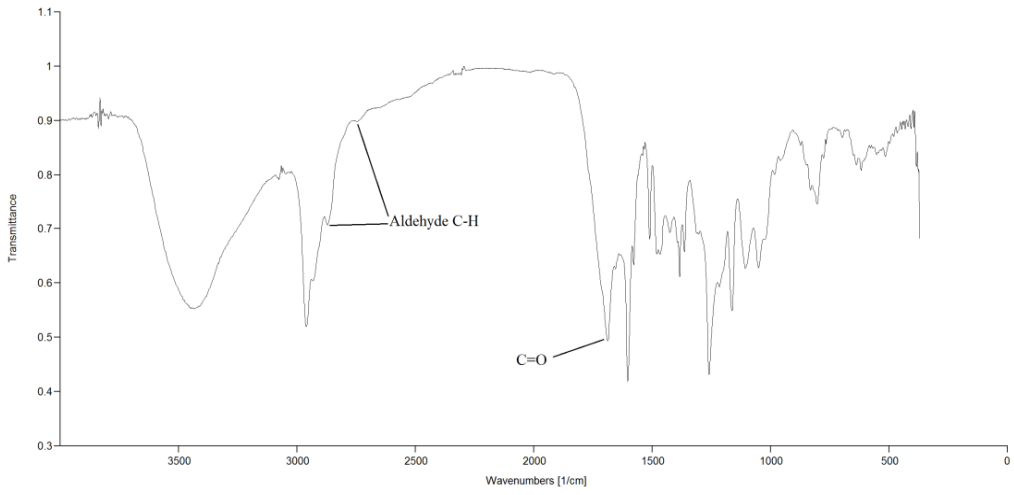

Figure 3.17: Infrared spectra of Cu(**7**)$(ClO_4)_2$.

The cobalt(II) perchlorate complexation reaction was performed in a similar fashion. After concentration of the liquid, a red solid was formed. The IR spectrum of the proposed complex Co(**7**)$(ClO_4)_2$ is shown in Figure 3.18. This was compared to the free ligand IR spectrum in Figure 3.10a. The appearance of a stretching band at 1651 cm^{-1}, which could be attributed to a conjugated aldehyde, is observed indicating that ligand hydrolysis has occurred. This assertion is backed up by the appearance of a stretching band at 2874 cm^{-1} which could be due to the aldehyde C-H. This data, along with analysis of the ^1H NMR spectra of the diamagnetic metals reaction, appears to indicate the presence of an aldehyde within the structure.

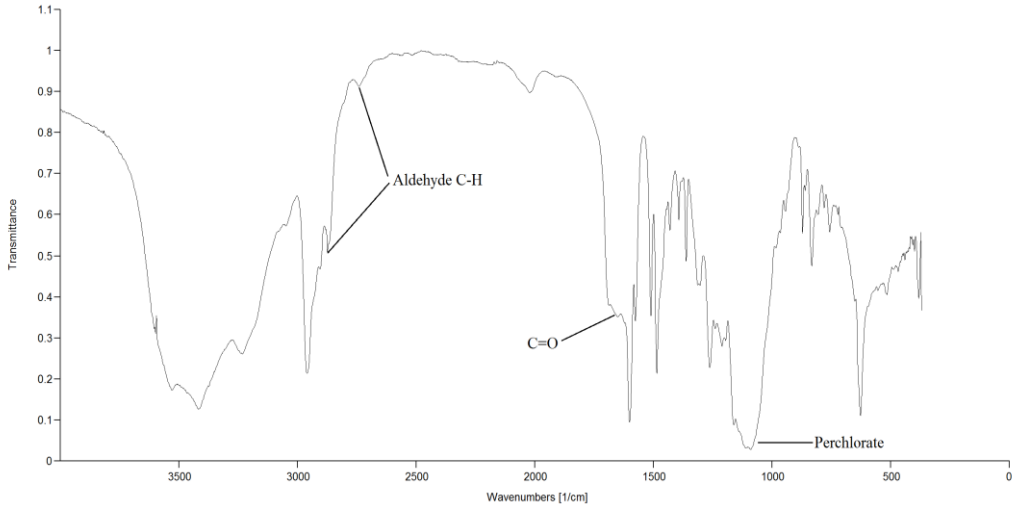

Figure 3.18: Infrared spectra of Co(**7**)$(ClO_4)_2$.

The metal complexation reaction with nickel(II) perchlorate proceeded in the same manner as the previously discussed reactions. The product from this reaction was obtained as a light yellow green solid. The infrared spectra of the ligand **7**, Figure 3.10a, was compared with that of the product from the complexation reaction Figure 3.19. A band at 1689 cm^{-1} is present, which is most likely a result of benzaldehyde in the product structure. Two stretching bands, which are attributable to the aldehyde C-H, are seen at 2743 cm^{-1} and 2872 cm^{-1}. This is consistent with the trends that have

been seen with other metal complexation reactions using ligand **7**. It was clear that perchlorate is also present in this structure which is seen by absorption bands at 1089 cm^{-1} and 1111 cm^{-1}. This indicates that some metal complexation has occurred.

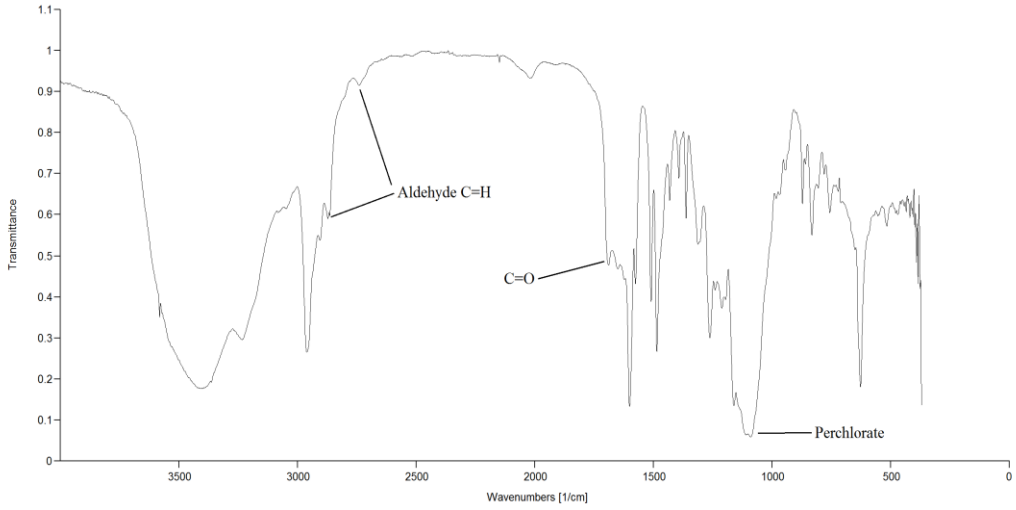

Figure 3.19: Infrared spectra of Ni(**7**)$(ClO_4)_2$.

3.3.5 Metal Complexation reactions of ligand 8

3.3.5.1 Reaction of 8 with zinc(II) perchlorate

A methanolic solution of zinc(II) perchlorate was added to a solution of ligand **8** (Figure 3.20) in chloroform, the resulting mixture was stirred for eight hours. After concentration of the solution a yellow solid was obtained. The ^1H NMR spectrum was analysed and is shown in comparison with the spectrum of the starting ligand **8**.

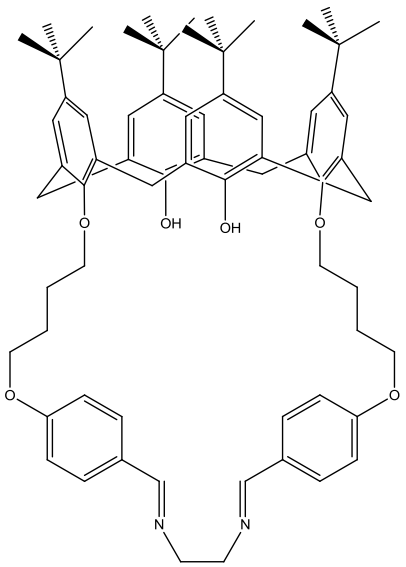

Figure 3.20: Ligand **8**.

The labelled peaks a-d correspond to the proton signals which appear to undergo the largest degree of shifting (Figure 3.21). As in the case of the ligand **7**, which differs by nature of its propyl chain, the most striking shift is that of signal H_d, which shifts from 8.05 ppm to 9.84 ppm. If this shift was due to the complexation of zinc it would be a shift of approximately 1.79 ppm, which in this context is a huge shift. The spectre of imine hydrolysis once again overshadows any attempted metal complexation.

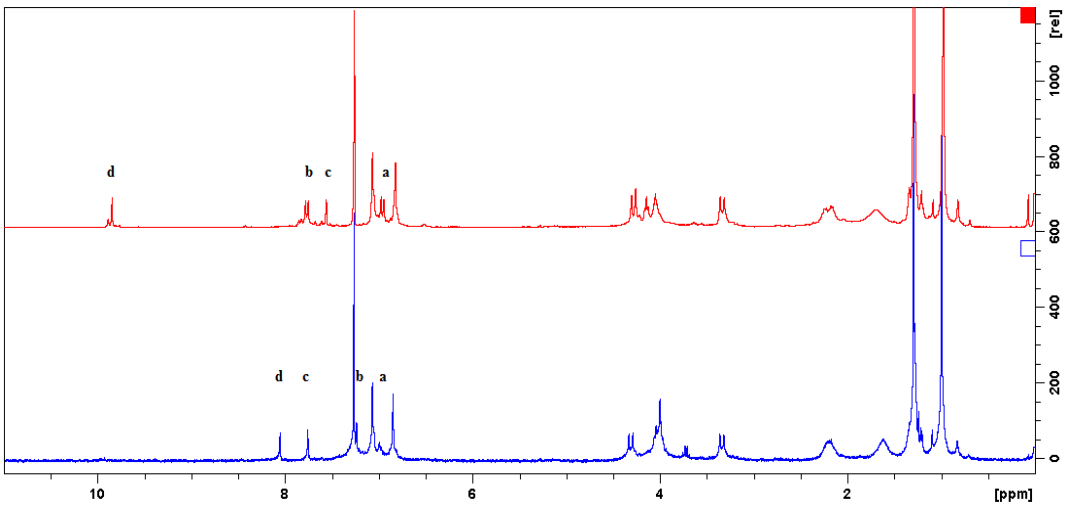

Figure 3.21: ^{1}H NMR spectra of **8** (blue) and Zn(**8**)$(ClO_4)_2$ (red).

The signal for the phenolic protons H_c experiences an upfield shift of 0.20 ppm from 7.76 ppm to 7.56 ppm; this could possibly be due to increased hydrogen bonding

within the lower rim cavity. The aromatics for what was the Schiff base moiety again show some shifting, but these are more prominent for signal H_b, which undergoes a downfield shift from 7.23 to 7.75 ppm, a 0.52 ppm shift. The signals for the butoxy chain are relatively unchanged with the exception of the disappearance of the bridging ethyl proton signal. As was the case with the zinc complexes of **7**, the ^{13}C NMR spectrum of **8** showed a signal at 190.7 ppm which would be indication that an aldehyde had been formed. If it was the case that it was a shifted imine carbon, this would be a shift downfield of almost 27 ppm. This is illustrated in Figure 3.22a and Figure 3.22b.

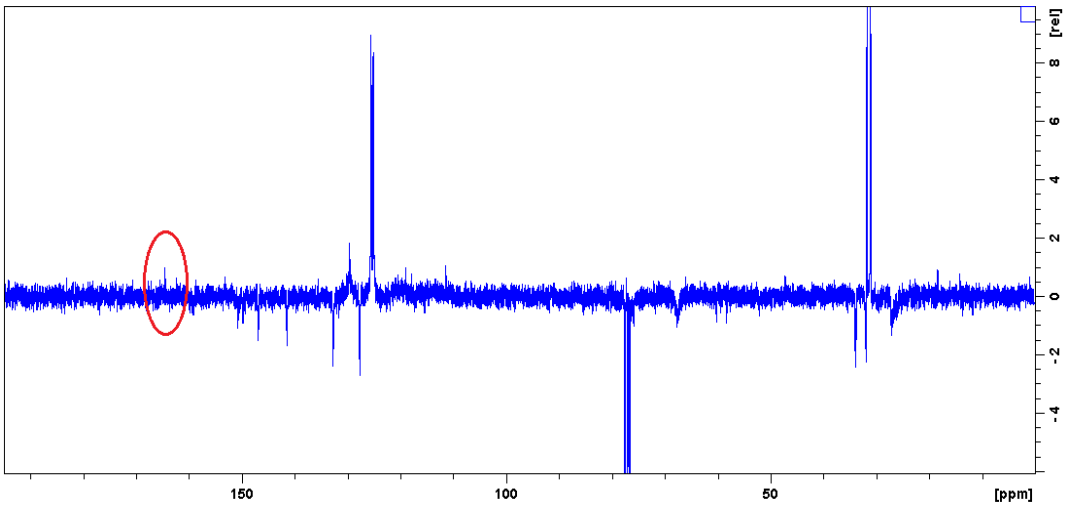

Figure 3.22a: DEPT135Q of **8** with imine carbon signal highlighted.

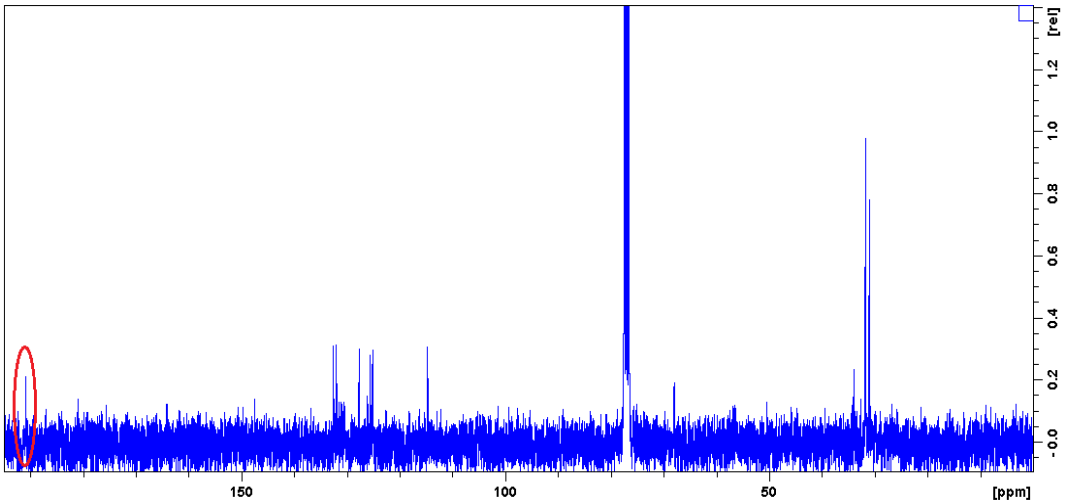

Figure 3.22b: ^{13}C NMR of Zn(**8**)$(ClO_4)_2$ with the shifted signal highlighted.

The IR spectrum of the product (Figure 3.23b) was compared to that of the uncomplexed ligand seen in Figure 3.23a. The stretching band between 1600 - 1700 cm^{-1} is observed at a different wavenumber. In the product from the metal complex reaction it is observed at 1694 cm^{-1} as a sharp medium band, while in **8** it occurs at 1644 cm^{-1} as a sharp strong absorption band. As has been previously discussed, a wavenumber this low is not uncommon for a conjugated aldehyde, such as benzaldehyde, which would be the likely product of imine hydrolysis in this reaction. Two absorption bands occur where the perchlorate anion would be expected to show, with stretching bands at 1109 cm^{-1} and 1122 cm^{-1}. This would seem to indicate some metal complexation had occurred.

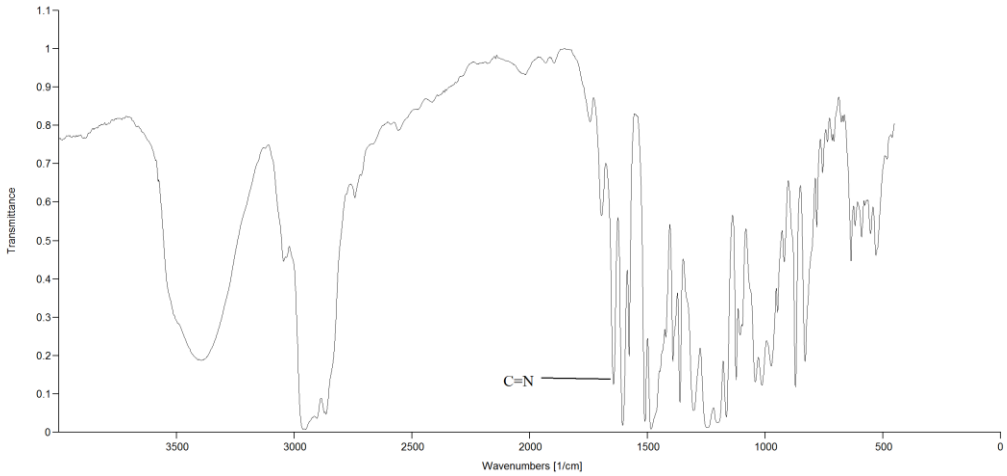

Figure 3.23a: IR spectrum of ligand **8**.

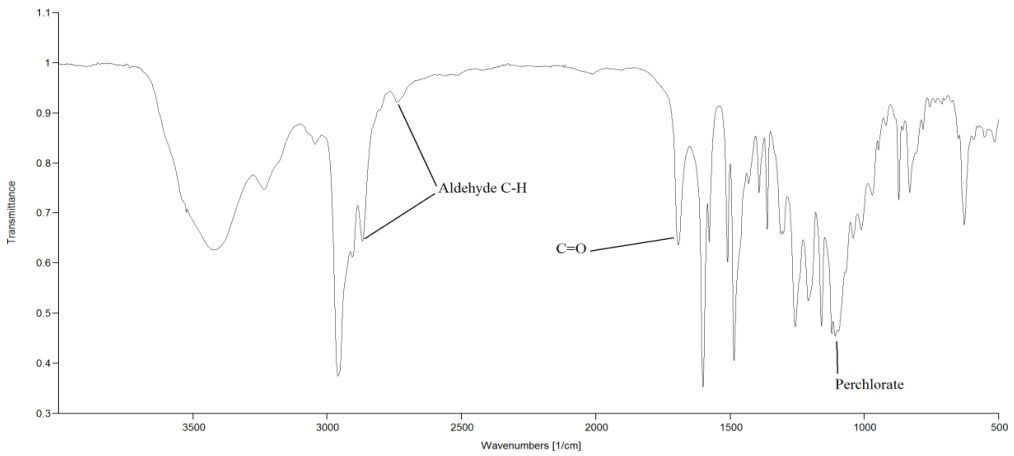

Figure 3.23b: IR spectrum of $Zn(\mathbf{8})(ClO_4)_2$.

3.3.5.2 Reaction of 8 with mercury(II) perchlorate

The attempted complexation of mercury(II) perchlorate was done in a similar fashion to the zinc(II) perchlorate reaction. The product was collected after concentration of the reaction mixture as a dark purple solid. This stark colour change was not anticipated as mercury complexes are expected to give a complex which bears the colour of the parent ligand. The ^{1}H NMR spectrum of the product was analysed and compared to the parent ligand. In comparison to the Zn(**8**)$(ClO_4)_2$ spectrum, the ^{1}H NMR spectrum is less clear but the same trends can be observed (Figure 3.24).

An aldehyde signal peak labelled H_a is seen to resonate at 10.34 ppm in the spectrum of the complex, which would represent a downfield shift of 2.29 ppm from the imine peak position in **8** of 8.05 ppm. As the signal resonates in the region where aldehydes are expected to occur, it is postulated that the ligand has undergone imine hydrolysis.

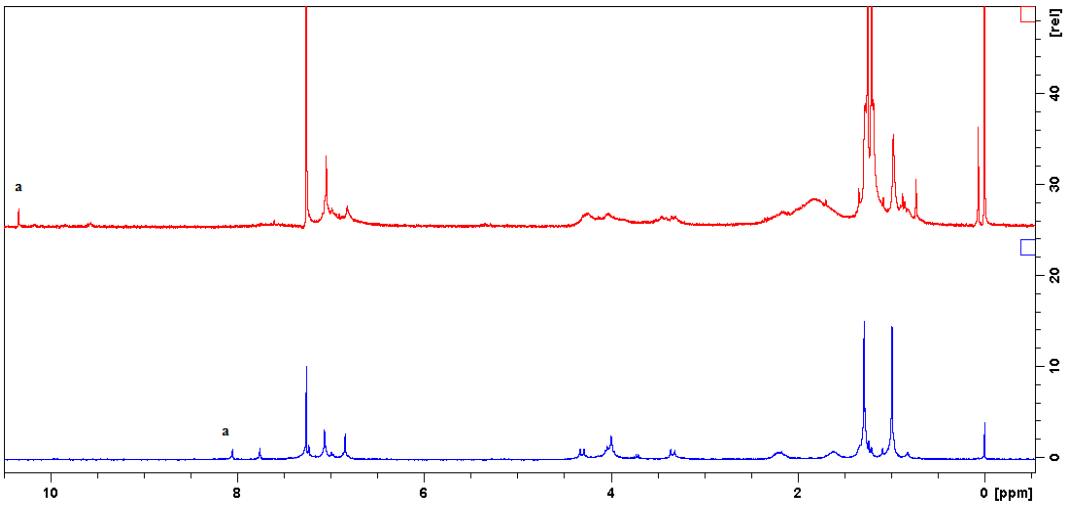

Figure 3.24: ^{1}H NMR spectra of **8** (blue) and Hg(**8**)$(ClO_4)_2$ (red).

The IR spectrum (Figure 3.25), shows more evidence of this ligand hydrolysis with an absorption band at 1693 cm^{-1}. This is a clear shift from the band observed for the free ligand (Figure 3.23a). The presence of the perchlorate stretch absorption bands at 1092

and 1109 cm^{-1} indicate that some degree of metal complexation is likely to have occurred.

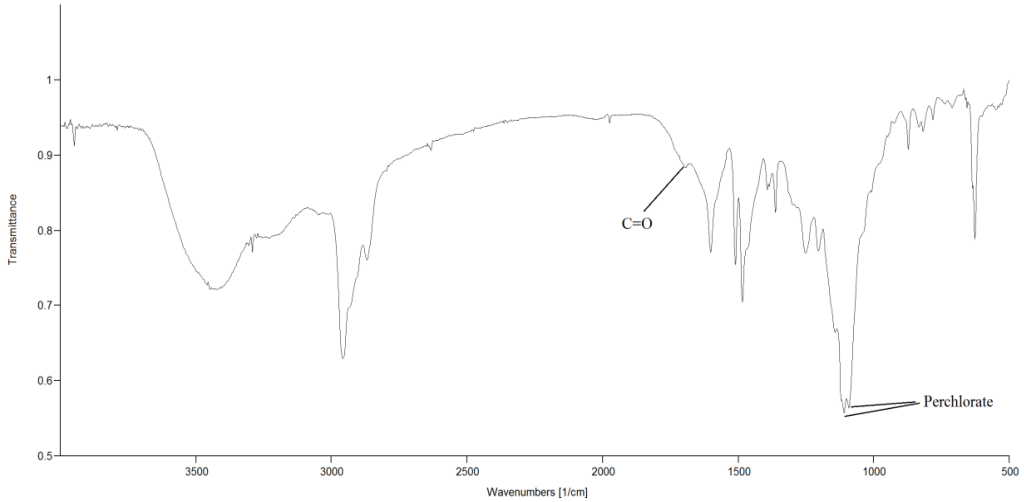

Figure 3.25: Infrared Spectrum of Hg(**8**)$(ClO_4)_2$.

3.3.5.3 Reaction of 8 with copper(II) perchlorate

The reaction between ligand **8** and copper(II) perchlorate followed a similar procedure to the metal complexation reactions above. The product from the reaction was obtained as a brown solid, this colour change was not promising for any potential complex as a green or blue colour would be expected. The IR spectrum (Figure 3.26) shows no clear evidence of aldehyde formation but does show a broad absorption band at 1628 cm^{-1}. However, the presence of two absorption bands which could represent the H-CO stretch are seen at 2781 cm^{-1} and 2870 cm^{-1}, providing some evidence which points toward the formation of an aldehyde. As was also seen in many of these infrared spectra, the perchlorate anion stretches are observed at 1089 and 1110 cm^{-1} indicating that some metal complexation is likely to have occurred.

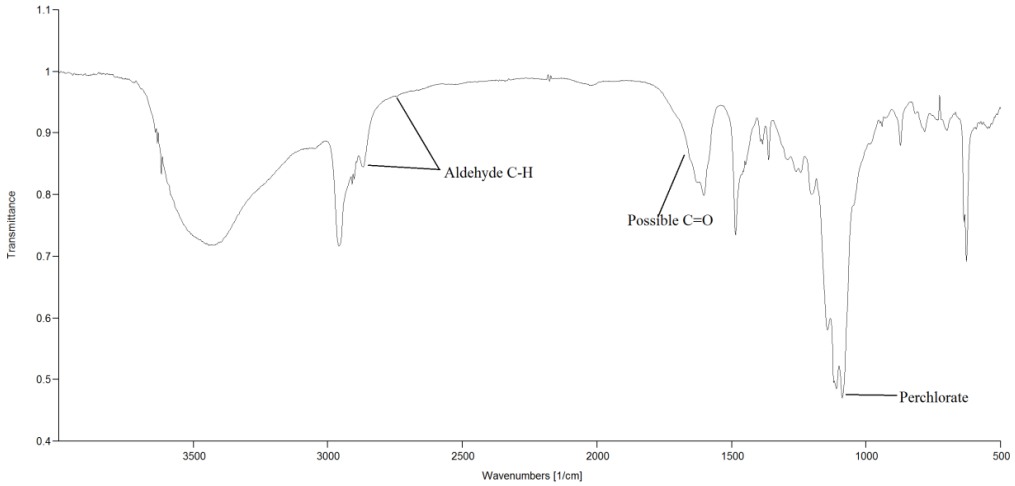

Figure 3.26: IR spectrum of Cu(**8**)$(ClO_4)_2$.

3.3.6 Metal Complexation reactions of ligand 10

3.3.6.1 Reaction of ligand 10 with zinc(II) perchlorate

A methanolic solution of zinc(II) perchlorate was added to a solution of ligand **10** (Figure 3.27) in chloroform. After stirring overnight no precipitate had formed.

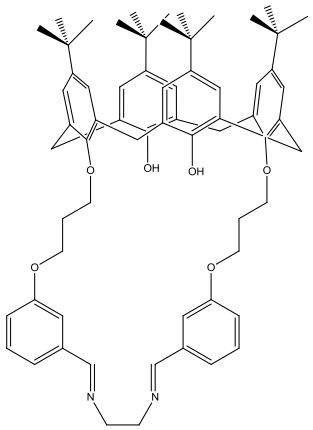

Figure 3.27: Ligand **10**.

The solution was reduced to dryness and the ^{1}H NMR spectrum was analysed and compared to the starting ligand (Figure 3.28). Once again, an apparent shift in resonance position is seen for proton H_d, which is representative of the imine proton in **10**. The shift is from 8.06 ppm to 9.88 ppm, a downfield shift of 1.82 ppm.

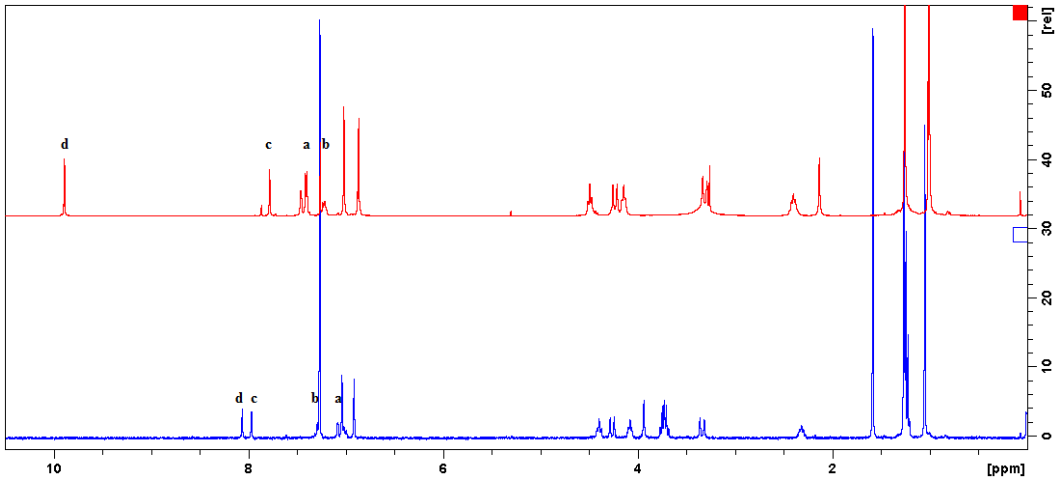

Figure 3.28: ^{1}H NMR spectra of **10** (blue) and Complex Zn(**10**)$(ClO_4)_2$ (red).

An upfield shift is noted for the phenolic proton signal H_c from 7.96 ppm in the starting ligand to a position of 7.78 ppm in the spectrum of the complex, resulting in an upfield shift of 0.18 ppm. Shifting can be seen in the pendant aromatic proton signals positions H_a and H_b. This trend was also seen in the products from earlier metal complexation reactions. The ^{13}C NMR spectrum was examined and compared to that of **10** (Figure 3.29a&b). Once again the formation of an aldehyde would be quite obvious from these spectra. The key difference in the spectrum is the region in which the highlighted signals resonate. In the spectrum obtained for the complex this peak resonates at 192.2 ppm, and once again this is much higher than would be expected for an imine carbon.

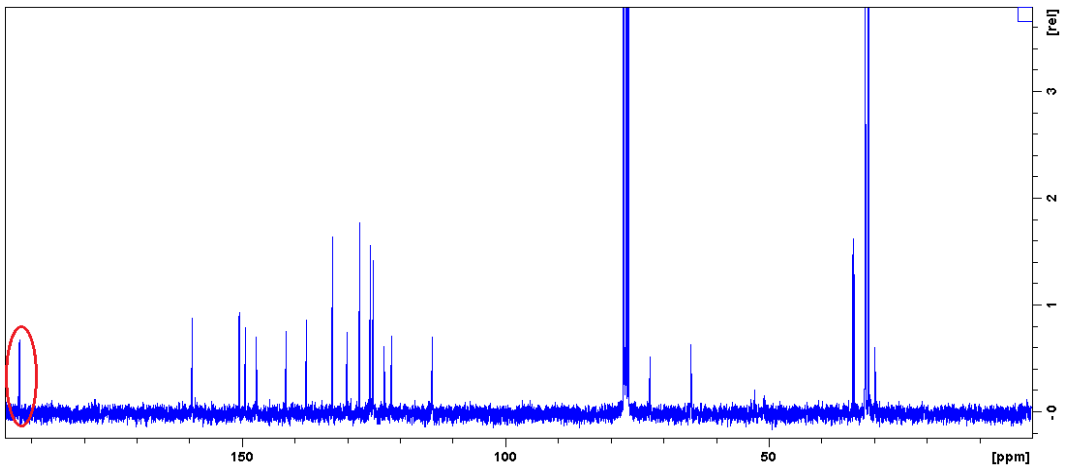

Figure 3.29a: ^{13}C NMR spectrum of Zn(**10**)$(ClO_4)_2$ with apparent aldehyde signal highlighted.

When it is compared to the spectrum of ligand **10**, which has a signal that resonates at 163.7 ppm, this would represent a shift of 28.5 ppm. This would denote a very large degree of shifting, and once again points to the occurrence of imine hydrolysis within the reaction system.

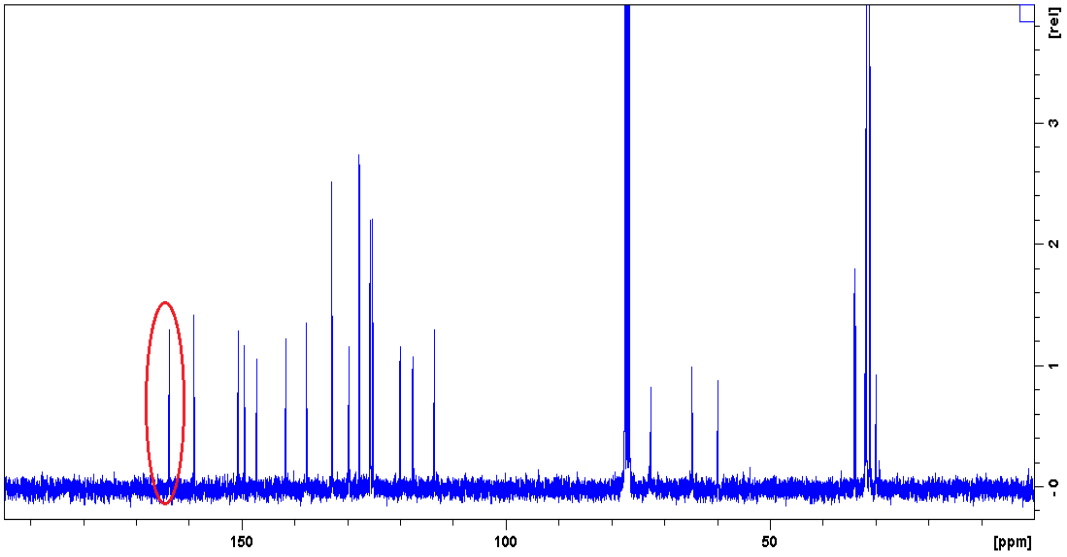

Figure 3.29b: ^{13}C NMR spectrum of **10** with imine signal highlighted.

The infrared spectrum was examined next, with the complex once again being compared to the free ligand (Figure 3.30a & Figure 3.30b). It can be seen that the strong sharp signal between 1600-1700 cm^{-1} no longer overlaps with the imine absorption band in the parent spectrum. This band now occurs at 1691 cm^{-1} which, as discussed previously, is common for benzaldehyde. This hypothesis is supported by the presence of two bands at 2726 cm^{-1} and 2870 cm^{-1}, which are the H-C aldehyde stretch bands. Once again, the perchlorate bands are noted within the spectrum and occur at 1099 cm^{-1} and 1151 cm^{-1}. This again shows that some metal complexation is likely to have occurred.

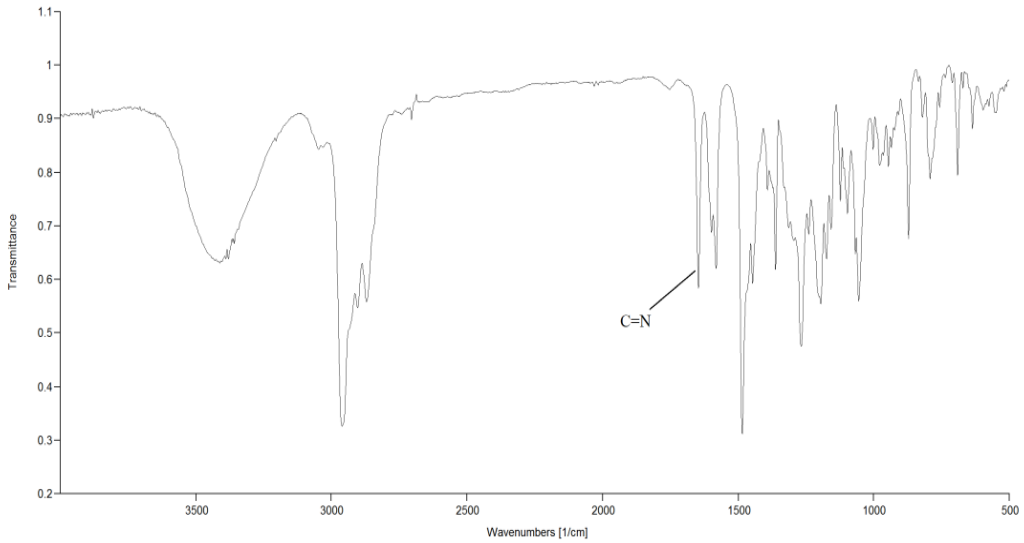

Figure 3.30a: IR spectrum of **10**.

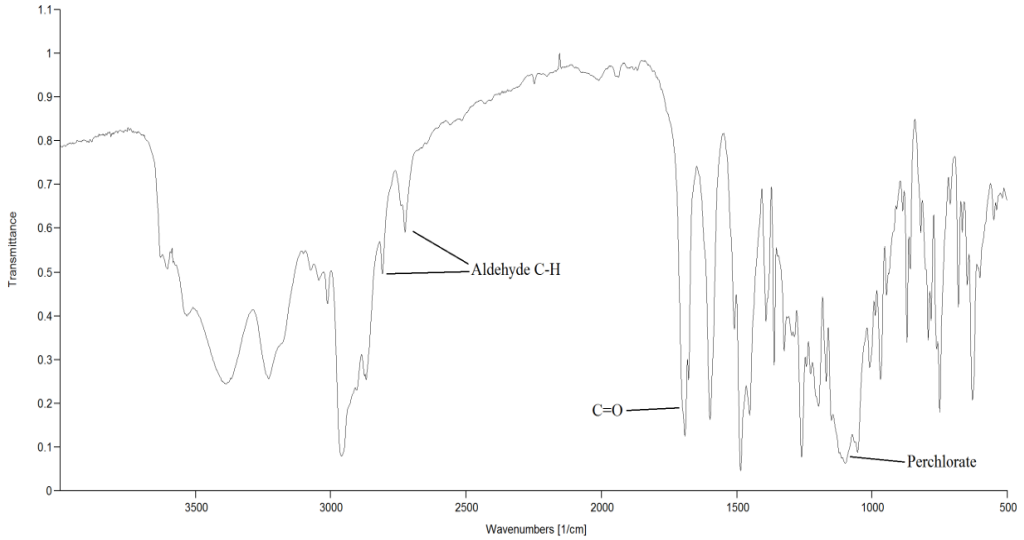

Figure 3.30b: IR spectrum of Zn(**10**)$(ClO_4)_2$.

3.3.6.2 Reaction of ligand 10 with copper(II) perchlorate

The attempted metal complexation reaction between **10** and copper(II) perchlorate was performed in the same manner as for the zinc(II) perchlorate reaction, with the product obtained as a pale green solid after reduction of the solution. Upon comparison to the parent ligand (Figure 3.30a), a few differences are notable in the spectrum obtained for the complex (Figure 3.31). A sharp absorption band occurs at 1698 cm^{-1} which would

seem to imply that an aldehyde has formed during the complexation reaction. This assertion is backed up by the appearance of two stretching bands, one at 2738 cm^{-1} and another at 2872 cm^{-1}, which represent the C-H aldehyde stretch. A pair of absorption bands, which could be attributed to the perchlorate anion are seen at 1102 and 1055 cm^{-1}. This, along with the colour change is indicative of metal complexation.

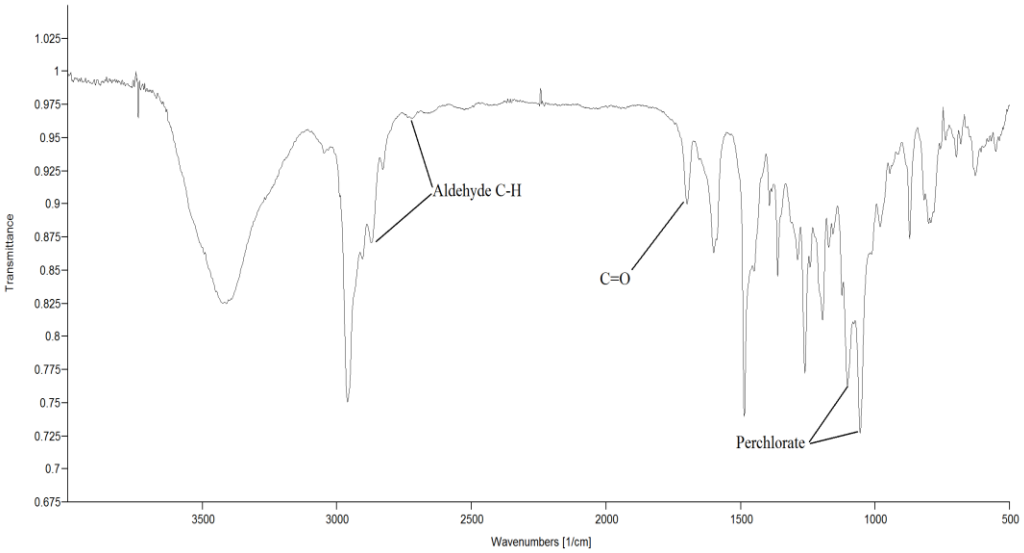

Figure 3.31: IR spectra of Cu(**10**)$(ClO_4)_2$.

3.3.7 Metal Complexation reactions of ligand 11

3.3.7.1 Reaction of 11 with zinc(II) perchlorate

A solution of **11** (Figure 3.32) in chloroform was stirred and to this a methanolic solution of zinc(II) perchlorate was added. After being cooled to room temperature, the solution was reduced to dryness under reduced pressure to yield an off white solid. The ^1H NMR spectrum of the product was analysed and compared to the spectrum of the parent ligand (Figure 3.33).

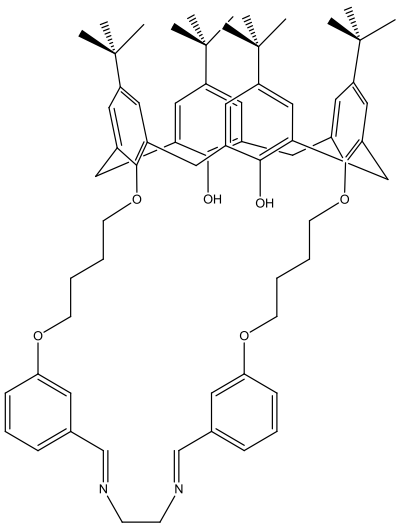

Figure 3.32: Ligand **11**.

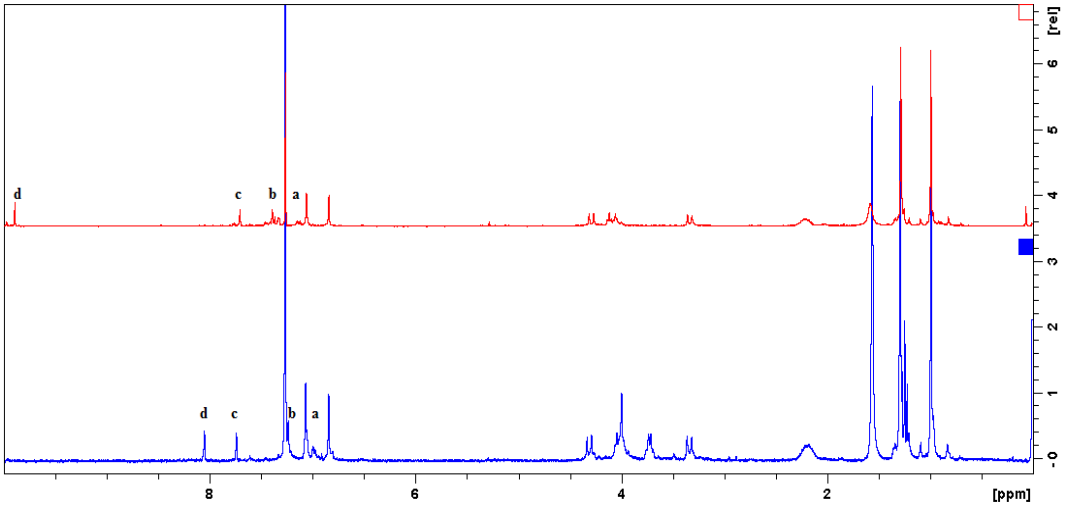

Figure 3.33: ^{1}H NMR spectra of **11** (blue) and Zn(**11**)$(ClO_4)_2$ (red).

The proton signal which is labelled H_d has been assigned to the imine proton in **11**, a large shift in this resonance position can be seen in the spectrum of Zn(**11**)$(ClO_4)_2$. The shift from 8.05 ppm in **11** to 9.89 ppm in Zn(**11**)$(ClO_4)_2$ is most likely due to imine hydrolysis resulting in a benzaldehyde. The phenolic proton signal H_c is seen to shift upfield by 0.04 ppm from 7.74 ppm in **11**, to 7.70 ppm in the product. As was the case with the previously discussed zinc complexes, a slight downfield shift is observed in the pendant aromatic protons. It is also noted that the bridging ethyl fragment signal is no longer present in the spectrum. The ^{13}C NMR spectrum of the product (Figure 3.34a) was analysed and compared to that of **11** (Figure 3.34b). The large shift

downfield of the highlighted signal in Figure 3.34a of 28 ppm from 164.4 to 191.13 ppm is indicative of aldehyde formation. This is in accordance with what has been previously discussed in sections 3.3.3, 3.3.4, and 3.3.5.

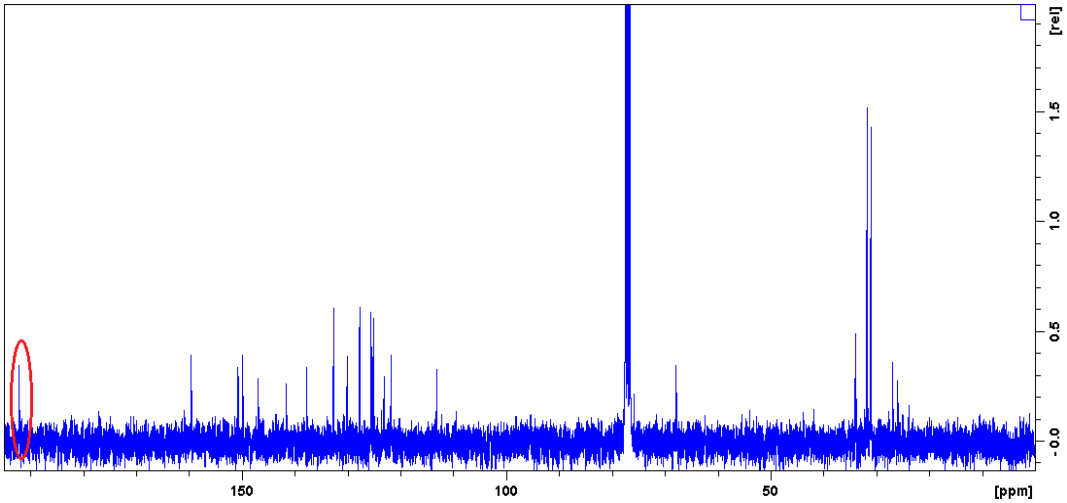

Figure 3.34a: ^{13}C NMR spectrum of Zn(**11**)$(ClO_4)_2$.

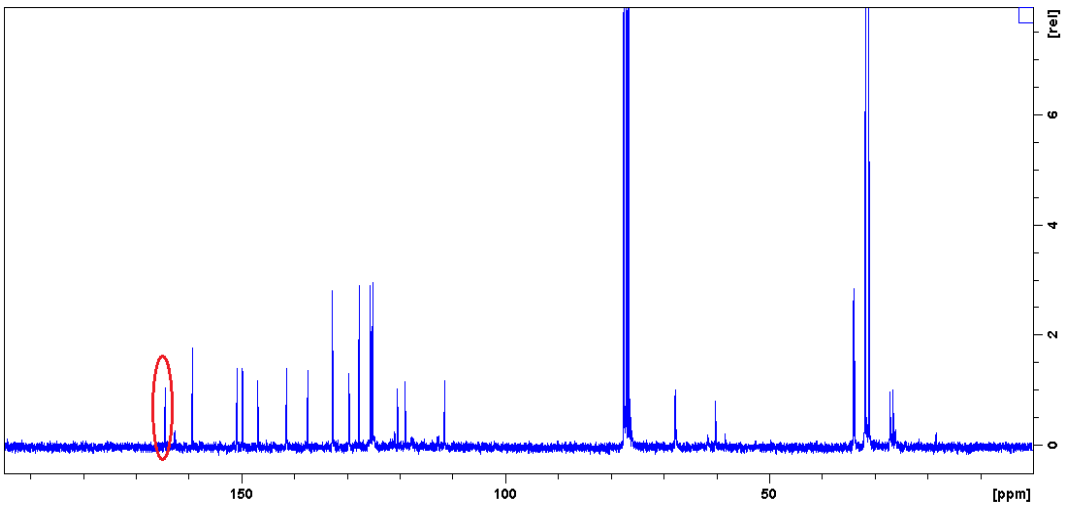

Figure 3.34b: ^{13}C NMR spectrum of **11**.

The IR spectrum was also examined and compared to the spectrum obtained for **11**. The spectra are shown in Figure 3.35a and 3.35b. A shift in the band, which occurs at 1646 cm^{-1} in **11**, can be seen at a new wavenumber of 1700 cm^{-1} for Zn(**11**)$(ClO_4)_2$. The new position is characteristic for a conjugated aldehyde such as benzaldehyde.

This is also backed up by the presence of two new peaks at 2741 and 2869 cm^{-1}, which are typical for the C-H aldehyde stretch.

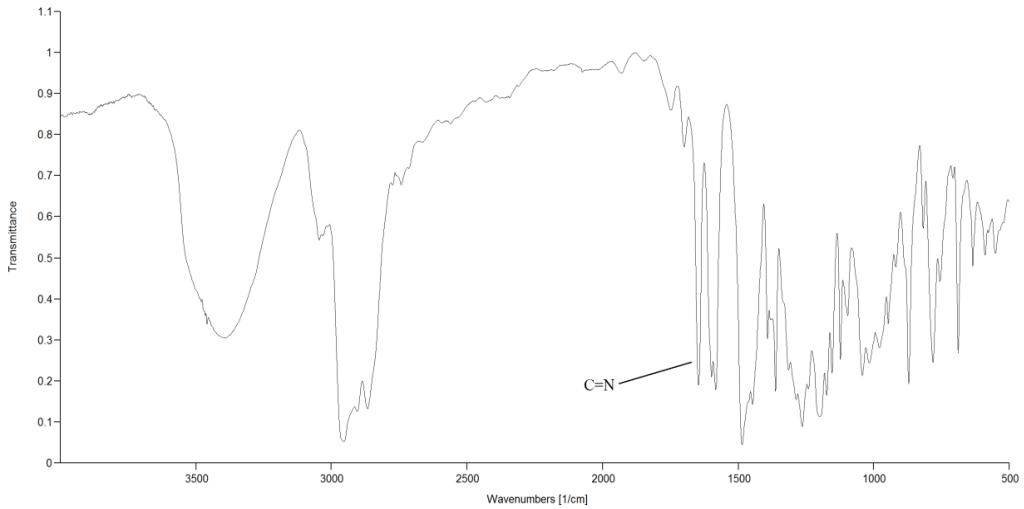

Figure 3.35a: IR spectrum of **11**.

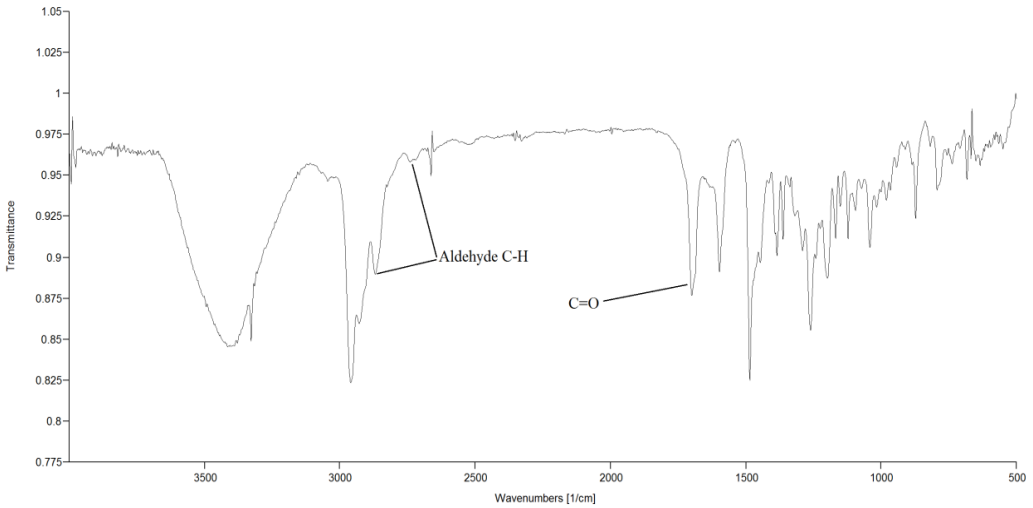

Figure 3.35b: Infrared Spectrum of Zn(**11**)$(ClO_4)_2$.

3.3.7.2 Reaction of 11 with mercury(II) perchlorate

The same general method as was used in the complexation reaction of **11** with zinc(II) perchlorate was used for the reaction between **11** and mercury(II) perchlorate, which yielded a brown solid. The ^{1}H NMR spectrum of the product was analysed and it can be clearly seen (Figure 3.36) that there is a large shift from the spectrum for **11** (red) to

the spectrum of the Hg(**11**)$(ClO_4)_2$. This once again is consistent with the aldehyde formation hypothesis.

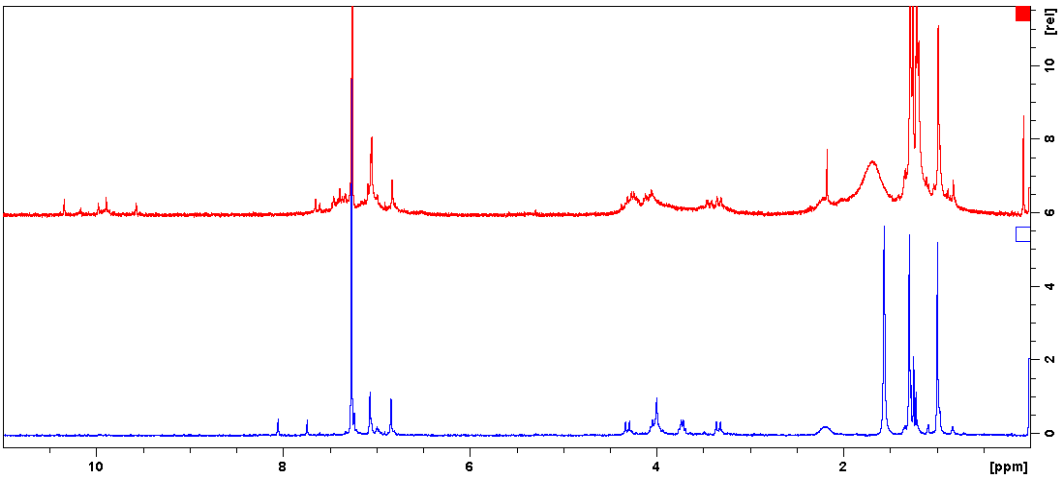

Figure 3.36: ^{1}H NMR spectra of **11** (blue) and Hg(**11**)$(ClO_4)_2$ (red).

The IR spectrum of the product Hg(**11**)$(ClO_4)_2$ (Figure 3.37) clearly shows a shift in the band in the region of 1600-1900 cm^{-1} when compared to the spectrum of **11** (Figure 3.35a). The band occurs at 1696 cm^{-1}, which is indicative of a benzaldehyde C=O stretch. This assignment is backed up by the observation of two aldehyde C-H stretch bands at 2725 cm^{-1} and 2870 cm^{-1}. It is also clear from the spectrum that the perchlorate anion is present in this compound from the bands at 1092 and 1108 cm^{-1}, which points to metal complexation occurring.

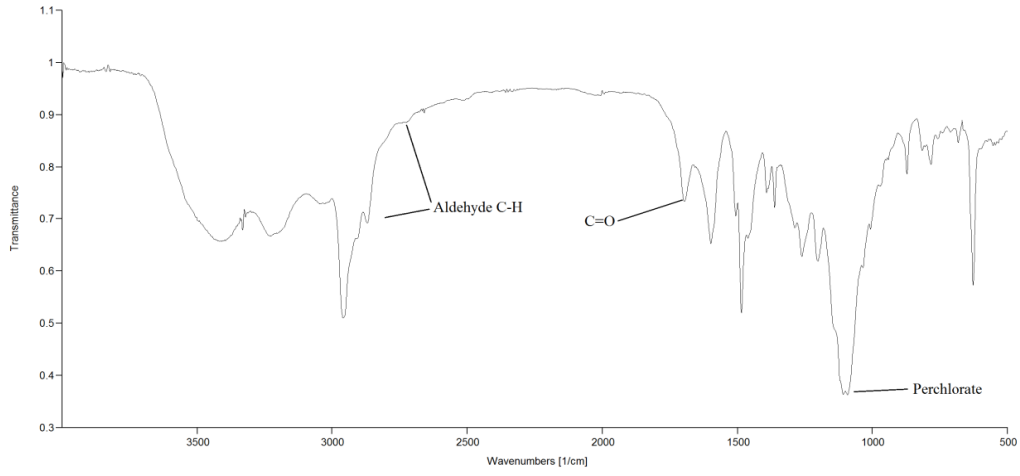

Figure 3.37: IR spectrum of Hg(**11**)$(ClO_4)_2$.

3.3.7.3 Reaction of 11 with paramagnetic perchlorate metal salts

The metal complexation reactions between the paramagnetic salts, copper(II) perchlorate, cobalt(II) perchlorate and nickel(II) perchlorate, and the ligand **11**, were performed in a similar fashion to the diamagnetic salts above. None of the reactions afforded the product as a precipitate, so all solutions were concentrated under reduced pressure to give solids. Cu(**11**)$(ClO_4)_2$ gives a blue green solid, of which the IR spectrum was recorded (Figure 3.38) and compared to the spectrum for **11** (Figure 3.35a). As was the case with the diamagnetic compounds, an absorption band is seen at 1694 cm^{-1}, which points to hydrolysis of the imine moiety in the complexation reaction. The aldehyde C-H stretching bands can be seen at 2739 cm^{-1} and 2869 cm^{-1}, which is in line with the original hypothesis.

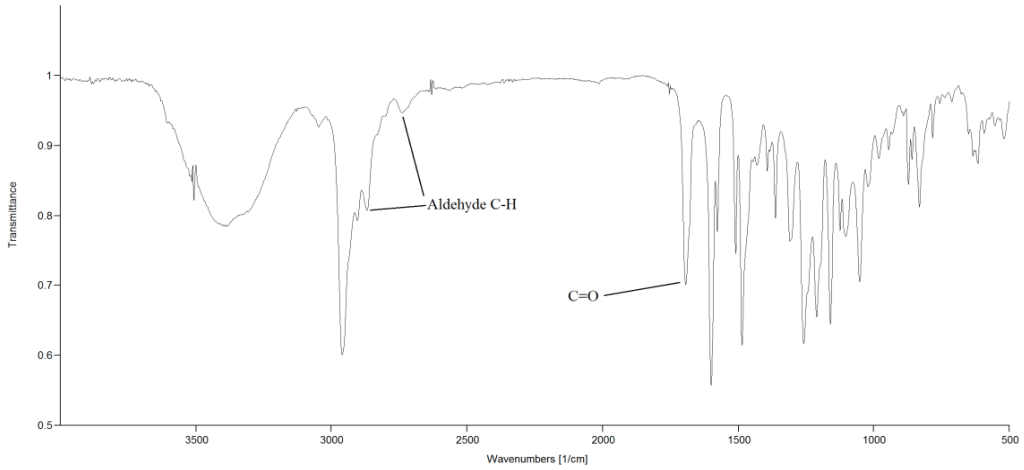

Figure 3.38: Infrared spectrum of Cu(**11**)$(ClO_4)_2$.

Co(**11**)$(ClO_4)_2$ is obtained as a red solid after reduction of the solution, the IR spectrum (Figure 3.39), was once again compared to that of the starting ligand **11**. A sharp absorption band is observed at 1698 cm^{-1} which is most likely due to the formation of an aldehyde, and once again this is solidified by the presence of the C-H stretching bands at 2726 cm^{-1} and 2869 cm^{-1}.

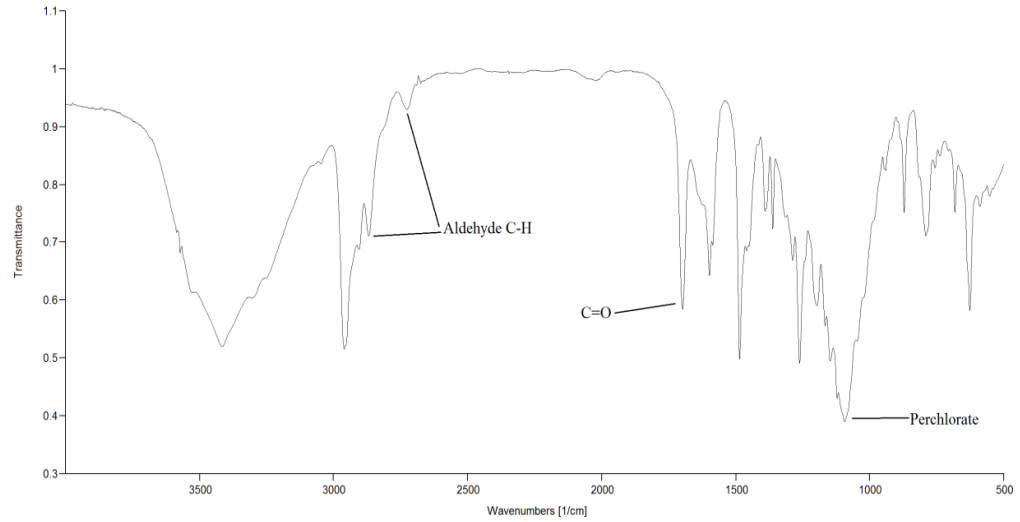

Figure 3.39: Infrared spectrum of Co(**11**)$(ClO_4)_2$.

Ni(**11**)$(ClO_4)_2$ was obtained as a yellow solid. Upon analysis of the IR spectrum (Figure 3.40), an absorption band is seen at 1698 cm^{-1}, which again points to hydrolysis of the imine moiety in the complexation reaction. The aldehyde C-H stretching bands can be seen at 2742 cm^{-1} and 2870 cm^{-1}, which backs up this original hypothesis.

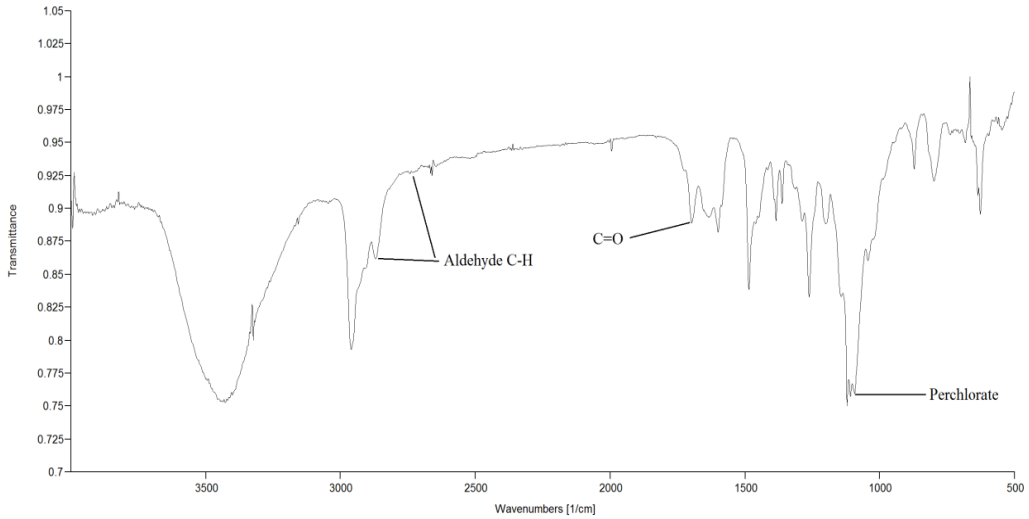

Figure 3.40: IR spectrum of Ni(**11**)$(ClO_4)_2$.

3.3.8 Metal Complexation reactions of ligand 14

3.3.8.1 Reaction of 14 with zinc(II) perchlorate

A methanolic solution of zinc(II) perchlorate was added to a stirring solution of **14** (Figure 3.41) in chloroform.

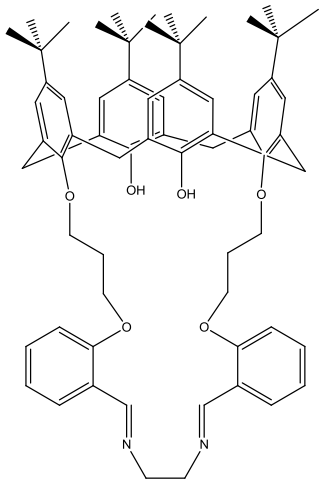

Figure 3.41: Ligand **14**.

After concentration of the solution a light brown solid was obtained. Analysis of the ^{1}H NMR spectrum (Figure 3.42) yields some interesting results.

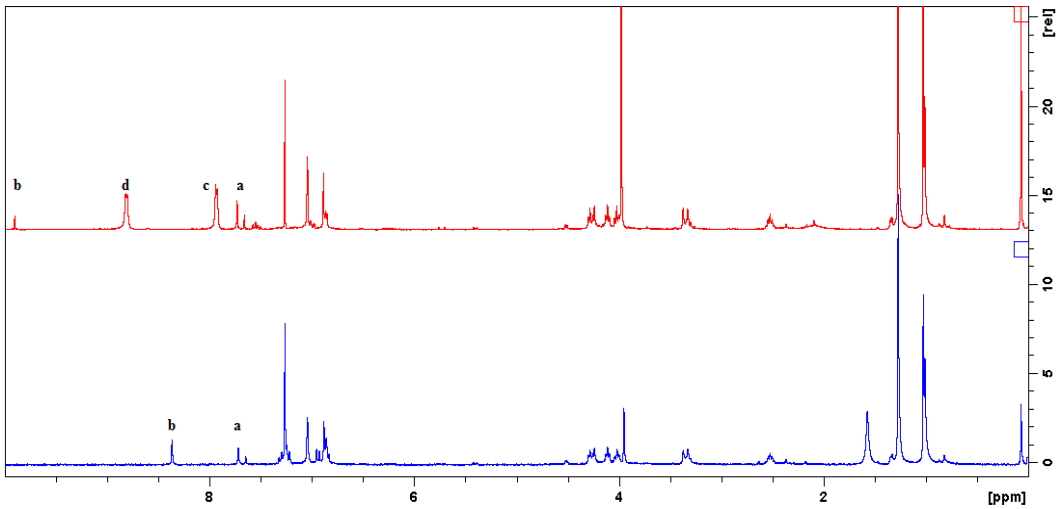

Figure 3.42: ^{1}H NMR spectra of **14** (blue), and Zn(**14**)$(ClO_4)_2$ (red).

When the IR spectrum of the product (Figure 3.43b) is compared to the ligand spectrum (Figure 3.43a), a noticeable change in position is seen for the sharp

absorption band which occurs at 1634 cm^{-1}. In the infrared spectrum of Zn(**14**)$(ClO_4)_2$ this band occurs at a higher wavenumber of 1732 cm^{-1}. This is a characteristic absorption band for the C=O stretch of the aldehyde product from the hydrolysis reaction. This is also backed up by the observation of two aldehyde C-H stretching bands at 2743 and 2868 cm^{-1}.

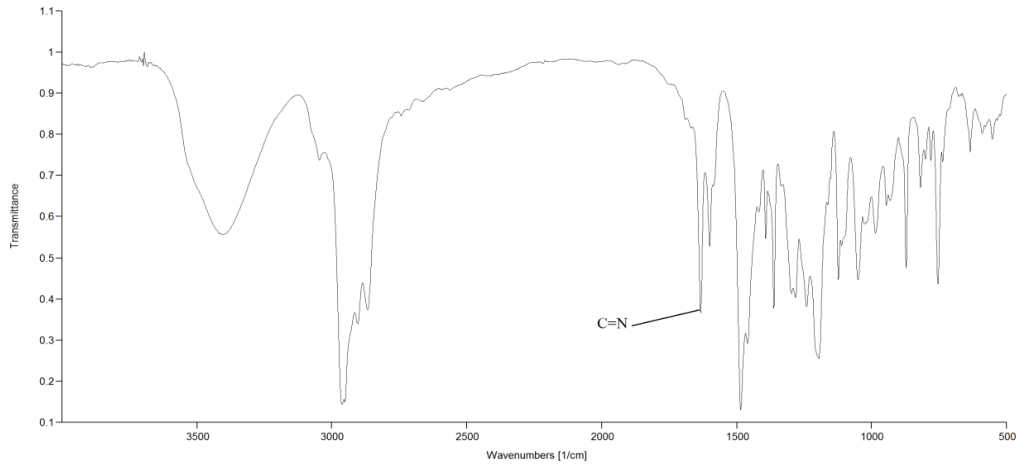

Figure 3.43a: IR spectrum of **14**.

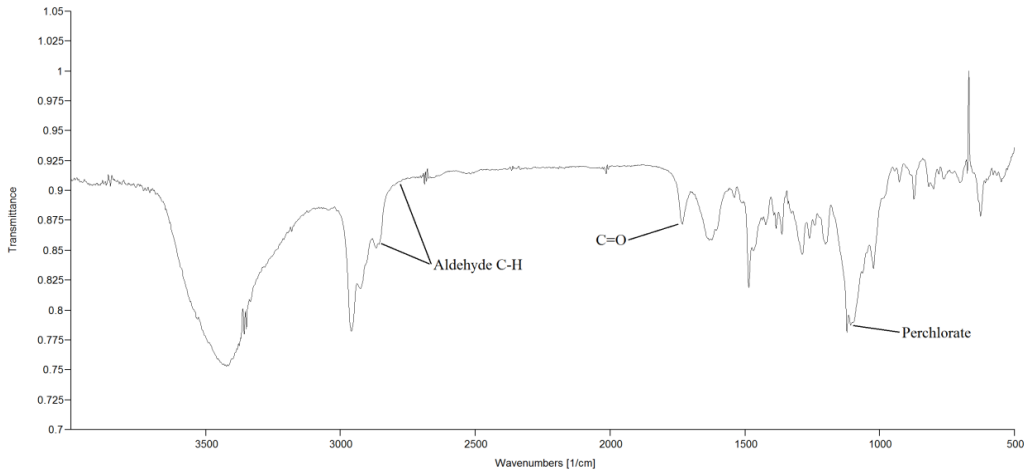

Figure 3.43b: IR spectrum of Zn(**14**)$(ClO_4)_2$.

3.3.8.2 Reaction of 14 with mercury(II) perchlorate

The reaction between **14** and mercury(II) perchlorate was carried out with the same method as the zinc(II) perchlorate complexation reaction. The product was obtained as

a brown solid from concentration of the solution. The ^{1}H NMR spectrum (Figure 3.44) was compared to that of the starting ligand **14**. A large downfield shift can be seen for the proton labelled H_b from a position of 8.36 ppm in **14**, to a resonance position of 10.34 ppm in Hg(**14**)$(ClO_4)_2$, resulting in a downfield shift of 1.98 ppm. The new downfield position of this proton would seem to suggest that imine hydrolysis occurred during the metal complexation reaction. The phenolic proton signal H_a experiences an upfield shift of 0.12 ppm from 7.73 ppm in **14**, to 7.60 in Hg(**14**)$(ClO_4)_2$.

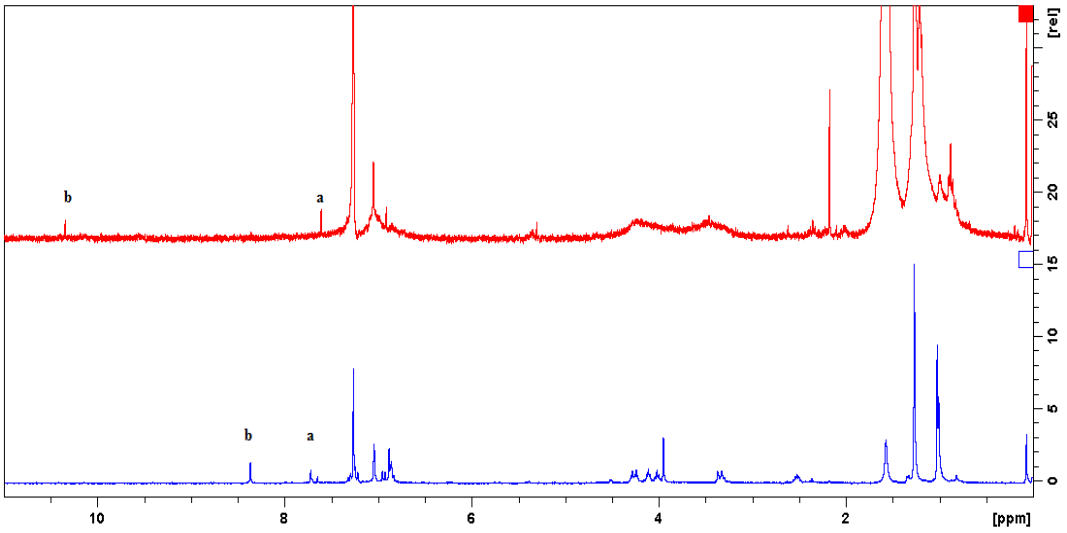

Figure 3.44: ^{1}H NMR spectra of **14** (blue) and Hg(**14**)$(ClO_4)_2$.

Comparison of the infrared spectrum obtained for the Hg(**14**)$(ClO_4)_2$ product (Figure 3.45) with that of the parent ligand, once again, shows a shifted position in the sharp band seen at 1634 cm^{-1} for **14**, to a higher wavenumber of 1658 cm^{-1}. Although this is somewhat low for an aldehyde, it is reasoned to represent benzaldehyde, which is consistent with imine hydrolysis. Once again the presence of aldehyde C-H stretching bands at 2746 cm^{-1} and at 2868 cm^{-1} supports this hypothesis. Metal complexation is thought to have occurred, as absorption bands which are attributed to the perchlorate anion are seen at 1108 cm^{-1} and 1121 cm^{-1}.

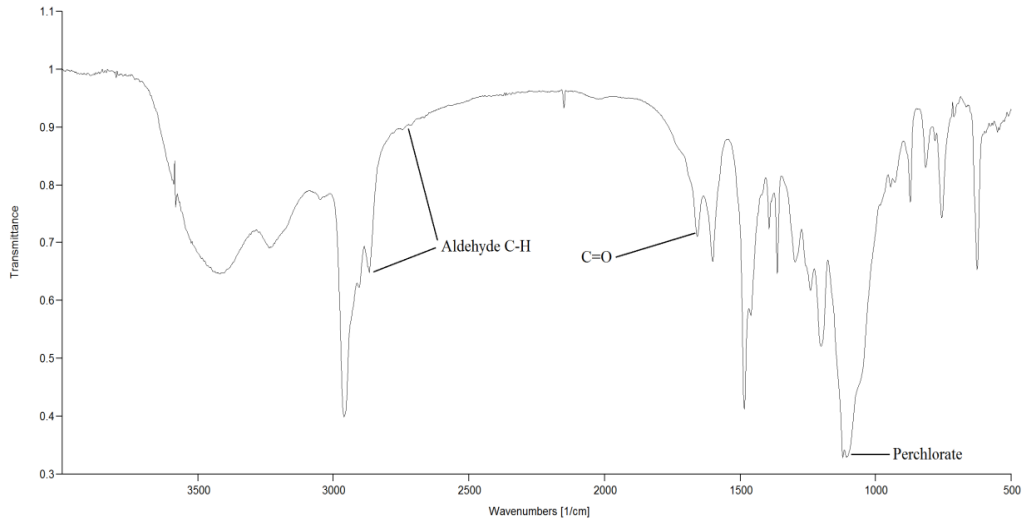

Figure 3.45: IR spectrum of Hg(**14**)$(ClO_4)_2$.

3.3.8.3 Reaction of 14 with paramagnetic perchlorate metal salts

The metal complexation reactions between the paramagnetic salts, copper(II) perchlorate, cobalt(II) perchlorate and nickel(II) perchlorate, and the ligand **14**, were performed in a similar fashion to the diamagnetic salts previously discussed. The product from the copper(II) perchlorate complex reaction Cu(**14**)$(ClO_4)_2$ is obtained as a green solid. The infrared spectrum of the product (Figure 3.46) was analysed and compared to the parent ligand. Since absorption bands, which pointed towards aldehyde formation, were seen in both diamagnetic complexes with **14**, the general broadening of the imine absorption band was somewhat unexpected. In the product spectrum it occurs at 1639 cm^{-1}, which would seem to suggest that metal complexation to the imine nitrogen has occurred. The absence of the C-H aldehyde stretching bands at ≈ 2750 cm^{-1} and ≈ 2850 cm^{-1} makes it difficult to suggest that imine hydrolysis has occurred.

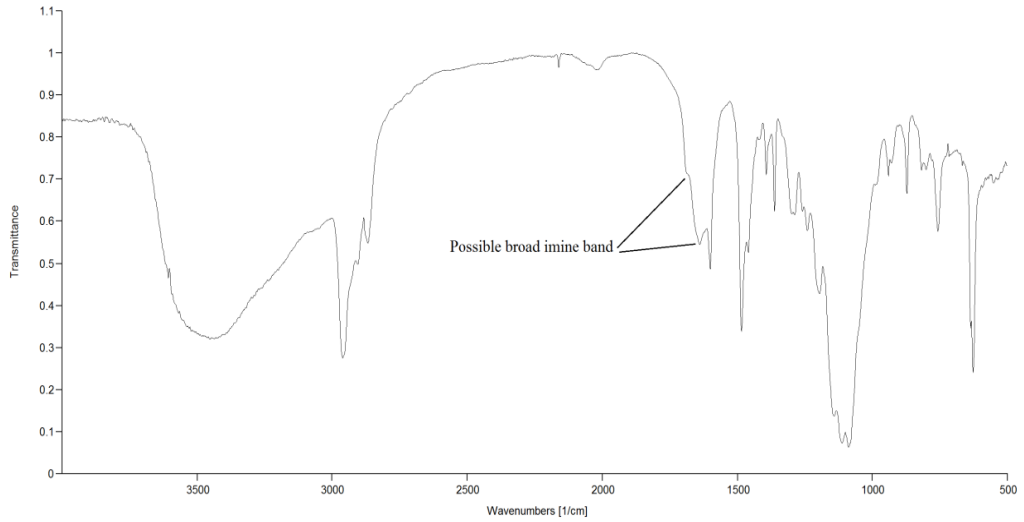

Figure 3.46: Infrared spectrum of Cu(**14**)$(ClO_4)_2$.

The nickel(II) perchlorate complex Ni(**14**)$(ClO_4)_2$ is obtained as a yellowish green solid. When the infrared spectrum is analysed (Figure 3.47) the general broadening observed for Cu(**14**)$(ClO_4)_2$ was again observed, but an absorption peak at 1687 cm^{-1} can be seen as a shoulder band. An absorption band is seen at 2872 cm^{-1}, which could be due to an aldehyde C-H stretching band, but no strong band is observed at 2750 cm^{-1}. As was the case with the copper complex, it cannot be said for certain that imine hydrolysis had occurred.

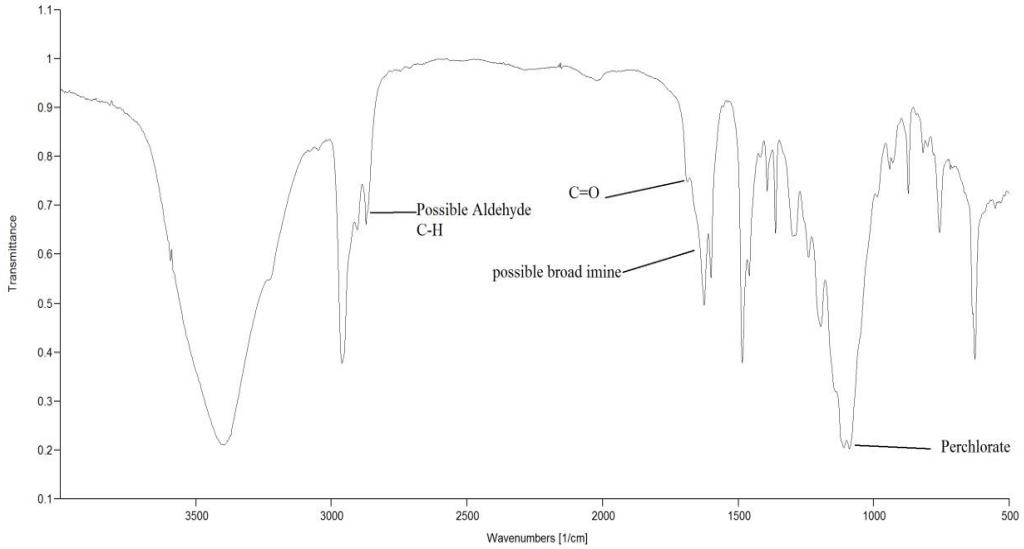

Figure 3.47: Infrared spectrum of Ni(**14**)$(ClO_4)_2$.

The same trends are seen in the IR spectrum of the Co(**14**)$(ClO_4)_2$ complex (Figure 3.48). The general broadening of the imine band is noted, but once again a shoulder aldehyde peak is observed at 1687 cm^{-1}. The presence of an aldehyde is further hinted towards due to the appearance of the C-H stretching bands at 2868 cm^{-1} and at 2747 cm^{-1}. However, it cannot be said with any certainty that imine hydrolysis had occurred with these metal complex reactions.

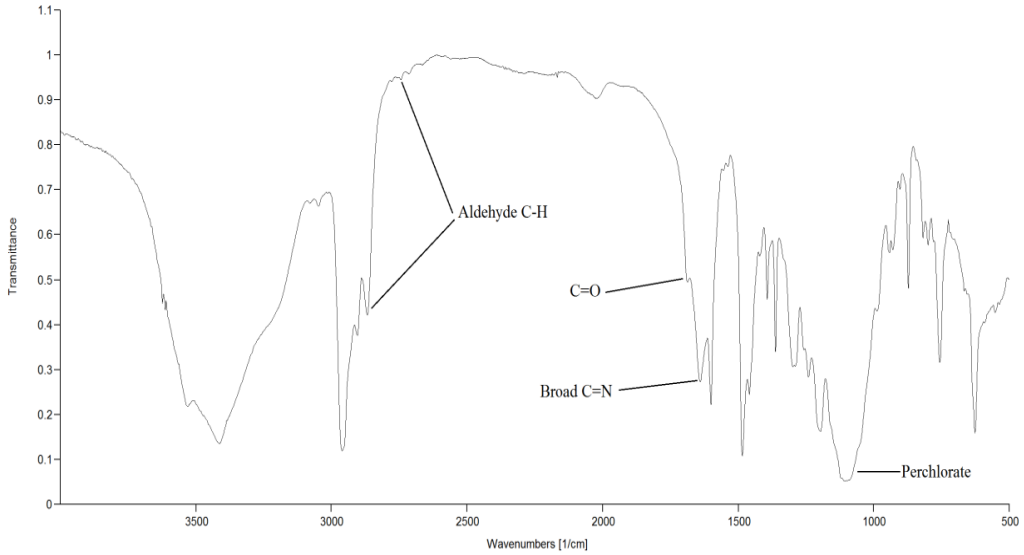

Figure 3.48: IR spectrum of Co(**14**)$(ClO_4)_2$.

3.3.9 Metal Complexation reactions of ligand 15

3.3.9.1 Reaction of 15 with zinc(II) perchlorate

This metal complexation reaction was attempted using a similar procedure to the previously discussed complexation attempts. After reduction of the solution a yellow solid was obtained.

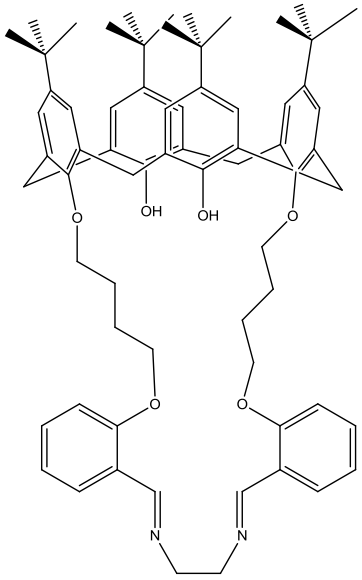

Figure 3.49: Ligand **15**.

The ^{1}H NMR spectrum was analysed and compared to the spectrum for **15** (Figure 3.50). The clear downfield shift in the proton labelled H_b from 8.72 ppm to 10.52 ppm, which is a downfield shift of 1.80 ppm, once again points to imine hydrolysis during the complexation reaction. The phenolic proton signal labelled H_a experiences an upfield shift of 0.25 ppm from 7.92 to 7.67 ppm. This trend was seen for all the attempted diamagnetic complexes.

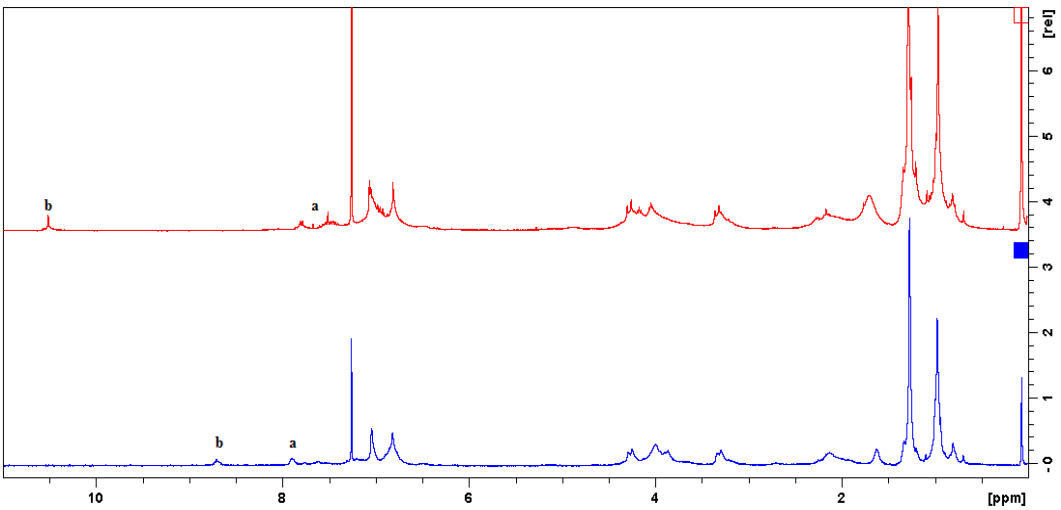

Figure 3.50: ^{1}H NMR spectra of **15** (blue) and Zn(**15**)$(ClO_4)_2$ (red).

Examination of the IR spectrum (Figure 3.51b) and comparison with the parent spectrum (Figure 3.51a), once again shows a change in position for the band which is at 1668 cm^{-1} in **15**; a shift is seen in this peak to 1690 cm^{-1} in Zn(**15**)$(ClO_4)_2$. This would suggest that an aldehyde had formed within our structure, as was the case with the previously discussed reactions. The observation of absorption bands at 2759 cm^{-1} and 2869 cm^{-1} indicates further that ligand hydrolysis has occurred, with these absorption bands representing the aldehyde C-H stretching bands.

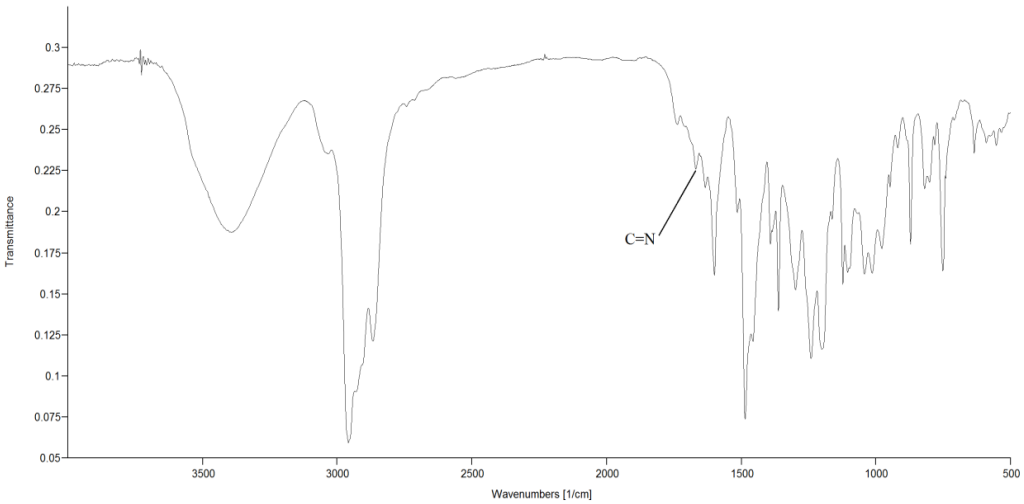

Figure 3.51a: IR spectrum of **15**.

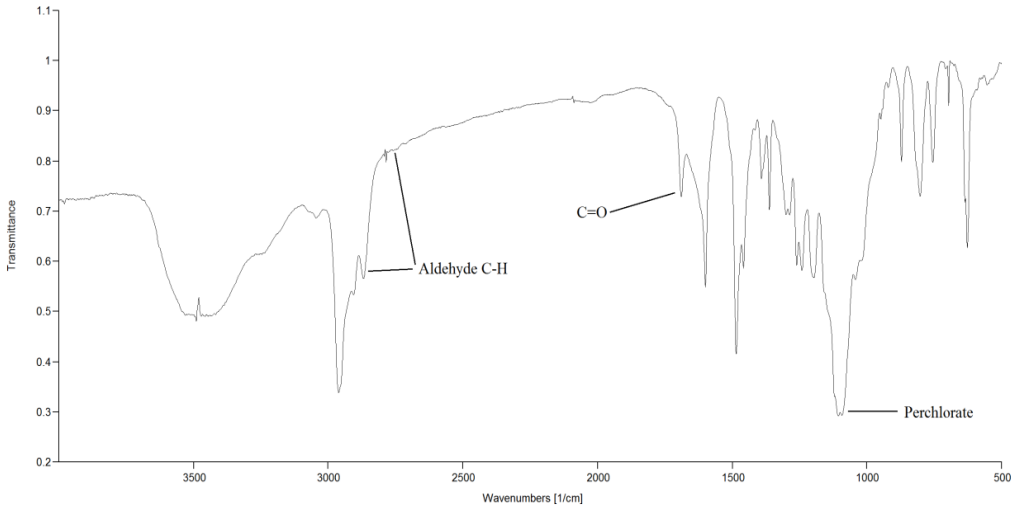

Figure 3.51b: IR spectrum of Zn(**15**)$(ClO_4)_2$.

3.3.9.2 Reaction of 15 with copper(II) perchlorate

The IR spectrum of the Cu(**15**)$(ClO_4)_2$ (Figure 3.52) when compared to the infrared spectrum of the parent ligand, shows the general broadening which has been seen with the paramagnetic complexes in Figures 3.47, 3.48 and 3.49. This absorption band occurs at 1600 cm^{-1} and is quite broad; a shoulder can be seen at ≈ 1720 cm^{-1} which could point to aldehyde formation. The C-H aldehyde stretching peaks can be seen at 2747 cm^{-1} and another at 2863 cm^{-1}. This provides additional indication that ligand hydrolysis has occurred.

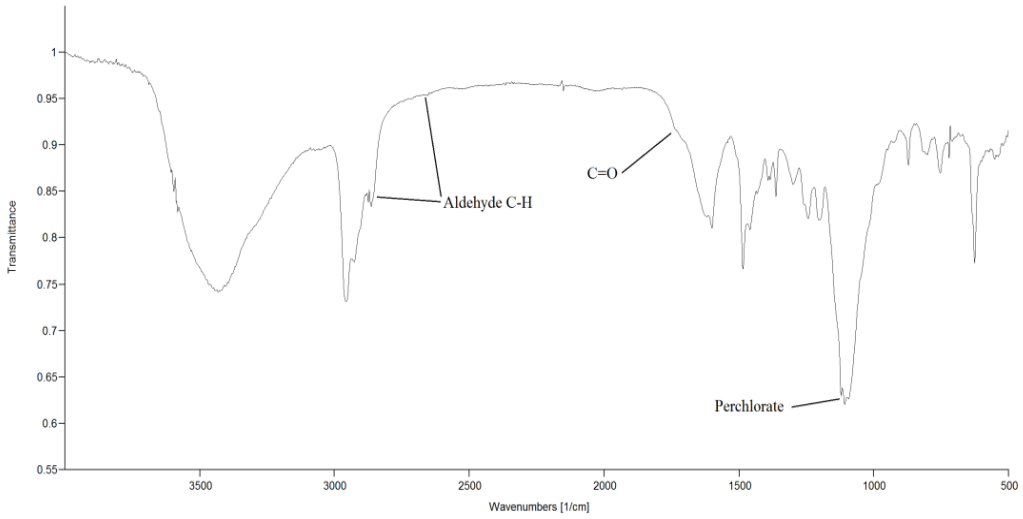

Figure 3.52: IR spectrum of Cu(**15**)$(ClO_4)_2$.

3.3.10 Imine hydrolysis products

The proposed structure for the hydrolysis product from the attempted metal complexation reactions is shown (Figure 3.53). This assignment is supported by the ^1H NMR, ^{13}C NMR, and IR spectroscopic data collected.

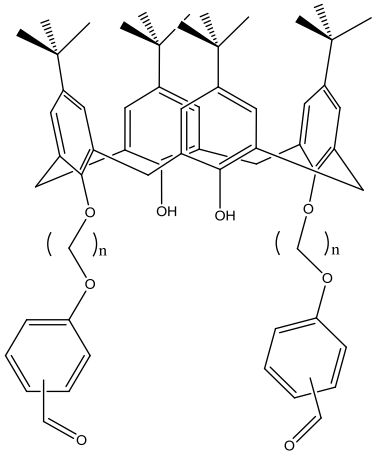

Figure 3.53: Proposed structure of the hydrolysis product from metal complexation reactions, where n = 3 or 4.

3.3.11 Spectroscopic Studies

The products from the metal complexation reactions which have the most interesting colour changes were screened to determine if they exhibited any fluorescent emission behaviour. The purple products from the mercury perchlorate complexes with **7** and **8** were tested as this colour change was unexpected. It was noted that the purple colour which was seen in the solid form was not observed in solution phase. Once in solution, a brown colour was noted. The UV-Vis spectra of the products from the metal complexation reactions were compared to that of the starting materials (Figure 3.54 & Figure 3.55).

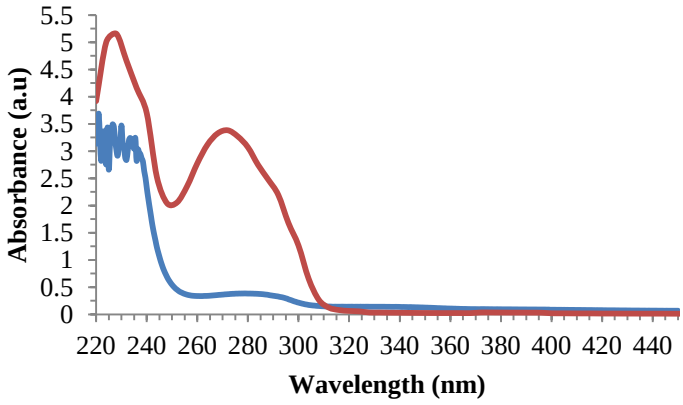

Figure 3.54: UV-Vis Spectra of **7** (red) and Hg(**7**)$(ClO_4)_2$ (blue).

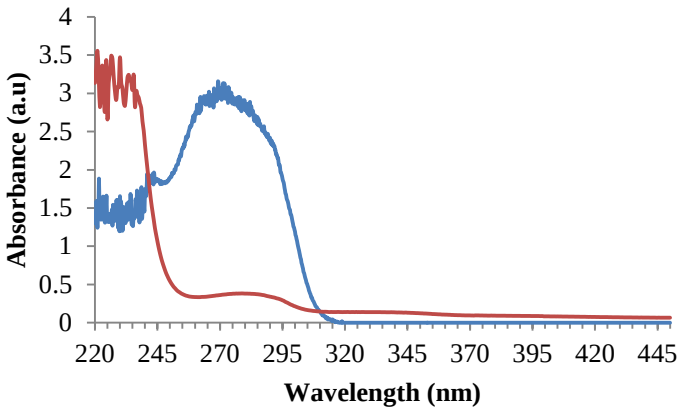

Figure 3.55: UV-Vis Spectra of **8** (blue) and Hg(**8**)$(ClO_4)_2$ (red).

A reduction in the degree of absorbance in the peak at 280 nm is observed in both spectra. The peak observed in the absorbance spectra were once again used as the excitation wavelength (λ_f^{ex} = 280 nm) to obtain a fluorescence emission spectrum. In a not unexpected result, no fluorescent behaviour was observed (NFO) for either of the complexes screened (Table 3.8).

Table 3.8: Excitation wavelength λ_f^{ex} for fluorescent emission spectroscopy and peak emission recorded, λ_f^{em}.

Sample no.	λ_f^{ex} (nm)	λ_f^{em} (nm)
Hg(**7**)$(ClO_4)_2$	280	NFO
Hg(**8**)$(ClO_4)_2$	280	NFO

3.4 Triazole linked calix[4]arenes

3.4.1 Overview

The goal for this section was to prepare a range of calix[4]arene triazole derivatives that could exhibit unusual metal binding behaviours, building from the Schiff base linked calixarenes prepared in **section 2.2**. In the years following Sharpless *et al.* reporting on click chemistry,[50] the use of the triazole moiety as an ionophore for metal ion sensors has been of interest with numerous examples prepared.[67,115,124,125]

Calixarene based sensors containing both an imine and triazole moiety for Zn^{2+} coordination have been reported by Pathak *et al.*[124] This group wanted to examine the effect of having more than one metal binding core in the structure upon selectivity for metal ions. To this end they prepared four ligands, one possessing just the triazole moiety and three with Schiff base linkages (Figure 3.56). Using fluorescence and absorption spectroscopy, this group has shown that Zn^{2+} is selectively recognized by the Schiff base and not the triazole moiety. They found that only L_2, L_3 and L_4 show any change in fluorescence upon titration of Zn^{2+}. Pathak also reports that L_4 can be used as a selective sensor for Zn^{2+} due to changes in the fluorescence only occurring upon titration of Zn^{2+} out of the ten divalent metal ions studied. Furthermore, this group reported on the suitability of this ligand L_4 for use in organic systems as binding was noted in aqueous solutions of MeOH and MeCN. L_4 was utilized for sensing Zn^{2+} in blood serum milieu which this group reported on in 2010.[125]

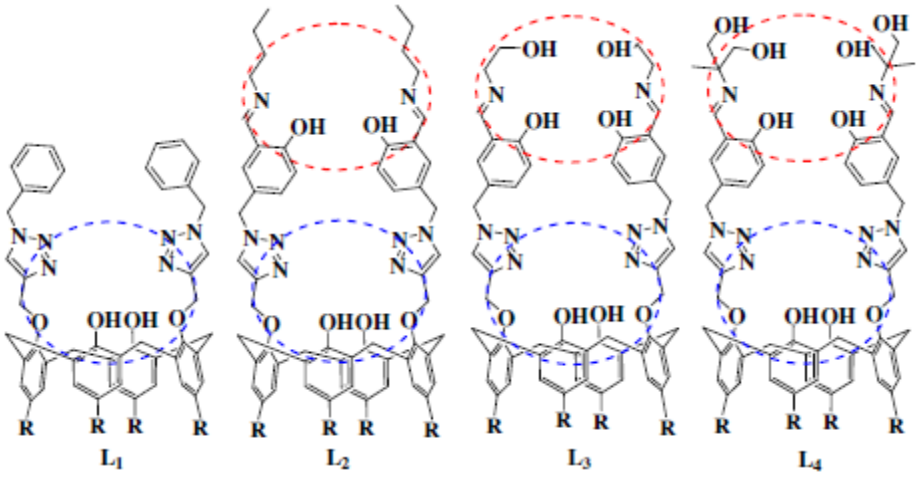

Figure 3.56: Ligands prepared by Pathak and co-workers.[124]

Therefore, the preparation of triazole linked Schiff base capped calix[4]arene was attempted to examine the effect of multiple binding sites within the molecule. The triazole would be formed by a Copper(I)-catalyzed Azide-Alkyne Cycloaddition (CuAAC),[50] which is a copper catalysed variant of the Huisgen 1,3-dipolar

cycloaddition.[126] Sticking with the compartmentalisation method, which had proved to be successful, a range of calix[4]arene azides were prepared (Scheme 3.9). These have been used previously as a basis for producing triazole linked calixarenes.[66,115]

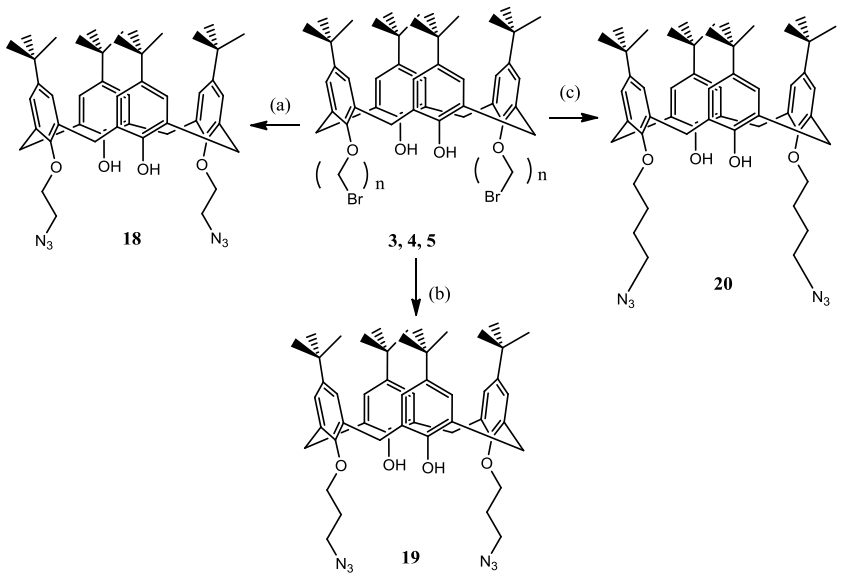

Scheme 3.9: Scheme for synthesis of azide-calixarenes **18**: n =2, NaN_3, CsCl, DMF, 90 °C. **19:** n = 3, NaN_3, CsCl, DMF, 90 °C. **20:** n = 4, NaN_3, CsCl, DMF, 90 °C.

The aim was to prepare *mono* and *bis* alkyne substituted di-imine bridged diphenol link units (Figure 3.57). It was initially envisaged that preparation of the *bis* variants would allow for the preparation of triazole linked analogues of the ligands prepared in Section 3.2. The *mono* derivatives would furnish a range of calixarene variants possessing flexible pendants arms which contain both a triazole and Schiff base moiety, similar to those prepared by Pathak.[124]

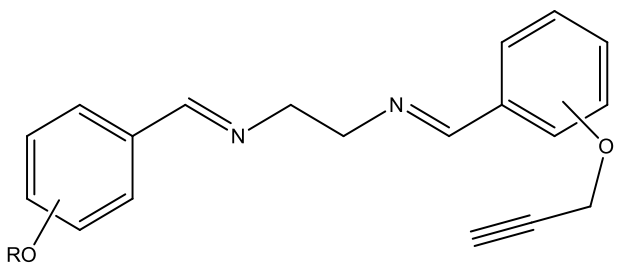

Figure 3.57: General structure of alkyne substituted di-imine diphenol units. R=H, $CH_2C{\equiv}CH$.

To ensure that the CuAAC method was advantageous for a calixarene based synthesis, a range of calixarene triazole linked benzaldehyde were synthesised. This was intended to serve as a model system upon which the Schiff base triazole reactions could be based. As was the case with the Schiff base linkers, the *ortho*, *meta* and *para* alkyne substituted benzaldehyde derivatives were prepared (Figure 3.58).

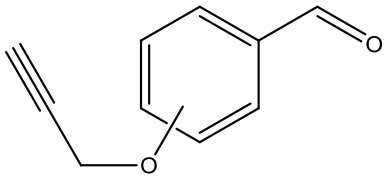

Figure 3.58: Structure of alkyne substituted benzaldehyde.

3.4.2 Synthesis and Characterisation of Calix[4]arene azide derivatives

The alkylazide substituted calix[4]arenes **18**, **19** and **20** were prepared by the method which is described by Tian *et al*.[115] The appropriate *bis*-bromoalkyl calix[4]arenes were dissolved in DMF (15 mL), to which sodium azide and caesium chloride was added. This reaction mixture was heated to 90 °C for a period of four hours. After the reaction is cooled to room temperature, the azidoalkyl calixarenes are precipitated from water as off white solids.

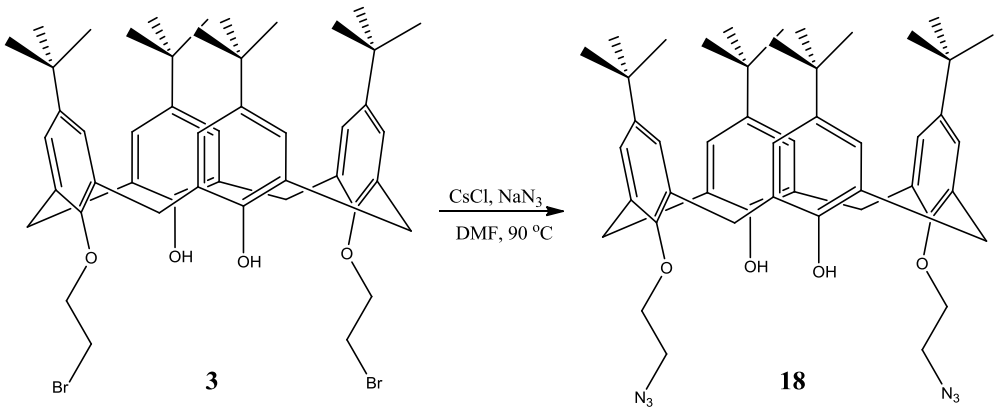

Scheme 3.10: Synthesis of **18** showing conditions used.

The resulting azides were characterised by their NMR and IR spectra. Upon analysis, it is found that the ^{1}H NMR spectra are broadly similar to the spectra obtained for the bromoalkoxy tetramers previously discussed. The effect that the symmetry of the 1,3-distal substituted calixarene has on the ^{1}H NMR spectrum of **18** is clear upon analysis. The *tert*-butyl group signals are seen to resonate as two singlets at 0.93 ppm and 1.30 ppm. Again, this effect is seen in the signals for the aromatic protons, which resonate as a pair of singlets at 6.77 ppm and 7.07 ppm. Once again, the diastereotopic nature of the methylene bridging protons is seen by the pair of doublets at 3.30 ppm and 4.30 ppm. The phenolic proton signal is seen to resonate as a singlet at 6.98 ppm. These signals show little or no shifting when compared to the 1,3-*bis*bromoethoxy calix[4]arene **3**. In comparison, the ethyl chain signal show the most significant amount of shifting. The ethyl chain is represented by two triplets at 3.81 ppm and 4.05 ppm. When compared to the spectrum of **3**, it is clear that the more downfield signal has been shifted upfield by approximately 0.23 ppm; this is due to the azide bound to this CH_2.

The 1,3-*bis*-azidopropoxy calix[4]arene **19** provides a similar spectrum to the bromopropoxy derivative **4**, which has been previously described.

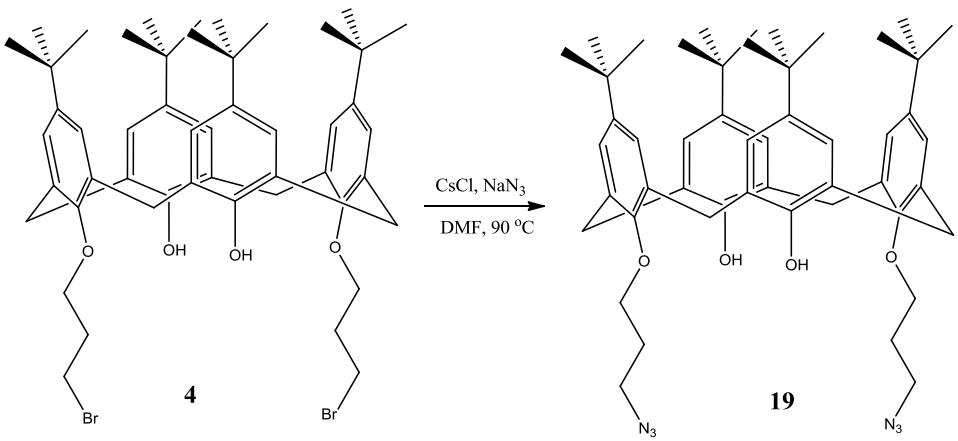

Scheme 3.11: Synthesis of **19** with conditions used shown.

Once again, the effect of symmetry on the spectrum is apparent from the pair of singlets at 1.00 ppm and 1.27 ppm. This effect is also clear from the pair of singlets that represent the aromatic proton signals at 6.85 ppm and 7.04 ppm. The signal for the phenolic proton is seen at 7.60 ppm. As in the case of **18**, the methylene bridges retain their diastereotopic nature and are represented as two doublets at 3.32 and 4.19 ppm. When compared to **4**, there is an upfield shift in the downfield doublet from 4.24 to 4.19 ppm. The propoxy chain is represented by a quintet and two triplets, which resonate at 2.21, 3.86 and 4.03 ppm. When these signals are compared to the starting bromopropoxy derivative, it is clear they experience the greatest degree of shifting, with upfield shifts of 0.28, 0.12 and 0.06 ppm.

The 1,3-*bis*butylazide derivative **20**, produces a ^{1}H NMR spectrum which is quite similar to the bromobutyl derivative **5**, which was discussed previously.

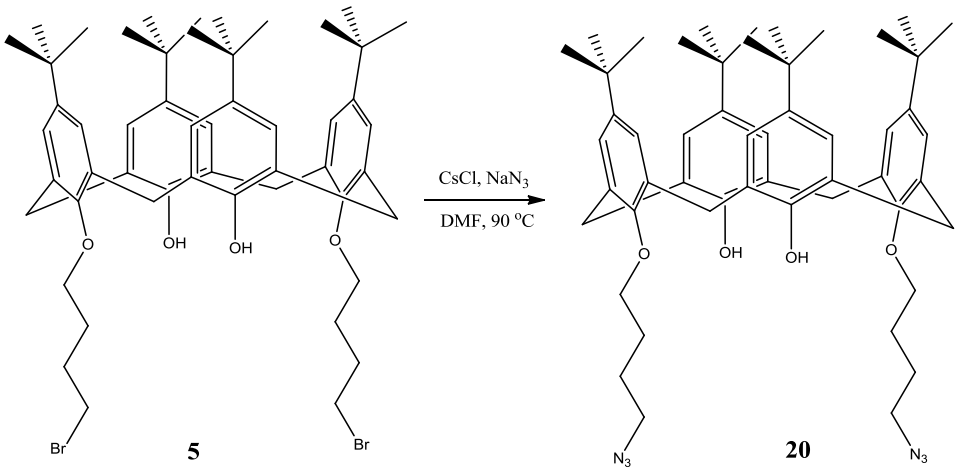

Scheme 3.12: Reaction conditions for synthesis of **20**.

The effect that symmetry has on the spectrum is clearly seen from the *tert*-Butyl groups, which resonate as two singlets at 0.96 and 1.28 ppm. It can also be seen from the appearance of the aromatic signals as two singlets at 6.80 ppm and 7.05 ppm. As has been the case with all the 1,3-distal-substituted calixarenes studied in this thesis, the butyl pendant arms experience the highest degree of shifting. The two central

methylene groups resonate as a broad singlet at 2.06 ppm which integrates for eight protons. The ether CH_2 and the CH_2 bound to the azide resonate as two triplets at 3.47 and 3.97 ppm, which represents an upfield shift of 0.13 ppm and a slight downfield shift, from the bromobutyl ligand.

3.4.3 Synthesis and Characterisation of alkynes

The synthesis of the 1,3-distal propargylcalixarene, **17**, is shown in Scheme 3.13. This alkyne substituted calixarene is widely used as the starting point for many triazole linked calixarene derivatives.[113,124,127] A mixture of the calix[4]arene and potassium carbonate was refluxed for two hours prior to addition of the alkyne to facilitate deprotonation of the phenolic groups. Trituration of the crude product with MeOH yielded a white solid which was recrystallized by slow diffusion. Further purification was carried out by column chromatography.

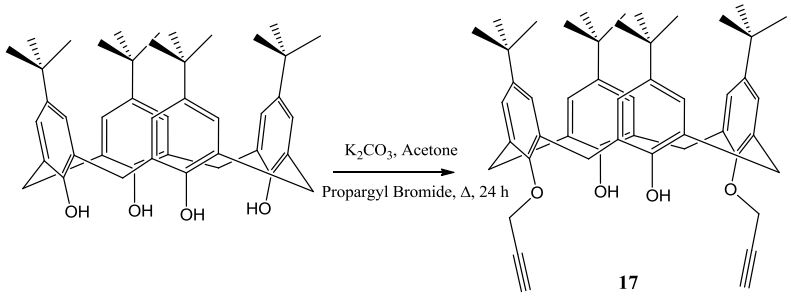

Scheme 3.13: Synthesis of 1,3-*Bis*alkyne Calixarene with conditions used shown.

As was expected, the symmetrical nature of the *bis*propargyl substituted calixarene was evident upon analysis of the ^{1}H NMR spectrum. The effect of symmetry is clearly seen by the appearance of two singlets which represent the *tert*-Butyl groups that resonate at 0.90 ppm and 1.30 ppm. This effect is also seen in the aromatic protons which resonate at 6.72 and 7.07 ppm as singlets. The phenolic proton signal resonates at 6.49 ppm as a singlet. This upfield shift is due to the extra hydrogen bonding which can occur due to the presence of the alkyne proton in close proximity to the phenol

groups. The methylene bridges are seen once again as two doublets which resonate at 3.31 and 4.35 ppm. It is clear that they retain the diastereotopic nature previously discussed. The ether CH_2 of the propargyl arm is represented by a doublet which resonates at 4.74 ppm with a coupling constant of J = 2.4 Hz. The alkyne proton signal resonates at 2.53 ppm as a triplet, with a coupling constant of J = 2.4 Hz, which is characteristic for a terminal alkyne. The ^{13}C NMR substantiates this assignment, as does the microanalysis which also includes a water molecule in the macrocyclic cavity.

The synthesis of the propargyl substituted benzaldehyde derivatives has been previously reported, by Giguère *et al.*[116] Magano *et al.*[123] and Pathak *et al.*[124] Therefore, these were selected as model compounds which would be linked by the triazole moiety to the calixazide scaffold. The general synthetic scheme is shown in Scheme 3.14. It is clear from the proposed structures that there is a high degree of symmetry in the compound. The effect of this on the ^1H NMR spectra is clear.

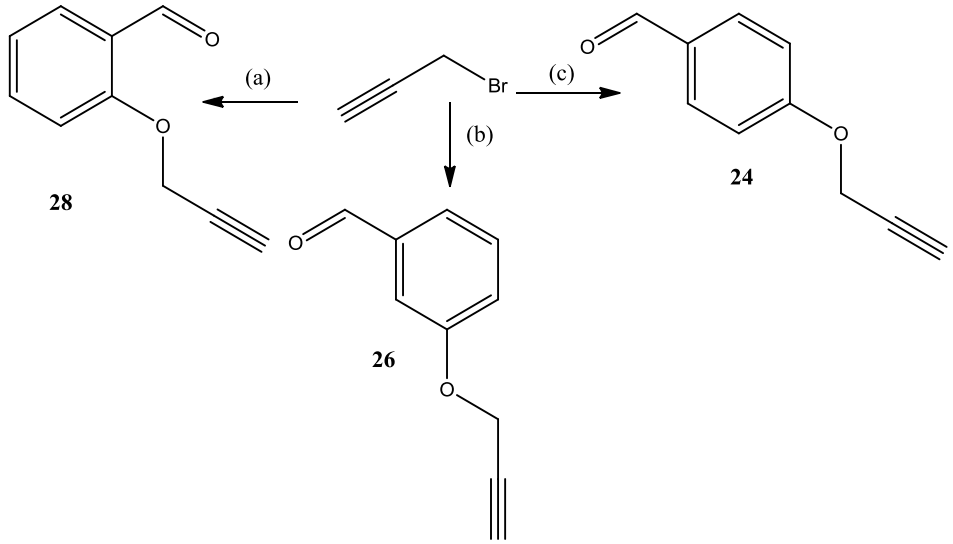

Scheme 3.14: General synthetic scheme for propargyl substituted benzaldehyde derivatives: **(a)** K_2CO_3, MeCN, 2-hydroxybenzaldhyde. **(b)** K_2CO_3, MeCN, 3-hydroxybenzaldehyde. **(c)** K_2CO_3, MeCN, 4-hydroxybenzaldehyde.

Upon analysis of the ^{1}H NMR spectrum of **24**, the distinct splitting pattern for a *para* di-substituted aromatic is observed. These aromatic protons resonate as a pair of doublets at 7.07 ppm and 7.83 ppm, with coupling constants of J = 8.7 Hz and J = 8.7 Hz. The aldehyde proton signal is seen as a singlet at 9.89 ppm, and the ether CH_2 resonates as a doublet at 4.77 ppm with a coupling constant of J = 2.4 Hz. The signal for the alkyne proton is observed as a triplet which resonates at 2.58 ppm, with a coupling constant of J = 2.37 Hz.

The *meta* substituted benzaldehyde **26** also exhibits the effect of symmetry in its ^{1}H NMR spectrum. The aromatic protons are represented by two multiplets which resonate at 7.25 ppm and 7.50 ppm; the aldehyde proton signal can be seen as a singlet which resonates at 9.98 ppm. A doublet which resonates at 4.75 ppm represents the ether CH_2 and has a coupling constant of J = 2.4 Hz. The alkyne proton is observed as a triplet which resonates at 2.55 ppm, with a coupling constant of J = 2.4 Hz.

Analysis of the ^{1}H NMR spectrum of the *ortho* substituted benzaldehyde **28** reveals the effect that the symmetrical nature of the compound has upon the spectrum. The aldehyde proton signal is seen as a singlet which resonates at 10.47 ppm. The aromatic proton signals resonate as two multiplets at 7.10 and 7.56 ppm and a doublet of doublets which resonates at 7.83 ppm. This splitting pattern was seen previously in the *ortho* substituted Schiff base linker **13**. Once again, the ether CH_2 resonates as a doublet at 4.82 ppm with a coupling constant of J = 2.4 Hz, and the alkyne proton signal is represented by a triplet which resonates at 2.58 ppm with a coupling constant of J = 2.4 Hz.

The deshielding effect, which is seen for the aldehyde proton signal when moving from *ortho* to *meta* to *para* (10.47 > 9.98 > 9.87 ppm), can be attributed to the induced magnetic field of the alkyne bond (Figure 3.59). The π electrons circulate the molecule

along the girth of the alkyne with both π bonds being involved. This movement of the π electrons produces a contribution to the induced magnetic field which opposes the applied field around the terminal proton (Figure 3.59). This produces a shielding effect on the alkyne, which explains the upfield position in contrast to alkenes. When the aldehyde proton is in the vicinity of this induced field it has the opposite affect and results in a downfield shift. The shift experienced by the *ortho* variant is larger due of the proximity aldehyde proton to the alkyne, which results in the downfield position of 10.47 ppm. The aldehyde protons of both *meta* and *para* derivatives, being more distant, are not as desheilded with shifts of 9.98 and 9.87 ppm, respectively.

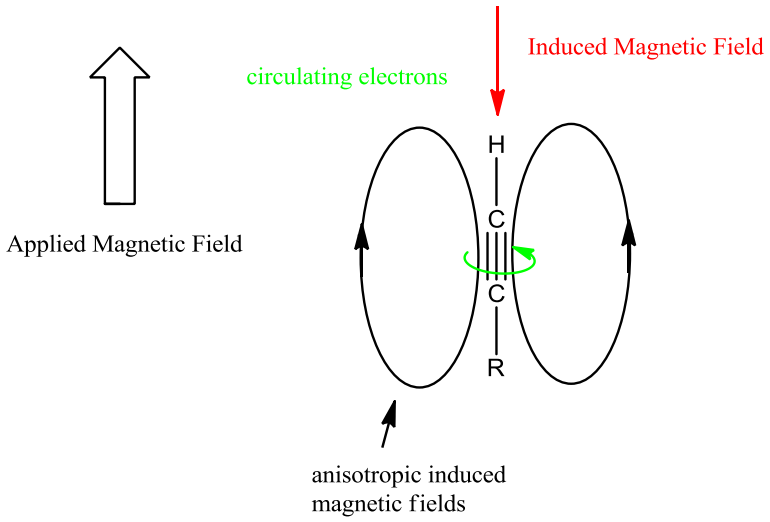

Figure 3.59: Applied and induced magnetic fields of a typical terminal alkyne.

As the *para*, *meta* and *ortho* propargyl substituted benzaldehyde derivatives were obtained as pure products, it was decided to synthesise a range of propargyl substituted variants of the Schiff base linkers from Section 2.2. It was originally planned to prepare a library of both *bis* and *mono* substituted derivatives of the *para*, *meta* and *ortho* linkers **6**, **9** and **13**. This was to continue the compartmentalisation ethic which was decided upon at the outset of this project. As the reaction conditions were practically identical to the pathway employed in the construction of the capped

calixarenes, it was expected that these Schiff base alkynes would be readily obtained. The reality was that there was mixed success in the synthesis of this family of linkers.

A *bis*-alkyne-substituted-*ortho*-Schiff base linker, **30**, was synthesised using similar conditions to all previous reactions with alkyl halide compounds reported in this thesis (Scheme 3.15). Analysis of the ^{1}H NMR spectrum of this compound clearly shows the effect that symmetry has on the NMR spectrum. The imine proton resonates as a singlet at 8.24 ppm and integrates for two protons. This is clear evidence of the presence of the imine within the compound.

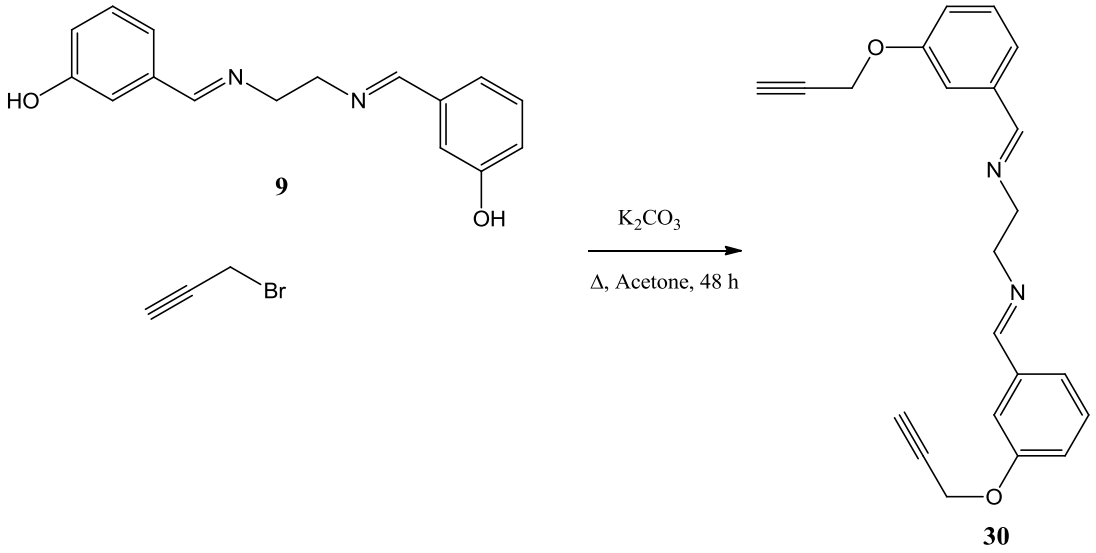

Scheme 3.15: Synthesis of *meta bis*-substituted Schiff base linker.

The characteristic triplet, which represents the alkyne proton, can be seen to resonate at 2.49 ppm with a coupling constant of J = 2.4 Hz. This signal resonates for two protons, providing evidence that a *bis* substituted alkyne has been formed. This postulation is further strengthened by the appearance of two signals, which resonate at 3.96 ppm as a singlet and at 4.70 ppm as a doublet. These represent the ethyl bridge within the Schiff base and the ether CH_2 of the alkyne, respectively. The aromatic protons resonate at 7.02, 7.28 and 7.32 ppm as three multiplets. The formation of this *bis*-alkyne Schiff

base is bolstered by the ^{13}C NMR spectrum. Elemental analysis reveals that some ethanol, which was used as the crystallisation solvent, is present.

Although the isolation of this product was successful, examination of the ^{1}H NMR of the crude product (Figure 3.60) reveals a familiar theme which was to be seen throughout the attempted synthesis of propargyl substituted Schiff bases. A new signal, H_a, appears at 9.97 ppm, which is in the region of the spectrum an aldehyde proton is expected to resonate. It is clear from the reaction conditions that no aldehyde is present, so this aldehyde must be formed due to imine hydrolysis.

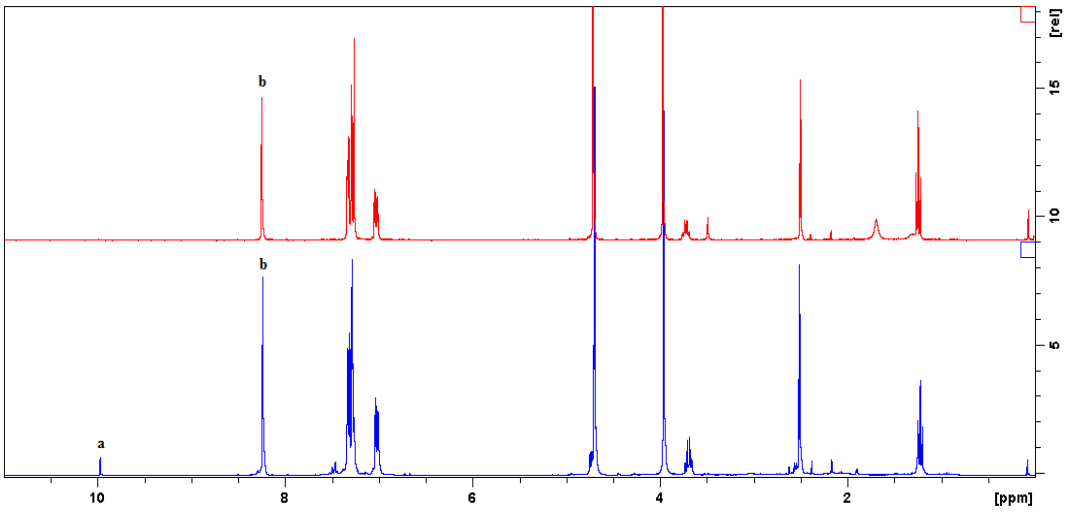

Figure 3.60: ^{1}H Spectra of crude product (blue) and **30** (red) with protons *a* and *b* highlighted.

Hydrolysis of the imine has been discussed at length in **section 3.3**. Comparison of the integrals for the imine H_b and aldehyde signals H_a reveal a ratio of product to aldehyde of 13:1, with the desired product as the major product. Although imine hydrolysis is known to occur even under mild conditions, this was somewhat unexpected due to the previously successful employment of similar reaction conditions to yield the capped calixarenes. Propargyl bromide has a lower acid disassociation constant (pK_a) in comparison to the alkyl halide calixarenes; this may lead to an acid catalysed hydrolysis of the imine to yield the aldehyde (Mechanism 3.2).[128] Although it is clear

from the formation of the desired compound **30**, that in this case the aldehyde is a minor side product, the instability of the imine bond under mild conditions could be problematic in further reactions of this type.

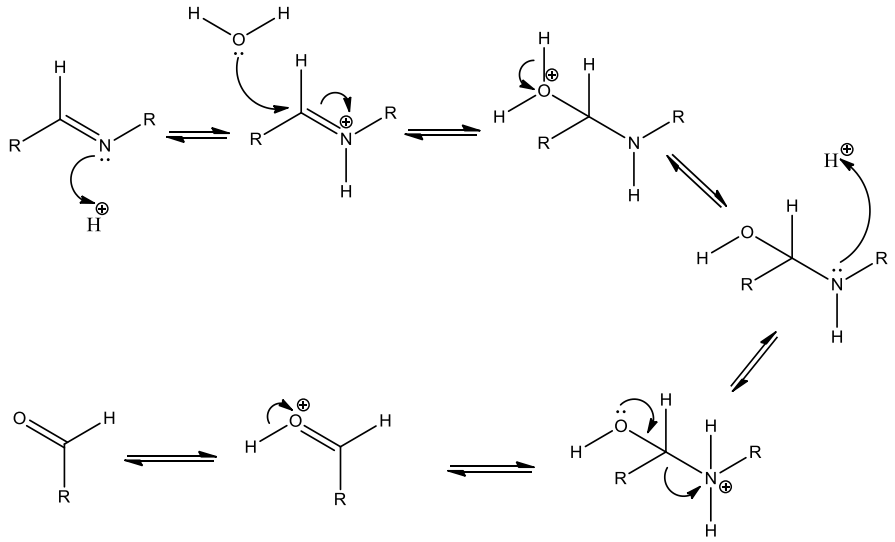

Mechanism 3.2: Acid catalysed imine hydrolysis.

A *mono* propargyl substituted variant of the *para* linker **6** was prepared in a similar fashion to **30** (Scheme 3.16). Due to the attempted *mono* substitution, the reaction period was half of that employed for the *bis* variant. This was also expected to help limit formation of the aldehyde.

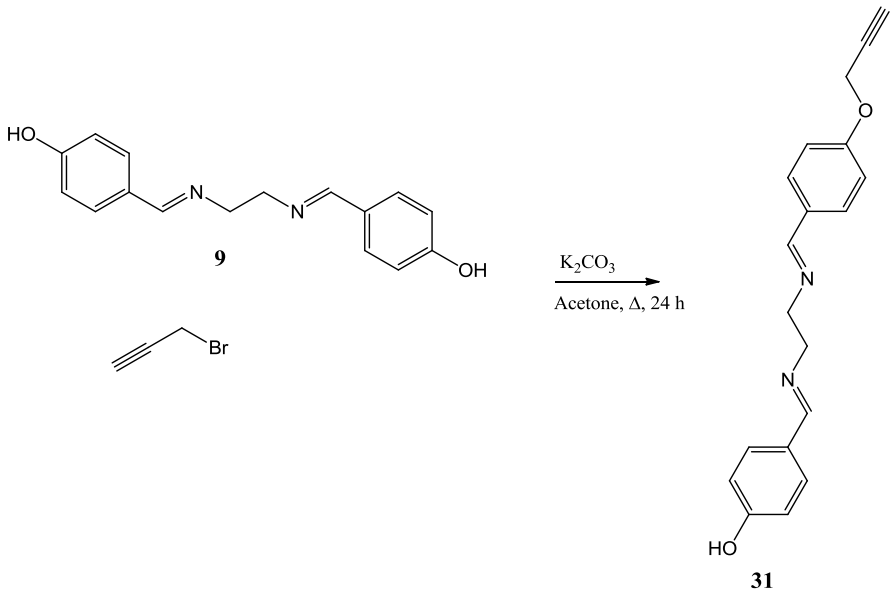

Scheme 3.16: Proposed synthesis of *mono* substituted *p*-Schiff base link.

^{1}H NMR spectral analysis of the crude product (Figure 3.61) clearly illustrates that aldehyde formation has indeed occurred. It is also indicated that the aldehyde is the major product from this reaction, which is the opposite of what was seen in the synthesis of compound **30**. Comparison of the integrals for the aldehyde signal (*a*) and the imine signal (*b*) reveal a ratio of 3.6:1 of aldehyde to the desired compound. The crude mixture was dissolved in DCM and petroleum ether was added to precipitate out the product.

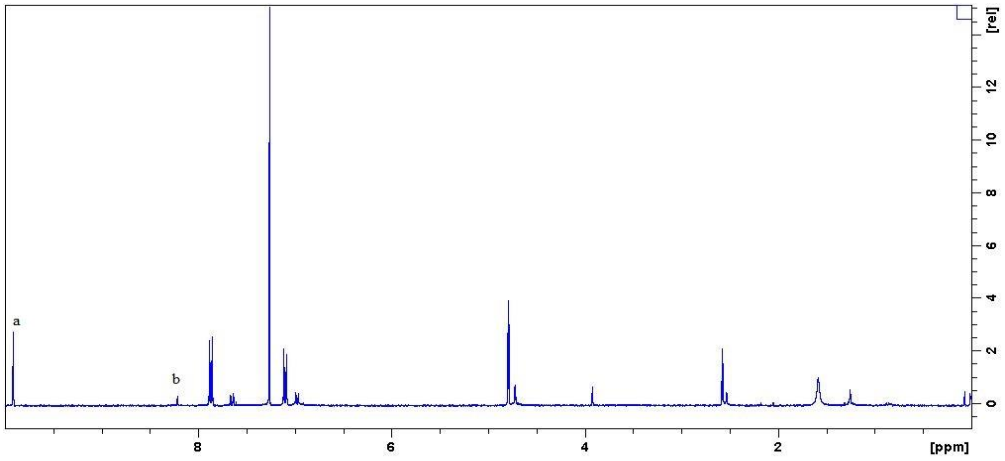

Figure 3.61: ^{1}H NMR spectrum of attempted synthesis of **31**.

A pale yellow solid was obtained and upon studying the ^{1}H NMR spectrum it is clear that this is the aldehyde hydrolysis product (Figure 3.62). The spectrum obtained is practically identical to that of the *p*-alkyne substituted benzaldehyde **24**.

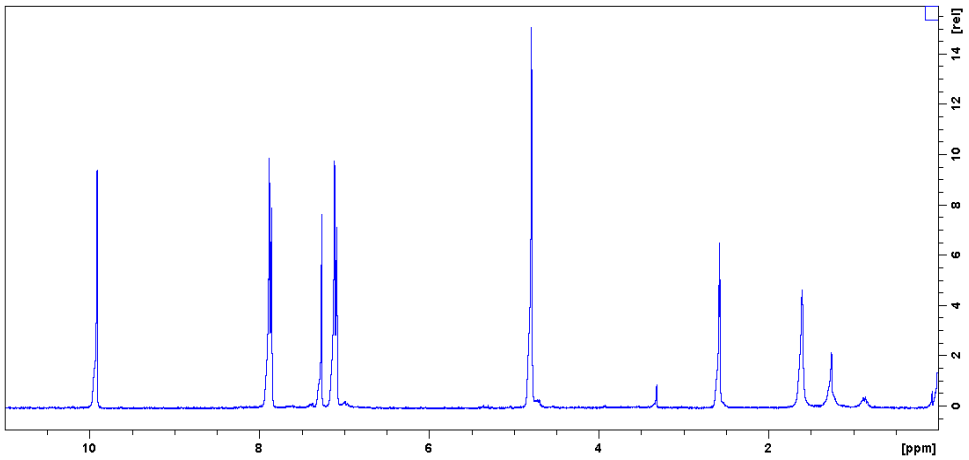

Figure 3.62: ^{1}H NMR spectrum of product of Schiff base hydrolysis.

Although some cleavage of the imine bond was expected, the predominance of the aldehyde product was not. The ^{1}H NMR spectrum of the remaining filtrate was analysed and compared with that of the isolated aldehyde (Figure 3.63) and it is clear that even in the filtrate the aldehyde is the dominant product; this trend was to be seen for the remaining attempts at synthesising propargyl substituted Schiff bases.

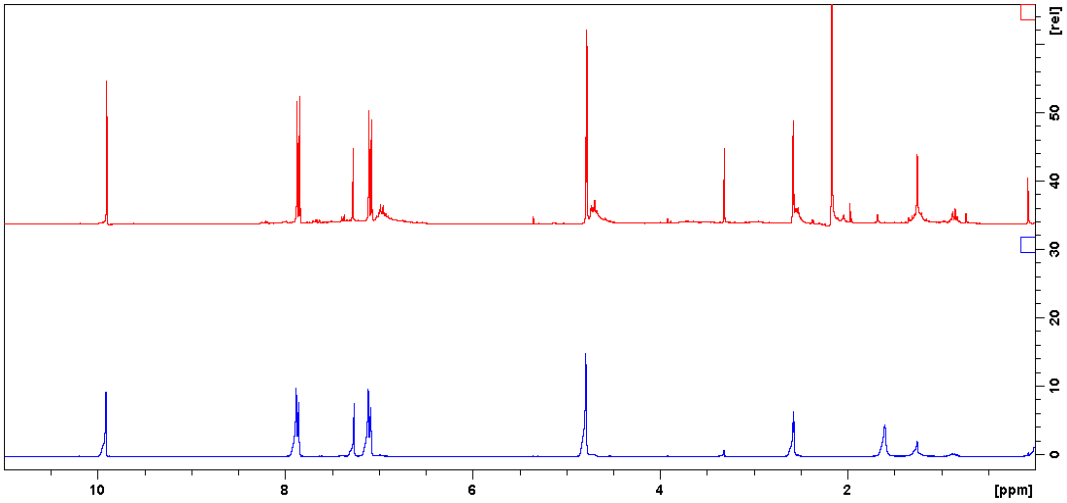

Figure 3.63: ^{1}H NMR spectra of the isolated aldehyde (blue) and the filtrate (red).

An *ortho-bis*-alkyne variant was attempted using similar reaction conditions to **30** (Scheme 3.17). As imine hydrolysis was observed in the previously attempted reactions, it was no surprise when, upon analysis of the ^{1}H NMR spectrum of the crude product, a characteristic aldehyde peak was observed.

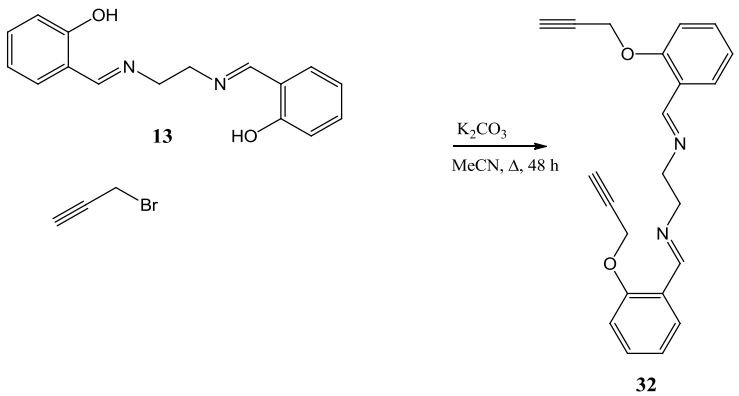

Scheme 3.17: Reaction scheme for attempted synthesis of **32**.

A TLC of the crude product revealed two spots, so column chromatography was utilized to separate the product. Schiff bases are very hard to separate using silica gel, but the propargyl substituted benzaldehyde derivatives are easily purified by this method, and as such it was assumed that it would be easily separated while leaving the desired product on the stationary phase. Comparison of the ^{1}H NMR spectra of the first product from the column with the crude spectrum (Figure 3.64) reveals that the *ortho* alkyne benzaldehyde **28** was isolated.

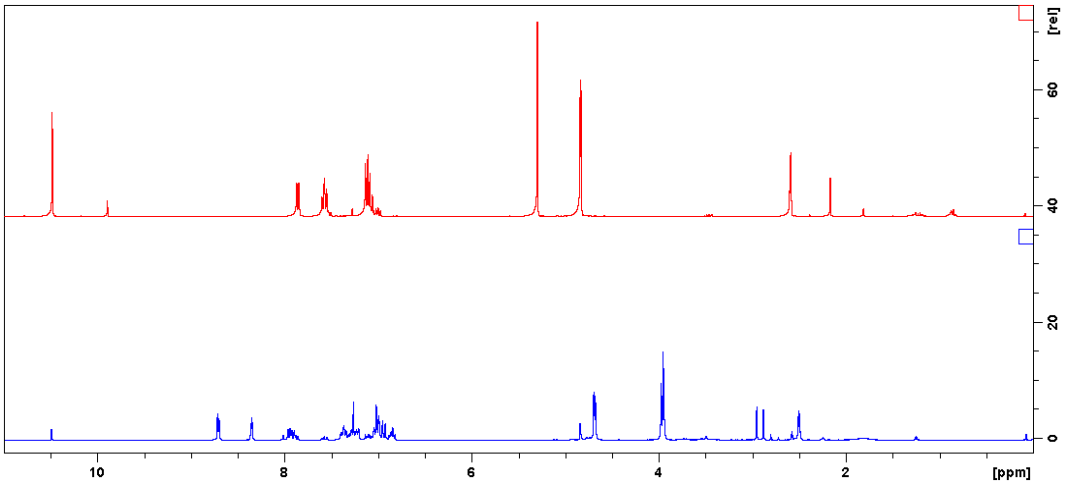

Figure 3.64: ^{1}H NMR spectra of **32** crude (blue) and first column product (red).

The column was flushed with MeOH, and it was thought this would yield the pure *bis*-alkyne product, but upon analysis of the ^{1}H NMR spectra (Figure 3.65) it is clear that the aldehyde is still present as a major constituent.

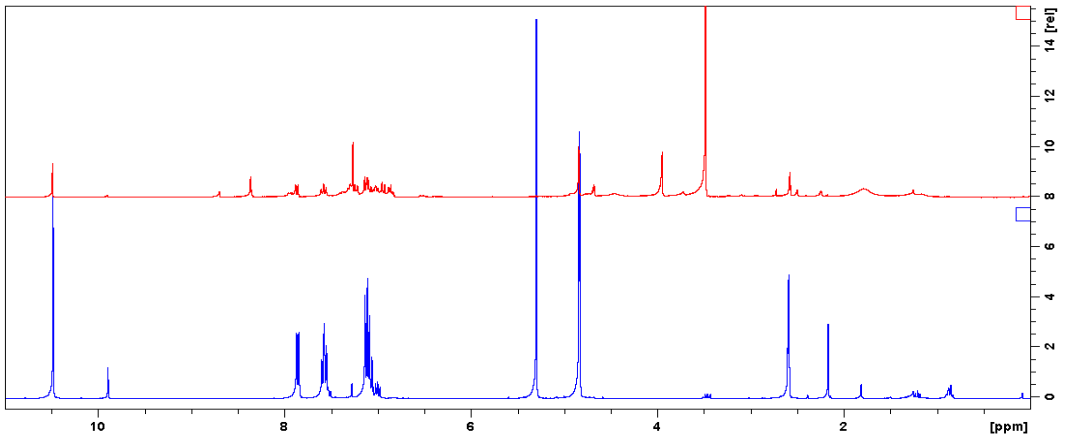

Figure 3.65: ^{1}H NMR spectra of aldehyde product (blue) and of column flush (red).

The final alkyne substitution reaction to be attempted was a *mono-ortho*-alkyne substituted Schiff base. Once again, this was prepared in a similar fashion to the previously discussed unsuccessful attempts; the reaction pathway is outlined in (Scheme 3.18).

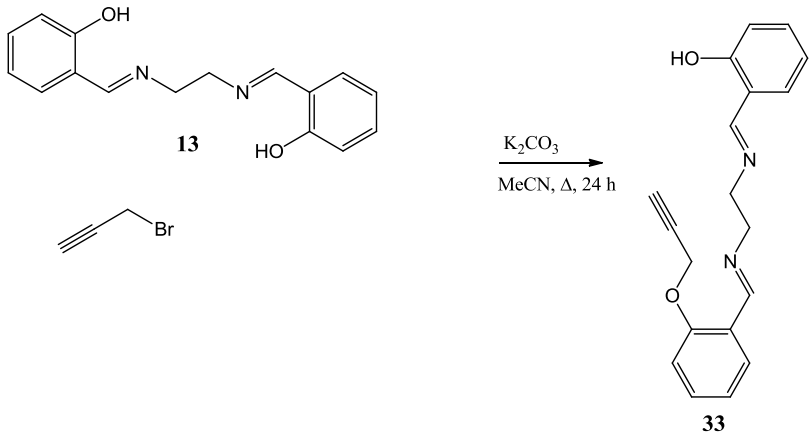

Scheme 3.18: Attempted synthesis of **33**.

Yet again, some degree of imine hydrolysis was expected, but the extent to which it occurs was still uncertain. Once again the ^{1}H NMR spectrum was obtained of the crude product (Figure 3.66).

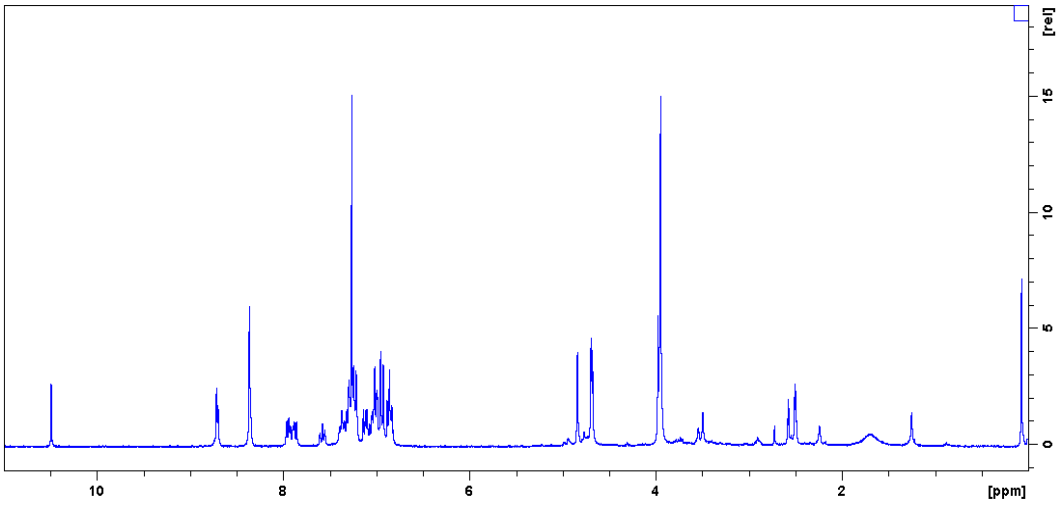

Figure 3.66: ^{1}H NMR spectrum of crude product from **33**.

It can be clearly seen that a peak is observed in the aldehyde region of the spectrum, at 10.49 ppm, which once again points towards hydrolysis of the imine. As column chromatography proved to be unsuccessful in obtaining the desired product for the *bis* derivative, a mixture of DCM and petroleum ether was attempted to isolate the product. However, this did not yield either the aldehyde hydrolysis product or the desired product. The major difference between the successful synthesis of **30** and the subsequent failed synthesis attempt is the choice of solvent, with acetone being used for the successful method and acetonitrile for the failed attempts.

3.4.4 Copper(I)-catalysed 1,3 Huisgen Azide-Alkyne Cycloaddition (CuAAC)

The proposed catalytic cycle for the copper(I)-catalysed 1,3 Huisgen azide-alkyne cycloaddition (CuAAC) reaction is shown in mechanism 3.3, which was proposed by Himo *et al*.[59] This mechanism has previously been discussed in detail in **Section 1.3.2**.

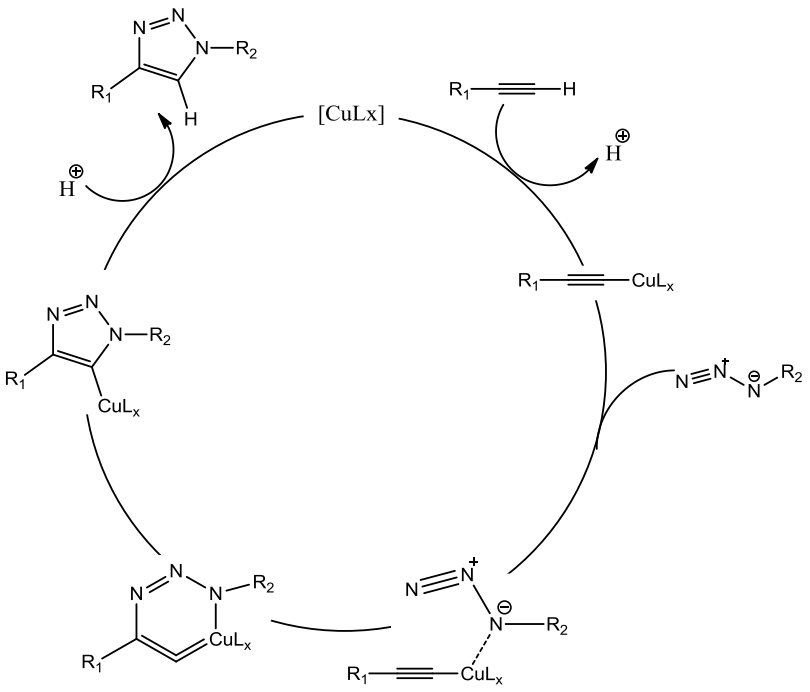

Mechanism 3.3: Proposed catalytic cycle for the CuAAC reaction.[55]

This type of cycloaddition was chosen as it is regioselective and results in only the 1,4-disubstituted triazole. The formation of this triazole is easily characterised from the

characteristic resonance position of the C_5 carbon in the ^{13}C NMR spectrum at approximately 120 ppm.[65] Figure 3.67 shows the standard nomenclature for assignment of triazole structure.

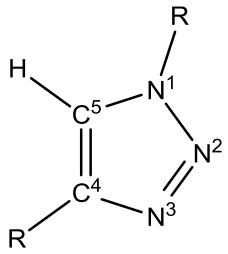

Figure 3.67: General 1,4-disubstituted-1*H*-1,2,3-triazole.

The Cu(I) catalyst is generated by *in situ* reduction of Cu(II), copper sulphate pentahydrate in this case. The addition of a reducing agent, sodium ascorbate for example, reduces Cu from the +2 to the +1 oxidation state. Using this method of Cu^{1+} generation negates the need for a base in the reaction. Another advantage of employing this method is that it does not require an inert atmosphere, despite the instability of Cu(I) in the presence of oxygen.[129]

3.4.5 Synthesis and Characterisation of Triazole linked Double Calixarenes

Using the successfully isolated calixarene-alkyne **17**, and the three calixarene-alkyl azides, **18**, **19** and **20**, three triazole linked double calixarenes were synthesised. The synthesis of the double calixarene **21** has been previously reported by Morales-Sanfrutos and co-workers[71] using copper iodide as the catalyst. The aim was to use copper sulfate as the catalyst, by way of the *in situ* reduction of Cu(II) to Cu(I), to perform a click reaction, yielding the desired double calixarenes. But, as will be seen in the discussion of each product, the requirement of column chromotography for purification means that these reactions do not adhere to the rules which Sharpless proposed for a reaction to be classed as click.[50]

Before arriving upon the reaction conditions which are shown in Scheme 3.19, a range of solvents, reaction temperatures and reaction times were attempted. Most of these conditions gave minimal yields, with some giving no indication of the desired product being formed. The conditions which were finally used had been previously reported by Tian in 2010 for the synthesis of a triazole-linked 8 oxyquinoline calix[4]arene.[115] It was found through several attempts that control of the reaction temperature was key to the formation of the triazole ring.

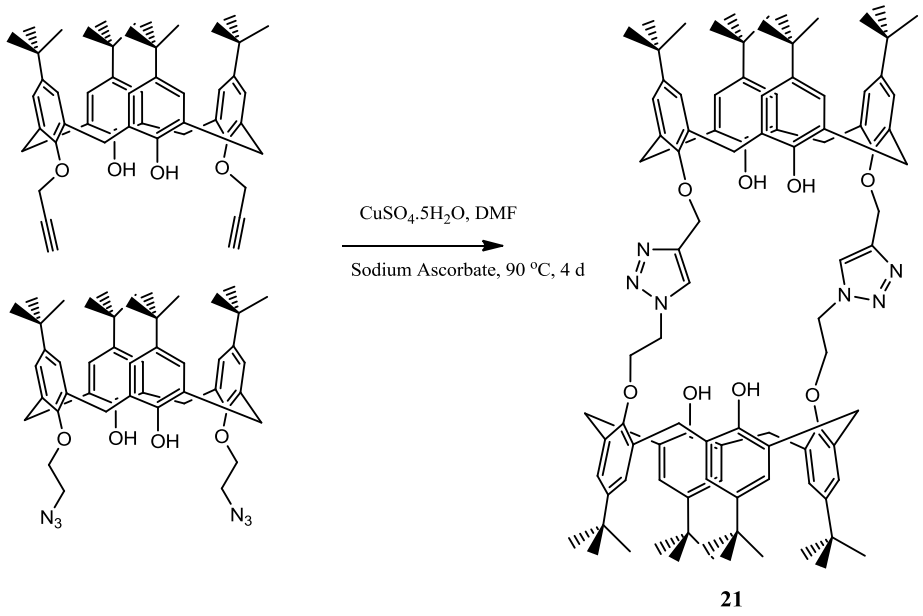

Scheme 3.19: Synthesis of **21** showing conditions used.

The *bis*-alkyne calixarene **17** and the *bis*-ethylazide calixarene **18** were dissolved in DMF. To this the copper sulphate and sodium ascorbate were added, and the stirring mixture was heated to 90 °C for 86 h. After the product was extracted with ethyl acetate from water, the solution was reduced to dryness. This residue was taken up in DCM, and a yellow solid was obtained through slow diffusion of DCM in methanol. This was then further purified by column chromatography to obtain **21** as an off white/yellow solid. Analysis of the ^{1}H NMR spectrum of the product indicates that the proposed structure from Scheme 3.19 has been obtained, and conforms well to the previously reported spectrum.[70]

As is the case for the majority of 1,3-*bis*-substituted calixarenes in this thesis, the *tert*-Butyl groups are seen as a set of singlets at 0.97 ppm and 1.28 ppm, but they integrate for thirty six protons each. Due to the fact there are two cavities for solvents to inhabit, an array of solvent signals can be seen in the *tert*-Butyl region. In the spectrum of the double calixarene duplication of the methylene bridge signals is noted, whereas in previously discussed calixarene derivatives the methylene bridges appear as two doublets. This is due to the methylene bridges being in slightly different chemical environments owing to the proximity to the triazole unit. In this spectrum the methylene bridges are represented by two multiplets which resonate at 3.29 and 4.10 ppm and integrate for eight protons each. Two triplets at 4.50 and 5.12 ppm represent the ethyl chain protons, and a signal at 5.25 ppm, which resonates as a singlet, represents the ether CH_2 between the calixarene and the triazole. The aromatic proton signals are represented by a singlet which resonates at 6.83 ppm and a multiplet which resonates at 7.02 ppm. These integrate as eight and sixteen protons, respectively. Two sets of signals are seen for the phenolic protons and resonate at 6.91 and 7.60 ppm as singlets. Finally, the triazole proton signal is observed as a singlet which resonates at 8.55 ppm. The ^{13}C NMR spectrum also indicates the formation of a doublet calixarene with the *tert*-Butyl carbon peak dominating the spectrum. Mass spectrometry of the product points towards the proposed structure with the M+H peak found at 1512.9443 *m/z*, which conforms well to the calculated value, and falls within the accepted 5 ppm error range. However, without a crystal structure this cannot be confirmed unambiguously.

With this synthetic route proving to be fruitful, a similar reaction was performed between the *bis*-propylazide calixarene **19** and **17** (Scheme 3.20). After removal of the solvents, the product **22** was obtained as an off-white solid. ^{1}H NMR spectral analysis (Figure 3.68) showed a similar spectrum to that of **21**.

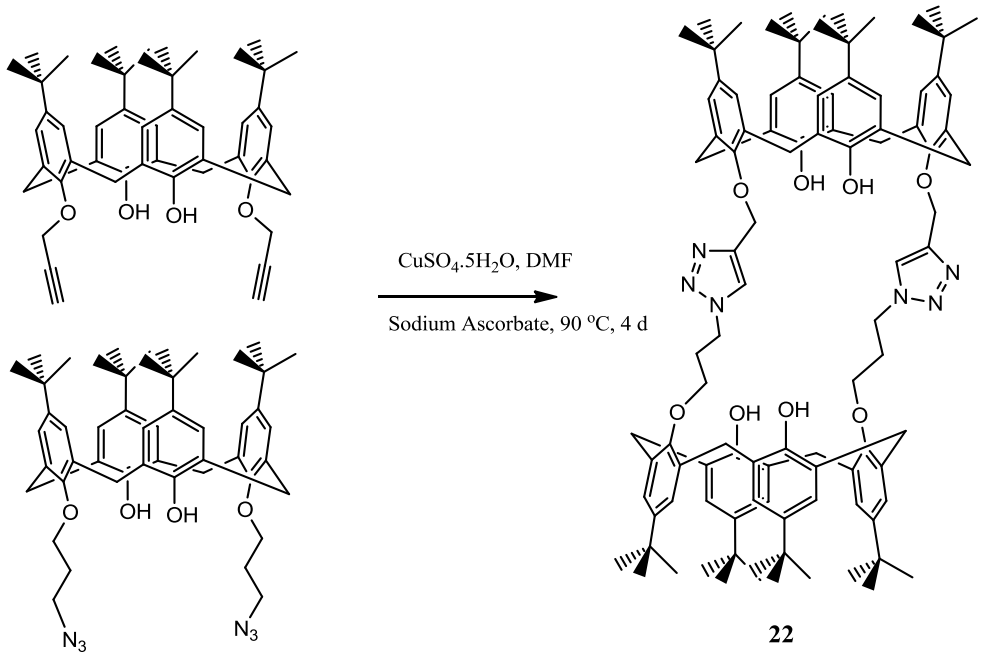

Scheme 3.20: Synthesis of **22** with conditions shown.

The effect of the highly symmetric nature of the product is clear on the spectrum. This is evident from the appearance of the *tert*-Butyl groups as four singlets which resonate at 0.95, 1.04, 1.27 and 1.29 ppm. Once again, there is duplication of the methylene bridge signals, which resonates as four doublets at 3.31, 3.35, 4.27 and 4.32 ppm. The propyl chain is represented by three signals which resonate at 2.67 ppm as a multiplet, at 4.18ppm as a triplet, and at 4.99 ppm as another triplet. The ether CH_2 between the calixarene and the triazole resonates at 5.41 ppm as a singlet. Symmetry is noted in the aromatic signals, which resonate at 6.81, 6.91, 7.04 and 7.06 ppm as singlets. As was seen for **21**, two separate signals are observed for the phenolic protons. These resonate as singlets at 7.22 ppm and at 7.93 ppm. The triazole proton is observed at 8.13 ppm and resonates as a singlet.

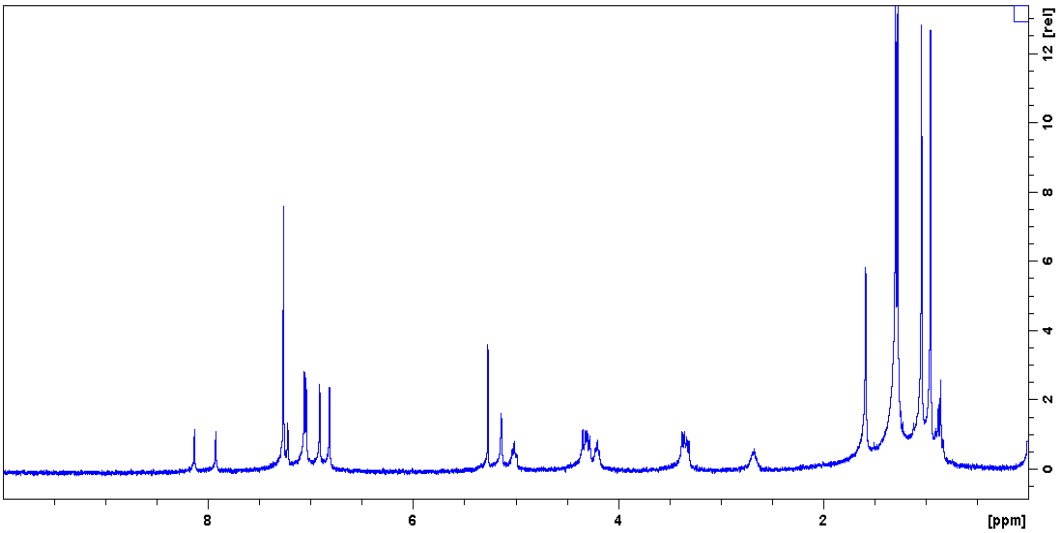

Figure 3.68: ^{1}H NMR spectrum of **22.**

This assignment of the ^{1}H NMR spectrum indicates that a triazole linked double calixarene has been successfully synthesised. This is further substantiated by the ^{13}C NMR spectrum and by mass spectrometry which found the M+H peak at 1540.9766 *m/z*, which compares well to the calculated value and is within the ppm error.

A similar reaction between the *bis*-butyl-azide calixarene **20** and **17** was attempted using comparable conditions to the previously isolated products **21** and **22**. This is described in Scheme 3.21. The product **23** was obtained as brown crystals from a mixture of dichloromethane and petroleum ether. The product was characterised by ^{1}H NMR spectroscopy and analysis of the product reveals a similar spectrum to that of **21** and **22**. Once again, the effect of symmetry is seen on the spectrum, with the *tert*-Butyl groups resonating as four singlets at 0.95, 1.03, 1.27 and 1.29 ppm. As was the case with **21**, the *tert*-Butyl region shows numerous solvents peaks.

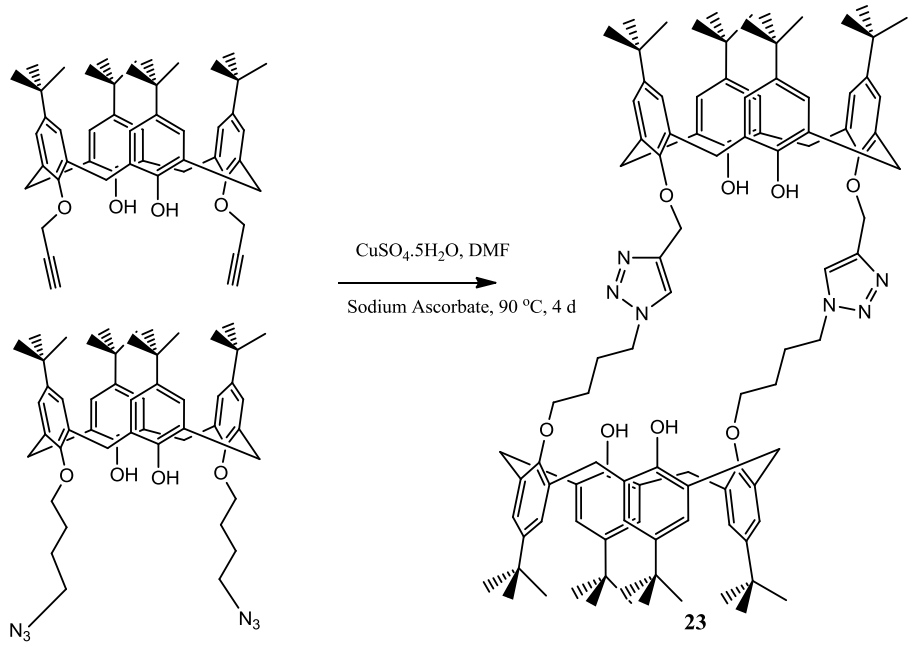

Scheme 3.21: Synthesis of **23** with conditions shown.

Once again, the duplication of the methylene bridge signals is seen by four sets of doublets which resonate at 3.30, 3.35, 4.27 and 4.31 ppm. The butyl chain is represented by two triplets that resonate at 4.18 and 4.98 ppm, a multiplet which resonates at 1.73 ppm, and another multiplet which resonates at 2.67 ppm. Once again, the ether CH_2 between the calixarene and the triazole resonates as a singlet at 5.13 ppm. As was the case for **22**, four signals can be seen for the aromatic protons, which resonate as singlets at 6.81, 6.90, 7.04 and 7.06 ppm. Two signals can be seen for the phenolic protons which resonate as singlets at 7.21 ppm and 7.90 ppm and, finally, the triazole proton resonates at 8.12 ppm as a singlet.

The structure proposed in Scheme 3.21 compares well to the ^{1}H NMR spectral assignment, and the ^{13}C NMR spectrum provides further evidence of this. Mass spectrometry was performed on this compound and although the accurate mass was not found, a fragmentation pattern which was consistent for the compound losing four protons was obtained. This once again strengthens the case for the proposed structure.

Although these compounds were successfully synthesised, the percentage yields were quite low, and as a result this route was abandoned at this stage.

3.4.6 Synthesis and Characterisation of Triazole linked Calixarene Benzaldehyde derivatives

Two sets of reaction conditions were used to synthesise the triazole linked benzaldehyde calixarene derivatives. The first method (a) using DMF as solvent gave higher yields (>85 %), but required column chromatography for purification and strict control of reaction temperature. The second method (b) used a solvent mixture of dichloromethane and water. Both methods have been previously reported in the synthesis of triazole linked calixarene derivatives,[115,124] and both have their advantages. This gave slightly lower yields (70-80 %) but did not require column chromatography for purification. As a result, the latter set of conditions were chosen where possible for the Huisgen cycloaddition to form the triazole linked calixarene benzaldehyde derivatives. The triazole linked calixarene benzaldehyde **30**, was synthesised *via* both methods (Scheme 3.22).

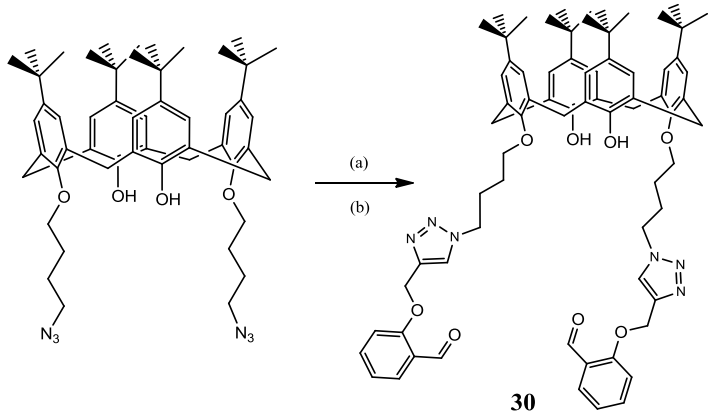

Scheme 3.22: Comparison the two reaction conditions employed for synthesis of **30**, **(a):** DMF, $CuSO_4.H_2O$, Sodium Ascorbate, 90 °C, 4 d **(b):** DCM:H_2O, $CuSO_4.H_2O$, Sodium Ascorbate, Δ, 5 d.

Analysis of both products using ^{1}H NMR spectroscopy (Figure 3.69) reveals that both reactions successfully yield the desired product. However, it is clear that method (b) affords a high degree of purity without the necessity to perform column chromatography. It is also notable that the residual solvent signals for DMF could obscure the triazole proton peak.

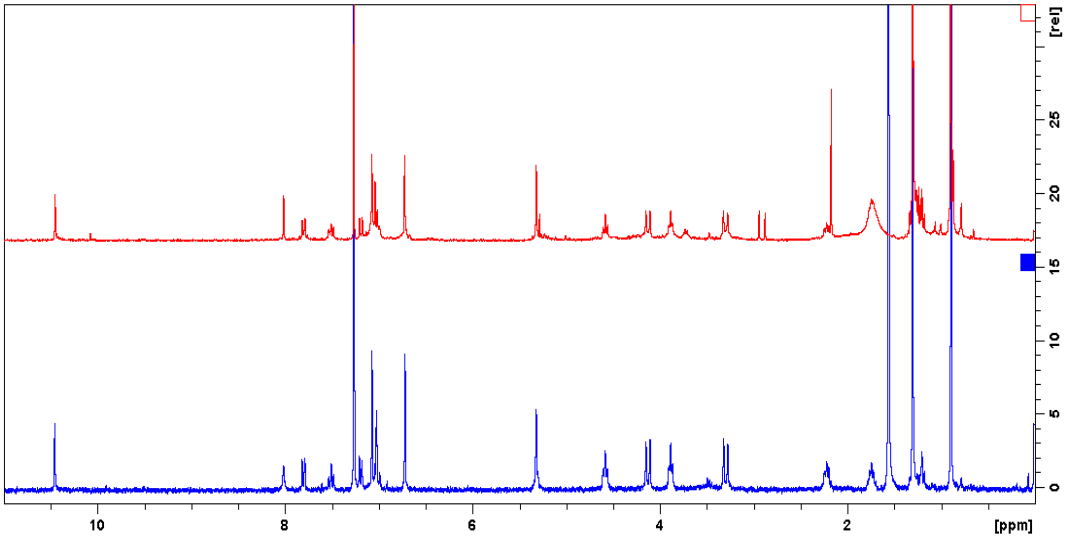

Figure 3.69: ^{1}H NMR spectra of **30** from reaction route **(a)** (red) and **(b)** (blue).

The ^{1}H NMR spectrum of the triazole linked *o*-benzaldehyde calixarene derivative **30** exhibits the tell-tale effect of a highly symmetrical compound. This is clear from the two *tert*-Butyl groups which resonate at 0.89 and 1.30 ppm. The effect is also seen in the aromatic proton signals which resonate as a pair of singlets at 6.72 and 7.07 ppm. A signal is observed at 7.02 ppm which represents the phenolic protons, and this resonates as a singlet. The methylene bridging protons are once again seen as two doublets, which resonate at 3.27 and 4.10 ppm. The butyl chain is observed as two quintets which resonate at 1.68 and 2.17 ppm, and by two triplets which resonate at 3.86 and 4.56 ppm. The ether CH_2 between the triazole and the benzaldehyde is represented by a singlet which resonates at 5.32 ppm. The aromatic proton signals for the benzaldehyde moiety are observed as a doublet of doublets which resonate at 7.78

ppm, a triplet at 7.48 ppm, a doublet at 7.17, and a multiplet at 7.04 ppm, which integrate for eight protons collectively. Finally, the aldehyde signal peak is clearly observed as a singlet which resonates at 10.45 ppm. This proposed structure is supported by the ^{13}C NMR spectral data (Figure 3.70) which shows a characteristic aldehyde peak at 189.6 ppm. The signal peak which resonates at 121.2 ppm, is in the region of the spectrum that the C_5 signal is expected for a 1,4-disubstituted-1*H*-1,2,3-triazole.[65]

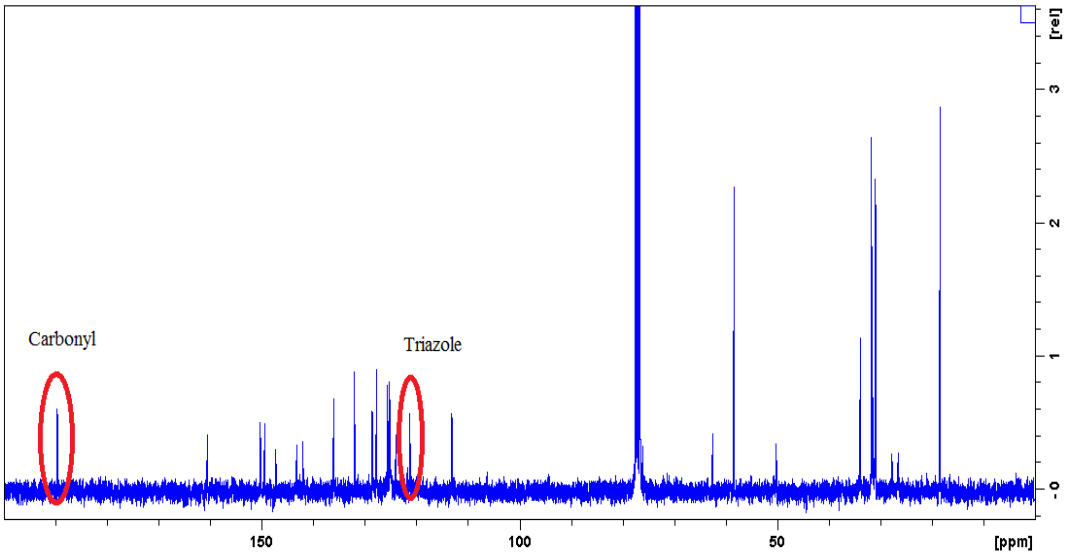

Figure 3.70: ^{13}C NMR of **30** with carbonyl and triazole carbon signals highlighted.

This structural assignment was further supported by the mass spectrum of the product, with the M+H peak observed at 1163.6608 *m/z*, which compares favourably with the calculated value. The IR spectrum of the product also supports the other spectroscopic data. The aldehyde represented by a C=O stretch is observed as a strong sharp band at 1688 cm^{-1} and two aldehyde C-H stretches at 2762 and 2868 cm^{-1}. The two C-N bonds in the triazole moiety are represented by a pair of absorptions bands at 1286 and 1337 cm^{-1}. The N=N stretch is represented by a stronger absorption band at 1485 cm^{-1}, which falls within the range previously reported for N=N bonds in IR spectroscopy.[130] A broad band at 3429 cm^{-1} is indicative of the phenolic OHs of the calixarene core.

The propyl *o*-benzaldehyde variant **29** was prepared by the same synthetic route (Scheme 3.23). This yielded **29** as an off-white solid which was characterised using ^{1}H NMR and ^{13}C NMR spectroscopic methods. The effect of symmetry is noted on the ^{1}H NMR spectrum once again (Figure 3.71). This is clearly seen in the *tert*-Butyl groups which resonate as a pair of singlets at 0.96 and 1.27 ppm, and this effect is also seen in the aromatic protons. These resonate at 6.81 and 7.05 ppm as two singlets, the phenolic proton is seen to resonate at 7.43 ppm as a singlet.

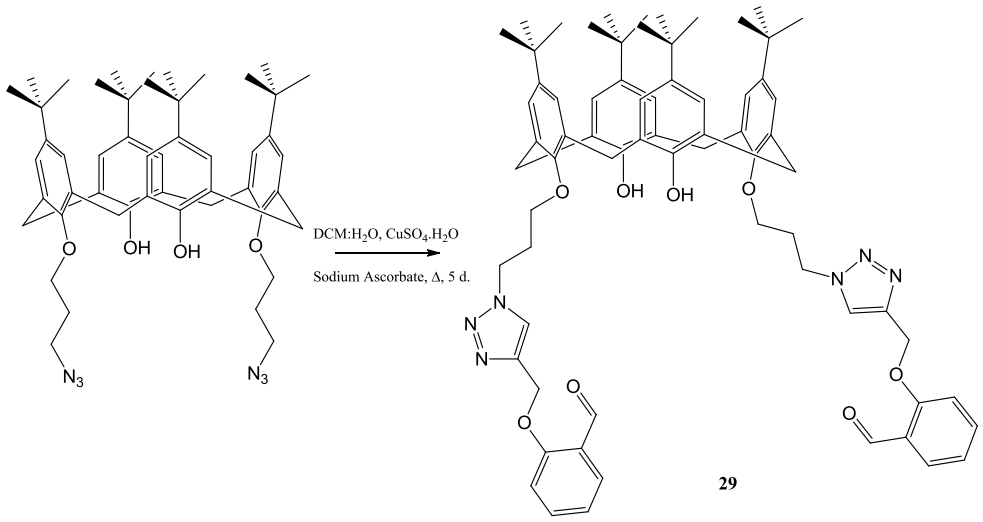

Scheme 3.23: Synthesis of **29** with conditions shown.

The propyl chain signals are observed as two triplets, which resonate at 3.99 and 4.87 ppm, and as a quintet that resonates at 2.59 ppm. The ether CH_2 between the triazole and the benzaldehyde is seen to resonate as a singlet at 5.29 ppm. Several signals are seen to resonate in the aromatic region of the spectrum. These signals, which represent the aromatic protons of the benzaldehyde, resonate as a doublet of doublets at 7.79 ppm, a triplet that resonates at 7.48 ppm, and two singlets which resonate at 7.15 and 7.12 ppm. The aldehyde proton signal is observed with a chemical shift of 10.40 ppm which resonates as a singlet. A singlet which is seen to resonate at 7.95 ppm represents the triazole proton.

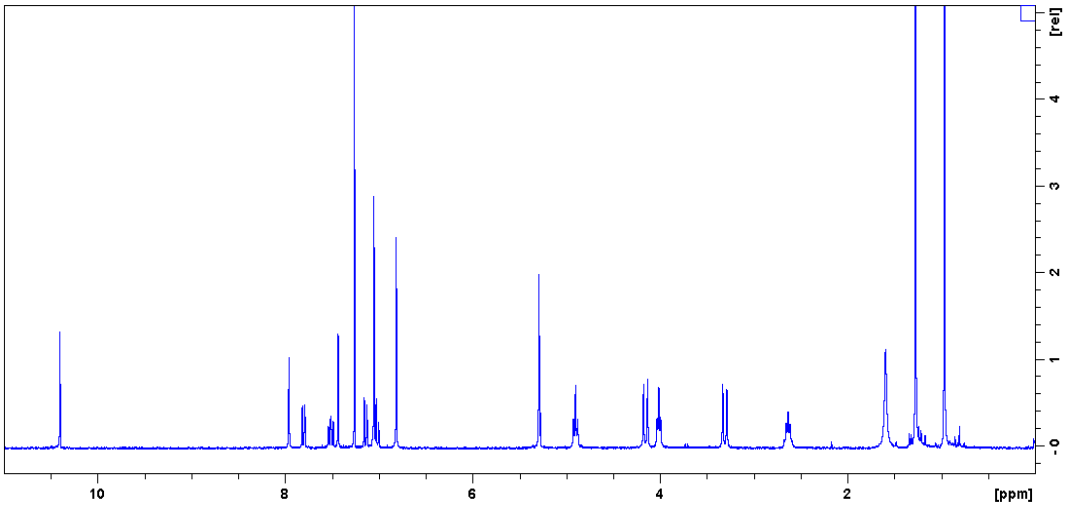

Figure 3.71: ^{1}H NMR spectrum of **29**.

This assignment is also supported by the ^{13}C NMR spectrum (Figure 3.72). Once again, the aldehyde carbonyl carbon signal is observed with a resonance of 189.6 ppm, which confirms that an aldehyde is present in the structure. The triazole C_5 is once again observed with a resonance of 121.2 ppm which, as discussed previously, is consistent with a 1,4-disubstituted-1*H*-1,2,3-triazole.

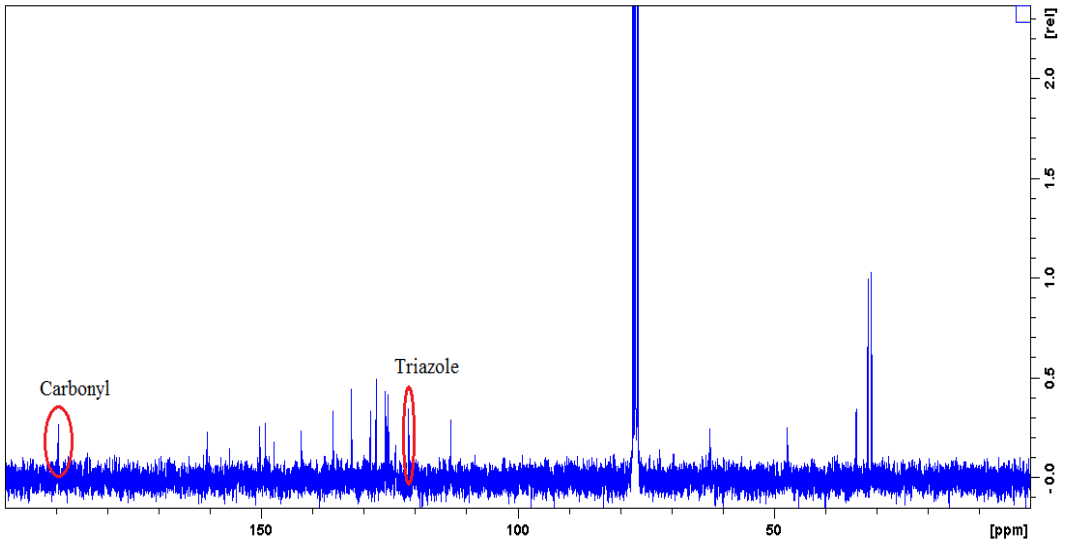

Figure 3.72: ^{13}C NMR Spectrum of **29**.

The structural assignment from the above data is reinforced by mass spectrometry. The *m/z* for the M+H is found at 1135.6191, which compares favourably to the calculated value. The IR spectrum, which is near identical to that of **30**, provides further evidence

that the desired compound was isolated. The aldehyde is represented by a C=O stretch that is observed as a strong sharp band at 1688 cm^{-1} and two aldehyde C-H stretches at 2762 and 2868 cm^{-1}. A broad band at 3432 cm^{-1} is indicative of the phenolic OHs of the calixarene core. The two C-N bonds in the triazole moiety are represented by a pair of absorption bands at 1286 and 1337 cm^{-1}. Once again, the N=N stretch is observed at 1485 cm^{-1}.

The *meta* and *para* benzaldehyde derivatives **27** and **25** are prepared using the same reaction conditions (Scheme 3.24). The ^{1}H NMR spectrum of triazole linked *m*-benzaldehyde calixarene **27** exhibits the tell-tale signs of a highly symmetrical molecule. This is clear from the pair of singlets that resonate at 0.97 and 1.28 ppm which are representative of the *tert*-Butyl groups. The pair of singlets which represent the calixarene aromatic protons resonate as singlets at 6.82 and 7.03 ppm, thus supporting the symmetrical structural assignment. The methylene bridging protons are represented by a pair of doublets which resonate at 3.29 and 4.14 ppm. The phenolic proton signal is observed as a singlet which resonates at 7.60 ppm. The propyl chain is represented by two triplets and a multiplet which resonate at 3.98, 4.85 and 2.54 ppm, which is similar to the spectrum of **29**. A singlet which resonates at 5.22 ppm represents the ether CH_2, which is between the triazole and the calixarene. The triazole proton signal resonates at 7.93 ppm as a singlet, and the aldehyde proton is observed at a resonance of 9.99 ppm as a singlet. The aromatic protons are observed to resonate as three multiplets and a singlet which resonate at 7.50, 7.46, 7.44 and 7.40 ppm. The proposed 1,4-triazole is supported by the ^{13}C NMR spectrum which shows a peak which resonates at 121.5 ppm. Once again, mass spectroscopy provided further evidence for the proposed structure, with an M+H peak found at 1135.6252 *m/z* which compares well with the calculated value.

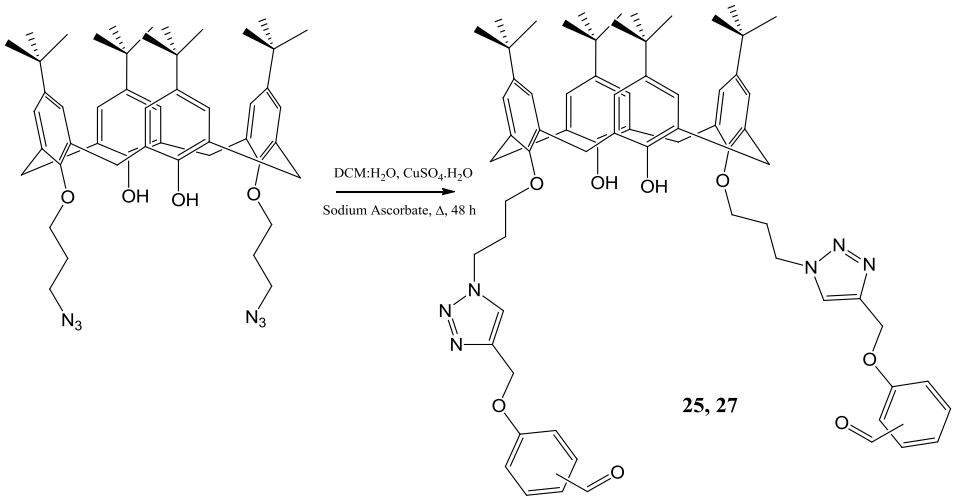

Scheme 3.24: Synthesis of **25** and **27** with conditions used shown.

The ^{1}H NMR spectrum of **25** is broadly similar to that of **27**, and once again the effect of symmetry is unmistakeable. The *tert*-Butyl groups resonating as two singlets at 0.96 and 1.29 ppm clearly illustrate this. In the aromatic region of the spectrum, the calixarene aromatic protons resonate as two singlets at 6.81 and 7.05 ppm. Once again, this is indicative of a highly symmetric structure. The phenolic proton signal is seen to resonate as a singlet at 7.42 ppm, which is the downfield position that has been previously discussed. Also supporting the symmetrical structure are the methylene bridges which are observed as two doublets that resonate at 3.29 and 4.13 ppm. The propyl pendant chain is represented by two triplets that resonate at 3.97 and 4.86 ppm, and a quintet which resonates at 2.57 ppm. The benzaldehyde aromatic proton signals are observed as a pair of doublets which resonate at 7.00 and 7.77 ppm. A singlet is observed with a chemical shift of 5.24 ppm which represents the ether CH_2 between the benzaldehyde and the triazole. The triazole proton signal is observed to resonate 7.95 ppm as a singlet, and the aldehyde proton signal is observed as a singlet which has a chemical shift of 9.85 ppm. The proposed 1,4-disubstituted triazole structure is corroborated by the ^{13}C NMR spectrum which has a signal peak that resonates at 121.4

ppm. Once again, mass spectroscopy was employed and the result of an M+Na of 1158.6119 *m/z* strengthens the case for the proposed structure.

3.4.7 Reaction between 30 and zinc(II) perchlorate

A metal complexation reaction was performed between **30** and zinc(II) perchlorate to establish the metal binding site within the structure. This was performed using the standard metal complexation system outlined previously in this thesis. The complex Zn(**30**)$(ClO_4)_2$ was obtained as a yellow solid and was analysed by ^{1}H NMR spectroscopy. It can be seen clearly when compared to the spectrum of **30** (Figure 3.73) that a significant degree of shifting has occurred for the triazole, aldehyde and ether CH_2 signals. A summary of the shifts up or downfield can be seen in Table 3.9. It is clear that the triazole proton experiences the highest degree of shifting, so with data and previously reported results,[67] the triazole unit was the most reasonable site of metal complexation.

Table 3.9: Upfield and downfield shifts observed for **30** and complexation with Zn.

Proton	δ_H **30** ppm	δ_H Zn(**30**)$(ClO_4)_2$ ppm	Shift +/- ppm
Ether CH_2	5.32	5.50	+ 0.18
Triazole-H	8.02	8.42	+ 0.42
Aldehyde-H	10.45	10.08	- 0.36

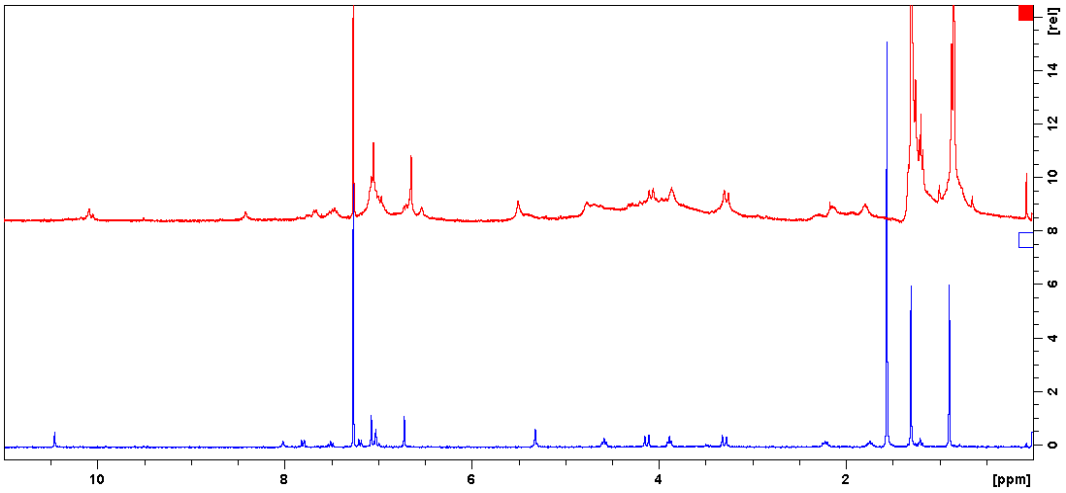

Figure 3.73: ^{1}H NMR spectra of **30** (blue) and Zn(**30**)$(ClO_4)_2$.

This is supported by the IR spectrum (Figure 3.74) which shows no significant shifting in the aldehyde absorption band, which would seem to indicate that binding has occurred at the triazole.

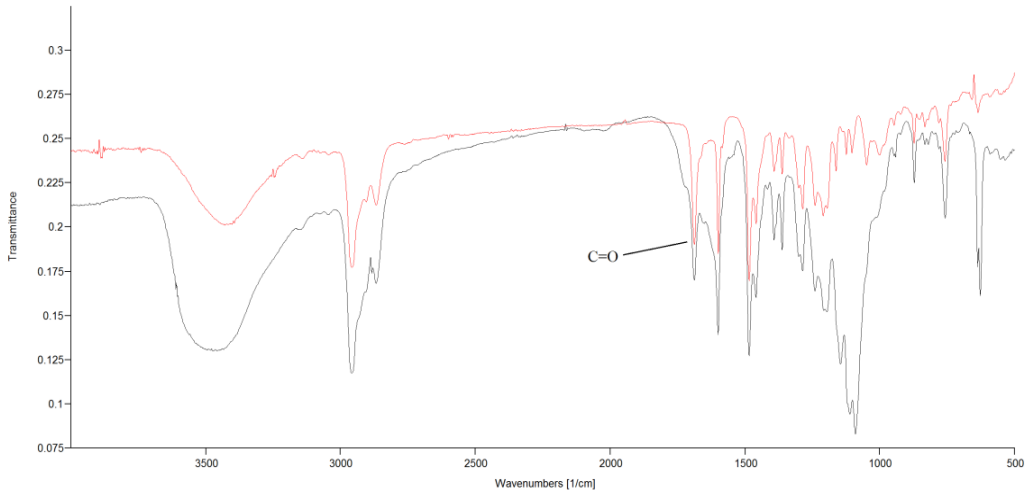

Figure 3.74: IR spectra of **30** (red) and Zn(**30**)$(ClO_4)_2$ (blue).

The potential metal binding sites are shown (Figure 3.75a) and are highlighted by encirclement. The data obtained from ^{1}H NMR and IR spectroscopy leads to the proposed mode of binding between the two triazole units (Figure 3.75b). This is observed as the downfield shift in the triazole proton. A shift of this nature has been observed previously in similar triazole modified calixarenes.[67]

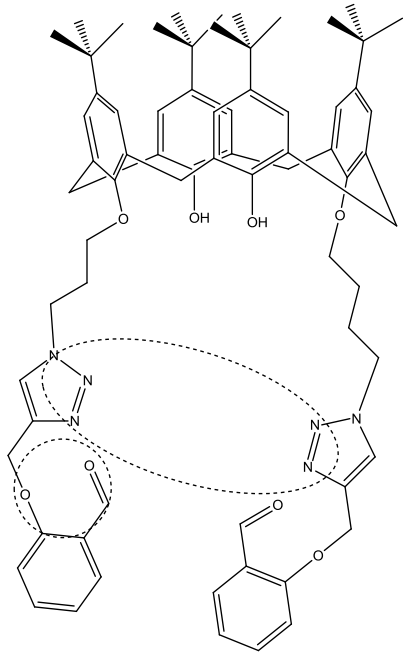

Figure 3.75a: Proposed structure for **30** with binding sites shown.

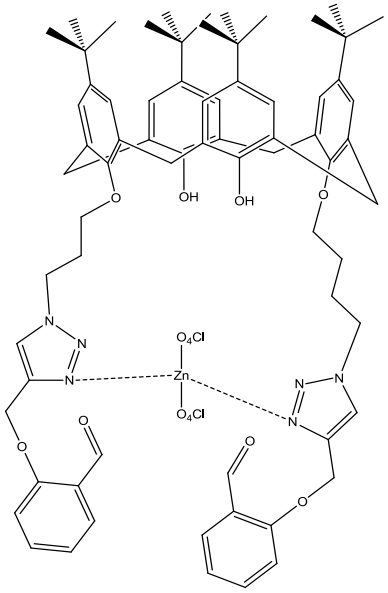

Figure 3.75b: Proposed structure of Zn(**30**)$(ClO_4)_2$.

3.4.8 Spectroscopic Studies

Having established that the benzaldehyde derivatives were suitable for metal complexation, their suitability for use as metal ion sensors was explored. Triazoles have been extensively employed as an ionophore in a range of calixarene based metal ion sensors, with the triazole moiety being used to link calixarene scaffolds to a range of reporter units, i.e. pyrene[67] and oxyquinoline.[115] Although the previously studied ligands from **Section 2.2** showed no fluorescent behaviour, it was expected that due to π-π stacking of the aromatic rings, the benzaldehyde calixarene derivatives would show some fluorescence emission spectra. As a result of this, the *ortho* benzaldehyde variants **29** and **30** (Figure 3.76), which were obtained in the highest yield and with the greatest purity were screened.

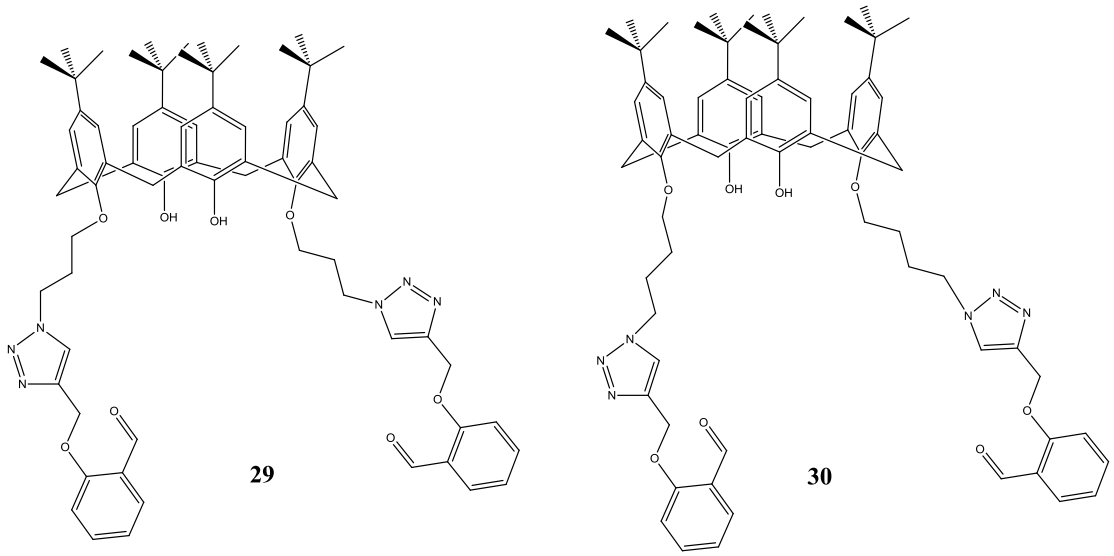

Figure 3.76: Structures of **29** and **30**.

Chloroform solutions of **29** and **30** were prepared at a concentration of 100 μM for UV-Vis spectroscopy. The spectra obtained are shown in Figure 3.77. The wavelength at which the absorption peaks occur is used as the λ_f^{ex} to obtain a fluorescence emission spectrum.

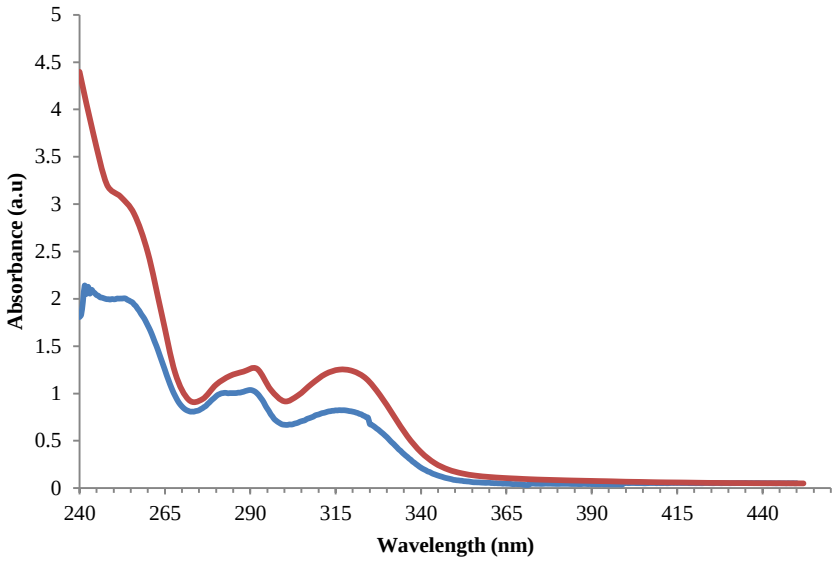

Figure 3.77: UV-Vis spectra of **29** (blue) and **30** (red).

The emission spectra were recorded for each excitation wavelength λ_f^{ex}, but it was found that not all of these exhibited fluorescence behaviour. The wavelengths which afforded a fluorescence emission spectrum were 292 nm for **29** and 290 nm for **30**. The emission spectra recorded are seen in Figure 3.78.

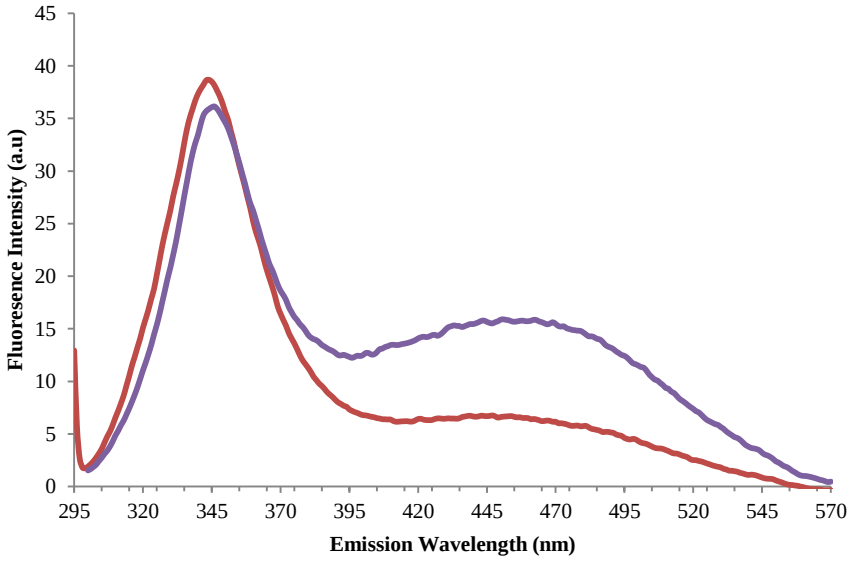

Figure 3.78: Fluorescence emission spectrum of **29** (red) λ_f^{ex} = 292 nm and **30** (purple) λ_f^{ex} = 290 nm (100 μM).

Although the ligands clearly exhibit some fluorescent behaviour, there are numerous factors which would limit their use as sensors: The concentration used of 100 μM is relatively high when compared to other calixarene based sensors[67] and the intensity of the peak emission λ_f^{em} is not of a sufficient strength to be used as an effective sensor. For these reasons, further spectral studies were not performed. A summary of the results of both the UV-Vis and fluorescence emission spectral data is presented in Table 3.10.

Table 3.10: UV-Vis and fluorescence emission data from **29** and **30**.

Sample	Absorption Peaks			λ_f^{ex}	λ_f^{em}
29	252	292	316	292	344
30	250	290	316	290	346

3.4.9 Reactions of 1,3-distal azidopropyl calixarene with dipropargyl Schiff base linker 30

It has been clearly established that standard click reaction conditions are suitable for the preparation of both the triazole linked double calixarenes and the triazole linked benzaldehyde calixarenes. As a result, the preparation of a Schiff base capped triazole calixarene was attempted, but using a modified synthetic route (Scheme 3.25). The need for a modified route was due to the presence of water in either the work up (DMF method) or as part of the solvent systems (DCM:H_2O), which would cause hydrolysis of the Schiff base moiety. As a result, methanol was chosen as the co-solvent due to the solubility of copper sulphate in this system. The copper sulphate salt was used in its pentahydrate form, and a consequence of this was the possibility for imine hydrolysis occurring. Therefore, to combat this a second reaction was attempted with the addition of a drying agent ($MgSO_4$) which has been reported previously in imine reactions.[131]

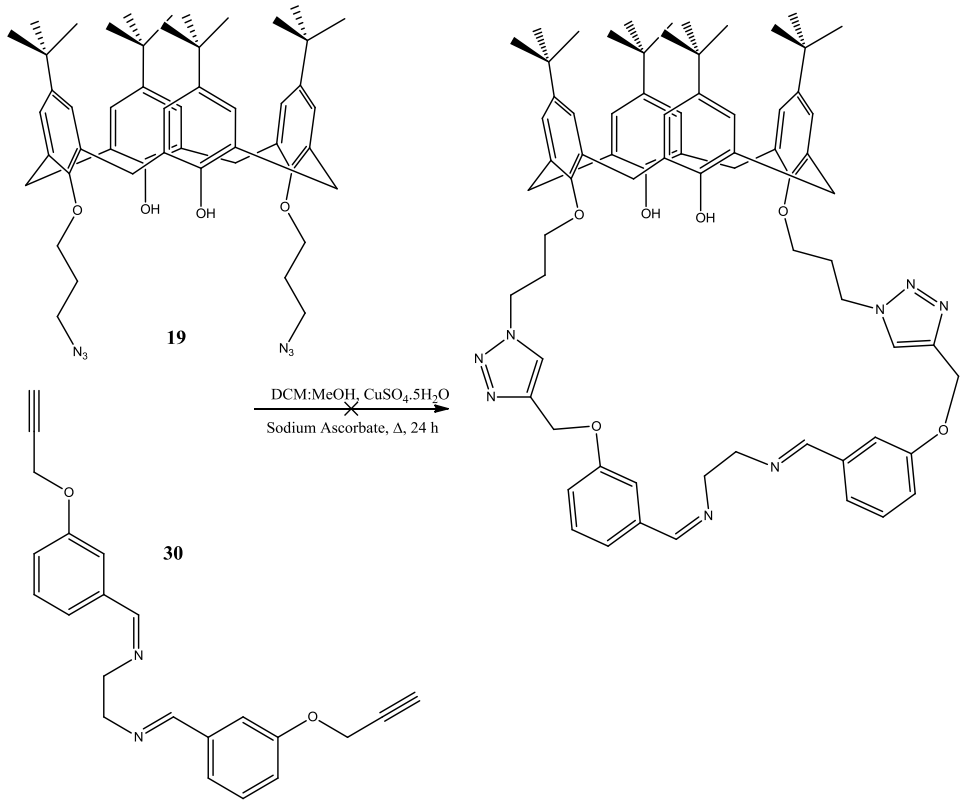

Scheme 3.25: Attempted synthesis of Schiff base capped triazole linker calixarene.

^{1}H NMR spectral analysis was conducted on the crude products from both reactions. It was suspected that some imine hydrolysis would occur due to the hydrated form of the metal salt being used as was previously seen in **section 3.3**. The ^{1}H NMR spectrum obtained for the crude product of reaction 2.4.16 (Figure 3.79) clearly displays the characteristic aldehyde proton signal, which is indicative of imine hydrolysis. This signal resonates as a singlet at 9.98 ppm labelled H_c. It appears that a triazole has been successfully formed, this is due to the observation of a singlet which resonates at 7.94 ppm labelled H_a. It also appears that the imine is still present in the spectrum. This could be due to some unused starting material which is indicated by a singlet that resonates at 8.26 ppm, labelled H_b. A triplet that resonates at 2.55 ppm points toward some unreacted alkyne being present.

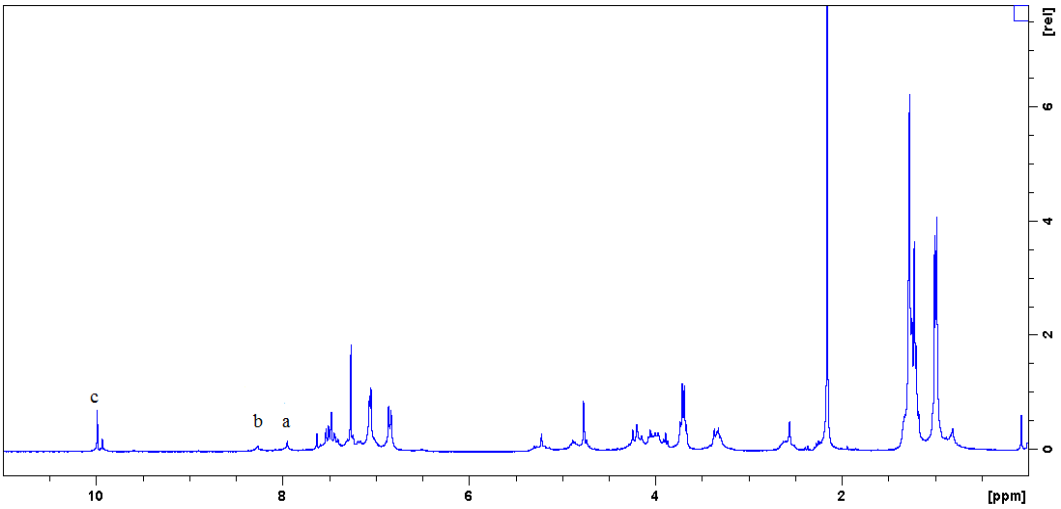

Figure 3.79: ^{1}H NMR of crude product from reaction 2.4.16 in absence of drying agent.

In light of evidence of imine hydrolysis occurring, it was decided to repeat this reaction in the presence of a drying agent. In this reaction, magnesium sulphate was added in the hope of removing water from the reaction system. Other than the addition of the drying agent, the reaction was performed using the same conditions. Once again, ^{1}H NMR spectroscopy was employed to determine if the product had been formed. Upon analysis of the ^{1}H NMR spectrum of the crude product (Figure 3.80), it is clear that imine hydrolysis has occurred once again. This is evident from a signal which resonates as a singlet at 9.93 ppm. As was observed with the product from the reaction without the drying agent, a peak which could represent the phenolic protons is observed at 8.01 ppm which resonates as a singlet. Another singlet is seen to resonate at 8.24 ppm which indicates that there is an imine in the product. As was the case with the product from reaction 2.4.16, it is thought that some unreacted dialkyne is present. This is supported by the presence of a triplet which resonates at 2.20 ppm. This chemical shift is indicative of an unreacted alkyne moiety.

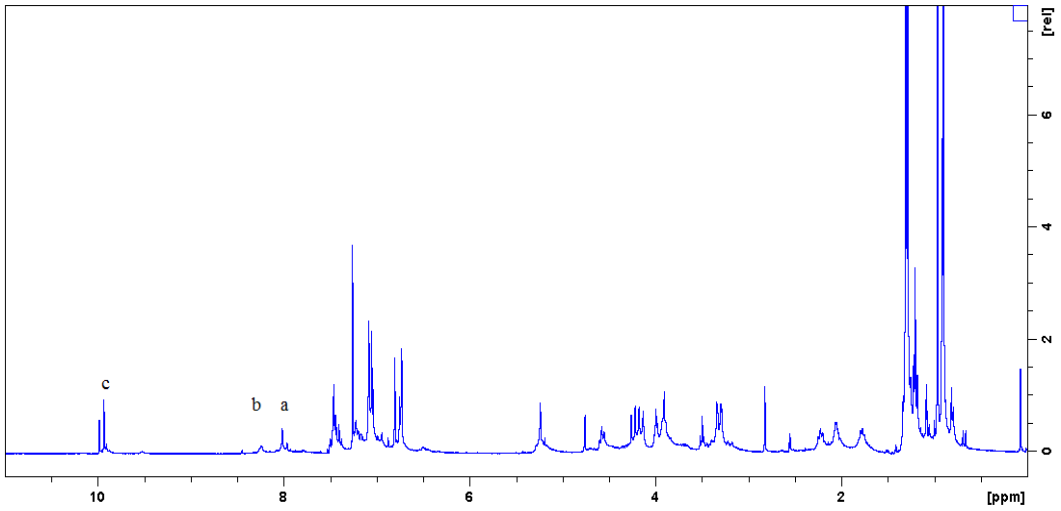

Figure 3.80: ^{1}H NMR spectrum of the crude product from reaction 2.4.17.

Due to the overwhelming evidence that the imine moiety undergoes hydrolysis in the presence of a hydrated metal, it is clear that any of the synthetic routes attempted in thesis are not suitable for the preparation of a Schiff base triazole linked calixarene. Furthermore, it is clear that due to the sensitivity of the imine bond even under mild conditions its usefulness as a metal ion binder is quite limited.

3.5 Isoxazole modified calix[4]arenes

3.5.1 Overview

In recent years there has been a huge increase in the number of publications which involve the copper promoted synthesis of triazoles, many of which are suitable for use as metal ion sensors.[67,115,124,125] In designing systems to detect copper ions, it is imperative that no trace of the catalyst contaminates the sensor and, since rigorous catalyst removal is often non trivial, alternative catalyst free approaches are desirable. As a result, copper free click reactions such as the Huisgen nitrile oxide-alkyne 1,3-dipolar cycloaddition reaction (NOAC) for the copper free formation of isoxazole linked conjugates has been of interest.[76,77,132] In comparison to the triazole based

sensors, isoxazole linked calix[4]arene sensors are less studied.[99,133] In collaboration with the Heaney group in NUI Maynooth, two calix[4]arene isoxazole derivatives, **PIC** and **AIC**, were synthesised and their ability to act as a metal ion sensors was assessed. The proposed structures are shown in (Figure 3.81).

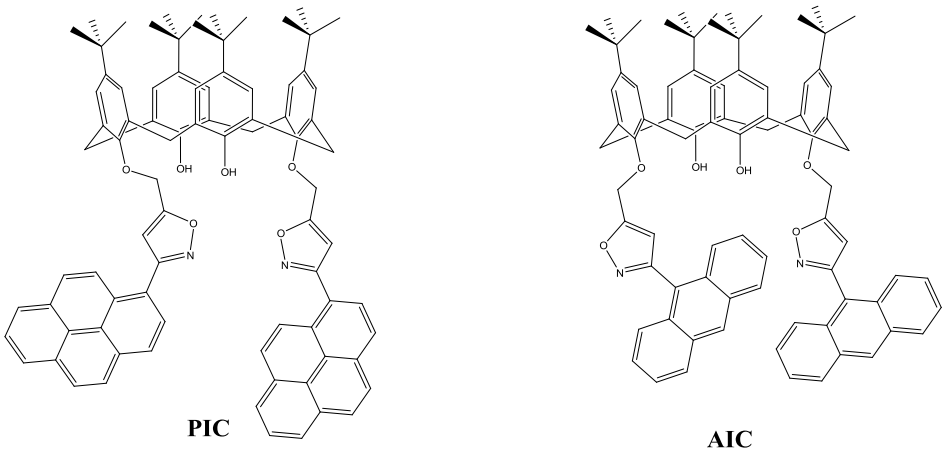

Figure 3.81: Structure of pyrene isoxazole calixarene (**PIC**) and anthracene isoxazole calixarene (**AIC**).

The fluorescence emission spectra of **PIC** and **PIM** have been previously discussed, and it was found that copper(II) was bound selectively. Therefore, with the anthracene analogue **AIC** the same trend was expected. The emission spectrum of **AIC** was recorded at 6 μM in MeCN. Metal titrations were performed to determine the effect, if any, different metal cations had on the recorded emission spectra at a range of concentrations. It was found that only Cu^{2+} had a significant effect upon the emission spectrum. To determine the effect which the anion had on the fluorescence emission profile different, Cu(II) salts were examined. To compare and contrast whether the calix[4]arene macrocycle had any enhancing or quenching effect on the emission characteristics, the model *tert*-butyl-phenoxy based sensors **AIM** and **PIM** were prepared. The structures of **PIM** and **AIM** are shown in Figure 3.82.

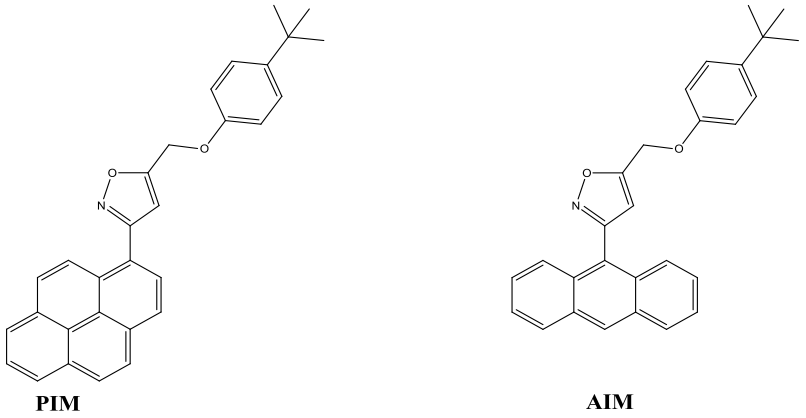

Figure 3.82: Proposed structures of pyrene isoxazole monomer (**PIM**) and anthracene isoxazole monomer (**AIM**).

3.5.2 Fluorescence studies on AIC *(anthracene isoxazole calixarene)* and AIM *(anthracene isoxazole monomer)*

3.5.2.1 UV/Vis spectral analysis of AIC and AIM

To determine the absorption wavelength of **AIC** and **AIM**, 6 μM samples were prepared for UV-Vis analysis in HPLC grade MeCN. The spectra were recorded using a standard procedure, i.e. a *background* spectrum was recorded (spectrum of MeCN), which was set as the baseline. The spectra recorded are shown in Figures 3.90a and 3.90b.

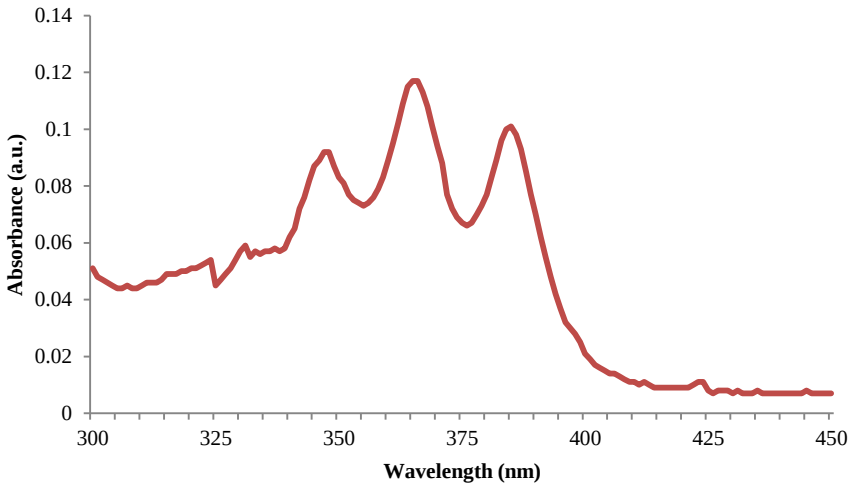

Figure 3.83a: UV-Vis absorbance spectrum of AIC (6 μM) in CH_3CN.

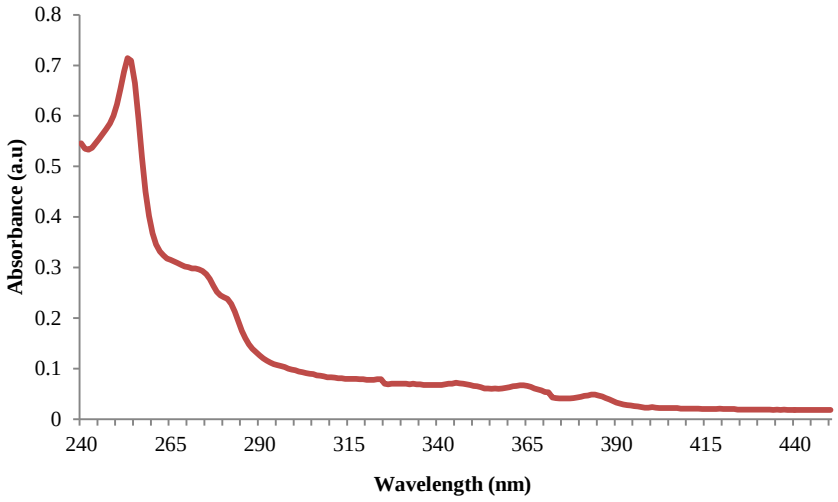

Figure 3.83b: UV-Vis absorbance spectrum of AIM (120 μM) in CH_3CN.

Analysis of the spectra revealed that **AIC** has three absorbance peaks at 348, 364 and 384 nm, and **AIM** has three absorbance peaks at 252, 364 and 384 nm. The information gleaned from these spectra was exploited in determination of the optimal wavelength for excitation (λ_f^{ex}) in subsequent fluorescence spectroscopy studies. Similar analysis was previously completed on the pyrene analogue. A summary of data extracted from the UV-Vis spectra is contained in Table 3.11.

Table 3.11: absorbance peaks and excitation wavelengths for 6.0 μM solutions **AIC**, **AIM**, **PIC**, **PIM** in MeCN.

Species	UV absorption (nm)			λ_f^{ex} (nm)
AIC	348	364	384	364
AIM	252	364	384	364
PIC	242	275	343	343
PIM	274		346	274

3.5.2.2 Fluorescence Spectroscopy of AIC and AIM

The fluorescence emission spectra were recorded in HPLC grade MeCN with excitation at a wavelength determined from UV-Vis spectral analysis Table 3.11. It was found that the MeCN solution of **AIC** (6 μM) exhibited fluorescence at 422 nm

and a slightly more intense fluorescence peak at 439 nm. A 6 μM MeCN solution of **AIM** yielded a structure-less emission spectrum with the peak emission occurring at 423 nm (Figure 3.84a). The more structured emission spectrum obtained for **AIC** is interpreted to suggest dynamic, intramolecular, face-to-face π-stacking of the anthracene units in solution. A stark difference is found between **PIC** and **PIM**, with the calixarene based sensor showing clear monomer and excimer emissions bands, while the monomer unit exhibits only the monomer emission (Figure 3.84b). This effect has been previously discussed by Kim *et al.*[134] An anthracene modified calixarene, which differs from **AIM** by the inclusion of a chlorine atom attached to the anthracene fluorophore, has been prepared by Chang *et al.* in 2008, reporting comparable emission spectra.[99] What is notable is that the peak emission (λ_f^{em}) for the emission spectrum of **AIM**, which is only the monomer emission, occurs at λ_f^{em} = 423 nm. This corresponds to the first emission peak observed in the emission spectra of **AIC**, so the second peak which is observed at λ_f^{em} = 439 nm is due to excimer emission.

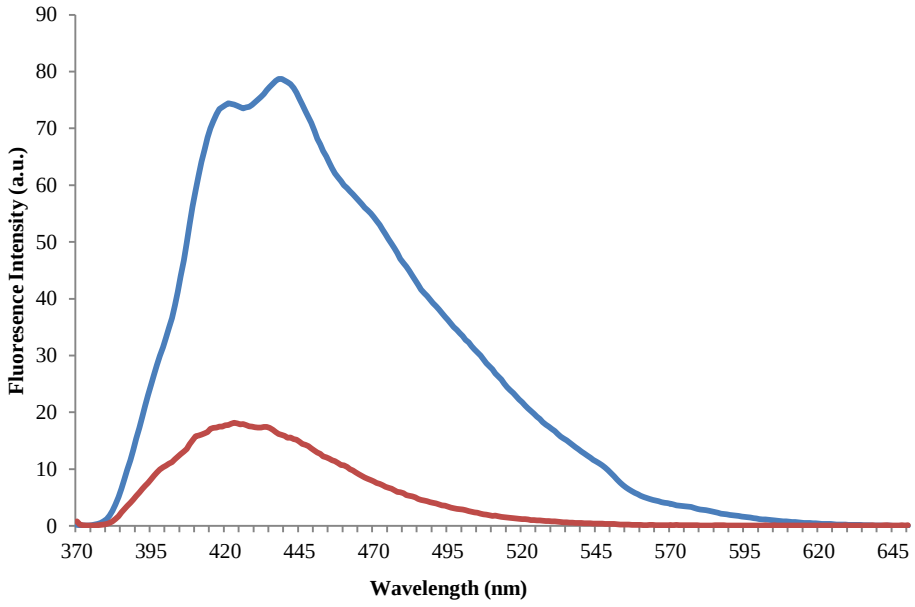

Figure 3.84a: Fluorescence emission spectra of **AIC** (blue) λ_f^{ex} = 364 nm and **AIM** (red) λ_f^{ex} = 364 nm (6 μM) in MeCN.

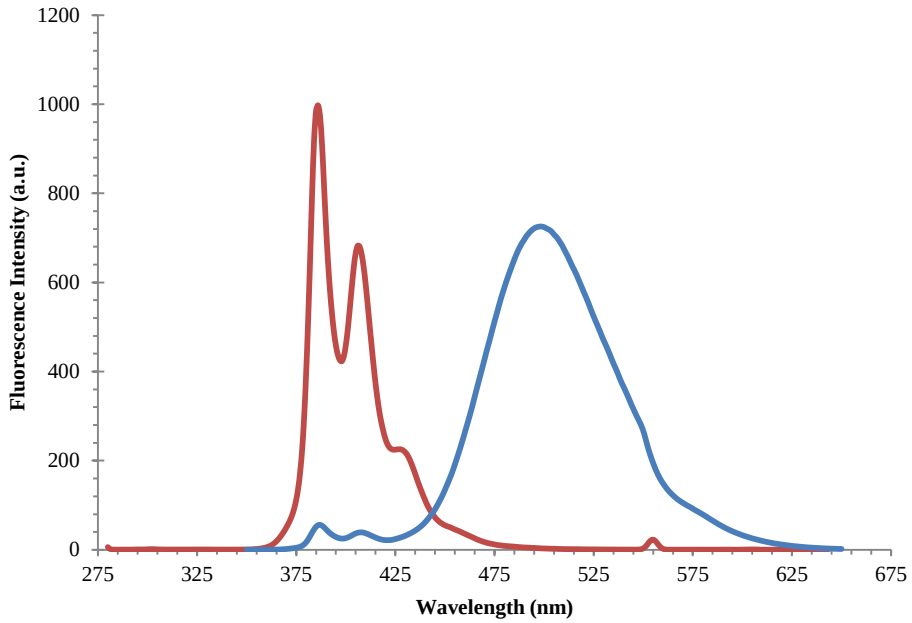

Figure 3.84b: Fluorescent emission spectrum for **PIC** (blue) λ_f^{ex} = 343 nm and **PIM** (red) λ_f^{ex} = 274 nm (6 μM) in MeCN.

3.5.2.3 Metal Perchlorate Titration Studies

The influence that a variety of metal perchlorate salts (Hg^{2+}, Ni^{2+}, Zn^{2+}, Co^{2+}, Fe^{2+}, Pb^{2+}, Cd^{2+} and Cu^{2+} derivatives) have on the fluorescent emission behaviour of a MeCN solution of **AIC** (6 μM) λ_f^{ex} = 364 nm was examined. The concentration of the metal perchlorate salts was varied from 6 μM to 600 μM. The results of this study are shown in Figure 3.85a-h. It can be seen clearly that only Cu^{2+} caused a dramatic spectral response.

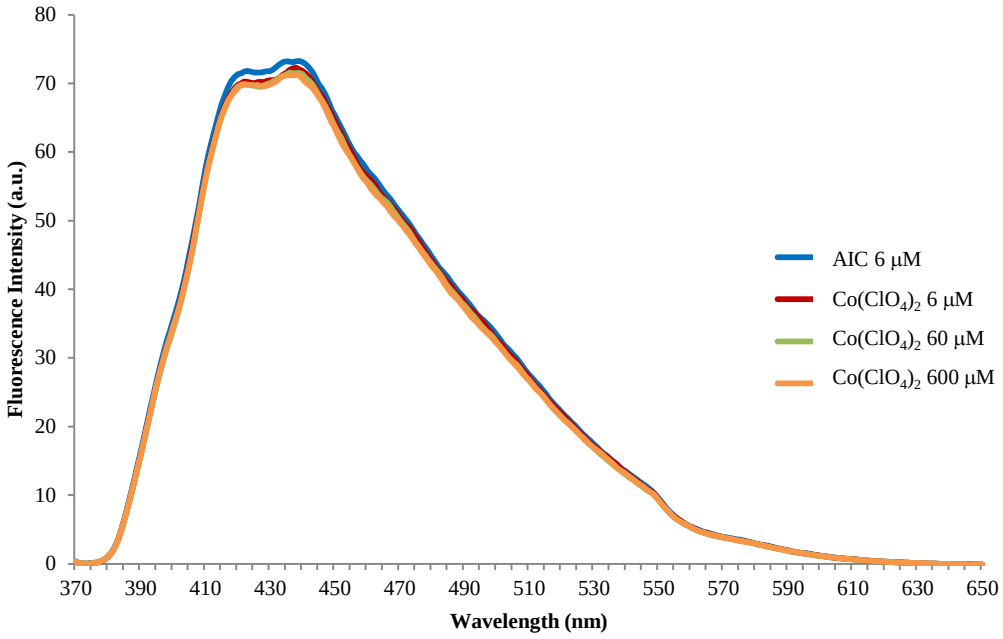

Figure 3.85a: Emission spectra of **AIC** 6 μM (MeCN) and in the presence of increase concentrations of cobalt(II) perchlorate, λ_f^{ex} = 364 nm.

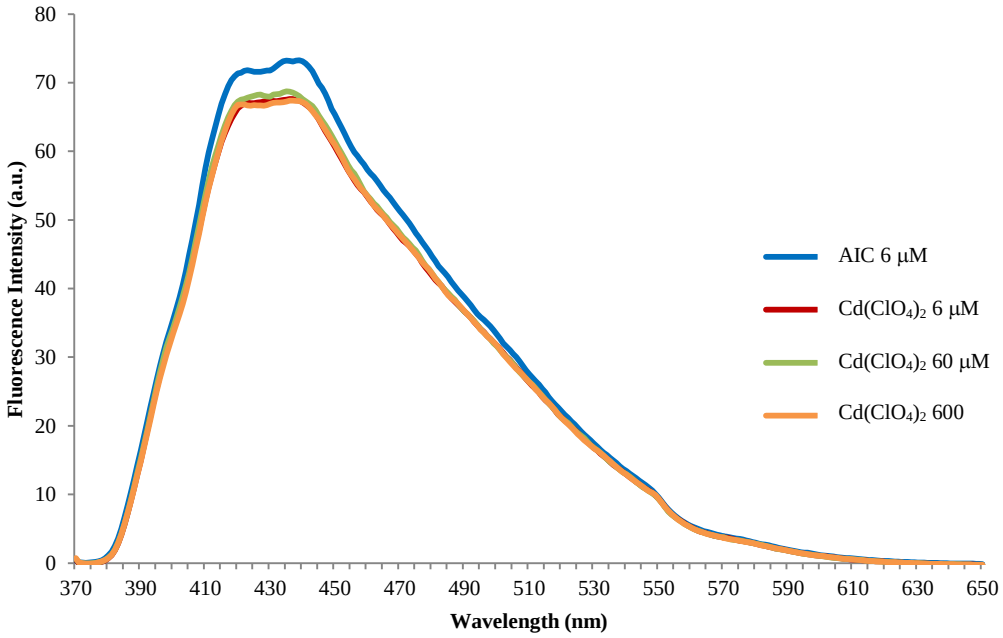

Figure 3.85b: Emission spectra of **AIC** 6 μM (MeCN) and in the presence of increase concentrations of cadmium(II) perchlorate, λ_f^{ex} = 364 nm.

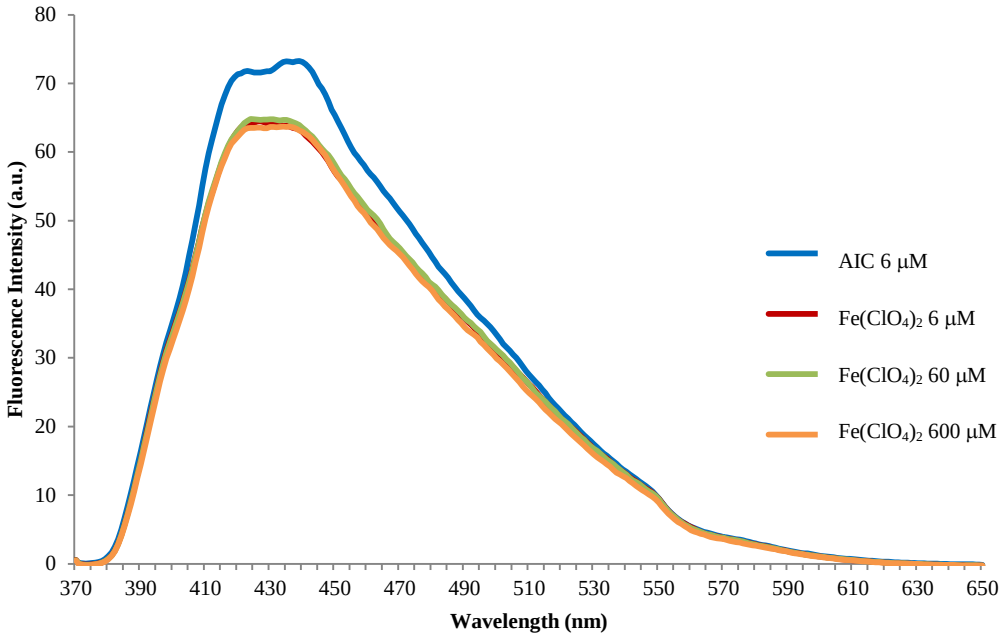

Figure 3.85c: Emission spectra of **AIC** 6 μM (MeCN) and in the presence of increasing concentrations of iron(II) perchlorate, λ_f^{ex} = 364 nm.

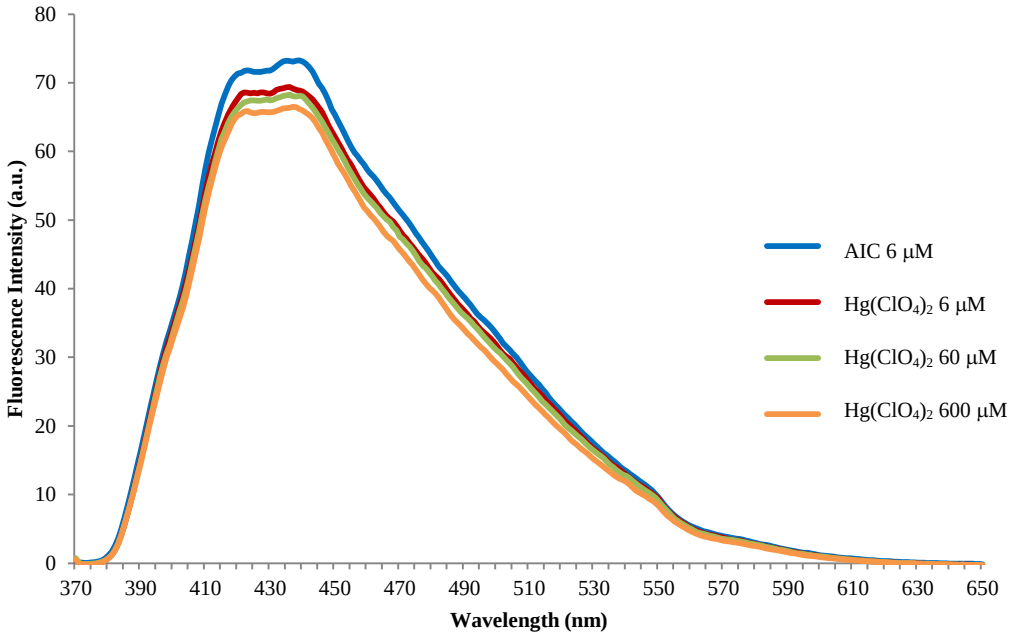

Figure 3.85d: Emission spectra of **AIC** 6 μM (MeCN) and in the presence of increasing concentrations of mercury(II) perchlorate, λ_f^{ex} = 364nm.

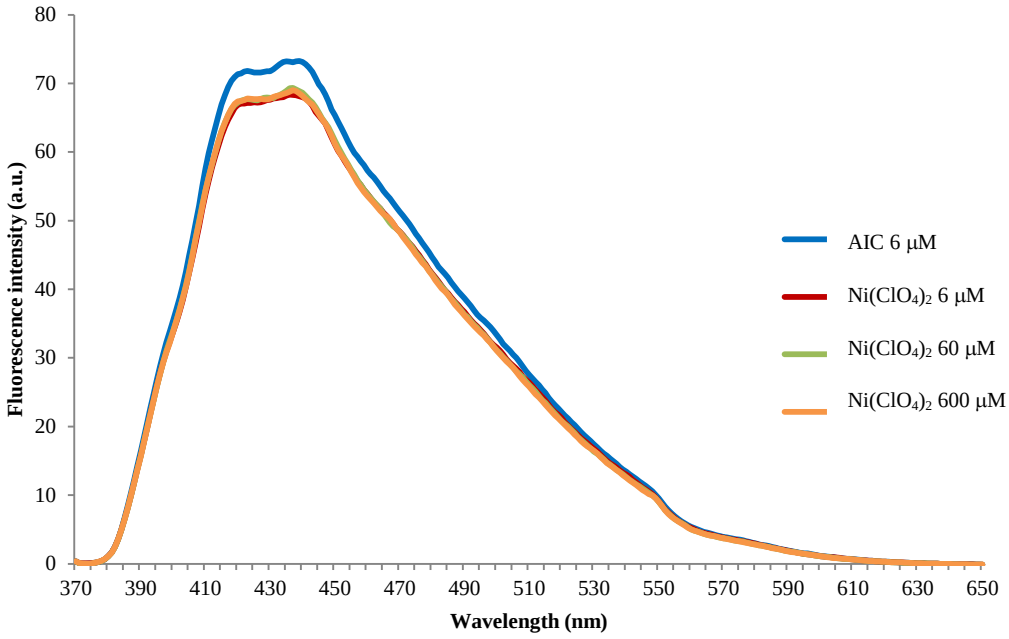

Figure 3.85e: Emission spectra of **AIC** 6 µM (MeCN) and in the presence of increasing concentrations of nickel(II) perchlorate, λ_f^{ex} = 364 nm.

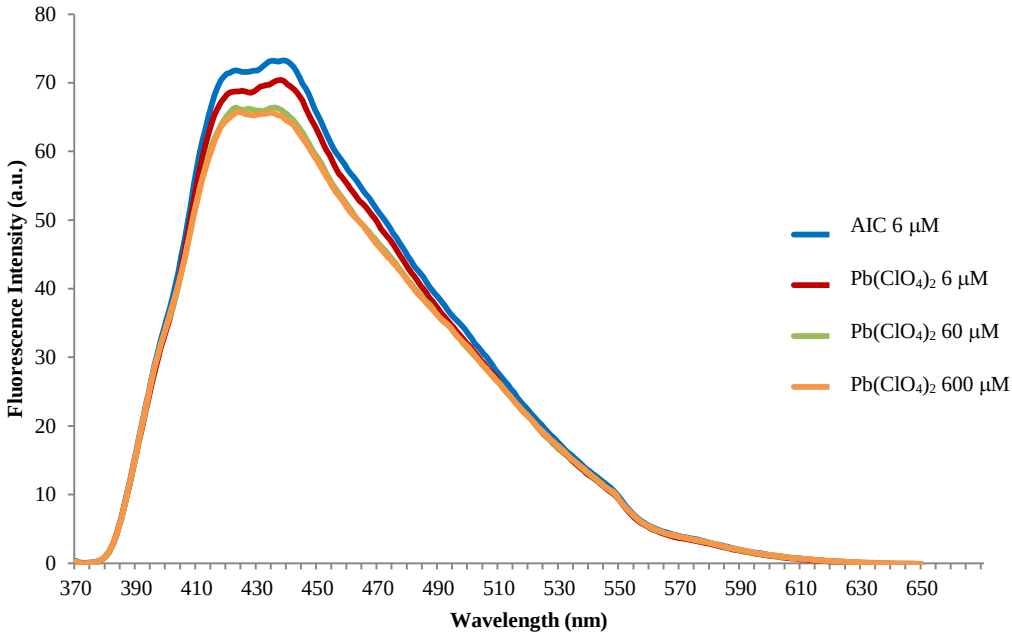

Figure 3.85f: Emission spectra of **AIC** 6 mM (MeCN) and in the presence of increasing concentrations of lead(II) perchlorate, λ_f^{ex} = 364 nm.

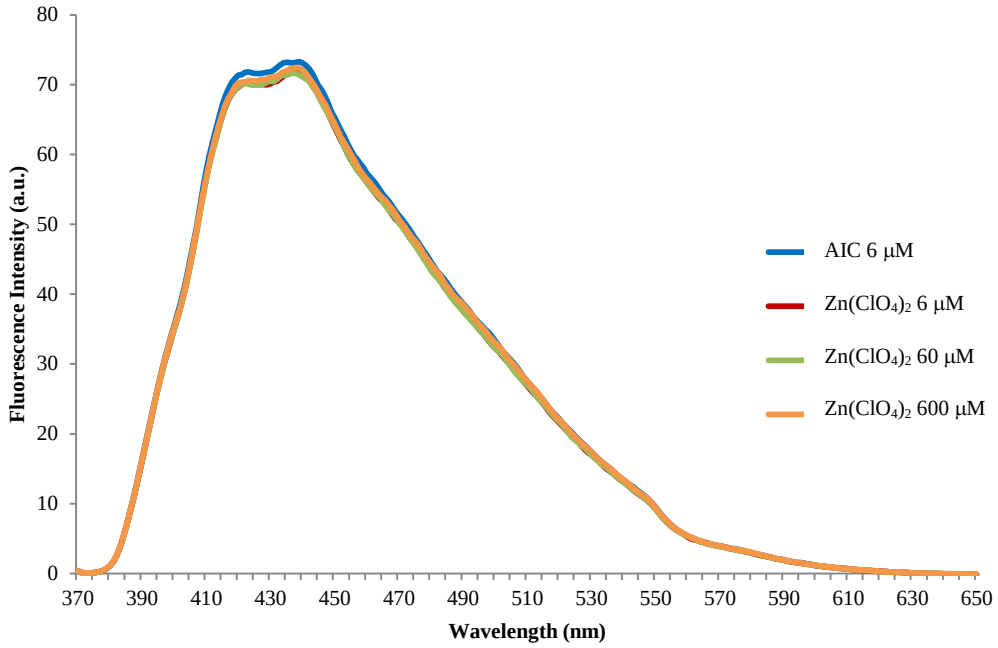

Figure 3.85g: Emission spectra of **AIC** 6 μM (MeCN) and in the presence of increasing concentrations of zinc(II) perchlorate, λ_f^{ex} = 364 nm.

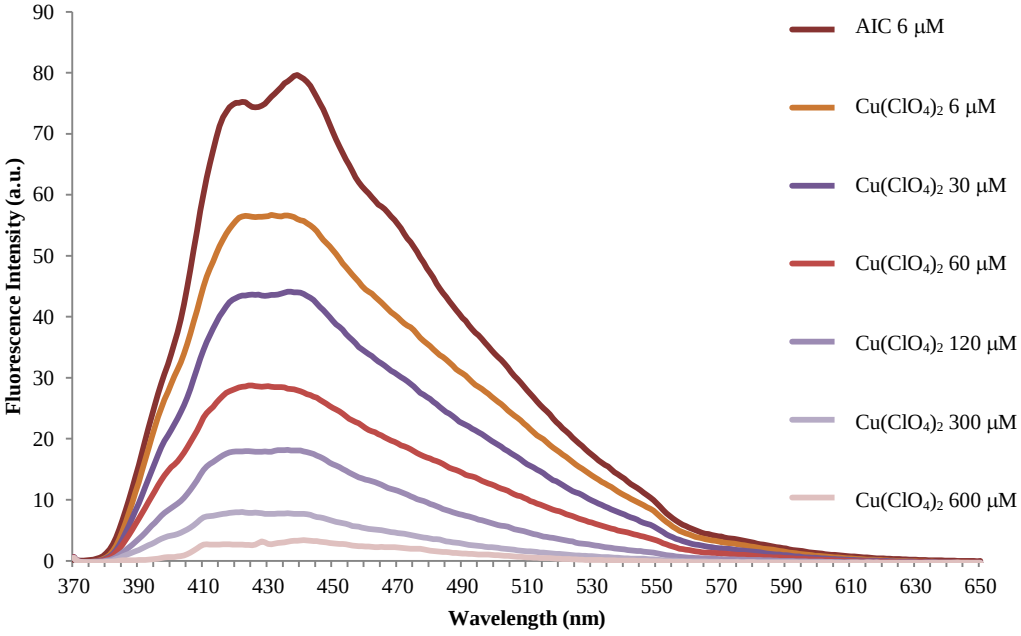

Figure 3.85h: Emission spectra of **AIC** 6 μM (MeCN) and in the presence of increasing concentrations of copper(II) perchlorate, λ_f^{ex} = 364 nm.

The quenching effect that the Cu^{2+} ion has on the spectrum is quite remarkable. Even in the presence of one molar equivalent of copper(II) perchlorate, the quenching effect is immediately noticeable. The peak emission is quenched by 30 % in comparison to that of the free **AIC**. This stark difference in quenching upon addition of different metals is clear from the emission spectra in Figure 3.86a. A graphical representation of the change in the peak fluorescent emission λ_f^{em} is shown in Figure 3.86b.

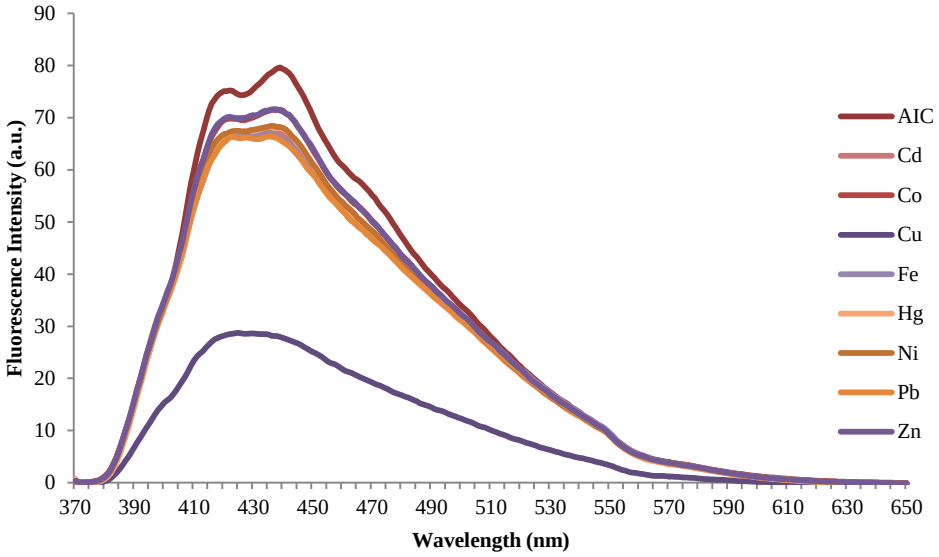

Figure 3.86a: Emission spectra of **AIC** 6 μM (MeCN) and in the presence of 120 μM of M^{2+}, λ_f^{ex} = 364 nm.

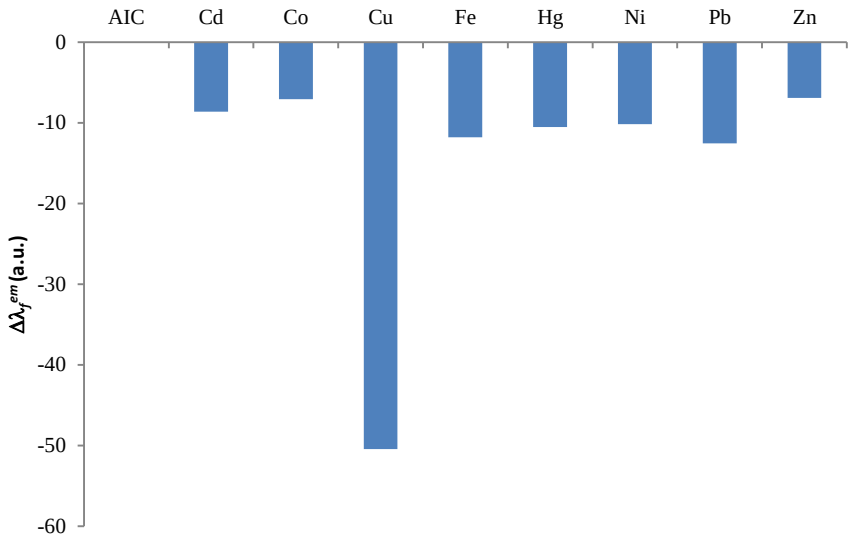

Figure 3.86b: Peak Fluorescent Emission Change for **AIC** with 120 μM of M^{2+} λ_f^{em} = 439 nm.

3.5.2.4 Anionic Effects

Having established that Cu^{2+} was the only metal ion to have any significant effect upon the emission spectrum, the influence of the nature of the anion was probed. To this end the emission spectrum of **AIC**, in the presence of a range of Cu(II) metal salts including (chloride, acetate, and nitrate) and also in the presence of Cu(I)Cl, was recorded. It is clear from the fluorescence emission spectra (Figures 3.94a-c) that the sensitivity of **AIC** towards Cu^{2+} is strongly influenced by the nature of the counterion. Quenching of the emission of **AIC** by chloride, nitrate and acetate salts was significantly lower, with the quenching effect at 600 μM being ~ 50 %, 40 % and 3% of that observed for copper(II) perchlorate, respectively. This is ascribed to the relative dissociation of these compounds in MeCN.

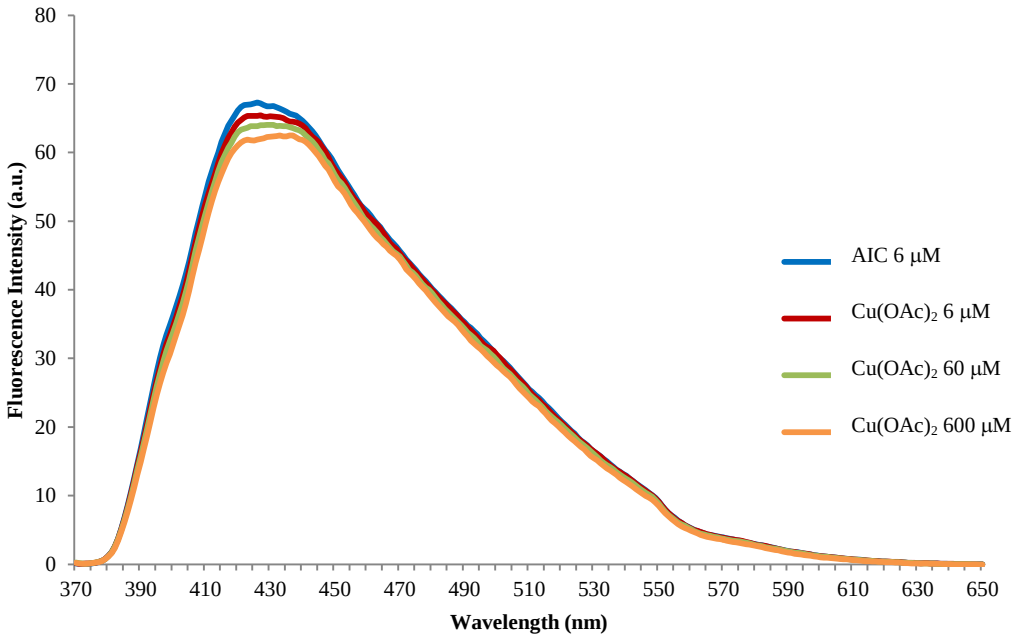

Figure 3.87a: Fluorescence emission spectra of **AIC** 6 μM (MeCN) and in the presence of increasing concentrations of $Cu(OAc)_2$, λ_f^{ex} = 364 nm.

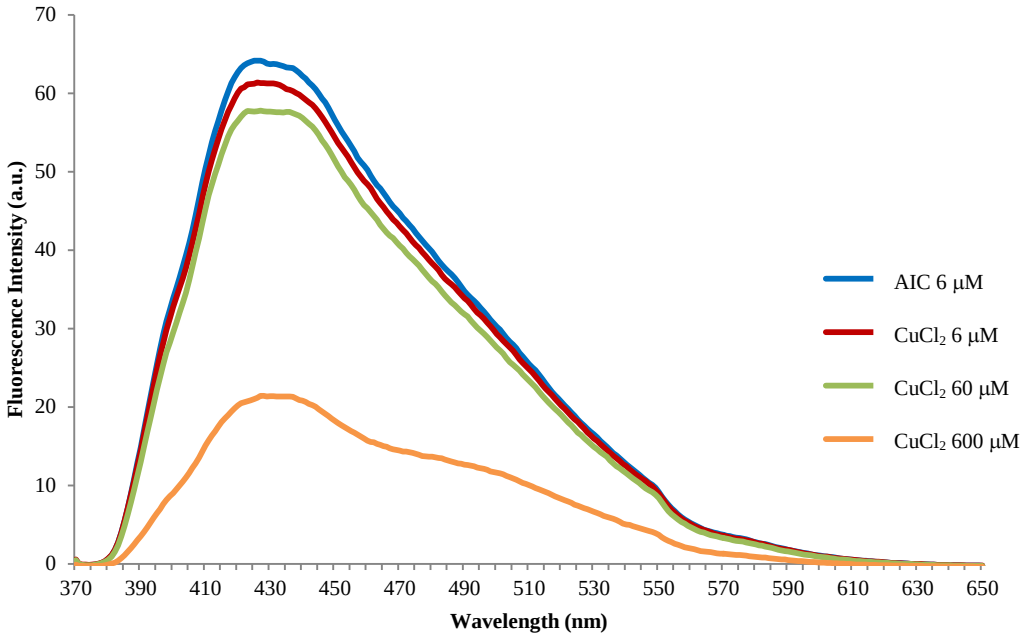

Figure 3.87b: Fluorescence emission spectra of **AIC** 6 μM (MeCN) and in the presence of increasing concentrations of $CuCl_2$, λ_f^{ex} = 364 nm.

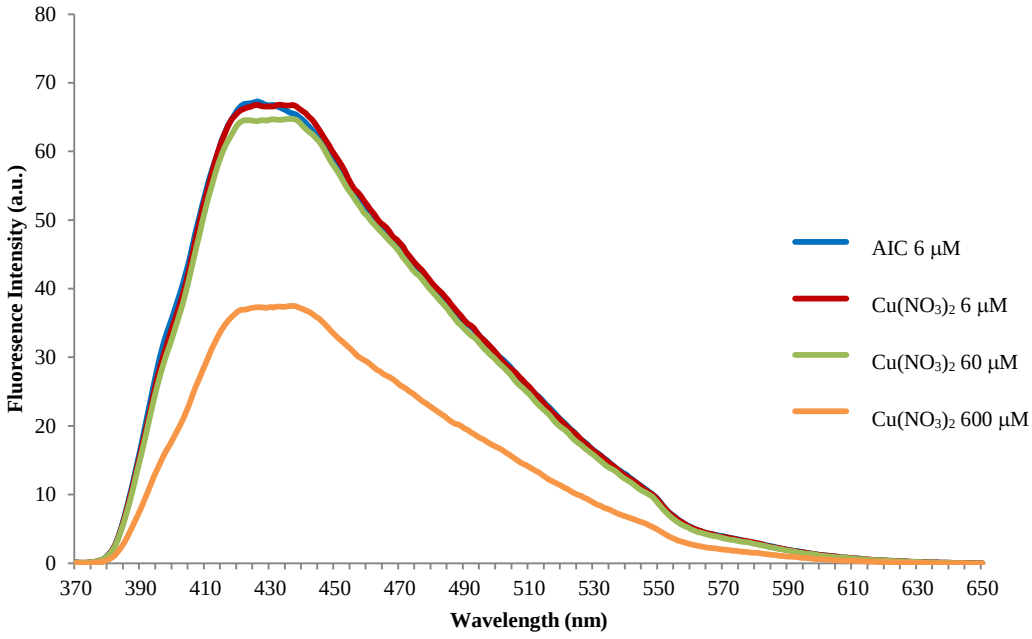

Figure 3.87c: Fluorescence emission spectra of **AIC** 6 μM (MeCN) and in the presence of increasing concentrations of $Cu(NO_3)_2$, λ_f^{ex} = 364 nm.

The emission spectrum of **AIC** in the presence of copper(I) chloride was also recorded (Figure 3.88). It is strikingly clear that the Cu^{+} ion has no quenching effect upon the emission spectrum. This is due to the different coordination geometries that Cu(I) and Cu(II) possess. Molecular modelling studies were performed on **PIC**, and it was found that the copper(II) ion is in a distorted square pyramid with one of the two isoxazoles acting as apical ligand. Cu^{2+} is known to adopt this coordination while Cu^{+} is not.[135] It is assumed that **AIC** adopts this same coordination geometry, but it cannot be stated unambiguously in the absence of crystallographic data.

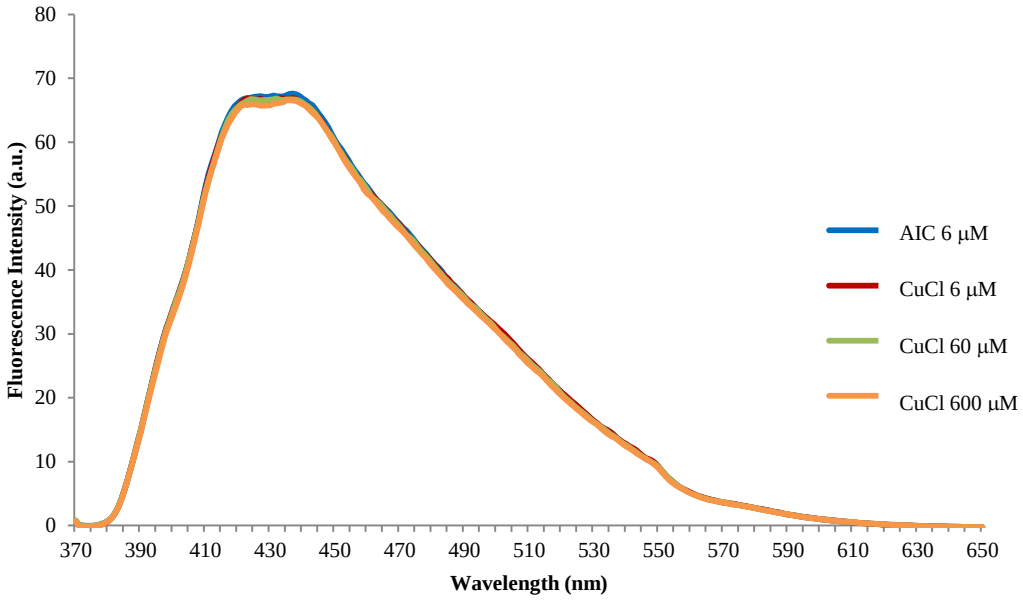

Figure 3.88: Fluorescence emission spectra of AIC 6 μM (MeCN) and in the presence of increasing concentrations of CuCl, λ_f^{ex} = 364 nm.

3.5.2.5 Quenching due to copper(II) perchlorate

It is clear from the data gathered that **AIC** is preferentially quenched by the copper(II) perchlorate salt, this was also seen for the pyrene analogue. To probe the sensing potential, the extent of fluorescence quenching of a solution of **PIC** (6 μM) as a function of Cu^{2+} concentration over the range (6 - 120 μm) was examined. Despite the

vast reduction in signal intensity, the spectral features are largely unchanged with proportionate quenching of both monomer and excimer bands upon the addition of increasing number of equivalents of Cu^{2+} ions (Figure 3.89). Although in comparison to **PIC**, which shows a reduction in peak fluorescence of ≈ 82 %, **AIC** has a somewhat reduced sensitivity with a reduction of ≈ 65 % observed.

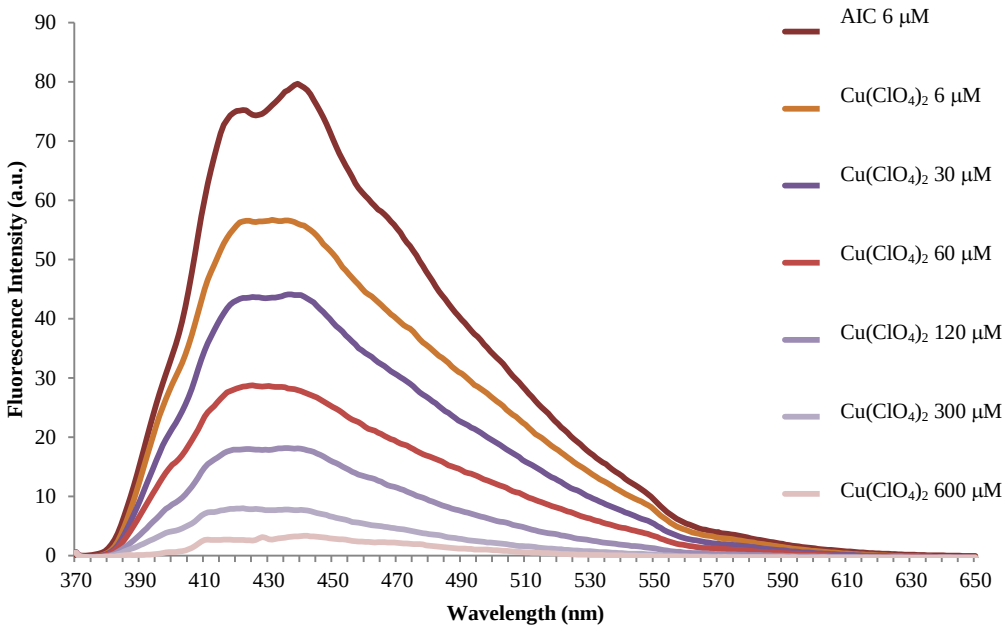

Figure 3.89: Fluorescence emission spectra of **AIC** 6 μM (MeCN) in the presence of 6, 30, 60, 120, 300 and 600 μM of $Cu(ClO_4)_2$, λ_f^{ex} = 364 nm.

PIC showed almost complete quenching at a concentration of 20 μM, however **AIC** requires a concentration of 300 μM of Cu^{2+} added to achieve this (Figure 3.89). Although the sensitivity of **AIC** for Cu^{2+} is reduced in comparison to **PIC**, it is found to be broadly similar to that of its 9-chloroanalogue reported by Chang.[99] What is significant however, is that even at a lower concentration of host (6 μM for **AIC**) the peak emission observed surpasses that of the 9-chloroanthracene analogue by a factor greater than 10. It is found that under the same conditions, weaker quenching is observed for the related isoxazolo-naphthyl calixarenes with unmodified upper rims.[88]

Evidently, binding of the Cu^{2+} ions to the calixarene host (**AIC**) has a significant effect on the spatial configuration of the arylisoxazole reporting units, thus diminishing the opportunity for the intramolecular communication leading to the excimer emission characteristic of **AIC**. Further isoxazole-copper chelation may enhance anthracene – Cu^{2+} π-cation interactions. A combination of the heavy metal ion effect and reverse PET from the anthracene groups to the isoxazole nuclei, which may have become electron deficient following metal complexation, may account for the reduction in monomer emission. It was found that in contrast to the calixarene based sensors, the fluorescence spectra of the model compound **AIM**, which has a single arylisoxazole unit, remained largely unchanged upon the addition of any of the nine metal perchlorates (Figure 3.90a). This suggests that there is a requirement for a hosting compound to have a well-defined positioning of the two fluoroionophore units for sensing of copper ions. The effect of an absence of conformational rigidity is seen clearly in Figure 3.90b, whereupon the addition of 50 molar equivalents of Cu^{2+} ions, only a slight reduction in the fluorescence intensity of a solution of **AIM** in MeCN (6 μM), is observed.

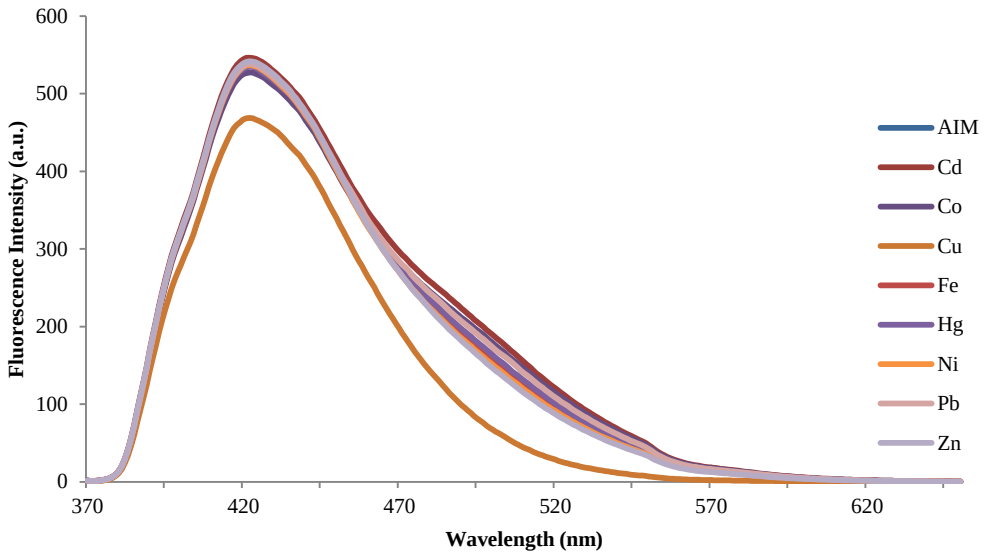

Figure 3.90a: Emission spectra of **AIC** 6 μM (MeCN) and in the presence of 120 μM of M^{2+}, λ_f^{ex} = 364 nm.

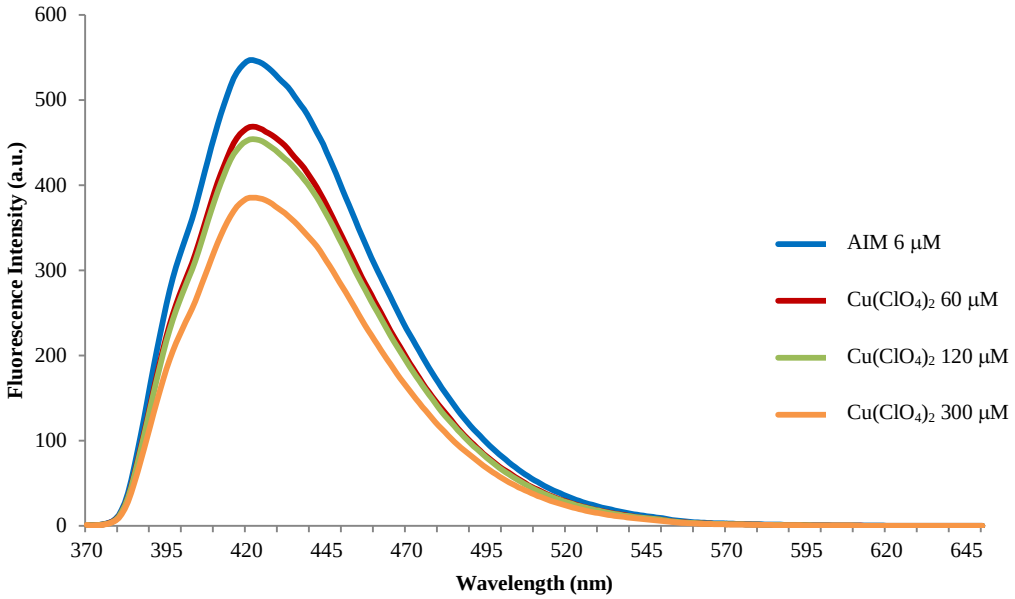

Figure 3.90b: Fluorescence emission spectra of **AIM** 6μM (MeCN) and $Cu(ClO_4)_2$ 60, 120, 300 μM, λ_f^{ex} = 364 nm.

Analysis of the emission profile of the *tert*-butyl phenol based sensor **AIM** reveals a much narrower emission spectrum when compared to that of calixarene based **AIC**. It is likely that only monomer emission is observed for **AIM**, and that the emission spectrum recorded for **AIC** is a combination of the both monomer and excimer. This phenomenon has been previously described for the pyrene analogues **PIM** and **PIC**. This lack of excimer emission points to the absence of π-π stacking of the extended aromatic systems (anthracene/pyrene moieties) of either the **PIM** or **AIM** sensors.

To determine the minimum concentration of Cu^{2+} that **PIC** and **AIC** can detect, (minimum detection limit) a plot of fluorescence intensity (y-axis) against the host concentration (x-axis) was constructed, using a method that has been previously employed by numerous groups.[136-138] The fluorescent emission spectra of the host ligand was recorded over a range of concentrations (0.5–7 μM). A set of corresponding data was obtained upon the addition of the copper(II) perchlorate guest, with the ratio of host to guest kept at 1:1 (Figures 3.98a & 3.98b).

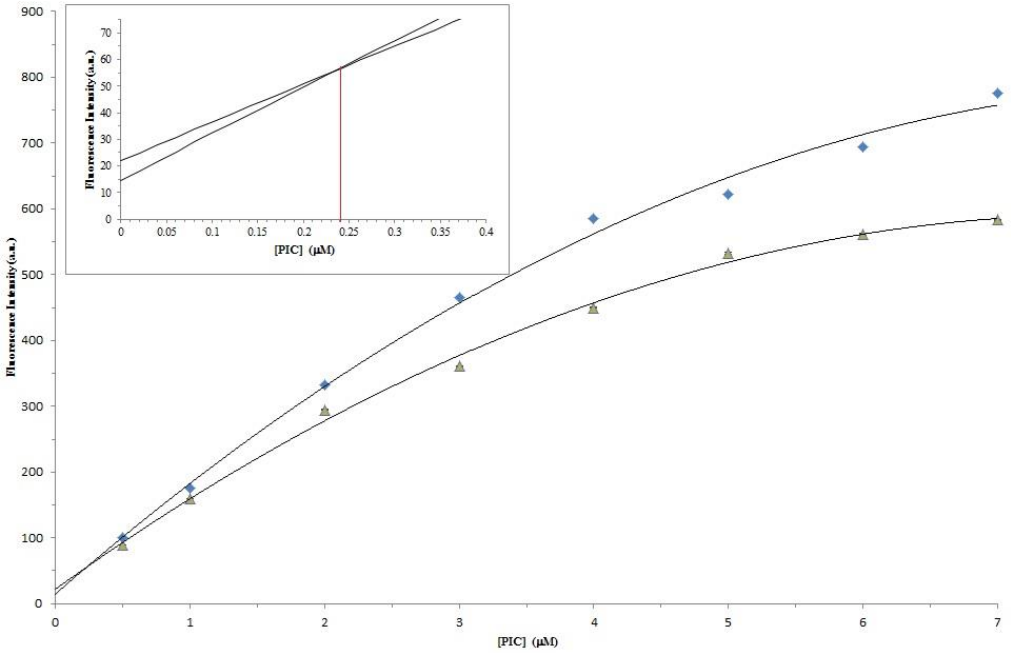

Figure 3.91a: Minimum detection limit plot for **PIC**: **PIC** ♦, **PIC** + Cu^{2+} ▲. Insert: Expansion of the intersection of the trend lines, (MeCN) λ_f^{ex} = 343 nm.

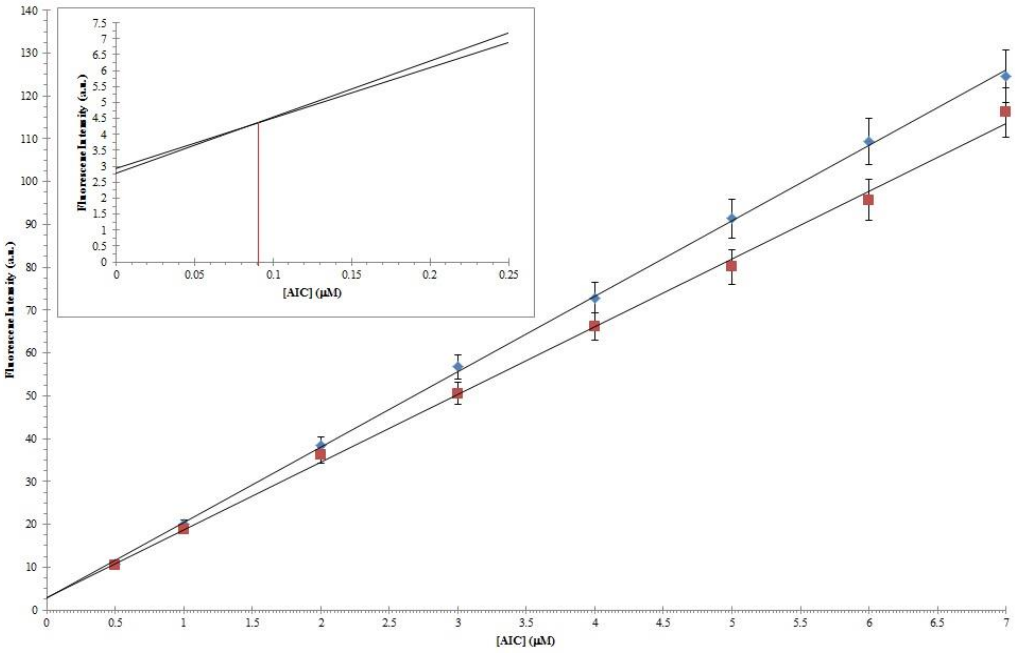

Figure 3.91b: Minimum detection limit plot for **AIC**: **AIC** ♦, **AIC** + Cu^{2+} ■. Insert: expansion of the intersection of the two trend lines, (MeCN) λ_f^{ex} = 343 nm.

The minimum detection limit is found to be the point at which the regression lines intersect. A line is then dropped to the x axis to obtain the concentration of Cu^{2+} which can be detected. The limits at which **PIC** and **AIC** can detect Cu^{2+} in MeCN solution

are determined from these plots to be 2.3 x 10^{-7} and 0.9 x 10^{-7} M, respectively. It is clear that this low limit of detection is in line with the limits previously reported by Wanichacheva *et al.* of 2.49 x 10^{-7} M.[137] As a result of these excellent minimum limits of detection, it is clear the both **PIC** and **AIC** are effective sensors for Cu^{2+} recognition.

In order to determine the stoichiometry of the binding between **AIC** and Cu^{2+}, a Job's plot was constructed using the method of continuous variation (Figure 3.92). In this method, the change in the peak fluorescence (ΔF^{em}*[X]) is plotted against the mole fraction [X], where the mole fraction is the ratio of host concentration to the host and metal concentration.[99,136]

$$[X] = \frac{[H]}{[H] + [Q]}$$

$$where, [H] = host\ concentration$$

$$[Q] = quencher\ concentration\ (Cu^{2+})$$

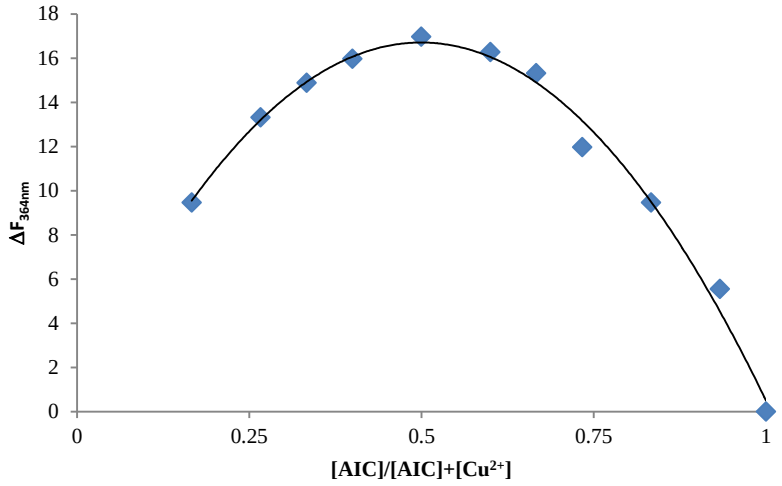

Figure 3.92: Job's plot of a complex of **AIC** with Cu^{2+}.

The characteristic parabolic curve is observed for the Job's plot of **AIC**. The peak fluorescence change is observed at a mole fraction of 0.5, which is indicative of 1:1

metal complex formation. This trend has also been observed for the pyrene analogous sensor **PIC**.

The ratio of the intensity of the fluorescence emission at 439 nm of **AIC** alone to that of following titration of Cu^{2+} (I_o/I) was plotted against the concentration of added Cu^{2+} [Q]. The Stern Volmer plot which arises from dynamic quenching follows Equation 1.

$$\frac{\phi_o}{\phi} = \frac{I_o}{I} = 1 + k_q\tau_o[Q] = 1 + K_{SV}[Q] \qquad \textbf{Equation 1}$$

I_o and I are the steady state fluorescence intensities in the absence of and in the presence of a quencher, respectively. And $k_q\tau_o$ is the Stern-Volmer constant K_{sv}. If this plot is linear, the slope gives the Stern-Volmer constant. From this, k_q can be calculated if the excited state lifetime in the absence of quencher is known.[92] For a bimolecular process where diffusion is limited, $k_q=k_1$ (k_1 being the diffusional rate constant), and when τ_o is equal to one, the slope of the plot is the association constant ($K_a = K_{sv}$) for the complex.[99] The resulting Stern-Volmer plot for **AIC** has an upward curvature which is suggestive of a combination of static quenching, arising from complexation, and dynamic quenching, arising from random collisional encounters, between an excited **AIC** and Cu^{2+} quencher (Figure 3.93). This has also been observed for the pyrene analogue **PIC**. This upward curve was unexpected when compared to similar sensors which follow Stern Volmer kinetics.[88,99,139] For a system which experiences both dynamic and static quenching, it will follow the equation below. Clearly it is less straight forward to obtain the K_a from Equation 2.

$$\frac{I_O}{I} = (1 + k_q\tau_O[Q])(1 + K_{SV}[Q]) \qquad \textbf{Equation 2}$$

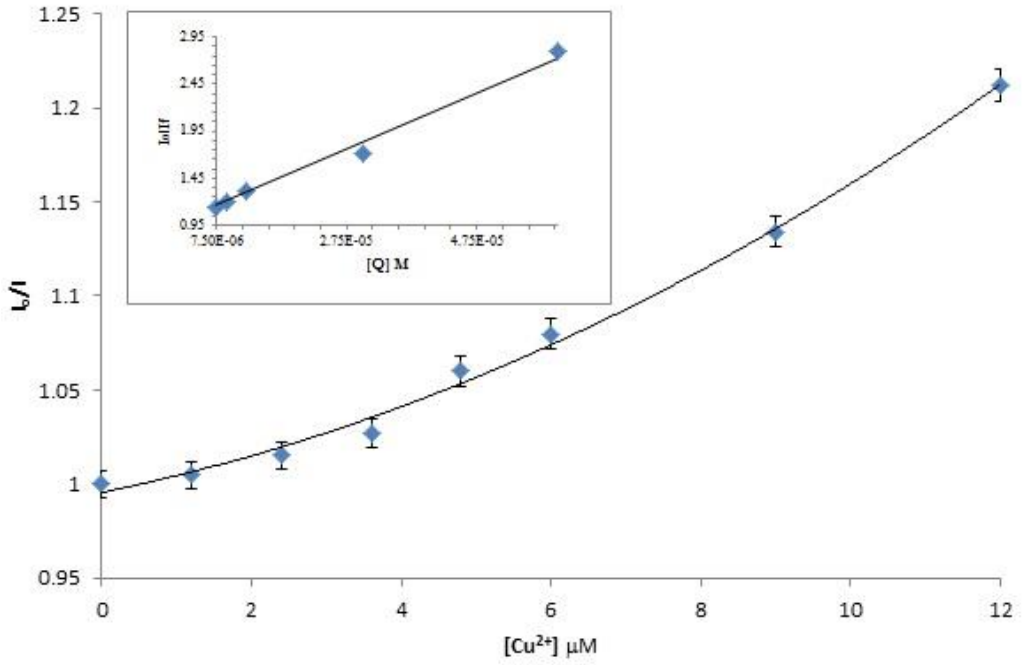

Figure 3.93: Stern Volmer type plot for **AIC**, insert high concentration showing more linear nature.

Overall, it appears that both dynamic and static quenching is occurring, however it can be seen that when more than 6 μM of Cu^{2+} is added, which is one molar equivalent, the curve appears to straighten (Figure 3.93 insert). This apparent return to linearity suggests that the quenching is more dynamic in nature. As has been described previously, dynamic quenching arises from random collisional encounters between an excited **AIC** and Cu^{2+} quencher. On the other hand, static quenching is due to complex formation, with the apparent drop off in static quenching above 1 equivalent of Cu^{2+} added; it is proposed that total complexation occurs at 1 molar equivalent of quencher added. This is in accordance with the result from the Job's plot (Figure 3.92).

Three methods for the determination of the stability constant K_s, which is equal to K_a, by fluorometry were described by Valeur in 1988.[100] For all the following methods, I_F^o is the peak fluorescence for the free ligand spectrum (**PIC**/**AIC**) and I_F^{max} is the maximum fluorescent emission observed in the presence of the quencher (Cu^{2+}). The concentration of the metal and ligand are given by [M] and [L].

Method One:

$$\frac{I_F - {I_F}^o}{{I_F}^{max} - I_F} = K_S[M]$$

In this method the ratio of $(I_F–{I_F}^o)$ / $({I_F}^{max}–I_F)$ is plotted against the metal concentration [M], and the stability constant K_s is obtained from the slope of the line. A major drawback of this method is the requirement to determine ${I_F}^{max}$. This is difficult to determine with a high degree of accuracy at high concentrations of metal ions. As quite concentrated solutions of Cu^{2+} were used as the quencher, this method was deemed to be unsuitable.

Method Two:

$$\frac{\left[1 - \left(\frac{{I_F}^o}{I_F}\right)\right]}{[M]} = K_S\left(\frac{b}{a}\right)\left(\frac{{I_F}^o}{I_F}\right) - K_S$$

This method is used when the determination of ${I_F}^{max}$ proves to be problematic.[103] K_s is determined from the intercept of a plot of $[1-({I_F}^o/I_F)]/[M]$ against ${I_F}^o/I_F$. Due to the emphasis that this method places on the error for the points close to ${I_F}^o$, it is unsuitable for weak variations in the fluorescence intensity. As a result, a third method was used which would be suitable for both **PIC** and **AIC**.

Method Three:

$$\frac{{I_F}^O}{I_F - {I_F}^O} = \left[\frac{a}{b-a}\right]\left[\left(\frac{1}{K_S[M]}\right) + 1\right]$$

For this method, ${I_F}^O/(I_F-{I_F}^O)$ is plotted against 1/[M] and the stability constant K_s is determined from the ratio of intercept to slope. This method was used to determine the

K_a of both **PIC** and **AIC**. The plots obtained for **PIC** and **AIC** are shown in Figures 3.101 and 3.102, respectively.

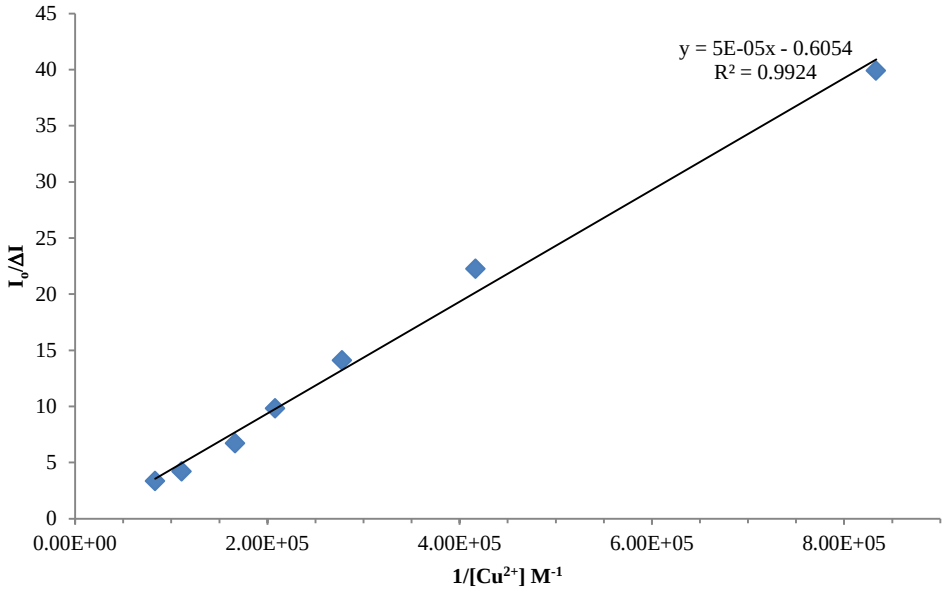

Figure 3.94: Plot for determination of K_a for **PIC**.

The plot for **PIC** has sufficient linear behaviour. Accordingly, the stability constant, given by the ratio of the intercept *vs* the slope (intercept = 0.6054, slope = $5x10^{-5}$), is estimated as 1.2×10^4 M^{-1}.

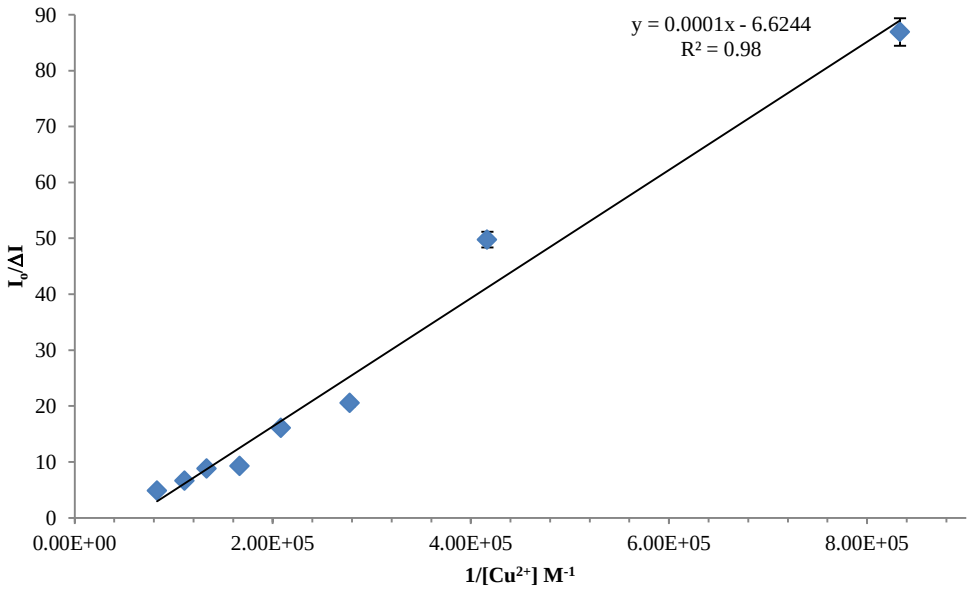

Figure 3.95: Plot for determination of K_a for **AIC**.

The same calculation was performed on the data obtained for **AIC** and the stability constant was consequently determined to be 7.0 x 10^4 M^{-1}. These values compare well with previously reported results for copper sensors, 1.58+/- 0.03 x 10^4 M^{-1} for a chloroanthracene analogue,[99] and 2.08 x 10^3 M^{-1} for a naphthalene based sensor.[88] A triazole based pyrene sensor for cadmium, developed by Kim *et al*., reported a K_a of 5.18x10^4 M^{-1}.[67]

Autoreduction of Cu^{2+} to Cu^{+} due to a phenol has been reported previously,[140] and Chung *et al*. have reported evidence of this with their chloroanthrancene analogue.[99] Evidence of this reduction can be gathered from an absorption titration experiment of **AIC** and **PIC** with Cu^{2+}. Copper(I) has a characteristic absorption peak at 450-480 nm, so if autoreduction was occurring a peak would be observed at this wavelength. To this end the absorption spectrum of both **PIC** and **AIC** were recorded in the presence of copper perchlorate (Figure 3.96a & Figure 3.96b). It can be seen clearly that there is no evidence of this absorption peak for Cu^{+}.

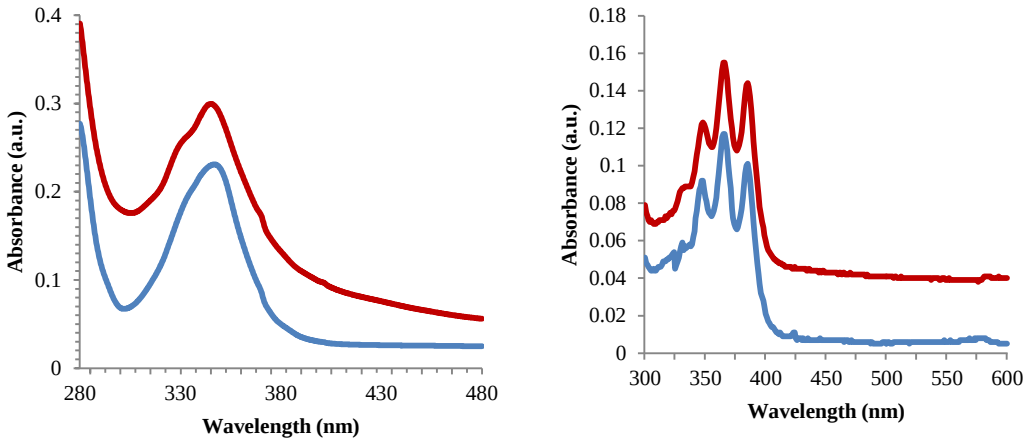

(a) *(b)*

Figure 3.96: (a) UV-Vis spectrum of **PIC** 6 μM (blue) and with $Cu(ClO_4)_2$ 120 μM (red) (MeCN) **(b) AIC** 6 μM (blue) and with $Cu(ClO_4)_2$ 120 μM (red) (MeCN).

3.5.3 Metal Titration ^{1}H NMR of PIC and AIC

In an attempt to determine where the metal binding site was within our sensors, metal titration ^{1}H NMR studies between **PIC**/**AIC** and both Cu^{2+} and Zn^{2+} were undertaken. The perchlorate salts of these metal ions were chosen as they are ions which either caused quenching of **PIC**/**AIC** or showed no effect on the fluorescence of **PIC**/**AIC**. Figure 3.97 shows the ^{1}H NMR spectra of a 0.65 mM solution of **PIC** in $CD_3CN:CDCl_3$ (3:1) and with addition of increasing concentrations of Cu^{2+}. It is abundantly clear that the addition of copper(II) ions causes a broadening, which further supports the assertion that no autoreduction of Cu^{2+} is occurring. If Cu^{2+} was reduced to Cu^{+}, a much sharper spectrum would be observed due to the diamagnetic nature of the Cu^{+} ion. Evidence of the effect this autoreduction has on the ^{1}H NMR spectra has been reported by Chung and co-workers.[99]

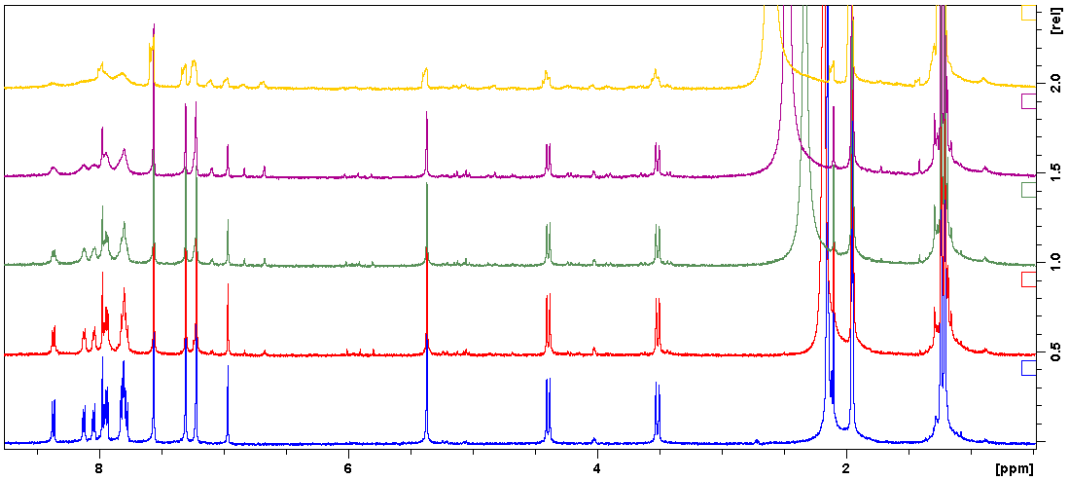

Figure 3.97: ^{1}H NMR spectrum of **PIC** 0.65 mM (blue) and in the presence of 0.5 (red), 1.0 (green), 1.5(purple), and 2.0 (yellow) equivalents of Cu^{2+}, in a $CD_3CN:CDCl_3$ (3:1) mix.

The isoxazole is represented by a singlet which resonates at 6.93 ppm, it was expected that this peak would experience a downfield shift upon complexation of the metal. This clear movement in the isoxazole signal has been reported before for isoxazole linked sensors,[99] and a similar shift has been reported for triazole linked sensors.[67] However,

what is observed for **PIC** in the presence of Cu^{2+} ions is quite different to this. The signals which represent the isoxazole and pyrene are found to broaden significantly, indicating that both are involved in copper coordination.

Upon titration of 0.5 equivalents of copper(II) perchlorate (0.325 mM), new signals are seen for the isoxazole proton which suggests that this is involved in binding. This is seen in all subsequent titration spectra (Figure 3.98). However, a single singlet is not observed which suggests that the binding is more complicated than the metal simply binding to the oxygen of the isoxazole ring. Furthermore, this suggests that other binding may be occurring, such as binding which involves a nitrogen atom from the triazole ring. While some broadening of the pyrene aromatic signals is observed below 2.0 equivalents, it is not until this concentration of Cu^{2+} ion is exceeded that dramatic broadening occurs.

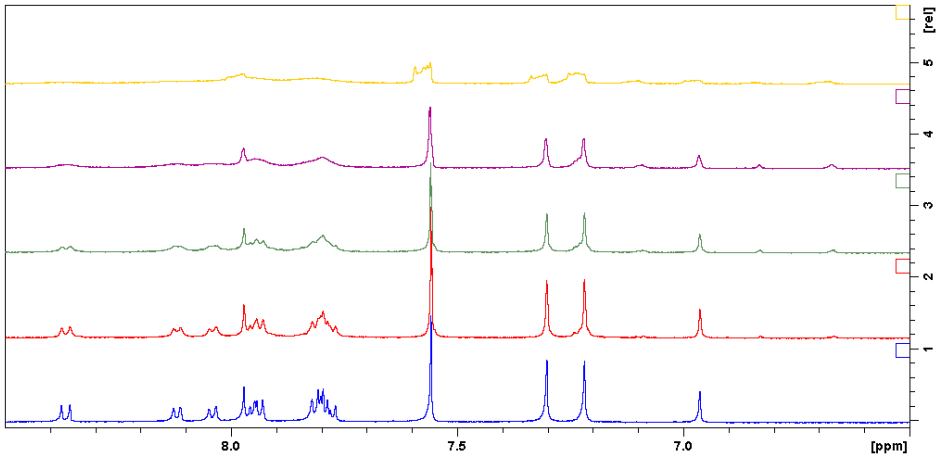

Figure 3.98: A section of the ^{1}H NMR spectra of **PIC** with 0.5 (red), 1.0 (green), 1.5 (purple) and 2.0 (yellow) equivalents of Cu^{2+}, CD_3CN:$CDCl_3$ (3:1).

With the introduction of two equivalents of Cu(II) ions, the pyrene signals begin to noticeably broaden. This can be seen in up to five equivalents of metal ion added (Figure 3.99). With this level of metal ion added, the pyrene signals are broadened beyond detection. Those signals associated with the calixarene core remained sharp

and appeared to be unaffected by the bulk paramagnetism. This suggests that there is some interaction between the Cu^{2+} and the pyrene, as well as with the isoxazole moiety.

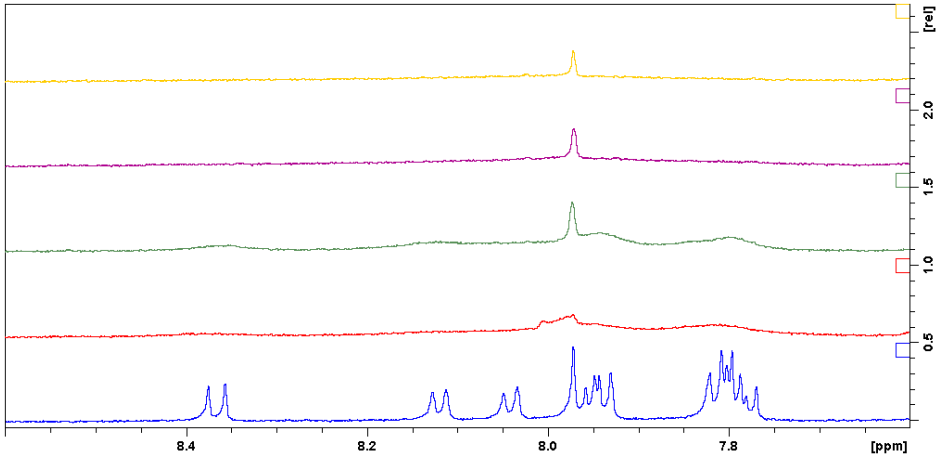

Figure 3.99: Expansion of the pyrene region of the ^{1}H NMR spectra of **PIC** with 2.0 (red), 3.0 (green), 4.0 (purple) and 5.0 (yellow) equivalents of Cu^{2+}, CD_3CN:$CDCl_3$ (3:1).

A similar set of experiments was performed using zinc(II) perchlorate, a metal salt which had little to no effect on the fluorescent emission spectra of **PIC**. No significant changes were observed in the isoxazole or pyrene signals, even upon addition of five molar equivalents of metal (Figure 3.100).

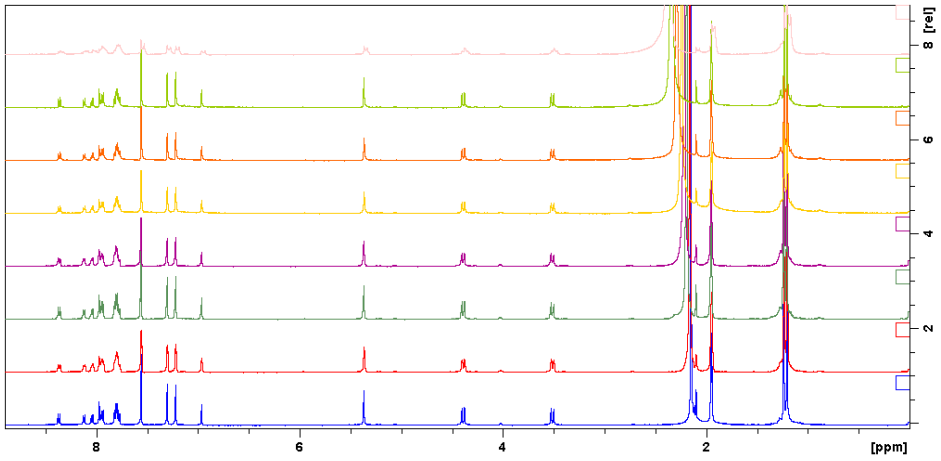

Figure 3.100: ^{1}H NMR spectra of **PIC** with 0.5, 1.0, 1.5, 2.0, 2.5, 3.0, 4.0 and 5.0 equivalents of $Zn(ClO_4)_2$, CD_3CN:$CDCl_3$ (3:1).

A parallel set of metal titration ^{1}H NMR studies were performed for the anthracene derivative (**AIC**) (Figure 3.101).

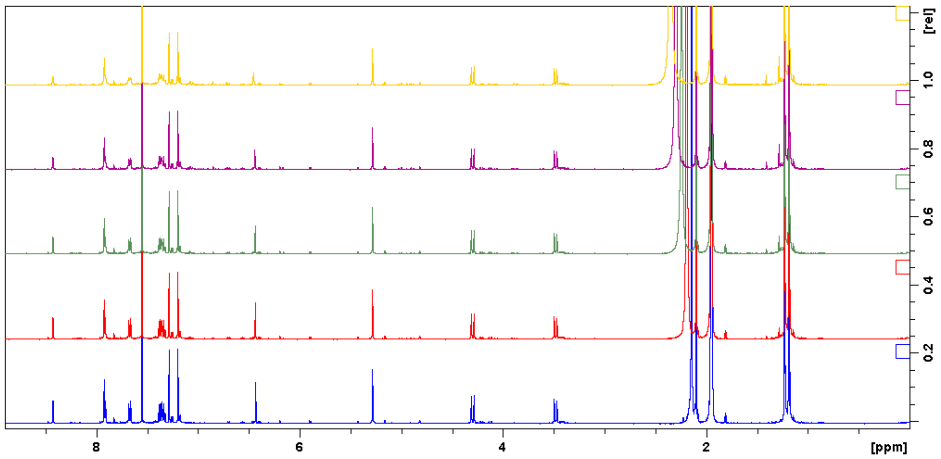

Figure 3.101: ^{1}H NMR spectra of **AIC** 0.65 mM (blue) with 0.5 (red), 1.0 (green), 1.5 (purple) and 2.0 (yellow) equivalents of $Cu(ClO_4)_2$, CD_3CN:$CDCl_3$ (3:1).

The isoxazole proton is represented by a signal which resonates as a singlet at 6.43 ppm, and it was expected that this peak would experience a downfield shift upon complexation of the metal ion. Once again, the result is not quite this simple, as upon titration of the Cu^{2+} ion this broadening can be seen in both the isoxazole and anthracene signals. This is consistent with what has been seen for the pyrene analogue **PIC**.

Addition of 0.5 equivalents of Cu^{2+} causes a slight downfield shift and broadening of the isoxazole signal. New signals are seen for the isoxazole proton which suggests that the isoxazole ring is involved in binding. This is seen in all subsequent titration spectra (Figure 3.102). As was the case for **PIC**, the binding does not appear to just involve the isoxazole moieties. Once again, some broadening of the fluorophore aromatic signals is observed below 2.0 equivalents, however it is not until this concentration of Cu^{2+} ion is exceeded that significant broadening occurs.

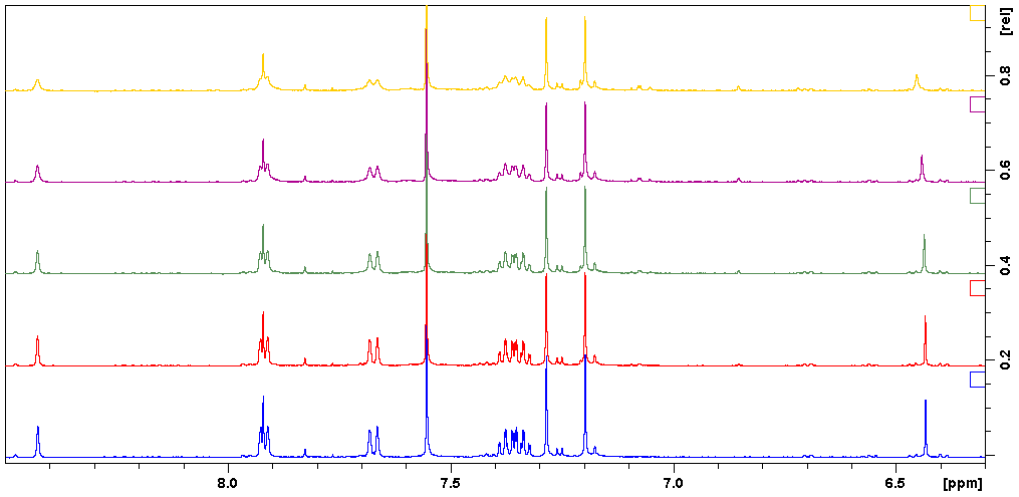

Figure 3.102: A section of the ^{1}H NMR spectra of **AIC** (blue) with 0.5 (red), 1.0 (green), 1.5 (purple) and 2.0 (yellow) equivalents of Cu^{2+}, CD_3CN:$CDCl_3$ (3:1).

Introduction of two equivalents of Cu^{2+} ions results in clear broadening of the anthracene signals. This can be seen for up to five equivalents of metal ion added (Figure 3.103). At this level of metal added, the anthracene signals broaden beyond detection. Once more, the signals which are associated with the calixarene core remained sharp and appeared to be unaffected by the bulk paramagnetism. This is very similar to the result obtained for the pyrene analogue **PIC**, and clearly suggests that there is an interaction between the Cu^{2+} ions and the anthracene units.

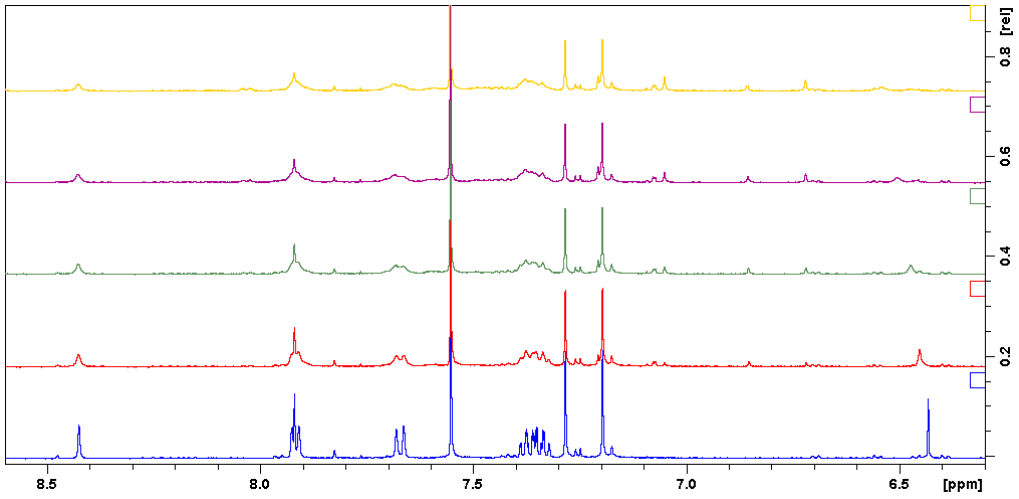

Figure 3.103: Expansion of the anthracene region of the ^{1}H NMR spectra of **AIC** (blue) with 2.0 (red), 3.0 (green), 4.0 (purple) and 5.0 (yellow) equivalents of Cu^{2+}, CD_3CN:$CDCl_3$ (3:1).

Zinc(II) perchlorate, a metal salt which had little to no effect on the fluorescent emission spectra of **AIC**, was tested using the same method. No significant changes were observed in the isoxazole or pyrene signals, even upon addition of five molar equivalents of metal (Figure 3.104). Once again, this is consistent with the data which was collected for the pyrene analogue **PIC** (Figure 3.100).

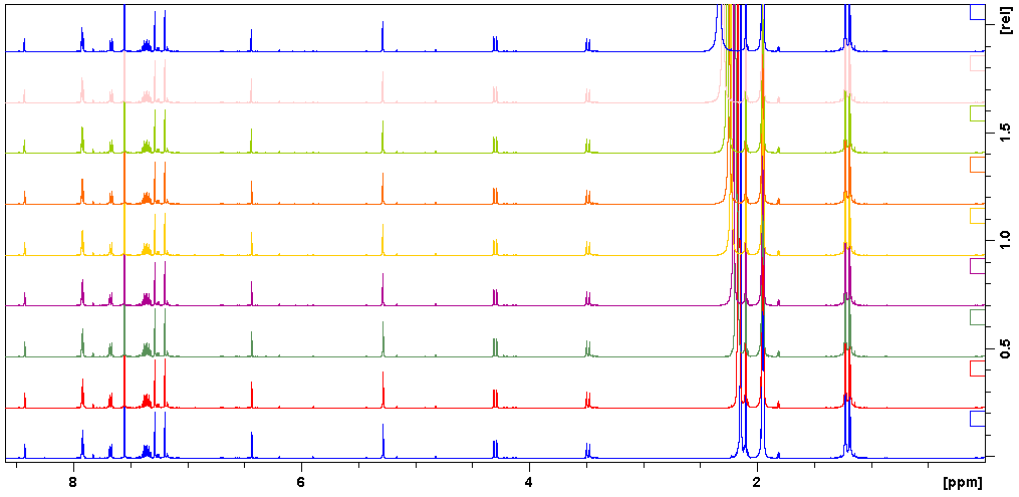

Figure 3.104: ^{1}H NMR spectra of **AIC** with 0.5, 1.0, 1.5, 2.0, 2.5, 3.0, 4.0 and 5.0 equivalents of $Zn(ClO_4)_2$, CD_3CN:$CDCl_3$ (3:1).

These results would suggest that possibly more than one metal ion is involved in the binding process. This is in direct contrast with the Job's plot which was obtained from fluorescence spectrometry and indicated the presence of a 1:1 **PIC**-Cu^{2+} complex in solution.

Two possible binding modes are proposed. Firstly, two interactions, one between the nitrogen and the Cu^{2+} and the other between the pyrene rings and a Cu^{2+} ion, are occurring. With this mode the Cu^{2+} ion is binding to the isoxazole ring and also binding to the pyrene ring, with rapid movement between both sites. A second binding mode is also proposed, where the Cu^{2+} ion sits between both pyrene rings and an isoxazole ring with one acetonitrile molecule occupying the fourth coordination site

(Figure. 3.112). The broad nature of pyrene signals in the ^{1}H NMR spectra supports both of these binding possibilities as does the appearance of a number of isoxazole signals. This is further supported by the appearance of several signals in the 1-1.5 ppm region of the spectrum (Fig. 3.104) which could be due to acetonitrile solvated both inside and outside the upper cavity of the calix[4]arene.

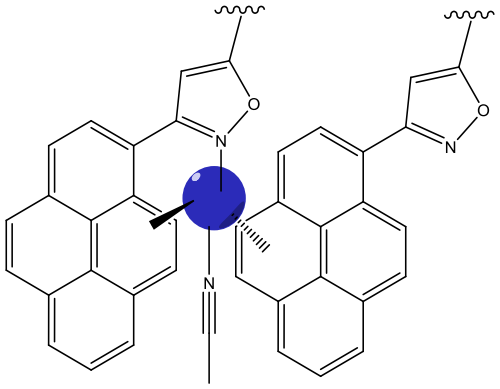

Figure 3.105: Proposed binding of Cu^{2+} ion (blue sphere) with pyrene rings (above and below), one isoxazole ring and MeCN molecule.

The results from the ^{1}H NMR spectral studies for **AIC** are nearly identical to the trend observed for **PIC**. Hence, a similar mode of binding is proposed for this sensor (Figure 3.106). Once again, the broad nature of anthracene signals in the ^{1}H NMR spectra supports both of these binding possibilities as does the appearance of a number of isoxazole signals. As was the case for **PIC**, further support is noted by the appearance of several signals in the 1-1.5 ppm region of the spectrum (Fig. 3.109) which could be due to acetonitrile being both inside and outside the upper cavity of the calix[4]arene.

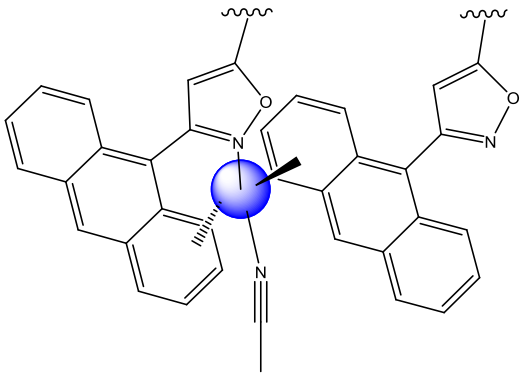

Figure 3.106: Proposed binding of Cu^{2+} ion (blue sphere) with anthracene rings (above and below), one isoxazole ring and MeCN molecule.

3.5.4 Computational Studies on PIC

Molecular modelling studies were performed on the calixarene base sensor **PIC** by Dr. Elisa Fadda of NUIM. The results from the fluorescence studies which have been previously discussed are somewhat surprising, as are the results of the ^{1}H NMR titration studies. It appears that **PIC** and **AIC** only bind to Cu^{2+} ions, but there should be no reason why the isoxazole units should only bind these ions in preference to other metal ions. Another possibility for binding is between the pyrene units in a ferrocene-type formation, but again this should bind all the metal ions and not the only Cu^{2+} ion.

The **PIC** ground state structure in the absence of a Cu^{2+} ion was obtained by geometric optimization in terms of redundant internal coordinates with the qNR algorithm implemented in the Turbomole program. The calculation was performed at the RI-B97D//def2-TZVP level of theory, where the B97 functional was augmented with Grimme dispersion correction.[141] The structure of the Cu^{2+}/**PIC** complex was found by optimizing the geometry of six unbiased starting conformations. These conformations were generated by placing the ion at six different positions along the y-axis within the calixarene crown of the minimum shown in Figure 3.107a, with distances between the ion and the nitrogen of the isoxazole ranging from 3.0 to 9.0 Å in 1 Å steps (Figure 3.107b). The geometric optimization of the Cu^{2+}/**PIC** starting complexes was run in two steps: **(i)** Berny algorithm at the ROHF//6-31G* level (Gaussian09),[142] **(ii)** qNR at the RI-B3LYP//def2-TZVP (Turbomole) for all atoms.

The optimized structures of both **PIC** and the **PIC** Cu^{2+} complex are shown in Figure 3.107a and 3.114c, respectively. The gas phase minimum found for **PIC** shows a distinctive intramolecular π-π stacking between the two pyrene moieties. In this conformation, the LUMO of one of the pyrene groups interacts with the HOMO of the other pyrene forming a stable excimer characterized by a broad emission band that

peaks at 498 nm. The introduction of a Cu^{2+} ion induces a radical conformational change in the **PIC** structure upon binding. It can be seen in Figure 3.107c that the Cu^{2+} ion is coordinated in a distorted square pyramid conformation, with one of the isoxazole rings acting as an apical ligand (Table 3.12). This involvement of the isoxazole results in significant rotation of one of the pyrenyl moieties relative to the other. Therefore, due to this rotation the intramolecular π-π stacking between the pyrene groups is broken, and this is most likely the cause for the excimer quenching. This is in agreement with work previously reported by Kim *et al.*[143] using an amide binding site. The quenching of the monomer emission band is possibly caused by reverse PET. This is where a pyrene moiety acts as the electron donor and the complexed isoxazole fulfils the acceptor role. The mechanism for monomer quenching has been discussed in earlier work by Chang *et al.*[99]

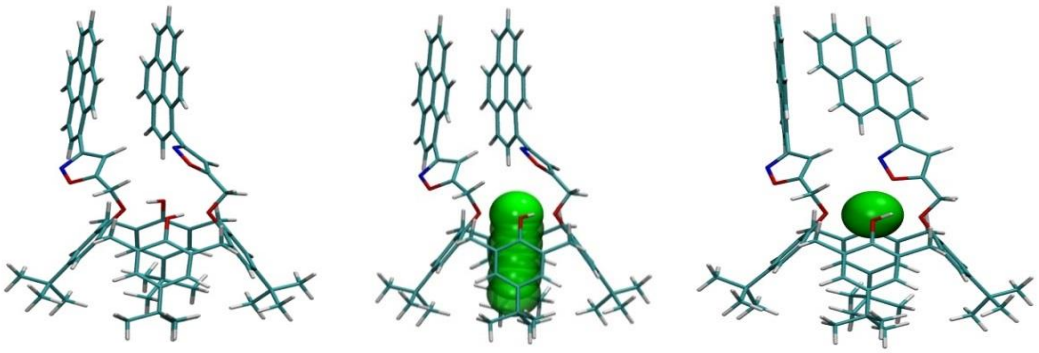

(a) *(b)* *(c)*

Figure 3.107: **(a)** Structure of the gas-phase ground state for the unbound **PIC (b)** Six starting positions selected to capture the effect of the entrance of a Cu^{2+} ion (shown as green spheres) in the **PIC** conformation **(c)** Gas phase ground state of the **PIC**-Cu^{2+} complex.

Table 3.12: Cu(II)-**PIC** distorted square planar coordination. Bond distances are expressed in Å.

Level of theory	Crown OH1	Crown OH2	Crown-O1 isooxazole	Crown-O2 isooxazole	O-isoxazole
B3LYP/def-SV(P)	2.1	2.1	2.2	2.1	2.4

As has been previously discussed, titration emission experiments with the other metal perchlorates (Co, Cd, Hg, Fe, Ni, Zn and Pb) had no effect on the fluorescence emission spectra of **PIC** or **AIC**. The results of the modelling studies indicate that the selectivity towards the Cu^{2+} ion could be explained in terms of the geometrical constraints of the **PIC** coordination site. As can be seen from the structure of the **PIC**-Cu^{2+} complex, the optimal coordination is square pyramidal. While the Cu^{2+} ion is known to adopt this coordination, both in chemistry[144] and biology,[145] the other divalent metal ions tested do not share the same propensity for a square pyramidal coordination sphere with oxygen. Additionally, based on the ground-state structure of the unbound **PIC**, the formation of any complex would have to be energetically favoured enough to account for the energy loss due to the breaking of the π-π stacking.

Attempts to model interactions between the Cu^{2+} ion and the pyrene rings of the **PIC** resulted in no observed minimum, indicating that such an interaction was not likely to exist. This was taken as further evidence that the main interactions between **PIC** and Cu^{2+} ions were likely to be between the isoxazole nitrogen atoms, the phenol groups and the Cu^{2+} ion. It is clear that this molecular modelling does not conform to the data which was obtained from the ^{1}H NMR spectra. However, this mode of binding would go towards explaining the remarkable selectivity which **PIC** and **AIC** exhibit for Cu^{2+}.

4. Conclusions

The work carried out in this thesis was undertaken with a goal of the preparation of a range of novel calix[4]arene based metal ion binders. These were to be based on Schiff base, triazole or isoxazole units. As these were envisioned to be used as sensors, many of the compounds prepared were screened for potential fluorescent behaviour. All the Schiff base ligands were subjected to metal complexation reactions, which resulted in hydrolysis of the ligand in all cases. Perchlorate salts of Co^{2+}, Cu^{2+}, Ni^{2+}, Hg^{2+} and Zn^{2+} were used and, in one case, the anhydrous chloride salt of Zn^{2+} was used.

Ortho, meta and *para*-hydroxybenzaldehyde were used to prepare three Schiff base linkers **13**, **9** and **6**. These compounds were then used to prepare six novel Schiff base capped calix[4]arenes **7**, **8**, **10**, **11**, **14** and **15**, using a compartmentalised pathway. The products were prepared in good yield and purification of the desired products was mainly a straightforward task. Metal complexation reactions were attempted with all these ligands, using perchlorate salts of Co^{2+}, Cu^{2+}, Ni^{2+}, Hg^{2+} and Zn^{2+}. In all cases, it appears that hydrolysis of the imine has occurred, even though precautions were taken to ensure anhydrous conditions were employed. However, the hydrated form that these metals were supplied in furnished enough water into the reaction system to facilitate imine hydrolysis. An attempt was made to exploit the anhydrous metal salt zinc(II) chloride to prepare a metal complex with **7** but once again the result was imine hydrolysis.

These ligands were screened for fluorescent behaviour, but no fluorescence emission spectra were obtained for any of the ligands. The products from the metal complexation reaction of mercury(II) perchlorate with **7** and **8** were obtained as purple compounds. As a result of this unexpected colour change, these compounds were screened for fluorescent behaviour. The results obtained were consistent with the parent ligands, and no fluorescent emission was recorded. Therefore, it is clear from

these spectroscopic results that this family of compounds is not suitable for use as a metal ion sensor.

As the compartmental route was a success, it was decided to expand the project to include a triazole binding site, with retention of the problematic imine moiety. It was expected that these compounds would provide two contrasting ionophores within a rigid scaffold. To this end propargyl bromide was employed to substitute *ortho*, *meta* and *para*-hydroxybenzaldehyde to isolate the benzaldehyde alkynes **28**, **26** and **19**. Using the copper catalysed 1,3 Huisgen azide-alkyne cycloaddition (CuAAC). these were attached to alkylazide calix[4]arene to yield the triazolelinked benzaldehyde calix[4]arenes **25**, **27**, **29** and **30**. This confirmed that the calix[4]arene was a suitable scaffold upon which CuAAC type chemistry could be performed. The mode binding was established by the metal complex reaction between the perchlorate salt of Zn^{2+} and **30**. NMR Spectroscopic studies revealed that the metal binding site was between the two triazole moieties.

Two of these compounds, **29** and **30**, were screened by fluorescence spectroscopy to determine if this family of compounds was suitable for use as fluorescent sensors. As expected, these compounds did exhibit a weak emission spectrum, which is due to π-π stacking between the two pendant benzaldehyde rings. However, the quality of the emission spectra recorded was deemed not to be of sufficient quality for development as a chemosensor for metal ions.

The CuAAC reaction was utilized to prepare three double triazole linked calixarenes two of which are novel *calixtubes*. The first step towards this goal was the synthesis of a 1,3-distal propargyl substituted calix[4]arene **17**. The synthesis of this compound is well known and uncomplicated, yielding a product of high purity and high yields. This

calixalkyne was reacted with the three *calixazides* prepared to yield the *calixtubes* **21**, **22** and **23**. These were prepared in low yields and required column chromatography for purification, in contrast to the benzaldehyde variants which were isolated through recrystallization. These *calixtubes* were synthesised successfully and were characterised using NMR spectroscopic methods, and this was supported by mass spectroscopy. However, these reactions were not high yielding even at the extended reaction times. It was decided, due to the above mitigating factors, to move away from this synthesis.

The goal of using CuAAC type chemistry was to create Schiff base capped calixarenes which bore two different metal bindings sites. This was undertaken with a view of facilitating unusual metal binding behaviour. The predisposition of the Schiff base linkers towards imine hydrolysis, even under mild condition, was seen before in the metal complexation studies conducted with the capped calixarene. However, it was expected that *mono* and *bis* propargyl substituted derivatives of these linkers would be isolated in a relatively straightforward manner. This was not the case, however. Only one *bis*-propargyl-Schiff base linker **30** was successfully isolated. All other attempts to synthesise either *mono* or *bis* propargyl variants of the Schiff base linkers resulted in hydrolysis of the imine bond and isolation of a *mono* propargylated benzaldehyde. While this was also seen as a minor product from the reaction which yielded compound **30**, it was the major product from all subsequent attempts at this type of synthesis. It is proposed that acid catalysed imine hydrolysis is occurring in these reactions. This is due to propargyl bromide having a lower acid disassociation constant (pK_a) than the alkyl halide calixarenes, which were successfully substituted with the Schiff base linkers.

Not being discouraged by the unwelcome hydrolysis of the imine, the final construction of a triazole linker Schiff base capped calix[4]arene was attempted. Using a modified synthetic scheme, CuAAC chemistry was applied between the calixazide **19** and the *bis* propargyl Schiff base linker **30**. NMR spectroscopic analysis of the crude product from this reaction revealed once more, that cleavage of the imine bond had occurred. This was not completely unexpected as the copper catalyst used was obtained in its hydrated form. The reaction was repeated in the presence of a drying agent, but unfortunately this did not surmount the problem of imine hydrolysis. Therefore, it is concluded that this family of Schiff bases are unsuitable for CuAAC using copper sulphate as the catalyst.

Isoxazoles were next to be used to modify the calixarene scaffold. As a result of collaboration with Haowen Diao, of the Heaney group, four novel chemosensors were prepared. It was decided to modify the calixarene with two well-known fluorophores, so pyrene and anthracene were selected. The effect of the macrocyclic nature on the emission spectrum was tested by the preparation of two *calixalkyne* based sensors **AIC**/**PIC** and two *tert*-Butyl phenol alkyne based **AIM/PIM**. The structures of the calixarene host ligands were confirmed by X-ray crystallography. These sensors were screened for any fluorescent emission behaviour. It was discovered that the macrocyclic nature of the calixarene had a profound effect on the nature of the emission. The calixarene based sensors **PIC** and **AIC** exhibited both monomer and excimer emission, whilst the phenol based **PIM**/**AIM** show only monomer emission. The perchlorate salts of Hg^{2+}, Ni^{2+}, Zn^{2+}, Co^{2+}, Fe^{2+}, Pb^{2+}, Cd^{2+} and Cu^{2+} were titrated against a fixed concentration of the host to determine the affect this had on the spectrum. As a result, it was found that only Cu^{2+} had any major effect on the emission spectra recorded.

To determine the role of the counter ion in quenching of the emission spectrum, various copper salts were studied in the same manner. It was found that the other Cu^{2+} salts screened acetate, chloride and nitrate had a reduced quenching action in comparison to the perchlorate salt previously studied. The Cu(I) salt CuCl was also screened in the same manner, and it was found to have no effect on the emission spectrum. Therefore, it is clear that Cu^{+} has no quenching effect on the emission spectrum.

The quenching effect that copper(II) perchlorate had on emission spectra of **PIC** and **AIC** was studied in greater detail. The minimum concentration at which Cu^{2+} was detected was found to be 2.3×10^{-7} and 0.9×10^{-7} M or **PIC** and **AIC**, respectively. This was somewhat surprising and the quenching action of **PIC** is much more visual striking than that seen for the anthracene analogues **AIC**. Job's method of continuous variation was used to determine the stoichiometry of the metal complex being formed. This experimental method revealed a 1:1 binding stoichiometry for both **PIC** and **AIC** with Cu^{2+}.

Next, a Stern-Volmer plot was constructed with a view to determining the K_a for **AIC** and Cu^{2+}. This plot deviated from linearity which was indicative of two quenching processes occurring simultaneously, both dynamic and static quenching. Another method was used to determine the stability constant K_s for both **PIC** and **AIC**, this was found to be 1.2×10^{4} M^{-1} and 7.0×10^{4} M^{-1}, respectively.

To determine where in the scaffold metal binding was occurring, molecular modelling and ^{1}H NMR metal titration studies were employed. Molecular modelling studies were performed on the pyrene sensor **PIC** by Dr. Elisa Fadda at NUIM. The results pointed towards complexation of the Cu^{2+} between one of the isoxazole rings and the lower rim of the calixarene. The coordination geometry which this exposes would go some

way towards explaining the selectivity that these sensors show towards Cu^{2+}. The twist which is caused by this would explain the quenching in excimer emission noted upon addition of the metal.

The results of the ^{1}H NMR were more complicated than was expected. With both **PIC** and **AIC** undergoing broadening of both the isoxazole signal and the fluorophore aromatic signals. This suggests that binding of Cu^{2+} involves an isoxazole and the fluorophore units, although in the absence of crystallographic data this cannot be stated unambiguously.

The Schiff base capped calix[4]arenes were successfully prepared using the compartmentalisation pathway. Attempts to utilize these compounds to form metal complexes proved to be unsuccessful due to imine hydrolysis. The role which imine hydrolysis plays in this thesis is not limited to the attempted metal complexation reactions with these capped calixarenes. In fact, this unfortunate side reaction in part leads to the numerous pathways which resulted in the diverse range of compounds prepared. This method of compartmentalisation was intended to be used to create a range of triazole linked Schiff base capped calixarenes. However, it was discovered that hydrolysis of the imine ensued not only during the CuAAC reactions but also during formation of propargylated Schiff bases. As a result of this, only a limited number of triazole linked benzaldehyde calix[4]arenes were prepared, however, this led to the shift towards isoxazoles. A pair of macrocyclic isoxazole modified chemosensors (**AIC** and **PIC**) were prepared by NOAC, a pair of monomeric phenol based model sensors were also prepared (**AIM** and **PIM**). After extensive fluorescent spectroscopic testing it was found that these sensors were selective for Cu^{2+} ions.

There are a number of routes by which future work on these compounds could progress. The five membered isoxazole rings could be exchanged for six membered

rings which could result in improved ion sensing. The carbon chain which links the isoxazole and the fluorescent moiety could be lengthened; this would result in a loss of conjugation which once again could affect the sensitivity or selectivity of these sensors. Alternatively, due to their remarkable selectivity these sensors could be incorporated into an electronic sensor to create a copper selective electrochemosensor. If successful, this would open up a wide range of electrochemical experiments to be performed using these sensors.

Bibliography

1. A. Baeyer, *Ber.*, 1872, **5**, 25.

2. A. Baeyer, *Ber.*, 1872, **5**, 280.

3. A. Baeyer, *Ber.*, 1872, **5**, 1094.

4. C. D. Gutsche, *Calixarenes: An Introduction*, 2nd ed. edn., Royal Society of Chemistry, Cambridge, 2008.

5. A. Zinke and E. Zeigler, *Ber.*, 1944, **77**, 264-272.

6. B. T. Hayes and R. F. Hunter, *Chemi. Ind.*, 1956, 193-194.

7. B. T. Hayes and R. F. Hunter, *Journal Of Applied Chemistry*, 1958, **8**, 743-748.

8. J. W. Cornforth, P. D. Hart, G. A. Nicholls, R. J. W. Rees and J. A. Stock, *British Journal of Pharmacology and Chemotherapy*, 1955, **10**, 73-86.

9. J. W. Cornforth, M. E. D., P. K. T. and R. J. W. Rees, *Tetrahedron*, 1973, **29**, 1659-1667.

10. G. D. Andreetti, R. Ungaro and A. Pochini, *J. Chem. Soc., Chem. Commun.*, 1979, 1005-1007.

11. J. H. Munch and C. D. Gutsche, *Organic Syntheses*, 1990, **68**, 243-246.

12. C. D. Gutsche, M. Iqbal and D. Stewart, *J. Org. Chem.*, 1986, **51**, 742-745.

13. C. D. Gutsche, A. E. Gutsche and A. I. Karaulov, *J. Incl. Phenom. Macro.*, 1985, **3**, 447-451.

14. C. D. Gutsche, D. E. Johnston and D. R. Stewart, *J. Org. Chem.*, 1999, **64**, 3747-3750.

15. P. D. Harvey, *Coord. Chem. Rev.*, 2002, **233-234**, 289-309.

16. B. S. Creaven, D. F. Donlon and J. McGinley, *Coord. Chem. Rev.*, 2009, **253**, 893-962.

17. C. Wieser, C. B. Dieleman and D. Matt, *Coord. Chem. Rev.*, 1997, **165**, 93-161.

18. E. M. Collins, M. A. McKervey, E. Madigan, M. B. Moran, M. Owens, G. Ferguson and S. J. Harris, *J. Chem. Soc., Perkin Trans. 1*, 1991, 3137-3142.

19. S. Veravong, V. Ruangpornvisuto, B. Poipoosananakaton, M. Sukwattanasinitt and T. Tuntulani, *ScienceAsia*, 2000, **26**, 163.

20. J. McGinley, V. McKee and J. M. D. Walsh, *Inorg. Chim. Acta*, 2011, **375**, 57-62.

21. N. I. Nikishkin, J. Huskens, S. A. Ansari, P. K. Mohapatra and W. Verboom, *New J. Chem.*, 2013, **37**, 391.

22. S. O'Malley, B. Schazmann, D. Diamond and K. Nolan, *Tetrahedron Lett.*, 2007, **48**, 9003-9007.

23. K. C. Gupta, A. Kumar Sutar and C.-C. Lin, *Coord. Chem. Rev.*, 2009, **253**, 1926-1946.

24. D. Iyaguchi, S. Kawano, K. Takada and E. Toyota, *Biorg. Med. Chem.*, 2010, **18**, 2076-2080.

25. H. Schiff, *Chem. Zentralbl.*, 1857, **2**, 185-189.

26. N. P. Kushwah, M. K. Pal, A. P. Wadawale and V. K. Jain, *J. Organomet. Chem.*, 2009, **694**, 2375-2379.

27. J.-C. Andrez, *Tetrahedron Lett.*, 2009, **50**, 4225-4228.

28. N. Singh, M. S. Hundal, G. Hundal and M. Martinez-Ripoll, *Tetrahedron*, 2005, **61**, 7796-7806.

29. P. A. Vigato, S. Tamburini and L. Bertolo, *Coord. Chem. Rev.*, 2007, **251**, 1311-1492.

30. P. A. Vigato and S. Tamburini, *Coord. Chem. Rev.*, 2004, **248**, 1717-2128.

31. G. Nocton, P. Horeglad, V. Vetere, J. Pecaut, L. Dubois, P. Maldivi, N. M. Edelstein and M. Mazzanti, *J. Am. Chem. Soc.*, 2009, **132**, 495-508.

32. T. M. Ross, S. M. Neville, D. S. Innes, D. R. Turner, B. Moubaraki and K. S. Murray, *J. Chem. Soc., Dalton Trans.*, 2010, **39**, 149-159.

33. M. Shibasaki and S. Matsunaga, *Synthesis*, 2013, **45**, 421-437.

34. E. N. Jacobsen, W. Zhang, A. R. Muci, J. R. Ecker and L. Deng, *J. Am. Chem. Soc.*, 1991, **113**, 7063-7064.

35. E. N. Jacobsen, S. E. Schaus and J. F. Larrow, *J. Am. Chem. Soc.*, 1996, **118**, 7420-7421.

36. E. N. Jacobsen, S. E. Schaus, J. F. Larrow, K. B. Hansen, A. E. Gould, M. E. Furrow, B. D. Brandes and M. Tokunaga, *J. Am. Chem. Soc.*, 2002, **124**, 1307-1315.

37. E. N. Jacobsen and G. M. Sammis, *J. Am. Chem. Soc.*, 2003, **125**, 4442-4443.

38. L. Li, Y.-Q. Dang, H.-W. Li, B. Wang and Y. Wu, *Tetrahedron Lett.*, 2010, **51**, 618-621.

39. Z.-K. Song, B. Dong, G.-J. Lei, M.-J. Peng and Y. Guo, *Tetrahedron Lett.*, 2013, **54**, 4945-4949.

40. B. Shaabani and Z. Shaghaghi, *Appl. Organomet. Chem.*, 2011, **25**, 317-322.

41. A. Sap, B. Tabakci and A. Yilmaz, *Tetrahedron*, 2012, **68**, 8739-8745.

42. R. Seangprasertkij, Z. Asfari, F. Arnaud, J. Weiss and J. Vicens, *J. Incl. Phenom. Macro.*, 1992, **14**, 141-147.

43. R. Seangprasertkij, Z. Asfari, F. Arnaud and J. Vicens, *J. Org. Chem.*, 1994, **59**, 1741-1744.

44. M. F. Mahon, J. McGinley, A. D. Rooney and J. M. D. Walsh, *Tetrahedron*, 2008, **64**, 11058-11066.

45. J. McGinley and J. M. D. Walsh, *Inorg. Chem. Commun.*, 2011, **14**, 1018-1022.

46. B. S. Creaven, M. Deasy, P. M. Flood, J. McGinley and B. A. Murray, *Inorg. Chem. Commun.*, 2008, **11**, 1215-1220.

47. K. C. Gupta and A. K. Sutar, *Coord. Chem. Rev.*, 2008, **252**, 1420-1450.

48. D. E. Herbert and O. V. Ozerov, *Organometallics*, 2011, **30**, 6641-6654.

49. K. Arunkumar, M. A. Reddy, T. S. Kumar, B. V. Kumar, K. B. Chandrasekhar, P. R. Kumar and M. Pal, *Beilstein Journal of Organic Chemistry*, 2010, **6**, 1174-1179.

50. K. B. Sharpless, M. G. Finn and C. K. Hartmuth, *Angew. Chem. Int. Ed.*, 2001, **40**, 2004-2021.

51. S. Ast, T. Fischer, H. Muller, W. Mickler, M. Schwichtenberg, K. Rurack and H. J. Holdt, *Chem. Eur. J.*, 2013, **19**, 2990-3005.

52. L. V. Lee, M. L. Mitchell, S.-J. Huang, V. V. Fokin, K. B. Sharpless and C.-H. Wong, *J. Am. Chem. Soc.*, 2003, **125**, 9588-9589.

53. K. Liu, W. Shi and P. Cheng, *J. Chem. Soc., Dalton Trans.*, 2011, **40**, 8475-8490.

54. V. V. Rostovtsev, L. G. Green, V. V. Fokin and K. B. Sharpless, *Angew. Chem. Int. Ed.*, 2002, **41**, 2956-2599.

55. V. V. Fokin, *Organic Chemistry*, 2012, 247-277.

56. V. D. Bock, H. Hiemstra and J. H. van Maarseveen, *Eur. J. Org. Chem.*, 2006, **2006**, 51-68.

57. M. Meldal and C. W. Tornoe, *Chem. Rev.*, 2008, **108**, 2952-3015.

58. J. Hu, M. Zhang, L. B. Yu and Y. Ju, *Bioorg. Med. Chem. Lett.*, 2010, **20**, 4342-4345.

59. F. Himo, T. Lovell, R. Hilgraf, V. V. Rostovtsev, L. Noodleman, K. B. Sharpless and V. V. Fokin, *J. Am. Chem. Soc.*, 2005, **127**, 210-216.

60. V. O. Rodionov, V. V. Fokin and M. G. Finn, *Angew. Chem. Int. Ed.*, 2005, **44**, 2210-2215.

61. J. E. Hein and V. V. Fokin, *Chem. Soc. Rev.*, 2010, **39**, 1302-1315.

62. N. Castellucci and C. Tomasini, *Eur. J. Org. Chem.*, 2013, **2013**, 3567-3573.

63. J. R. Johansson, P. Lincoln, B. Norden and N. Kann, *J. Org. Chem.*, 2011, **76**, 2355-2359.

64. V. V. Fokin, G. Jia, Z. Lin, H. Zhao, L. Zhang, L. K. Rasmussen, S. Narayan and B. C. Boren, *J. Am. Chem. Soc.*, 2008, **130**, 8923-8930.

65. X. Creary, A. Anderson, C. Brophy, F. Crowell and Z. Funk, *J. Org. Chem.*, 2012, **77**, 8756-8761.

66. S. Thulasi, A. Savithri and R. L. Varma, *Supramol. Chem.*, 2011, **23**, 501-508.

67. S. Y. Park, J.-H. Yoon, C. S. Hong, R. Souane, J. S. Kim, S. E. Matthews and J. Vicens, *J. Org. Chem.*, 2008, **73**, 8212-8218.

68. N.-J. Wang, C.-M. Sun and W.-S. Chung, *Sensor. Actuat, B-Chem.*, 2012, **171-172**, 984-993.

69. S. Sameni, C. Jeunesse, D. Matt and J. Harrowfield, *Chem. Soc. Rev.*, 2009, **38**, 2117-2146.

70. F. G. Calvo-Flores, J. Isac-García, F. Hernandez-Mateo, F. Pérez-Balderas, J. A. Calvo-Asín, E. Sanchéz-Vaquero and F. Santoyo-Gonzalez, *Org. Lett.*, 2000, **2**, 2499-2502.

71. J. Morales-Sanfrutos, M. Ortega-Munoz, J. Lopez-Jaramillo, F. Hernandez-Mateo and F. Santoyo-Gonzalez, *J. Org. Chem.*, 2008, **73**, 7768-7771.

72. T. Müller, B. Willy and F. Rominger, *Synthesis*, 2008, **2008**, 293-303.

73. K. Takenaka, S. Nakatsuka, T. Tsujihara, P. S. Koranne and H. Sasai, *Tetrahedron: Asymmetry*, 2008, **19**, 2492-2496.

74. Z. Yang, K. Zhang, F. Gong, S. Li, J. Chen, J. S. Ma, L. N. Sobenina, A. I. Mikhaleva, G. Yang and B. A. Trofimov, *Beilstein Journal of Organic Chemistry*, 2011, **7**, 46-52.

75. M. S. Munsey and N. R. Natale, *Coord. Chem. Rev.*, 1991, **109**, 251-281.

76. F. Heaney, *Eur. J. Org. Chem.*, 2012, **2012**, 3043-3058.

77. V. Algay, I. Singh and F. Heaney, *Organic & Biomolecular Chemistry*, 2010, **8**, 391-397.

78. H. Feuer, *Nitrile Oxides, Nitrones, and Nitronates in Organic Synthesis*, 2nd edn., Wiley, New Jersey, 2008.

79. B. C. Sanders, F. Friscourt, P. A. Ledin, N. E. Mbua, S. Arumugam, J. Guo, T. J. Boltje, V. V. Popik and G. J. Boons, *J. Am. Chem. Soc.*, 2011, **133**, 949-957.

80. E. Coutouli-Argyropoulou, P. Lianis, M. Mitakou, A. Giannoulis and J. Nowak, *Tetrahedron*, 2006, **62**, 1494-1501.

81. T. Pasinszki, B. Hajgato, B. Havasi and N. P. Westwood, *PCCP*, 2009, **11**, 5263-5272.

82. M. T. Nguyen, S. Malone, A. F. Hegarty and I. I. Williams, *J. Org. Chem.*, 1991, **56**, 3683-3687.

83. V. Padmavathi, K. V. Reddy, A. Padmaja and P. Venugopalan, *J. Org. Chem.*, 2003, **68**, 1567-1570.

84. K. M. L. Rai and A. Hassner, *Synth. Commun.*, 1997, **27**, 467-472.

85. S. Grecian and V. V. Fokin, *Angew. Chem. Int. Ed.*, 2008, **47**, 8285-8287.

86. T. M. Kaiser, J. Huang and J. Yang, *J. Org. Chem.*, 2013, **78**, 6297-6302.

87. Y.-J. Shiao, P.-C. Chiang, A. Senthilvelan, M.-T. Tsai, G.-H. Lee and W.-S. Chung, *Tetrahedron Lett.*, 2006, **47**, 8383-8386.

88. A. Senthilvelan, I. T. Ho, K. C. Chang, G. H. Lee, Y. H. Liu and W. S. Chung, *Chem. Eur. J.*, 2009, **15**, 6152-6160.

89. C.-C. Tsai, I. T. Ho, J.-H. Chu, L.-C. Shen, S.-L. Huang and W.-S. Chung, *J. Org. Chem.*, 2012, **77**, 2254-2262.

90. C. C. Tsai, K. C. Chang, I. T. Ho, J. H. Chu, Y. T. Cheng, L. C. Shen and W. S. Chung, *Chemical Communications (Cambridge)*, 2013, **49**, 3037-3039.

91. A. Sharma and S. G. Schulman, *Introduction to Fluorescence Spectroscopy*, 1st ed. edn., John Wiley & Sons, New York, 1999.

92. B. Valeur, *Molecular Fluorescence Principles and Applications*, 1st ed. edn., John Wiley & Sons, Weinheim, 2002.

93. J. R. Lakowicz, *Principles of Fluorescence Spectroscopy*, 3rd ed. edn., Springer, New York, 2006.

94. J. B. Birks and L. G. Christophorou, *Spectrochim. Acta*, 1963, **19**, 401-410.

95. J. S. Kim and D. T. Quang, *Chem. Rev.*, 2007, **107**, 3780-3799.

96. T. Jin, K. Ichikawa and T. Koyama, *J. Chem. Soc., Chem. Commun.*, 1992.

97. M. Zheng, H. Tan, Z. Xie, L. Zhang, X. Jing and Z. Sun, *ACS Appl Mater Interfaces*, 2013, **5**, 1078-1083.

98. K. Ghosh and T. Sen, *Beilstein Journal of Organic Chemistry*, 2010, **6**, 44.

99. K.-C. Chang, L.-Y. Luo, E. W.-G. Diau and W.-S. Chung, *Tetrahedron Lett.*, 2008, **49**, 5013-5016.

100. S. Fery-Forgues, M.-T. Le Bris, J.-P. Guetté and B. Valeur, *J. Phys. Chem.*, 1988, **92**, 6233-6237.

101. M. I. Rodriguez-Caceres, R. A. Agbaria and I. M. Warner, *J. Fluorsec*, 2005, **15**, 185-190.

102. R. K. Pathak, V. K. Hinge, P. Mondal and C. P. Rao, *J. Chem. Soc., Dalton Trans.*, 2012, **41**, 10652-10660.

103. N. Mataga and S. Tsuno, *Bull. Chem. Soc. Jpn.*, 1957, **30**, 368-374.

104. C. D. Gutsche, B. Dhawan, K. H. No and R. Muthukrishnan, *J. Am. Chem. Soc.*, 1981, **103**, 3782-3792.

105. P. Jurečka, P. Vojtíšek, K. Novotný, J. Rohovec and I. Lukeš, *J. Chem. Soc., Perkin Trans. 2*, 2002, 1370-1377.

106. Z.-T. Li, G.-Z. Ji, C.-X. Zhao, S.-D. Yuan, H. Ding, C. Huang, A.-L. Du and M. Wei, *J. Org. Chem.*, 1999, **10**, 3572-3584.

107. V. Böhmer, J. Zhao, M. Bolte, C. Dordea and B. Grüner, *Synthesis*, 2009, **2009**, 4063-4067.

108. J. H. Billman, J. Y. Chen Ho and L. R. Caswel, *J. Org. Chem.*, 1952, **17**, 1375-1378.

109. A. H. Channar, A. A. Sheikh, M. Y. Khuhawar, S. A. Majidano and T. Pirzada, *J. Chem. Soc. Pak.*, 2013, **35**, 151-156.

110. A. E. Frost and H. H. Freedman, *J. Org. Chem.*, 1959, **24**, 1905-1907.

111. P. Bhowmik, K. Harms and S. Chattopadhyay, *Polyhedron*, 2013, **49**, 113-120.

112. Z. Asadi and M. R. Shorkaei, *Spectrochim. Acta, Part A*, 2013, **105**, 344-351.

113. Z. Asfari, A. Bilyk, C. Bond, J. M. Harrowfield, G. A. Koutsantonis, N. Lengkeek, M. Mocerino, B. W. Skelton, A. N. Sobolev, S. Strano, J. Vicens and A. H. White, *Organic & Biomolecular Chemistry*, 2004, **2**, 387-396.

114. M. J. Chetcuti, A. M. Devoille, A. B. Othman, R. Souane, P. Thuery and J. Vicens, *J. Chem. Soc., Dalton Trans.*, 2009, 2999-3008.

115. D. Tian, H. Yan and H. Li, *Supramol. Chem.*, 2010, **22**, 249-255.

116. J.-B. Giguère, D. Thibeault, F. Cronier, J.-S. Marois, M. Auger and J.-F. Morin, *Tetrahedron Lett.*, 2009, **50**, 5497-5500.

117. R. H. Hans, E. M. Guantai, C. Lategan, P. J. Smith, B. Wan, S. G. Franzblau, J. Gut, P. J. Rosenthal and K. Chibale, *Bioorg. Med. Chem. Lett.*, 2010, **20**, 942-944.

118. G. Zi, F. Zhang, L. Xiang, Y. Chen, W. Fang and H. Song, *J. Chem. Soc., Dalton Trans.*, 2010, **39**, 4048-4061.

119. A. Fleming, F. Kelleher, M. F. Mahon, J. McGinley and V. Prajapati, *Tetrahedron*, 2005, **61**, 7002-7011.

120. M. F. Mahon, J. McGinley, A. Denise Rooney and J. M. D. Walsh, *Inorg. Chim. Acta*, 2009, **362**, 2353-2360.

121. S. Chattopadhyay, P. Chakraborty, M. G. B. Drew and A. Ghosh, *Inorg. Chim. Acta*, 2009, **362**, 502-508.

122. R. P. Saini, V. Kumar, A. K. Gupta and G. K. Gupta, *Med. Chem. Res.*, 2013.

123. J. Magano, M. H. Chen, J. D. Clark and T. Nussbaumer, *J. Org. Chem.*, 2006, **71**, 7103-7105.

124. R. K. Pathak, S. M. Ibrahim and C. P. Rao, *Tetrahedron Lett.*, 2009, **50**, 2730-2734.

125. R. K. Pathak, A. G. Dikundwar, T. N. Row and C. P. Rao, *Chemical Communications (Cambridge)*, 2010, **46**, 4345-4347.

126. R. Huisgen, *Proc. Chem. Soc.*, 1961.

127. H. Li, J. Zhan, M. Chen, D. Tian and Z. Zou, *J. Incl. Phenom. Macro.*, 2009, **66**, 43-47.

128. R. J. Bergeron and P. G. Hoffman, *J. Org. Chem.*, 1979, **44**, 1835-1839.

129. S. Schindler, *Eur. J. Inorg. Chem.*, 2000, **2000**, 2311-2326.

130. F. Zimmermann, T. Lippert, C. Beyer, J. Stebani, O. Nuyken and A. Wokaun, *Appl. Spectrosc.*, 1993, **47**, 986-993.

131. D. F. Donlon, Institute of Technology Tallaght Dublin, 2010.

132. I. Singh, J. S. Vyle and F. Heaney, *Chemical Communications (Cambridge)*, 2009, 3276-3278.

133. A. Kumar, P. Sharma, L. K. Chandel and B. L. Kalal, *J. Incl. Phenom. Macro.*, 2008, **61**, 335-342.

134. S. K. Kim, S. H. Kim, H. J. Kim, S. H. Lee, S. W. Lee, J. Ko, R. A. Bartsch and J. S. Kim, *Inorg. Chem.*, 2005, **44**, 7866-7875.

135. F. A. Cotton and G. Wilkinson, *Advanced Inorganic Chemistry*, 5th ed. edn., John Wiley & Sons, New York, 1988.

136. R. Joseph, B. Ramanujam, H. Pal and C. P. Rao, *Tetrahedron Lett.*, 2008, **49**, 6257-6261.

137. N. Wanichacheva, S. Watpathomsub, V. S. Lee and K. Grudpan, *Molecules*, 2010, **15**, 1798-1810.

138. M. Shortreed, R. Kopelman, M. Kuhn and B. Hoyland, *Anal. Chem.*, 1996, **68**, 1414-1418.

139. O. Sahin and M. Yilmaz, *Tetrahedron*, 2011, **67**, 3501-3508.

140. A. S. Hay, H. S. Blanchard, G. F. Endres and J. W. Eustance, *J. Am. Chem. Soc.*, 1959, **81**, 6335-6336.

141. S. Grimme, *J. Comput. Chem.*, 2006, **27**, 1787-1799.

142. M. J. Frisch and *e. al*., Gaussian, Inc., Wallingford CT, 2009, vol. Revision A.1.

143. S. K. Kim, S. H. Lee, J. Y. Lee, J. Y. Lee, R. A. Bartsch and J. S. Kim, *J. Am. Chem. Soc.*, 2004, **126**, 16499-16506.

144. N. Zhao, *Acta Crystallogr C*, 2013, **69**, 348-350.

145. X. Le, S. Liao, X. Liu and X. Feng, *J. Coord. Chem.*, 2006, **59**, 985-995.